# Deformation of Walls Retaining Soft Clay Backfills

By
G. K. Spencer, Ph.D., M.I.E.Aust.
(Engineer, Coffey and Hollingsworth, Melbourne)
AND
P. J. Moore, Sc.D., M.I.E.Aust.
(Senior Lecturer in Civil Engineering, University of Melbourne)

SUMMARY.- The inter-relationship between the deformation and the lateral restraint of a retaining wall has been investigated both experimentally and theoretically. A rigid model wall retaining a soft clay backfill was allowed to yield by reducing the lateral support on the wall. Observations were made of the amount and rate of lateral wall deformation. These observations indicated that the rate of wall movement was inversely proportional to the lateral restraining force and for the very soft clays the rate of wall movement finally became constant. Predictions of the wall deformation as a function of time were made by means of the rate process theory supported by data from a series of torsion shear tests. These theoretical predictions were in reasonable agreement with the observations.

## I.- INTRODUCTION

The Civil Engineering Code of Practice (Ref.1) expressions for active earth pressure have been used extensively during the past twenty years for the design of rigid retaining structures supporting clay masses. In this conventional analysis it is assumed that the minimum or active earth pressures which are used for design exist after a finite outward wall movement. Following development of this active pressure distribution the wall movements were assumed to cease.

In situations in which yielding of the retaining wall is prevented it has been proposed (Refs. 2, 3,4) that the wall should be designed to resist the "at rest" lateral earth pressure. With a cohesive backfill, Taylor (Ref.3) concluded that it was reasonable to design a wall on the basis of active pressure if continuous movements can occur without serious consequences. He considered that the shearing stresses within a clay backfill undergo slow relaxation so that as the shear stress decreases the lateral pressure must gradually increase to maintain equilibrium. Tschebotarioff (Ref.4) and Vidmar (Ref. 5) have conducted model retaining wall tests which have produced results that confirm the shear stress relaxation concept presented by Taylor.

In order to examine quantitatively the inter-relationship between wall movement and the lateral force exerted by a cohesive backfill, a rigid model retaining wall was designed and built.

## II.- NOTATION

| | |
|---|---|
| $P$ | lateral restraining force applied to retaining wall |
| $c_u$ | undrained cohesion |
| $\tau_o$ | relaxed shear strength |
| $\tau$ | shear stress |
| $c_w$ | wall adhesion |
| $t$ | time |
| $t_1$ | reference time |
| $c_r$ | residual cohesion |
| $D$ | creep deviator stress |
| $\dot{\varepsilon}$ | strain rate |
| $\dot{\delta}$ | deformation rate |
| $\dot{\delta}_w$ | wall displacement rate |
| $A$ | strain rate at time $t_1$ |
| $m$ | negative slope of the plot between log of strain rate and log of time |
| $\alpha$ | coefficient in rate process theory |
| $\phi$ | inclination of failure plane to horizontal |

## III.- EXPERIMENTAL APPARATUS

The model retaining wall is shown in Figure 1. The bin containing the clay backfill was 18 inches wide, 20 inches long and 15 inches high. The kaolin soil in the bin was supported on one side by a moveable metal plate ¼ inch thick, 18 inches wide and 12 inches high. The retaining plate was permitted to move horizontally by a system of three roller bearings which roll in tracks between metal guides. During placement and consolidation of the backfill a horizontal proving ring connected between the retaining wall and a rigid frame provided lateral support and also a measure of the total earth pressure.

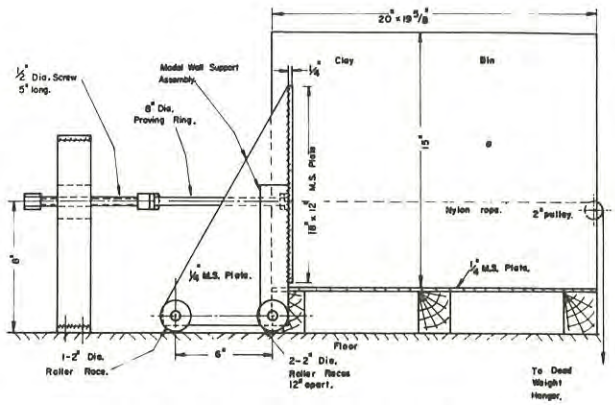


Fig.1. Model Retaining Wall

Prior to the wall moving, the proving ring restraint was replaced by dead weights via a pulley system from the retaining plate to the rear of the bin. Once this transfer of lateral support was achieved the proving ring was removed; wall movements were induced by removing a portion of the dead weights. A calibration test carried out on the wall system indicated that a frictional force of approximately ½ lb. exists as the wall is moved away from the backfill.

The horizontal displacements of the retaining wall were measured with two dial guages, which were independently fixed onto the rigid base of the bin having no contact with the proving ring. The backfill surface was surcharged with a uniformly distributed load. The settlements of the soil surface were measured with two vertical dial guages.

Determination of the shear stress-deformation characteristics of the clay backfill was obtained from torsion shear tests on remoulded Kaolin samples. The torsion shear apparatus was basically the same as that described by Hvorslev (Ref.6) with a few modifications made to simplify the construction. The apparatus permitted progressive shearing to occur during the test and the shearing resistance characteristics after initial failure, including the residual shearing resistance, to be fully explored.

## IV.- EXPERIMENTAL TEST RESULTS

Two stress controlled tests involving the small retaining wall were conducted. In Test No.1 for which the post consolidation water content and unit weight were respectively 78% and 98 lb./ft.$^3$, the total lateral force in the restraining proving ring after consolidation of the backfill was 102 lb. To produce wall displacements, loads were removed from the dead weight hanger such that the restraining force on the wall was less than the equilibrium value of 102 lb. To achieve an appreciable lateral wall movement within a period of about 5 days, lateral loads of less than 60 lb. were used. The load required to resist the hydrostatic water pressure alone was calculated to be 44 lb. The wall displacement variations with time corresponding to loads of 56,54,52 and 48 lb. are shown in Figure 2. The rates of wall movement extracted from these plots and which are listed in Table I reveal two important features:

(a) after a period of approximately 2 days the wall movements for all levels of restraining force appear to be linear with time, and

(b) the rate of wall movement is inversely proportional to the lateral restraining force.

The aim of Test No.2 for which the post consolidation water content and unit weight were respectively 52% and 106 lb./ft.$^3$, was to verify the above conclusions for a clay backfill placed at a consistency which resembles prototype conditions. The total lateral force in the restraining proving ring after consolidation was 125 lb. The external load required to resist the hydrostatic water pressure alone was found to be 44 lb.

TABLE I - WALL DEFORMATION BEHAVIOUR

| TEST NO.1 (backfill surcharge 0.41 lb/in.$^2$) | |
|---|---|
| Lateral Restraining Force Applied to Retaining Wall P,(lb.) | Horizontal Rate of Wall Movement (in./day) |
| 56 | 0.0035 |
| 54 | 0.008 |
| 52 | 0.012 |
| 48 | 0.020 |

| TEST NO.2 (backfill surcharge 0.53 lb/in.$^2$) | | | | | |
|---|---|---|---|---|---|
| Lateral Restraining Force Applied to Retaining Wall P,(lb.) | Horizontal Rate of Wall Movement (in./min.) x $10^{-6}$ | | | | |
| | Day: | 3 | 4 | 5 | 6 |
| 60 | | 4.2 | 3.6 | 3.1 | 2.1 |
| 45 | | 12.6 | 10.4 | 8.3 | 6.3 |

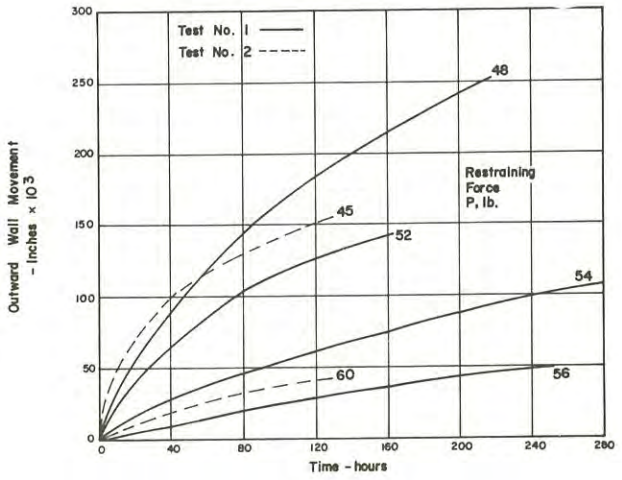


Fig.2. Retaining Wall Creep Tests

It was again found necessary to reduce the external loads such that an appreciable lateral wall movement was obtained within a 5 day period. The wall displacement variations with time corresponding to loads of 60 lb. and 45 lb. are shown in Figure 2. The plots reveal that for all levels of restraining force the rate of horizontal wall movement decreases with time. This result is contrary to that of Test No.1 in which a constant rate of wall creep was observed. The results of Test No.2 are tabulated in Table I.

A comparison of the test results suggests that the horizontal creep behaviour of the wall is a function of the stiffness of the backfill material, since all other variables are the same in both tests. In Test No.1, where a constant rate of wall movement

was observed, the moisture content of the clay backfill was 78% which is just above liquid limit of the soil. In Test No.2, the moisture content was 52% and produced a decreasing rate of wall movement. This apparent discrepancy may be explained if in Test No.1 the wall movement is considered to be decreasing at an extremely slow rate. Therefore, it can be postulated that as the natural moisture content of a clay backfill decreases, the decrease in the rate of outward wall movement becomes more apparent.

In all retaining wall tests the undrained shear strength of the clay backfill after consolidation was determined by vane apparatus. These insitu values of the undrained cohesion, $c_u$ were determined at various depths throughout the clay profile. The main advantage of this apparatus is that it permits values of shear strength to be obtained in extremely soft soils. The vane shear strength variation with depth corresponding to Test Nos.1 and 2 are shown in Table II.

In addition to the vane tests, strain-controlled torsion shear stage tests were conducted on kaolin samples duplicating the vertical effective stress and moisture content of the clay backfills. The values of the undrained shear strength, $c_u$ and the residual shear strength, $c_r$ from the torsion shear tests are also shown in Table II. During the tests it was observed that the undrained shear strength was compatible with a finite strain rate, since the shear stress decreased immediately deformation was terminated. It was noted that after all shearing stages, the shear strength of the sample relaxed and fell to a fixed level which was compatible with zero displacement. The shear stress corresponding to this level may be termed the "relaxed" shear strength, $\tau_o$ of the soil, the values of which are tabulated in Table II corresponding to Tests Nos. 1 and 2.

In addition to the strain-controlled torsion shear tests, creep tests were performed on Kaolin samples corresponding to the stress conditions at the mid-depths of the backfills in Test Nos. 1 and 2. These were essentially stress-controlled tests in which a constant shear stress was applied to the samples and the deformation characteristics observed. The magnitude of the constant shear stress, $\tau$ used in the creep tests ranged from 50% to 88% of the drained peak shear strength. It was observed that creep did not occur if the applied shear stress was below the relaxed shear stress, $\tau_o$ . Typical results of the creep tests are provided in Figure 3. As expected, the creep behaviour is similar to that observed with the retaining wall. A tabulation of results for both series of creep tests is given in Table III.

TABLE II - SHEAR STRENGTH OF CLAY BACKFILL AFTER CONSOLIDATION

| Test No. | Vane Tests $c_u$(psi) | Torsion Shear Stage Tests $c_u$(psi) | $c_r$(psi) | $\tau_o$(psi) |
|---|---|---|---|---|
| 1, 8" above base | 0.19 | - | - | - |
| 6" above base | - | 0.22 | 0.22 | 0.08 |
| 2" above base | 0.23 | - | - | - |
| 2, 8" above base | 0.23 | - | - | - |
| 6" above base | - | 0.25 | 0.25 | 0.10 |
| 2" above base | 0.27 | - | - | - |

TABLE III - TORSION SHEAR CREEP TEST

| Creep Test No. | Applied Shear Stress (psi) | Observed Deformation Rate (in./min.) | | | | |
|---|---|---|---|---|---|---|
| C.T.1 | 0.27 | $2.3 \times 10^{-4}$ | | | | |
| | 0.22 | $5.6 \times 10^{-6}$ | Constant Creep Rate | | | |
| | 0.17 | $7.6 \times 10^{-8}$ | | | | |
| | 0.15 | $7.6 \times 10^{-9}$ | | | | |
| | | Day | 2 | 5 | 7 | Factor |
| C.T.2 | 0.30 | | 34 | 20 | 18 | $\times 10^{-6}$ |
| | 0.25 | | 3.33 | 2.00 | 1.85 | $\times 10^{-6}$ |
| | 0.20 | | 0.30 | 0.18 | 0.17 | $\times 10^{-6}$ |
| | 0.17 | | 0.07 | 0.05 | 0.04 | $\times 10^{-6}$ |

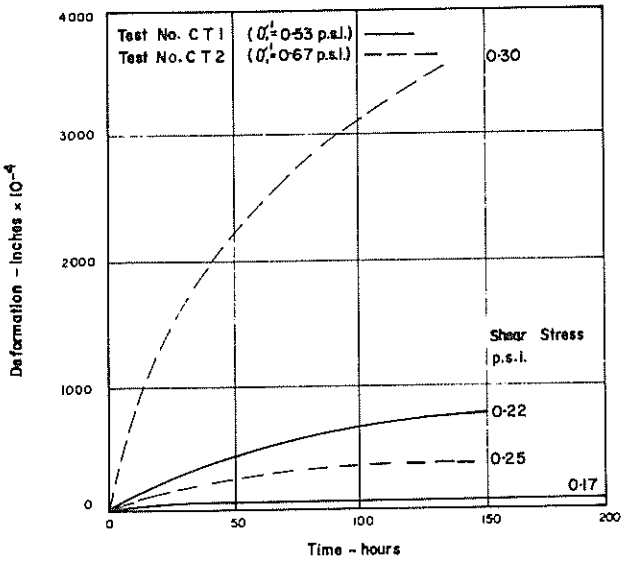


Fig.3. Torsion Shear Creep Tests

These results tend to confirm the earlier statement that the creep behaviour of a soil is dependant upon the stiffness of the material. It seems that an almost constant rate of creep can be expected for very soft soils, whereas for stiffer clays the creep rate has been observed to decrease with time.

## V.- THEORETICAL ANALYSIS

To predict the deformation behaviour of retaining walls the theory of absolute reaction rates, commonly known as rate process theory (Ref.7) has been used to describe the creep behaviour of clay under stress. In particular Mitchell, Campanella and Singh (Ref.8) have adopted the principles of the rate process theory to determine a simple three parameter expression for the creep rate, under conditions of constant temperature and over a stress range of engineering interest. The expression has been derived using experimental test results and is given below:

$$\dot{\epsilon} = A.(t_1/t)^m . e^{\alpha.D} \qquad ...(1)$$

In its present form equation (1) is unsuitable as a means of predicting retaining wall behaviour from torsion shear creep tests. If the strain rate $\dot{\epsilon}$ is replaced by the deformation rate, $\dot{\delta}$ and the shear stress increment $(\tau-\tau_o)$ substituted for the deviator stress (D), then the creep equation becomes:

$$\dot{\delta} = A_1.(t_1/t)^{m_1} . e^{\alpha_1.(\tau-\tau_o)} \qquad ...(2)$$

Equation (2) can now be used to predict deformation rates from the results of torsion shear creep tests allowing values of the constant $A_1, m_1$ and $\alpha_1$ to be found.

The creep equation derived above only gives the displacement rate along a failure plane within the soil mass which, according to the conventional analysis, passes through the base of the wall and slopes at an angle $\Theta$ to the horizontal. Therefore the horizontal wall displacement rate, $\dot{\delta}_w$ can be determined from:

$$\dot{\delta}_w = \dot{\delta}.\cos\Theta$$

where from the conventional analysis:

$$\Theta = \arctan(1/\sqrt{1 + c_w/c_u})$$

If a typical value of $c_w$ is assumed such that $c_w/c_u$ is equal to 0.33, then it can be shown that:

$$\dot{\delta}_w = 0.76\,\dot{\delta} \qquad ...(3)$$

## VI.- DISCUSSION OF EXPERIMENTAL RESULTS

As derived earlier the expression for the rate of displacement along an assumed failure plane by the theory of rate processes is given by equation (2). For the conditions corresponding to Test No.1, the observed results from the torsion shear and retaining wall tests revealed that after a period of transient creep, deformation occured at a constant rate so that $m_1$ is zero in equation (2). Also, since the observed behaviour corresponds to the fully active condition (P = 54 lb.) in which the undrained shear strength, $c_u$ is mobilized then equation (2) becomes:

$$\dot{\delta} = A_1 . e^{\alpha_1.(c_u-\tau_o)} \qquad ...(4)$$

To determine the constants $A_1$ and $\alpha_1$ it is necessary to plot the shear stress increment, $(\tau-\tau_o)$ against the logarithm of the deformation rate, $\dot{\delta}$ from the torsion shear creep tests. This plot is shown in Figure 4. The slope of the line of best fit passing through the experimental points gives the value of $\alpha_1$, which in this case is 88.0. The value of $A_1$ is $3.1 \times 10^{-11}$. obtained from the intercept where $(\tau-\tau_o)$ is zero. Therefore the deformation rate along the assumed failure plane within the clay backfill is given by:

$$\dot{\delta} = 3.1 \times 10^{-11}\, e^{88.0(c_u-\tau_o)} \qquad ...(5)$$

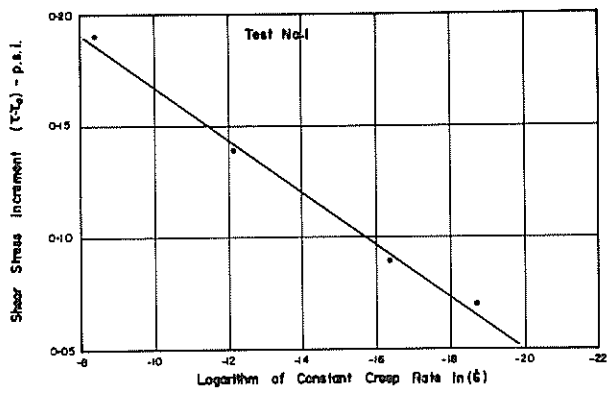


Fig.4. Plot of $(\tau-\tau_o)$ Versus LN($\dot{\delta}$)

If 0.14 psi, which is the shear stress increment corresponding to the 56 lb. lateral restraining force, is substituted for $(c_u - \tau_o)$, then the deformation rate, $\dot{\delta}$ is equal to 0.009 in./day, which in terms of the rate of outward wall movement, $\dot{\delta}_w$ is 0.0068 in./day. The comparison between the predicted rate of 0.0068 in./day and the observed rate of 0.0080 in./day is extremely good.

In Test No.2 the deformation behaviour corresponding to lateral restraining forces of 60 lb. and 45 lb. were observed. From considerations of equilibrium of the failure wedge the shear stress developed along the plane failure surface passing through the toe of the wall and corresponding to the above lateral forces are 0.26 psi and 0.29 psi respectively. Since the relaxed shear strength $\tau_o$ is equal to 0.10 psi, the shear stress increments, $(\tau - \tau_o)$ corresponding to lateral forces of 60 lb. and 45 lb. are 0.16 psi and 0.19 psi, respectively.

The results of the torsion shear creep tests have been analysed by plotting the logarithm of deformation rate, $\dot{\delta}$ versus the logarithm of time, $t$ as shown in Figure 5. This plot produces four nearly parallel straight lines, each corresponding to a level of applied shear stress, $\tau$. The slope of these lines ranged from 0.56 to 0.51, having an average value of 0.53 which is the magnitude of $m_1$ in the rate process theory equation.

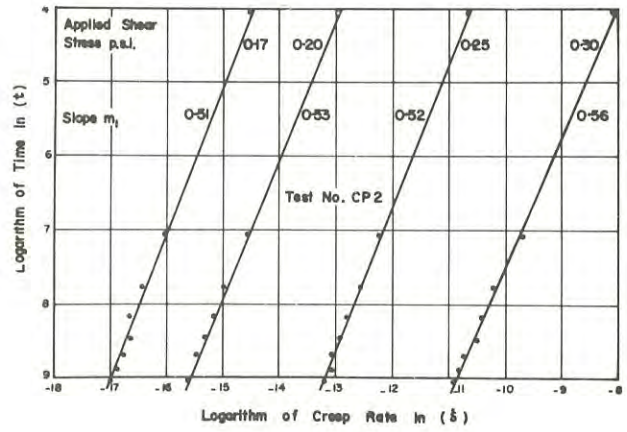


Fig.5. Plot of LN($t$) Versus LN($\dot{\delta}$)

The values of $A_1$ and $\alpha_1$ in this equation were obtained by plotting the deformation rate at various times after commencement of the creep test versus the shear stress increment $(\tau - \tau_o)$. This plot of LN $(\dot{\delta})$ versus $(\tau - \tau_o)$ is shown in Figure 6 for the four creep stresses at times corresponding to 1,3 and 6 days after each test was begun. This plot produced three parallel straight lines which correspond to the above times. For calculation purposes the unit time, $t_1$ was chosen to be 1 day. From the 1 day line in Figure 6, the slope $\alpha_1$ was found to be equal to 49.0 and the intercept where $(\tau - \tau_o)$ is zero, $A_1$ equal to $3.2 \times 10^{-9}$. If these values are substituted into the equation derived from the rate

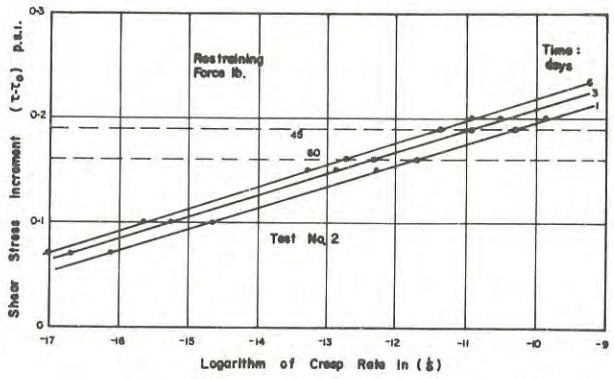


Fig.6. Plot of $(\tau - \tau_o)$ Versus LN($\dot{\delta}$)

process theory, then the deformation rate along the assumed failure plane within the clay backfill is given by:

$$\dot{\delta} = 3.2 \times 10^{-9} \left(\frac{1}{t}\right)^{0.53} e^{49.0(\tau - \tau_o)} \qquad \ldots(6)$$

From the above expression the rate of displacement along the failure plane can be determined at any time, $t$ (days) and at any value of the mobilized shear stress, $\tau$ along the failure surface. The horizontal wall movement, $\dot{\delta}_w$ can be found from equation (3). The observed rates of outward wall movement variation with time for restraining forces of 60 lb. and 45 lb. have been plotted in Figure 7. Superimposed on this figure is the theoretical behaviour predicted from the rate process theory. The average difference between the observed and predicted behaviour is approximately 15%, thus indicating that the adopted theory provides a reasonable method of estimating rates of wall movement.

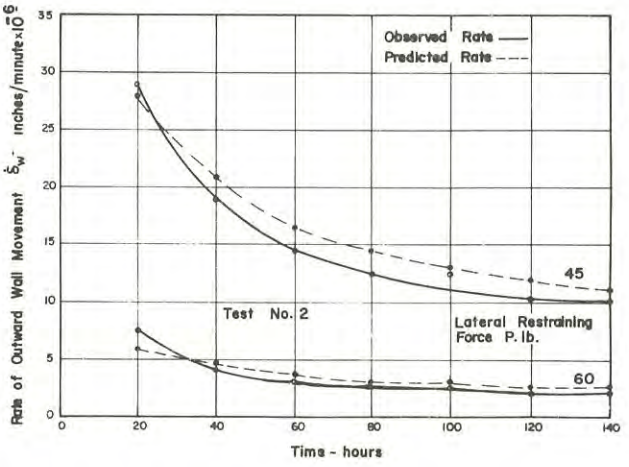


Fig.7. Comparison of Observed & Predicted Rates of Outward Wall Movement

## VII.- CONCLUSIONS

The results of torsion shear tests on soft clays have indicated that in order to keep the undrained shear strength mobilized, a definite rate of deformation must be applied to a shear surface. Similarly, to maintain a mobilized shear stress less than the failure stress along a failure plane within a clay backfill, the retaining structure must continually creep to achieve equilibrium. The relaxed shear strength is the shear stress which is compatible with zero deformation along a shear surface. If a retaining wall is designed on the basis that the relaxed shear strength is the maximum stress acting across a failure plane, then outward wall displacements will be zero.

The results of measurements of the relaxed shear strength $\tau_o$ in the torsion shear stage tests suggests that continual creep of walls will occur if shear stresses in a backfill are larger than $\tau_o$. For prototype backfill materials, the results from the model retaining wall and torsion shear creep tests reveal that deformations occur at a decreasing rate. The rate process theory was used to derive an expression for the rate of deformation along an assumed plane failure surface. The constants in the expression were calculated from the results of a series of torsion shear creep tests and the deformation rate converted into an equivalent wall movement. The observed and predicted outward wall displacement rates disagreed by about 15%. Thus it seems that deformation of a retaining structure can be predicted within reasonable limits by considering the rate process theory equation applied to the failure surface within a soil mass.

## REFERENCES


1. CIVIL ENGINEERING CODE OF PRACTICE, "Earth Retaining Structures", No.2, 1951.

2. TERZAGHI, K. - "Theoretical Soil Mechanics", Wiley, New York, 1943.

3. TAYLOR, D.W. - "Fundamentals of Soil Mechanics", Wiley, New York, 1948.

4. TSCHEBOTARIOFF,G.P. - "Large Scale Earth Pressure Tests with Model Flexible Bulkheads", Bureau of Yards and Docks, Dept. of the Navy, 1949.

5. VIDMAR, S. - "Relaxation Effects on the Earth Pressure of Cohesive Soils", Proc. of the Int. Conf. on Soil Mech. and Found. Engg., Hungarian Academy of Science, Budapest, 1963.

6. HVORSLEV, M .J.- "Torsion Shear Apparatus and Testing Procedures", Waterways Experimental Station, Corps. of Engrs. U.S.Army, Bull. No.38, 1952.

7. GLASSTONE, S., LAIDLER, K., and EYRING, H. - "The Theory of Rate Process", McGraw Hill Book Co., Inc., New York, 1941.

8. MITCHELL, J.K., CAMPANELLA, R.G., and SINGH, A. - "Soil Creep as a Rate Process", J.Soil Mech. and Found. Div. Proc. A.S.C.E., Vol. 94, SM1, 1968.

# Rock Structures and Associated Rock Alteration, Danjera Creek Dam, N.S.W.

By
A. D. M. Bell, M.Sc., M.Aus.I.M.M.
(Lecturer in Engineering Geology, The University of New South Wales)

Alteration.
* Chemical instability
Slides.

SUMMARY. - Danjera Creek damsite is an interesting case history of the association of rock structure and rock alteration. The most critical conditions are where fracture zones form permeability paths for hypogene and supergene circulations. Petrographic studies combined with structural analysis indicated sub-surface rock defects. At this damsite bedrock is comprised of steeply dipping intercalations of low-grade meta-sediments and basalt. Rock defects are caused by a combination of fracture and alteration associated with possible thrust faults. The "axial plane" of an anticline is parallel to the valley and dips 70°W. The resultant discontinuity pattern is asymmetric to the valley profile and rock cuts in the right abutment are less stable than those in the left abutment. Later deformation produced two fault/fracture sets at 50° and 90° to the valley axis. Secondary fracture porosity is greatest at the intersection of faults and is associated with alteration within basalt. Decomposition of basalt was initiated by hypogene circulations producing sulphide mineralization and weathering of basalt to clay is deepest in zones previously effected by hypogene alteration. Geological investigations during preliminary excavation work were utilised to redesign the concrete foundations.

## INTRODUCTION

Danjera Creek is a right bank tributary of the Lower Shoalhaven River in the central coastal belt of New South Wales. The dam is located 15 miles west of Nowra and is being constructed to augment water storage for the Shoalhaven Shire Council.

Wallis (Ref.1) has described the preliminary investigations of 1965/66. 16 vertical diamond holes were drilled during 1965 in the dam foundations. The area was geologically mapped and bulldozer trenching utilized to gain further geological information. Electromagnetic survey of a quartzite breccia zone associated with a suspected fault in the eastern part of the valley floor was interpretated to indicate this fault zone had a steep easterly dip (Note that excavation showed this fault dipped 70°W). Six additional angle diamond holes were then drilled into this zone.

The geology of Danjera Creek damsite provides an interesting case history concerning the affect of rock structures and hypogene rock alteration on the engineering properties of rock foundations. The occurrence of rock decomposition resulting from hypogene processes, i.e. hydrothermal activity, mineralization, auto-metamorphism, etc., is of specific importance in foundation studies in view of its persistance at depth. Normal weathering by supergene water percolation is on the other hand a surface phenomenon. Hypogene rock alteration is most extensive in chemically unstable igneous rock. It is difficult to recognise hypogene rock alteration in the surface exfoliated zone where it is normally masked by weathering.

Basaltic rocks are particularly prone to alteration. Auto-metamorphism (decomposition by entrapped volatiles) in extrusive basalt complexes is widespread in Eastern Australia and recent investigations in northern N.S.W. indicate that rock structures partly control the extent of decomposition in basalt flows where contemporaneous movements have occurred. At Danjera Creek, basalt forms sill-like masses in which auto-metamorphic alteration is slight and extensive alteration is associated with sulphide mineralization in zones of fracture along faults.

## GEOLOGY

The dam is founded on steeply dipping intercalations of Upper Devonian sediments and basalt, part of the western limb of an asymmetric anticline. The sediments consist of massive units of interbedded silty-mudstone and siltstone which contain thin beds of fine-grained quartzite and tuffaceous sandstone. These sediments have been affected by low-grade metamorphism and the rocks are indurated and cleaved, particularly parallel to a prominent "axial plane" cleavage trending 20°E of N and dipping 70°W. Bedding is indistinct, the few measurements possible indicate the bedding strikes 20°E of N and dips 60°W. The rock masses are isotropic, the asymmetric of the discontinuities resulting in the right bank foundations being less stable than the left bank in open cut.

The basalt varies in texture from sub-vitreous fine-grained to coarse-grained. Glassy material occurs near the sediment contact and it is assumed the basalt masses are sill intrusions. Decomposition of the basalt has selectively occurred along fault planes in association with pyrite/galena mineralization. Frequently the meta-sediment/basalt contacts are faulted.

Meta-sediments form the rock foundation in the abutments and basalt in the valley floor - see Fig. 1.

## ROCK STRUCTURES

The fold axis trends 20°E of N and is parallel to the river course. An "axial plane" cleavage dips 70° W with two complementary sets dipping 35°/40°W and 50°E. Two near-vertical joint sets trend 40° and 80° W of N. Faults in the latter directions have displaced

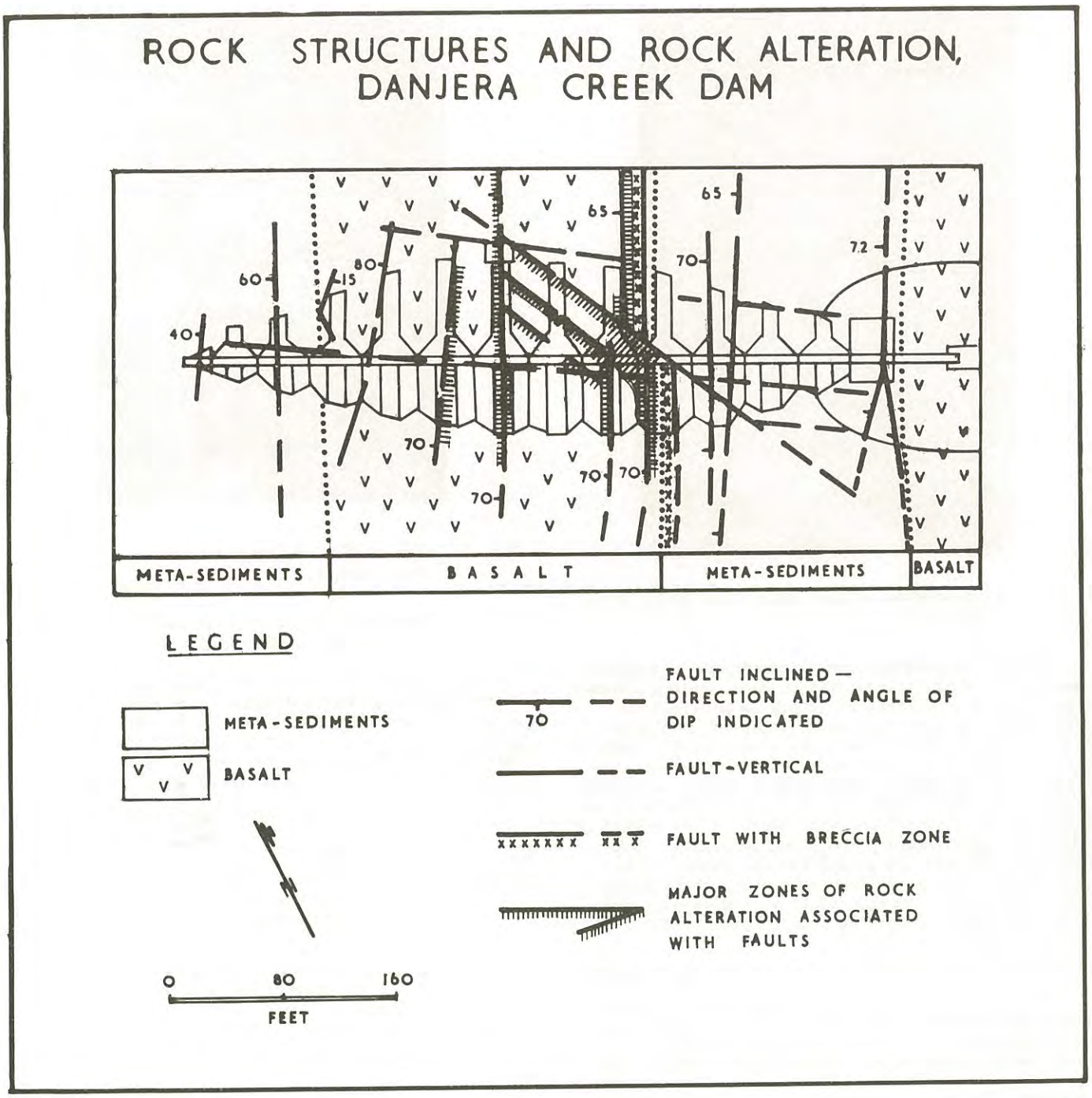


Fig.1

the "axial plane" faults. Many joints show displacement within the rock while major faults have sheared or brecciated the bedrock. The "axial plane" faults appear to be thrust planes and the sill-like basalt sheets may be repeated by faulting. The fault forming the eastern boundary of the valley floor basalt is associated with a mineralized quartzite breccia which appeared on the surface as a quartzitic gossan. Other faults were masked by the weathered mantle.

WEATHERING (SUPERGENE) AND ALTERATION (HYPOGENE)

An open jointed exfoliation zone extends 20' - 30' below the surface in the valley slopes. Basalt is completely to highly weathered in this zone and the meta-sediments less weathered with clay filled joints. Below the exfoliation zone the meta-sediments are slightly weathered with limited development of clay in joints. Seams of altered fractured basalt along faults are completely weathered to clay immediately below the exfoliation zone.

Fig. 2 - Slip surface on low-angle cleavage in meta-sediments.

Sulphide mineralization is prominent in faulted basalt with a quartz, calcite, pyrite, galena assemblage. Wallrock alteration occurs in mineralized zones with the rock substance grading from plastic clay to clay-basalt of moderate strength. The zone of alteration is a few feet wide along fault lines increasing in thickness within highly fractured basalt at fault intersections. The strength of fractured decomposed basalt increases with depth as the effect of supergene groundwater percolation decreases. The most critical zone of alteration was found in the eastern part of the valley floor where three fault sets intersected. A mass of clay, clay-basalt and fractured basalt extending over an area of 30' x 60' was excavated to 30' depth.

TREATMENT OF THE FOUNDATION ZONE DURING CONSTRUCTION

The dam is an articulated diamond head buttress design approximately 120 feet in height (see Fig.4) which has relatively low foundation loading, but needs uniform foundation conditions and stable abutment slopes. At the initial excavation stage (1969) it became apparent that the bedrock was highly fractured in fault zones and that rock alteration associated with mineralization would occur within the basalt. Three problems were to be expected:-

i) Instability in the right abutment where three discontinuities trending parallel to the slope form potential slip planes viz. bedding planes with dip 60°W; "axial plane" faults and cleavage with dip 70°W; cleavage with dip 35°/40°W.

ii) The presence of zones of alteration in fault zones within the valley floor basalt - see Fig. 3.

iii) The irregular depth to sound bedrock due to fracture in the meta-sediments and chemical alteration in the basalt.

Fig. 3 - Clay seams and altered fractured basalt in fault trench.

The initial excavations were carefully mapped and three additional angle diamond holes were drilled which located additional faults. As these investigations proceeded the results were utilised to modify the footings to suit the rock conditions. It was found necessary to carry out additional work viz:

a) Lowering the buttress foundation level in the abutments to alleviate slip on the low angle (35°) cleavage planes.

b) Excavation of highly fractured fault zones then backfilling with mass-concrete to a height which would effectively buttress less stable slopes - see Fig. 5.

c) Where a bed of quartzite formed a natural face this was maintained and rock-bolts used to stabilize the cut.

d) Buttress footings were extended to bridge fault zones.

e) Examination of the basalt was initiated, weak rock excavated and backfilled with mass concrete. Longitudinal faults (i.e. normal to the dam wall) were trenched and sealed with concrete to increase the permeability path of water circulation below the structure and prevent scouring.

f) Cross-faults in the valley floor basalt were excavated and the excavations utilized to pour concrete ribs between buttress footings. This method of strutting between buttresses will resist any earth pressures which might develop tending to rotate the buttresses in the valley floor.

Fig. 4 - Right abutment.

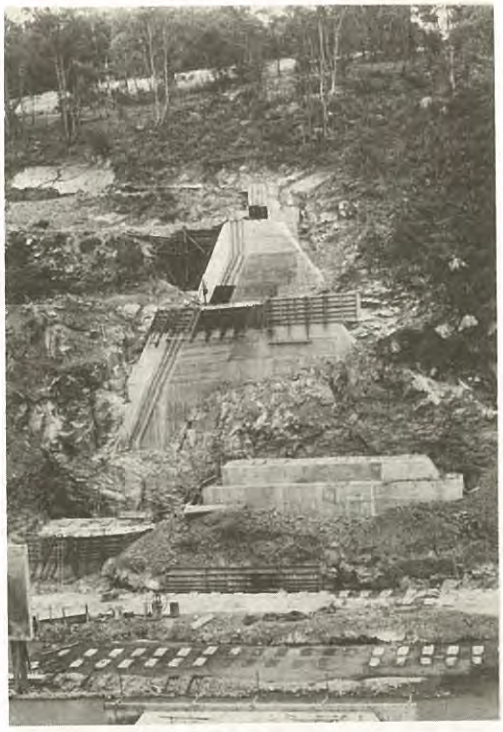

Fig. 5 - Left abutment - note buttress foundation supporting base of cut.

## CONCLUSION

This case history illustrates the need to gather all available geological information in order to present the engineer with a true picture of the foundation conditions (Ref.3).

Alteration of bedrock is frequently associated with rock structures and may be more important than fracturation in chemically unstable rock. As supergene weathering masks alteration effects in the surface soil zone, careful examination of drill cores is essential. The association of alteration with orientated rock structures emphasizes the value of structural analysis in engineering geology. Directed angle-drill holes are the best method of locating thin sheets of altered rock which may not be obvious in geophysical traverses.

Borehole-log sheets using a degree of weathering classification should be replaced by those differentiating weathering and alteration, such as the type proposed by Dixon (Ref. 2).

## ACKNOWLEDGEMENTS

The assistance received from officers of the Shoalhaven Shire Council and its consultant engineers Gutteridge, Haskins and Davey of Sydney, in particular R.A. Smith, Project Engineer, who provided the photographs is gratefully acknowledged. Most of the later geological work was carried out by C.R. Matson (Ref. 4) as part of his undergraduate thesis project and his observations particularly those dealing with the petrography of the bedrock have been invaluable.

## REFERENCES

1. WALLIS, G.R. - Engineering Geology of the Danjera Creek Damsite, Yalwal. Dept. of Mines, N.S.W., July, 1966.

2. DIXON, H.W. - Decomposition Products of Rock Substances - Proposed Engineering Geological Classification. Syd.Div.I.E.Aust. and Syd. Brch.Aust.I.M.M. - Rock Mechanics Symposium, Feb. 1969, pp. 39-44.

3. KNILL, J.L., and JONES, K.S. - The Recording and Interpretation of Geological Conditions in the Foundations of the Rosieres, Kariba and Latiyan Dams. Geotechnique, Vol. 15, No. 1, Mar. 1965, pp. 94-124.

4. MATSON, C.R. - The Geology of the Danjera Creek Dam - Yalwal, N.S.W. Ungrad. thesis, Univ of N.S.W., 1970.

# Some Effects of Structure on the Behaviour of Argillaceous Sediments

By

P. M. James, B.Sc., M.Sc. (Eng.), Ph.D., D.I.C.

(Senior Lecturer in Civil Engineering, University of Queensland)

SUMMARY.- Structure of clays and clay shales is discussed from three points of view.

(i) Directional effects, along or across the bedding, which appear to control the path or strain requirements in moving from peak to residual conditions. Examples are given to indicate that much smaller strains will be required to produce the residual strength along the bedding, although its ultimate value may be independent of direction.

(ii) Tectonic effects are briefly reviewed. Faulting, folding of sedimentary series, and also the general consolidation and erosion cycle stress changes are all found to produce similar shear zones within argillaceous sediments. Examples of flexural slip are given.

(iii) Mineralogical effects, taken to include the presence of slightly variable seams or layers in otherwise "homogeneous" clay formations. Examples from sites both in Australia and overseas are given to demonstrate how such layers will often control stability. In many cases the untypical behaviour can be put down to the localisation of montmorillonite during deposition of the formation.

## I.- INTRODUCTION

Argillaceous sediments, comprising the bulk of rocks on the earth's surface, are consequently of major importance in many aspects of human activity. They also, by their very nature, envelope the widest spectrum of soil mechanics problems. In this paper some attempt is made to outline the behaviour with respect to structure of one general class, the clay shales, (which is taken to include most overconsolidated clays),

Over the past decade it has become increasingly apparent that attention to what might be termed minor geological or structural details forms one of the most important facets of an engineering geologist's role; for example, observation of small slickensides in a shale interbedded with sandstones, which is the sort of phenomenon likely to be overlooked in a regional survey. Secondly, while the geological observation and recording of such details are essential, the observations themselves must be further subjected to scrutiny from the mechanics point of view. To continue the example: if the slickensides above are present, is the shale layer at or near its residual strength condition and what effect will this have on the stability of structures associated with the formation?

It is in this latter transition from observation to meaningful interpretation that communication between geology and engineering is most critical and where, unfortunately, it is most likely to break down.

Below some common and some less common effects of structure in clay shales are discussed from this point of view. The subject is treated, for convenience, under three headings: directional properties, tectonic effects, and mineralogical effects.

## II.- DIRECTIONAL PROPERTIES

In any sediment there will generally be a pronounced preferred orientation parallel to the bedding. This will occur for two reasons, the first being that deposition under gravity of non spherical particles will favour such a structure. The effect of this on field permeability is well documented. Secondly, it has been observed that consolidation of argillaceous sediments causes severe re-orientation of the clay platelets in a direction normal to the consolidating load, i.e. giving a horizontal orientation under gravity loadings. This will tend to override the physio-chemical effects of deposition.

Little work has been done, to the author's knowledge, concerning the effects of this bedding orientation on the shear strength properties of overconsolidated clays. However, an extensive set of triaxial tests on the London Clay by Bishop et al (1965) indicated that both peak and residual strengths were sensibly constant whether samples were cut across or parallel to the bedding. London Clay is, of course, a relatively isotropic formation and more shale like material may be expected to produce a marked variation in the peak strength; mainly peak strength for it is considered unlikely that the ultimate value of the residual strength would be much affected by direction even in shales. Residual strength is generally taken as an intrinsic property of a particular material and,

as such, independent of sample disturbance, strain rate etc; and, by inference, direction.

It should be noted here that the majority of published results to date are concerned largely with the magnitude of the parameters in relation to direction, rather than with behaviour during shear and when the actual path between peak and residual strengths is investigated, some variations in behaviour may be seen. Some multiple reversal shear box tests were undertaken by the author, James (1970), both along and perpendicular to the bedding in Oxford Clay. The Oxford Clay is a heavily over-consolidated formation from the Upper Jurassic of U.K. with the following properties.

| L.L. | P.L. | P.I. | C.F. | Activity |
|---|---|---|---|---|
| 50-75 | 20-32 | 25-50 | 40-60% | 0.6-1.1 |

Peak Strength $\phi'$ (= $30^{\circ}$ unweathered)
(= $22^{\circ}$ weathered )
c' variable

Residual Strength $\phi'_R$ (= $16^{\circ}$ unweathered )
(= $14\text{-}15^{\circ}$ weathered)
c' assumed = zero.

The results of the shear box tests are shown in Fig. No. 1.

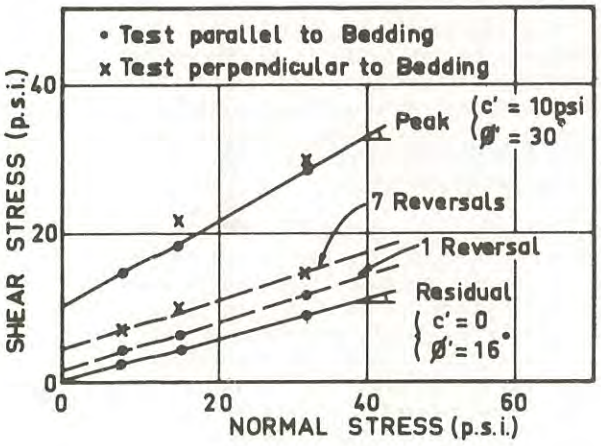


Fig 1. Directional shear tests on Oxford Clay

From the figure it may be seen that while the peak strengths, i.e. first travel strengths, are again reasonably consistent in either directions, (as found elsewhere) the behaviour on repeated shearing differs widely. One reversal in the test parallel to the bedding caused a greater reduction in strength than seven reversals in the test perpendicular to the bedding. Further, in the former test, parallel to the bedding, after one travel of the shear box the strength fell 90% of the way from peak to residual.

This then suggests that particle orientation resulting either from depositional characteristics or the consolidation of the formation has an important bearing on the path to the residual in any particular direction. This could be taken a step further, namely, that exceptionally large strains will be required to produce residual conditions in a slip plane or shear zone passing across the bedding, whereas residual conditions would be relatively quickly attained where the deformation was located along a bedding plane. Most slips in clay cuttings will, of course, consist of a combination of both conditions, and the strength along a slip zone could therefore increase from probably the residual near the toe to something only slightly less than the peak near the back scarp. This variation should be borne in mind if any sampling or insitu testing of a slip zone is to be made.

It is of interest to note here that the residual condition, involving as it does an almost complete orientation of clay particles parallel to the direction of straining, is a condition which does not normally heal with time. The existence of Pleistocene slips which today have factors of safety still in the vicinity of unity may be cited as evidence. It is not, however, known whether reconsolidation of a slip zone, by further deposition say, would cause some small healing. If so, this may prove a useful method of dealing with stabilizing slips in some circumstances.

## III.- TECTONIC EFFECTS

The structures of shear zones associated with conventional tectonic activity have been treated in papers by Skempton (1966), Skempton & Petley (1967) and Fookes & Wilson (1966). Shear zones associated with faulting are usually well defined and easily recognisable in the field. Less common in the literature and often less obvious in the field are the shear zones associated with folding of competent and incompetent beds, i.e. flexural slip zones. There are, however, three sites where this phenomenon has been investigated: Mangla Dam, described in the above mentioned papers; Muda Dam (Malaya) described by Taylor & James (1967) and Clarke, James & Morgenstern (1970); and Meadowbank Dam (Tasmania) described by Maddox, Kinstler & Mather (1967).

In all three cases the foundation rocks consisted of interbedded argillaceous and arenaceous sediments. In at least the former two cases the series had been subjected to fairly intense folding thereby causing flexural slip at the interface of the mudstones or shales with the sandstones. Along the mudstone boundaries then, shear zones had developed reducing the strength of the argillaceous material to or near to the residual. At the Muda site intense shearing and subsequent weathering had sometimes produced a thin layer, ½ inch to 1 inch thick, of soft clayey gouge against the sandstone interface. Properties obtained on this site were as follows.

| | |
|---|---|
| Weathered Mudstone: Peak Strengths (applicable only in unsheared mudstone, often towards the middle of each mudstone layer) | $\phi' = 26\text{-}27^{o}$ <br> $c' = 2\text{-}10$ psi |
| Weathered Mudstone: Residual Strengths (applicable towards the boundaries of each mudstone layer) | $\phi'_r = 18\text{-}20^{o}$ <br> $c'_r = 0$ approx |

The effects on the design of engineering structures associated with such conditions is obvious.

To take the lesson of these examples a step further, it is the author's opinion that any alternating sedimentary series should be treated with caution and examined for the presence of slickensides or other unusual characteristics at the various interfaces, whether differential movement of the rocks appears to have occurred or not.

The recent small slip in Kemp Place, Brisbane, occurred in a cutting through the moderately hard rock series of the Brisbane Tuff, which overlies the Brisbane Phyllites. The upper boundary of the Phyllite series is known to be weathered and the slip took place along the junction, which at this point dipped into the cutting at around $20^{o}$ to $30^{o}$. Inspection of the material at the interface, in the vicinity of the slip, revealed it to be highly clayey, (L.L. = 40% P.L. = 25%), with an abundance of slickensides and larger undulatory shear zones present. Multiple reversal shear box tests gave a value of $\phi'_r = 17^{o}$ for the residual strength of this interface material, that is, the strength likely to obtain along this plane of weakness which, as mentioned before, exists in an otherwise moderately hard rock cutting.

A relatively large degree of folding and subsequent flexural slip has occurred in these formations since deposition, which is again no doubt the reason for the presence of this degraded interface between the two rock types.

Finally, the presence of minor shear zones has been noted in clays which have remained largely undisturbed in their history, i.e. clays subjected to little or no tectonic activity. Tchalenko (1968) describes the presence of shear zones at depth in the London Clay; shears which, in themselves, bear all the characteristics of those resulting from landslips. Tchalenko also notes that these shears have developed when the clay has been fairly well consolidated, thus tending to discount the possibility of synaerisis. These discontinuities may have been the result of unequal straining either during latter stage consolidation or, more likely, during the stress release of the erosion cycle since the clay at the location where the shears were found has undergone very little movement during its history.

Hence it seems likely that shear zones within argillaceous sediments may be relatively common, ( for reason other than past landslip movements), while any alternating sedimentary series, unless completely undisturbed, should be regarded as potentially weak along lithological boundaries. Dessication shears have been documented, as well, Stapledon (1970).

## IV.- MINERALOGICAL EFFECTS

The presence of lithological alternations, e.g. layers of shale within a largely sandstone series, poses relatively straightforward problems in most cases. Less easily recognisable, however, are alternations of a mineralogical nature within a formation which appears to be homogeneous, e.g. thin montmorillonite seams in a clay-shale formation. The problem is rendered more difficult again since investigations into clay formations, in general, will be directed mainly towards the characteristic formation properties necessary for, say, deformation problems, whereas in stability problems it is likely to be the untypical characteristics which control the behaviour.

In most clay formations it is the presence of montmorillonite which appears to produce the major problems: high index properties, high swelling potential, low angle of shearing resistance, etc. The problem is not alleviated where the montmorillonite occurs in localised seams, especially in the realm of slope stability.

In Table No. I a number of formations are presented to illustrate what is believed to be the effect of montmorillonite seams. The table summarises a large number of landslips analysed by the author, James (1970), in which further references and information on the slips are available.

In the table only the parameters $\phi'$ and $\phi'_r$ have been quoted for simplicity. At residual conditions the parameter $c'_r$ may be taken as zero and while some effective cohesion will be acting at peak conditions, this will be variable and dependent on the age of the cutting, Skempton (1970). The values of $\phi'$ (peak) are nevertheless well documented and reasonably reliable.

It may be seen that where the occasional large discrepancy between laboratory and field exists, this is in the residual stage and* is known to contain localised seams of montmorillonite, e.g. the Lias and the Gault formations. The evidence is not conclusive in itself yet on engineering geological grounds, it provides sufficient indication to warrant detailed investigation in any major future works to determine whether montmorillonite is present at the site. Properties of bentonitic shales are given for comparison.

Other active clay minerals will have similar effects. An example of this is given in Table I.

* the formation

TABLE I

| Formation | Mineralogy | Applicable angle of shearing resistance ($\phi'$) | | | | Remarks |
|---|---|---|---|---|---|---|
| | | Peak $\phi'$ (degrees) | | Residual $\phi_r'$ (degrees) | | |
| | | Laboratory | Field | Laboratory | Field | |
| London Clay | Illite dominant, with kaolinite, vermiculite and occasionally montmorillonite. | 19 - 21 | 20 | 14 | 14 - 15 | Montmorillonite, when present appears to be disseminated in mass. May be absent altogether from the London area |
| Oxford Clay | Illite dominant, with kaolinite, lime secondary. Montmorill-onite generally absent from the areas studied. | 22 | 22? | 14 - 15 | 15 | |
| Lias Clay | Illite dominant, some lime content. Montmorillonite in Lower Lias occasionally. | 24 | 24 | 17 - 18 | 18 | One site in Lower Lias (Lyme Regis) gave a value of $\phi_r'$ (req) = $11^o$. |
| Gault Clay | Illite dominant, with kaolinite. Montmorillonite present and usually localised at certain levels, some lime content. | ? (high) | ? | 12 - 16 | 12 - 19 | Two slips at Folkestone-Warren (Hutchinson 1969) gave $\phi_r'$ (req) = $8^o$ |
| Bentontic Clays | Montmorillonite | ? | ? | 6 - 8 | Variable, usually 6 - $10^o$ range | |

(a) Maroon Dam Site

Maroon Dam is an earth-rockfill dam at present under construction in S.E. Queensland. The dam site is situated in a sedimentary series of mudstones and sandstones, of soft to moderate rock strength, gently dipping at a few degrees towards the valley on the right bank. During excavation of the culvert trenches along the stream bed the right bank of the valley became unstable, part of it moving forward several feet and consequently necessitating considerable regrading of the slope. The toe of the slip was readily visible, being confined to a distinctly weak bedding plane or zone approximately 1 foot wide in which slipping appeared to have occurred at two distinct horizons.

Figure No. 2 shows a cross section of the material of the landslip zone, with the relative properties of the various layers. The shear parameters were obtained in the direct shear apparatus. The zones containing slickensides may be seen to exhibit very much higher liquid and plastic limits, but unfortunately no mineralogical data is available.

The slip at this site is presumably wedge shaped, failing along this weak bedding plane. An analysis by the I.W.S. (personal communication) gave substantially the same value of $\phi'$ required ($16^o$) for stability as indicated by laboratory shear box tests. It also appears possible that the site has undergone a previous slip at some stage - one which has involved the whole right bank of the valley, since slickensiding was observed by the author within the same weak layer at locations outside the present extent of the slip.

| Scale | | DESCRIPTION OF STRATA | PROPERTIES | | | | | REMARKS |
|---|---|---|---|---|---|---|---|---|
| | | | L.L. | P.L. | P.I. | $\phi'_{peak}$ | $\phi'_R$ | |
| 1' 0" | 1 | Brown Mudstone jointed, fairly massive. | | NON PLASTIC | - | — | — | Strata 1 & 6 are similar |
| | 2(a) / 2(b) | Grey / Black } Laminated Shaley Clay | 89 | 25 | 64 | — | — | |
| | 3 | White & Brown soft Mudstone, (Slickensided) | 124 | 41 | 83 | 22°? | 14-18° | Variable test results |
| 2' 0" | 4 shear planes | Black / Grey } Shaley Clay | 95<br>94 | 38<br>26 | 57<br>68 | 18° | 14-15° | Tests on Shear Planes |
| | 5 | Grey & Brown Mudstone Not Slickensided | 66 | 21 | 45 | — | — | Similar appearance to stratum 3 |
| 3' 0" | 6 | Brown Mudstone | NON-PLASTIC | | | — | — | |

Fig.2. Slip zone at Maroon Dam

## V.- DISCUSSION

The problem therefore arises in determining the presence of structures described above, or in predicting the presence of seams of different (deleterious) mineralogy in a clay formation. Such a procedure, or an attempt at it, should preferably be made in the site investigation stage of any project. Unfortunately in a number of cases conventional drilling techniques have not provided the necessary core recovery in soft or slickensided shales or clays within a harder formation to give a true picture of subsurface conditions. The presence of such layers then becomes known only later, and usually through some semi-catastrophic event. Conversely, it would be equally uneconomical to design a slope, say, on the assumption that a weak layer may be present in a formation without specific confirmation of this by the site investigation.

A multi-stage approach for major works appears necessary. Firstly, a thorough engineering geological appraisal of the project which, in addition to the conventional aspects, should also include index properties of fault gouges, shear strength parameters along discontinuities, and perhaps a preliminary analysis of the mechanics of the structure/subsurface interaction. (This appraisal will often be extended to run concurrently with the excavation phase.) Secondly, drilling or boring techniques should be maintained at the highest standards for all engineering investigations to provide good continuous samples, if not in all drill holes, then in a selected number. This would be of particular importance in alternating sedimentary series. Finally, trial pits or adits should be excavated for detailed mapping of the accessible sub-strata and the findings be scrutinised by both the engineering geologist responsible and the design engineers.

## VI.- ACKNOWLEDGEMENTS

The majority of the work on which this paper is based was carried out while the author was a research assistant at Imperial College, London. In this country the author wishes to acknowledge Messrs Coffey & Hollingsworth, Consulting Engineers, with whom inspection of the Kemp Place landslide was made, and the Irrigation and Water Supply Commission for allowing the sampling, testing and publication of the information at Maroon Dam.

## VII.- REFERENCES

Bishop, A.W., Webb, D.L., Lewin, P.I. (1965) Undisturbed samples of London Clay from the Ashford Common Shaft:Strength-effective stress relationships. Geotechnique XV:1:1-31.

Clarke, C.L., James, P.M., Morgenstern, N.R. (1970) Foundation Conditions at Muda Dam. 2nd Int. Congress Rock Mechanics, Belgrade, September 1970.

Fookes, P.G. & Wilson, D.D. (1966) The geometry of discontinuities and slope failures in Siwalik Clay. Geotechnique 17:4:305-320.

Hutchinson, F.N. (1969) A reconsideration of the coastal landslides at Folkestone-Warren, Kent, in terms of effective stress. Geotechnique 19:1:6-38.

James, P.M. (1970) Time effects and progressive failure in clay slopes. Ph.D. Thesis, University of London.

Maddox, J.M., Kinstler, F.L., Mather, R.P. (1967). Foundation studies for Meadowbank buttress dam. Trans 9th Int. Cong. Large Dams Vol 1, 123-142.

Skempton, A.W. (1966) Some observations on tectonic shear zones. 1st Congress Rock Mechanics, Lisbon, Vol I p329-335.

Skempton, A.W. & Petley, D.J. (1967) The strength along structural discontinuities in stiff clays. Proceeds Geotech. Conf. Oslo; Vol 2, p3-20.

Skempton, A.W. (1970) First time slides in over-consolidated clays. Geotechnique XX:3:320-324.

Stapledon, D.H. (1970) Changes and Structural defects developed in some South Australian Clays, and their engineering consequences. I.E.A., Symposium of Soil and Earth Structures in Arid Climates. Adelaide May 1970.

Taylor, R.G. and James, P.M. (1967) Geotechnical aspects of the Muda Irrigation Project. Proc. 1st S.E. Asian Conf. Soil Eng. (Bankok) 33-42.

Tchalenko, J.S. (1967) The influence of shear and consolidation on the microscopic structure of some clays. Ph.D. Thesis, Univ. of London.

# An Investigation of Moisture Changes and Soil Structure in Earth Dams

By
M. S. Kotowicz, M.E.
(Design Engineer, Snowy Mountains Hydro-Electric Authority)
AND
S. N. Kiek, M.S., M.I.E.Aust.
(Engineer, Snowy Mountains Hydro-Electric Authority)

SUMMARY.- The results of field and laboratory work during construction of several earth and rockfill dams are presented to demonstrate that optimum moisture content is not constant under uniform compaction but varies with the initial moisture content of the soil before the compaction test. Furthermore, moisture content itself in sealed storage is not absolutely constant. The validity of the standard compaction test as a determinant of certain soil properties is considered.

## I.- INTRODUCTION

In the construction of earth dams optimum moisture content (OMC) is an accepted value governing soil placement moisture limits. It is also used during the materials investigations to determine the moulding moistures for testing.

In research into engineering behaviour and structure of soils, moisture contents are frequently reported in relation to OMC. In some cases, OMC is quoted as being the moisture which governs the behaviour of compacted soils and thus marks a boundary between soil structures. Reference is made to works of Aitchison et al (Ref. 1), Leonards and Narain (Ref. 2), Clegg and Paul (Ref. 3), Lambe (Ref. 4 and 5) and Seed and Chan (Ref. 6) and others.

Most workers, with given soil, compaction and water, assume OMC constant. It will be demonstrated here that such an assumption is invalid. In small earth structures the changes may not be significant and probably escape unnoticed. On large dams, for instance, accurate pore pressure prediction is of considerable economic value and thorough knowledge of all factors affecting it is necessary.

## II.- FIELD EXPERIENCE

On various dams of the Snowy Mountains Hydro-electric Authority involving detailed soil investigation and stringent construction control, it has been found that discrepancies existed between the values of soil properties recorded during and immediately after placement and those measured later in the laboratory. In particular, differences were noted in the values of OMC and the soil moisture content. Whilst the latter changes were attributed, at the time, to either drying of soil samples during storage or to ingress of moisture during handling in a humid room, no satisfactory reasons were found to explain the apparent changes in OMC. The matter was not pursued in depth as long as the changes, though mathematically significant, had no known effect on the engineering properties of soils in the embankment. On some projects it was found, however, that the changes caused considerable pore pressure variations necessitating, in some cases, a complete review of the placement moisture content.

During construction of Jindabyne Dam the behaviour of compacted core departed markedly from that anticipated. The pore pressures were much lower than expected. In fact, instead of positive pressures expected from the placement moisture content, large negative pressures developed and suction values of up to 2.8 pF were measured. Comparison of field and laboratory results showed that after several weeks storage of soil samples from the embankment the measured OMC increased by approximately 2.5 per cent. This increase indicated that the actual placement moisture content which, as is usual in dam construction was related to OMC, could have been too low. Empirical calculations suggested uniform increase of placement moisture content to bring the pore pressures to the desired level. This was done and positive pore pressures quickly developed and reached the predicted values. No cause of the phenomena was suggested at the time.

During construction of Talbingo Dam the pore pressures in the earth core were considerably higher than anticipated. After an extensive series of checks of all placement and testing procedures which ruled out some simple reason for the excess pore pressure, it was found that there was an apparent difference of about 1.5 per cent between the OMC determined under field conditions and that measured later in the laboratory on soil samples from the embankment. The field OMC appeared to be always higher than the laboratory one. A flat decrease of placement moisture content was applied and the pore pressures were reduced.

## III.- INVESTIGATION AT BLOWERING

### (a) Procedure

During construction of Blowering Dam a relatively large scale field investigation of factors affecting compaction test results was carried out. A testing programme was set out to establish the effects of a different initial moisture content and the length of curing time on compaction results. In addition, the influence of maximum particle size

was studied. The soil was taken from the impervious core of the dam after compaction by an average of eight passes of a heavy sheepsfoot roller. Thus it was ensured that breakdown of soil particles would have already occurred before laboratory compaction tests. The soil was broken down by hand and passed through a 1 in BS sieve. The sample was then mixed and quartered until a final sample was obtained. The soil was divided into 100 lb subsamples and stored in plastic bags inside metal containers. Compaction tests were carried out under conditions of controlled temperature and humidity using a mechanical compactor to eliminate human error, as much as possible. Compaction was done by 25 blows of a 5.5 lb hammer falling 18 inches on three layers of soil in a 1/20 cubic foot mould. Testing was performed using soil at different initial moisture contents. In one series of tests, moisture was introduced into the soil in carefully measured increments, normally at actual moisture content plus two, four and six per cent. Testing was then done after varying periods of curing ranging from one hour to several weeks. Another portion of the soil was first dried out on electric dryers and then conditioned by adding measured amounts of water. Varying periods of curing were again allowed. In all, over 1,000 tests were carried out with at least three repetitions at each initial moisture content and curing time. Moisture contents were determined using the whole of each compacted specimen subdivided into three subsamples of approximately 2 lb each, and the dry density of soil determined. Classification tests were performed for each 100 lb subsample.

(b) Results

The average results of all classification tests are shown on Table I. The compaction test results, in simplified form, are shown on Figure 1. At least five points were used for each OMC-maximum dry density determination as well as results from the three point rapid method (Ref. 7). Whilst the maximum particle size had a significant effect on compaction results, only the corrected resultant variations of OMC are shown here. It can be seen that OMC changed with change in initial moisture content. The upper limit, however, was not conclusively established because the apparent levelling of the curve could be partly attributed to errors arising from testing soil with an excess of water. The observed change of OMC was most marked after curing time of up to about 24 hours. The soils cured for longer periods showed lesser OMC movement but still significant enough to affect the behaviour of an earth core. The time dependent OMC changes were studied further and, after analysis, it was concluded that the actual moisture content (w) of soil also changed during curing. In general, the moisture content remained relatively constant after conditioning for a period of about 24 hours. During longer curing the moisture content became progressively less. The change was most marked within a certain overall range of initial moisture content. Below and above this range the moisture changes diminished (Fig. 2).

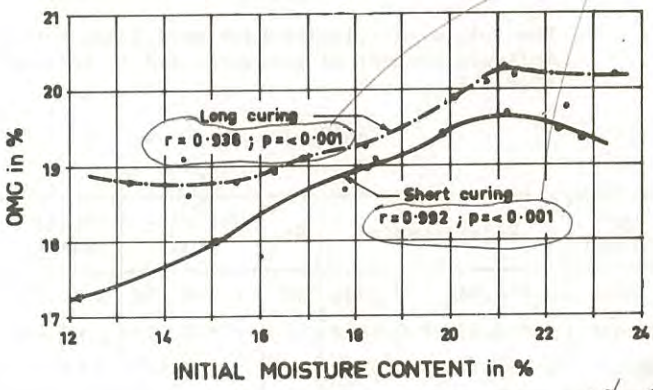


Figure 1

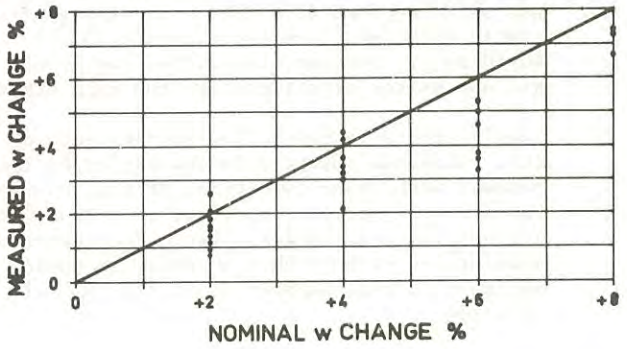


Figure 2

TABLE I

CLASSIFICATION TEST RESULTS

| $W_L$ | $W_P$ | $I_P$ | LS* | G | PERCENTAGES PASSING BS SIEVE | | | | | | | | | | CLAY |
|---|---|---|---|---|---|---|---|---|---|---|---|---|---|---|---|
| | | | | | 1" | 3/4" | 3/8" | 3/16" | 7 | 14 | 25 | 52 | 100 | 200 | |
| 45 | 23 | 22 | 8 | 2.75 | 100 | 99 | 96 | 90 | 89 | 80 | 74 | 68 | 62 | 55 | 30 |

* LS = LINEAR SHRINKAGE

## IV.- INVESTIGATION AT TALBINGO

(a) Procedure

During the construction of Talbingo Dam an investigation was made of moisture content and OMC movement during storage of soil in airtight containers. One hundred and ten samples were taken. Moisture content and OMC were determined during placement and after varying time intervals. Moisture contents on sampling and testing were compared. In moisture content subsampling losses were inevitably associated with the removal of the rock fraction. These were evaluated by specially controlled tests on 17 samples. A study was also made of changes in OMC using 24 of the 110 samples mentioned above.

(b) Results

The following relationships were found between moisture content of placement and at testing (Table II):

TABLE II

| Age (days) | Relationship | No. | Correlation | Significance |
|---|---|---|---|---|
| 0-40 | $y = 4.960 + 0.590x$ | 58 | $r = 0.718$ | $p < 0.001$ |
| 40-80 | $y = 3.632 + 0.666x$ | 22 | $r = 0.639$ | $p < 0.001$ |
| 80 + | $y = 5.143 + 0.628x$ | 30 | $r = 0.570$ | $p < 0.001$ |

where y = moisture content at testing and x = moisture content at placement. The relationship for samples aged more than 80 days was shown by Student's t test to be significantly different from those aged 0-40 and 40-80 days. However, the latter two groups did not differ significantly from each other.

The 17 specially controlled samples showed that, although moisture losses caused by rock removal were about two-thirds of the observed variation in moisture content, they could not account for the changes alone. Furthermore, similar losses must have occurred in taking moisture content subsamples at the time of sampling.

The relationship between OMC at the time of placement and OMC tested after storage in the laboratory (y and x respectively) was:

$y=1.740+0.833x \quad r=0.939 \quad p < 0.001....(1)$

Furthermore, there was an association with the difference between OMC and moisture content at placement, and the change in OMC during storage. Relationships for samples wet of OMC differed from those dry (Table III):

where y = increase in OMC during storage and x = difference between moisture content and OMC at the time of placement. There was no relationship for samples within 0.5 per cent of OMC.

TABLE III

| Relation to OMC | Relationship | No. | Correlation | Significance |
|---|---|---|---|---|
| Over 5% Dry | $y = 1.090x - 2.262$ | 7 | $r = 0.854$ | $p < 0.01$ |
| Over 5% Wet | $y = 0.535x - 1.012$ | 34 | $r = 0.722$ | $p < 0.001$ |

## V.- SPECIAL INVESTIGATION

(a) General

As each layer of soil was placed at four selected sites at Talbingo Dam, quadruplicate samples were taken in airtight jars. The places were marked with plastic markers. Sampling was repeated for each layer through a rise of about 5 feet. Sampling times were recorded. Afterwards excavations were made and a corresponding series of samples taken from the same places. Embedment varied from 1½ hours to several weeks. The fourth site was in finer plastic soil. A fifth site was selected for soil structure studies. Only one level was sampled but undisturbed samples were taken.

(b) Moisture Content

Moisture content changes, other than those within experimental error, were in the same direction in the embankment as in storage. Changes in the embankment always exceed those in storage. These remarks apply equally to 105°C and 200°C moisture contents.

For 38 routine control samples from Talbingo, 105°C and 200°C moisture contents were very significantly related:

$y=1.84+0.978x \quad r=0.892 \quad p < 0.001....(2)$

where y = 200°C and x = 105°C moisture content.

For 70 specially controlled samples from the special investigation, changes in 105° and 200°C moisture contents were very significantly related:

$y=0.781x-0.173 \quad r=0.758 \quad p < 0.001...(3)$

where y = 200°C and x = 105°C moisture content changes during storage.

The change in 105°C moisture content was very highly significantly related to "adsorbed" (105°C-200°C) moisture for 69 points:

$y=1.552-0.504x \quad r=0.628 \quad p < 0.001...(4)$

where y = adsorbed moisture, x = 105°C moisture content change on storage.

Soils stored after a period of embedment behave in the same way during storage as those sampled immediately on placement.

For the specially controlled samples there was a significant relationship between the change in 105°C moisture content and time of embedment. This did not apply to longer periods than 75 hours.

(c) Differential Thermal Analyses

Differential thermal analyses (DTA) were made to check that adsorbed moisture was driven off at 200°C. The DTA showed that there was a significant loss of material between 105°C and 200°C. This material was collected and shown to be water.

(d) Exchangeable Sodium Percentage

A relationship was considered (Ref. 1) between exchangeable sodium percentage (ESP), soil moisture electrolyte concentration and soil structure. Some adsorbed cations and soluble salts determinations were made so that structural changes could be investigated.

Changes in ESP after embedment were slight and random. Electrolyte concentration of soil moisture had more variation but did not show a recognisable trend. Results did not indicate structural change.

(e) Specific Surface

Specific surfaces of soil crumbs passing No.7 BS sieve were determined to ascertain whether structural changes could be detected this way but embedment did not produce any recognisable trend.

(f) Base Exchange

For Site 4 samples, base exchange capacity was found. It was highly significantly related to moisture content change on storage. The correlation was sufficiently close to enable moisture content change to be estimated from base exchange capacity. The relationship was:

$$y=0.0600x-0.98 \quad r=0.8 \quad p < 0.001 \ldots\ldots (5)$$

where y = % moisture change at 105°C,
x = base exchange capacity in milliequivalents per 100 grams.

However, all the soils were from one place, and only eight results were available from which to compute the relationship.

(g) Microscopy

Slides were made from the two undisturbed samples from Site 5 by the method used in CSIRO (Ref. 8). These were used both for optical and electron microscopy. Optical examinations revealed nothing of soil structure, but electron micrographs of cracks in the slides permitted examination in depth. Maximum magnification was 2000. Stereoscopic pairs showed conclusively that no structural change had occurred during 45 hours embedment. This agrees with the observations of other workers (Ref. 9,10).

Moisture changed by 0.9 per cent.

## VI.- DISCUSSION

(a) Moisture Interchange

Whatley (Ref. 11) after considerable investigation, demonstrated also that both moisture content and OMC are not constant during storage. He believed that changes in both moisture content and OMC resulted from changes from flocculated to deflocculated soil structure. This, he considered, caused interchange between adsorbed and free moisture, the former being that driven off between 105°C and 200°C. The results (equations 2, 3 and 4) demonstrated that no such interchange occurred as increases in 105°C moisture content were matched by equivalent increases in 200°C moisture content.

(b) Movement Toward Equilibrium

Since no structural change had been found, consideration was given to the concept of an equilibrium moisture content related to the Thornthwaite Climatic Index (Ref. 12). It appeared possible that the soil moisture content could tend toward such an equilibrium and thus explain the observed moisture movements. Unfortunately, the necessary climatic data for computing the Index were not available at the site.

(c) Source of Adsorbed Moisture

From the adsorbed cations tests, using published figures for ionic and hydration shell radii (Ref. 13), the amount of hydration shell moisture was computed. The published radii are based on transport experiments and are not a direct measure of the dimensions at rest. Clay thixotropy and some published work (Ref. 14) suggest that shells may slide over each other more readily in rapid motion. Dimensions could be greater at rest. If computed hydration moisture is plotted against adsorbed moisture for Sites 1, 2 and 3, all points lie close to a line whose slope is 1 : 5. This would be explained if hydration shells have five times the volume at rest as in transport. The relation certainly suggests that hydration shell moisture is associated with 105°-200°C moisture.

Soils from Site 4 did not conform. These contained abundant expanding lattice clay. Adsorbed moisture there was less than the relationship would suggest. The deficiency was related to base exchange capacity, which was highly significant. The base exchange capacity could reflect the proportion of expansive clay, in which case the interlayer hydration water may be removed at 105°C, whereas other hydration water may not.

## VII.- CONCLUSIONS

From the foregoing results it may be concluded that OMC of soil tested under uniform compactive effort changes with the initial moisture content. The magnitude of the change is greatest within a

certain initial moisture range and also dependent, to a degree, on curing time. Accompanying changes of the actual soil moisture content during curing were also observed.

The implication of these findings is considered to be of practical importance for the design and construction of projects where a small change of placement moisture content, even of the order of one half of a per cent could have serious economic and engineering repercussions.

The present work was carried out by Snowy Mountains Authority, an organisation which does not carry out fundamental research but undertakes investigations only to a point required by current construction needs. Thus, although the reasons for the observed changes remain unknown, from the available results it appears that changes of OMC are not caused by structural rearrangement and consequent transfer between adsorbed and free moisture. The possibility of movement toward equilibrium is worthy of further investigation.

With more frequent construction of high earth structures, testing procedures must be constantly updated to keep pace with more refined design requirements. It appears that the standard compaction test, which for decades has remained basically unchanged in concept, may now require a review. In the meantime, construction of trial embankments during investigation, where the design and the size of a project warrants it, remains as the only means of accurate assessment of soil properties.

VIII.- ACKNOWLEDGMENTS

The authors wish to acknowledge assistance received as follows:

- Mr R. ATTRIDGE for carrying out most of the work at Blowering.
- Mr J.I. HILTON for valuable suggestions during the course of the work and for review of this paper.
- Maj. N.J. WHATLEY, Royal Engineers, who conducted the initial phases of the work at Talbingo.
- Dr B. FILSHIE, CSIRO Division of Entomology, who made the electron micrographs.
- Dr D.F. LAFEBER for advice and help with the technique of soil slide preparation.
- The SNOWY MOUNTAINS HYDRO-ELECTRIC AUTHORITY for permission to publish this work. The opinions expressed here, however, are those of the authors and not necessarily those of the Authority.

REFERENCES

1. AITCHESON, D.G., INGLIS, O.G. and WOOD, C.C. "Post Construction Deflocculation as a Contributory Cause in the Failure of Earth Dams" Proc. 4th A.N.Z. Conf. Soil Mech. and Found. Eng. 1963.
2. LEONARDS, G.A. and NARAIN, J. "Flexibility of Clay and Cracking of Earth Dams" Jour. Soil Mech. and Found. Div. Proc. ASCE 1963.
3. CLEGG, B. and PAUL, M.J. "The Effect of Compaction Method on Pore Pressure in Laboratory Test Specimens" Proc. 5th A.N.Z. Conf. Soil Mech. and Found. Eng. 1967.
4. LAMBE, T.W. "The Structure of Compacted Clay" Jour. Soil Mech. and Found. Div. Proc. ASCE 1958.
5. LAMBE, T.W. "The Engineering Behaviour of Compacted Clay" Jour. Soil Mech. and Found. Div. Proc. ASCE 1958.
6. SEED, H.B. and CHAN, C.K. "Compacted Clays, A Symposium. Structure and Strength Characteristics" Proc. ASCE 1961.
7. HILF, J.W. "A Rapid Method of Construction Control for Embankments and Cohesive Soils" USBR Eng. Monograph No. 26 1959.
8. WALSH, J.D. and HOLLINGSWORTH, Judith "Sampling and Preparation of Natural Soils for Quantitative Three Dimensional Analysis" CSIRO Soil Mech. Div. Tech. Rep. No. 7 1968.
9. BARDEN, L. and SIDES, G.R. "Engineering Behaviour and Structure of Compacted Clays" Jour. Soil Mech. and Found. Eng. Proc. ASCE 1970.
10. BARDEN, L., SIDES, G.R. and KARUNARATNA, J.P. "A Microscopic Examination of Aspects of Clay Structure" Proc. S.E. Asia Conf. Soil Mech. and Found. Eng. Singapore 1970.
11. WHATLEY, N.J. "Report on High Pore Pressures at Talbingo Dam" SMHEA Cooma 1969.
12. RICHARDS, B.G., MURPHY, H.W., CHAN, C.Y.L. and GORDON, R. "Preliminary Observations on Soil Moisture and Dry Compaction in Pavement Design on the Darling Downs" 5th Conf. Aust. Road Research Board Canberra 1970.
13. BOCKRIS, J.O'M. and CONWAY, B.E. "Modern Aspects of Electrochemistry", Butterworth, London 1954.
14. NICOL, S.K. and HUNTER, R.J. "Some Rheological and Electrokinetic Properties of Kaolinite Suspensions" Aust. Jour. Chem., CSIRO Melbourne 1970.

# Fabric Symmetry and Mechanical Anisotropy in Natural Soils

By

D. Lafeber, D.Sc.

(Assistant Chief, Division of Applied Geomechanics, C.S.I.R.O.)

AND

D. R. Willoughby, B.Sc.

(Experimental Officer, Division of Applied Geomechanics, C.S.I.R.O.)

SUMMARY.- Current opinion in soil mechanics considers mechanical anisotropy of natural soils as being primarily due to gravitational compaction and consolidation, and practically ignores all other patterns of anisotropy. This type of anisotropy ('cross-anisotropy') is characterized by a vertical n-fold axis of symmetry ($n = \infty$), and, consequently, a horizontal plane of isotropy. The present paper accepts the process of natural compaction and consolidation, but emphasizes that this process may be *preceded* by one or other depositional process possessing only a single vertical plane of symmetry. This single plane contains the usually near-horizontal transport direction of the depositional process involved, and is indicative of a much lower order of symmetry, namely monoclinic symmetry.

Fabric analyses and mechanical (triaxial) testing have been performed on several dozens of oriented undisturbed specimens of two commonly occurring soils (a recent beach sand, and a residual silty clay of uniform composition). The results of these studies indicate that both soils *lack* a vertical n-fold axis of symmetry ($n = \infty$) in their original, pre-testing geometrical fabric. They exhibit only a single vertical plane of symmetry, i.e. monoclinic symmetry, as a result of the geological process involved. It is further demonstrated that a vertical n-fold axis of symmetry ($n = \infty$) is *absent* in the two soils as far as such mechanical properties as the secant modulus are concerned. It is finally shown that the presently hypothetical symmetry elements of the secant modulus distribution pattern can be related in a simple and logical manner to those of the original, pre-testing geometrical fabric, and these in turn to the major terrain features such as the direction of the coastline, or the orientation of the terrain slope.

On the basis of these results it is suggested that current ideas on the frequency of occurrence of cross-anisotropy in natural soils need to be reviewed.

## I.- INTRODUCTION

The need for a systematic study of the relationships between natural soil fabric or structure and soil mechanical properties has already been foreshadowed in Terzaghi's classical 'Erdbaumechanik' (Ref. 1). One of the major obstacles, however, in the development of a real engineering soil fabric analysis has been the fact that, particularly in soil mechanics, it has not been fully appreciated that many natural depositional processes are characterized by a directed, *horizontal movement* or *transportation component*. In nearly all anisotropy studies carried out by soils engineers, e.g. Bishop (Ref.2), and many others, the view has been adopted that soil anisotropy is primarily due to *gravitationally controlled consolidation and compaction*, and consequently characterized by the presence of a horizontal plane of isotropy and a vertical n-fold axis of symmetry ($n = \infty$).

In the present paper fabric and mechanical properties of undisturbed samples of two common types of soil will be described and their mutual relationship discussed. The two soils, although of Australian origin, have been chosen in such manner that they are comparable or similar to soils that are of common occurrence in many other parts of the world. It will be shown that in the two soils a horizontal plane of isotropy (or a vertical n-fold axis of symmetry, $n = \infty$) is *absent* as far as the fabric or the mechanical properties are concerned.

The fabric analysis techniques referred to in this paper are those developed by the senior author and his co-workers (Lafeber, Ref. 3, 4 and 5; Willoughby, Ref. 6; Walsh and Hollingsworth, Ref. 7; Willoughby and Walsh, Ref. 8). The mechanical testing techniques used are standard procedures, except where mentioned otherwise in the text.

## II.-SOIL FABRIC CHARACTERISTICS

The first of the soils selected for this study is a *recent beach sand* from near Portsea, Victoria. The second soil is a red-coloured, Fe-rich, *silty clay soil* (krasnozem) from near Silvan, Victoria.

In contrast to common practice in many soil mechanics fabric studies, the relevant fabric or structural criterion in the present paper will *not* be the clay platelet or domain arrangement in the soil. The reasons for this approach are twofold:

(a) The beach sand does not contain any clay size-fraction at all.

(b) The major fabric characteristics of a natural soil are not necessarily or even generally expressed in the clay fabric only (Ref. 3, 5, 9, 10, 11 and 12), but also are usually

reflected in the arrangement patterns of the *other* major soil components. Often they can be determined more conveniently in the latter.

For the beach sand, therefore, the preferred orientation of the skeleton grains is the only 'micro' criterion that can be used to define the fabric (Ref. 3 and 13). In the krasnozem soil, although there is a small percentage of the clay material showing preferred orientation (associated with the planar pore pattern), the three-dimensional arrangement of the planar pores (Ref. 3) will be used as a criterion to define the fabric.

(a) Fabric Criteria of Portsea Beach Sand

The particular material is a fine to medium-grained, rather well-sorted beach sand with an average grain diameter of approximately 0.5 mm (Fig. 1). The major constituent is quartz with smaller amounts of rock fragments, a few well-worn shell fragments, and possibly a very minor quantity of other organic material (Fig. 2). The majority of grains is subangular to subrounded, and in thin-sections a substantial percentage of elongated grain cross-sections can be observed.

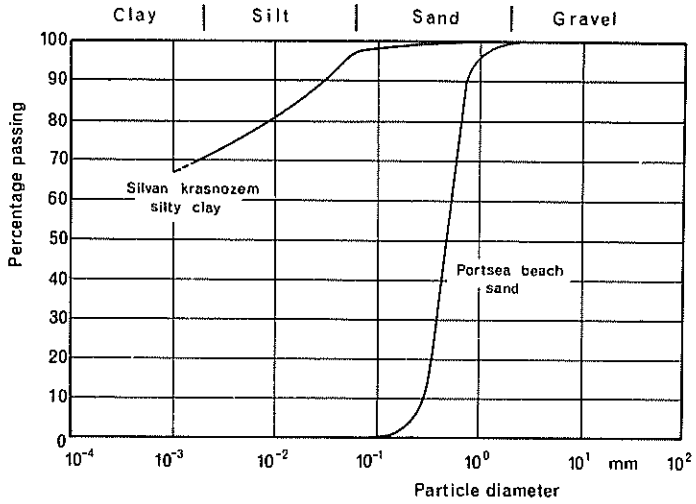


Fig. 1.- Grain size distribution of Portsea beach sand and Silvan krasnozem silty clay

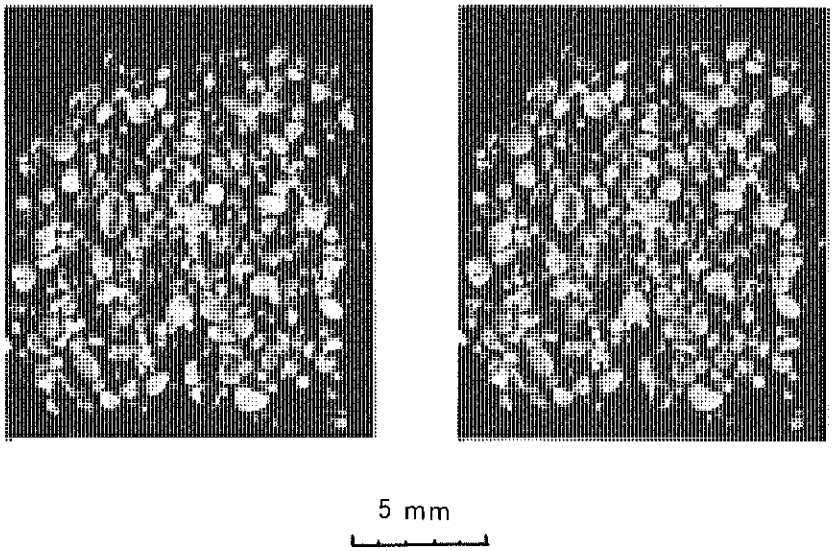


Fig. 2.- Stereopair of Portsea beach sand grains, showing their composition, shape, and roundness. Ordinary reflected light

In undisturbed vertical cross-sections through the deposit a distinct *bedding* can usually be seen, dipping seaward at an angle of about 5 degrees. Closer inspection indicates that relatively small differences in average grain size, and possibly also small variations in the amount of darker coloured grains are responsible for the bedding (Fig. 3). A number of vertically and horizontally oriented thin-sections has been prepared from undisturbed specimens with known orientation (one series of sections vertical and parallel to the coastline, another series vertical but perpendicular to the coastline, and the third series horizontal). In each of these thin-sections the orientation of the long axes of elongated grain cross-sections has been measured for several hundreds of grains. The results are shown in Fig. 4, and indicate a distinct, preferred orientation of the long axes in all three instances. The simplest interpretation of the diagram is that in the particular beach sand a substantial number of more or less platy grains, i.e. grains in which the two longest of the three geometrical axes are of approximately the same magnitude, are oriented in such manner that one of these long axes is parallel to the coastline, whereas the other dips *landward* at an angle of approximately 10 degrees. In other words, these grains show a very distinct *imbrication*. In other samples, however, a preferred grain orientation corresponding to the bedding plane has also been observed.

In conclusion, it can be stated that the major fabric characteristics of the particular beach sand are the bedding plane and the plane of imbrication. These two plane surfaces are oriented in such way that their intersection line is horizontal and parallel to the coastline. Since it cannot be assumed *a priori* that the two planes are of identical significance in regard to the mechanical behaviour of the undisturbed sand, the fabric pattern must be considered as having only one plane of symmetry, namely a vertical plane perpendicular to the coastline. This single symmetry plane, that also contains the transport direction in the depositional phase (Ref. 14, 15, and 16) is the characteristic feature of a *monoclinic* fabric.

It should be pointed out and emphasized at this stage, that the determination of the critical fabric

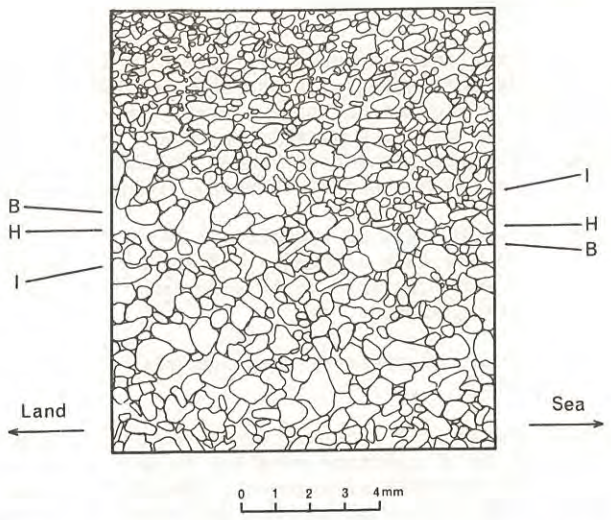


Fig. 3.- Vertical cross-section (perpendicular to the coastline) through undisturbed Portsea beach sand.
B = dip direction of bedding plane, H = horizontal plane, and I = dip direction of imbrication plane

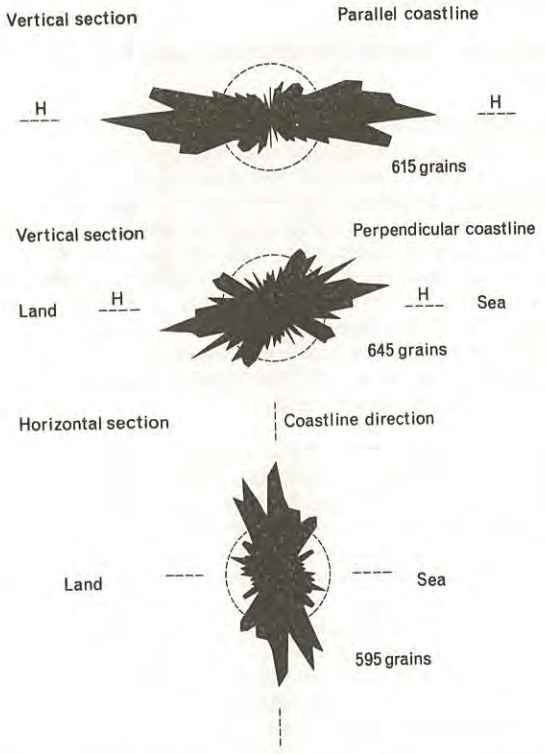


Fig. 4.- Preferred orientation of long axes of elongated sand grains in Portsea beach sand in differently oriented sections. The relative frequencies (%) of the long axes *versus* their orientation directions (5° intervals) have been plotted in polar co-ordinates. The broken circle (radius = 2.77%) represents a uniform distribution over all orientation directions. (Ref. 5)

features in many instances may not require the application of sophisticated research techniques, but can be based on an evaluation of purely geological factors instead (Ref. 13). In the present instance this would be only the bedding and the orientation of the coastline, where the strike of the bedding would be parallel to the coastline. In addition, the dip of the bedding is parallel to the transportation direction and to the vertical symmetry plane. Very obviously, *this common type of beach deposit does not show a vertical* n-fold *axis of symmetry* (n = ∞) in its geometrical or morphological fabric, nor a horizontal plane of isotropy.

(b) Fabric Criteria of Silvan Krasnozem Silty Clay

The krasnozem silty clay is a partly saturated, red-coloured soil with 10-20 per cent (by volume) of silt-sized skeleton grains (Fig. 1), largely consisting of quartz, and a non-swelling member of the chlorite-group as the major clay mineral. The particular soil is associated with and possibly derived from a moderately acid to intermediate volcanic rock (dacite), and occurs mostly in deep, rather homogeneous and uniform profiles, frequently in rolling to hilly country. This is also the case at the particular sampling site near Silvan, Victoria, where the terrain slope strikes N 29 E with a northwesterly dip of 5 degrees (both determined by theodolite measurement).

Planar pore analysis techniques (Ref. 3) have been applied to three oriented (fabric-wise) undisturbed samples of the soil collected at the particular site. The results, amounting to a total of nearly 700 planar pore poles, have been combined in the compound fabric diagram shown in Fig. 5. It will be seen in this figure that the position and distribution of the maxima and of the areas of high pole density are clearly asymmetrical in regard to the primitive circle (Ref. 17). There is a very distinct indication of a 'girdle-like' arrangement along the margin of the projection area, but the width of this girdle is substantially less in the north-western quadrant of the projection area than in the south-eastern quadrant. This characteristic suggests immediately:

(i) the girdle axis is *not* vertical, but tilted, and

(ii) the girdle shows a close geometrical relationship with the actual terrain slope at the sampling site.

The simplest and most logical assumption then is that the girdle axis is located in the vertical symmetry plane of the local terrain configuration, i.e. the vertical plane perpendicular to the strike of the terrain slope. This plane also contains the transportation direction associated with local hill creep.

The appropriate outer boundary of the 'best-fitting' girdle has been indicated in Fig. 5, and appears to be characterized by an axis tilting 5 degrees 'backwards' or 'uphill' (G in Fig. 5), and making, therefore, an angle of approximately 10 degrees with the pole of the terrain slope (D in Fig. 5). The figure demonstrates clearly that the bulk of the maxima and of the areas of high pole density is contained within the annular zone between the boundary curve and the primitive circle. Expressed in quantitative terms in regard to the original pole diagram, it appears that the girdle annulus contains 55.4 per cent of all the poles in the diagram, whereas for a uniform dis-

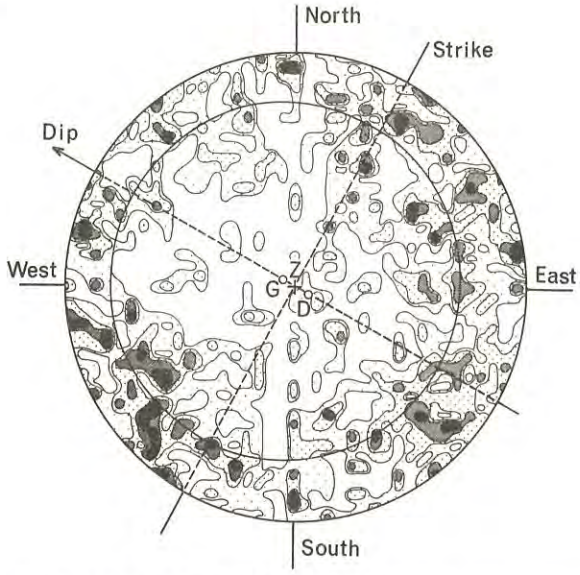


Fig. 5.- Preferred orientation of planar pores in Silvan krasnozem silty clay. Equal-area projection, horizontal projection plane, lower hemisphere. Composite diagram, 691 poles. Pole densities, 0, 1, 2, 3, and 4 or more (max.6) poles per unit area (=0.14%) of total area). Strike and dip are those of the terrain slope at the sampling site; D = pole of the terrain slope, G = pole of the tilted orientation girdle, Z = vertical co-ordinate axis.

tribution of poles over the whole projection area, the annular area would be expected to contain only 42.0 per cent of the poles. Formal application of the $\chi^2$ criterion (Ref. 18) indicates the difference between the two values (actually between the corresponding pole frequencies) to be statistically significant. The position of the girdle axis in the symmetry plane of the local terrain configuration obviously leads, as with the previously discussed Portsea beach sand, to a *monoclinic symmetry* of the whole system. This again means the *absence of a horizontal plane of isotropy or a vertical* n-fold *symmetry axis* ($n = \infty$).

As with the Portsea beach sand site it should be emphasized that an appreciation of the local topographical and geological conditions, i.e., orientation of the terrain slope, and a deep uniform soil profile, may eliminate the need for refined research techniques to determine the attitude of the relevant fabric symmetry elements: the presence and the orientation of the previously mentioned symmetry plane and the absence of a horizontal plane of isotropy may be predicted with near certainty on the basis of these macro-features.

It may finally be pointed out that the monoclinic symmetry is not very strongly expressed (the angle between the tilted girdle axis and the vertical is only 5 degrees!). This may well account for the observation, discussed later in this paper, that the discontinuity pattern developing in the samples after triaxial testing does not produce clear evidence for the presence of a monoclinic symmetry in the deformation process.

## III.-MECHANICAL ANISOTROPY

The initial purpose of the present investigation was to study the geometry of the deformation patterns and failure phenomena in the two previously mentioned types of soil. In view of this purpose, the triaxial testing arrangement has been chosen deliberately because of the 'high' initial symmetry, consisting of:

(i) a n-fold axis of symmetry ($n = \infty$) coinciding with the axis of the cylindrical test specimen and with the axis of loading in the triaxial testing machine, and

(ii) a plane of symmetry perpendicular to this axis.

Provided the soil is isotropic or 'cross-anisotropic' with the plane of isotropy parallel to the symmetry plane of the triaxial arrangement, the deformation patterns, the failure phenomena, and also the strength and elastic modulus patterns would be expected to show the same 'high' symmetry as the triaxial test itself. If, however, the soil is neither isotropic nor 'cross-anisotropic', one or more or all of these properties would be expected to show only those symmetry elements that are common to the triaxial testing arrangement and the soil. In the case of the two types of soil, discussed here, this would be *only the single* (vertical) *monoclinic symmetry plane*. It will be shown that this condition is indeed characteristic for the two soils examined.

### (a) Sampling, Sample Preparation, and Testing Procedures

In view of the original purpose of the investigation the sampling technique and sample preparation have been rather different for the two types of soil. The main problems relating to the loose, non-indurated beach sand are: to obtain undisturbed, oriented samples of the appropriate size and shape, and to place these in the undisturbed state in the triaxial apparatus, and to recover the loaded and eventually failed specimens from the apparatus in such a manner that the least possible disturbance occurs, and the specimens or parts of them can be studied more closely by means of thin-sections, etc.

These problems have been solved satisfactorily by developing a special technique (Ref. 8) that can be briefly described as field sampling in the fully saturated state, i.e. close to the waterline, followed by a two-stage total replacement of the original seawater in the specimens by polyethylene glycol ('Carbowax 4000'). The triaxial testing of the specimens is performed while, as a result of heating, the polyethylene glycol is completely molten. After completion of the testing procedure, the polyethylene glycol is allowed to solidify before the specimens are taken out of the testing apparatus. The same sampling and preparation techniques have been used for vertically and horizontally oriented samples. It may finally be noted that all triaxial tests on the beach sand samples have been carried out as *'drained'* tests and with standard ceramic endplates.

For the sampling of the krasnozem silty clay specimens, two different techniques have been used:

(i) all vertical specimens have been obtained by means of a three-inch auger core sampler, and

(ii) all horizontal specimens have been cut and shaped manually from oriented block samples.

Furthermore, the krasnozem specimens have been tested at field moisture content, and under *'undrained'* conditions. In a number of instances, low-friction, highly polished brass endplates have been used. In all other cases, however, these have been replaced by (high-friction) standard ceramic endplates.

(b) Test Results of Portsea Beach Sand

In the triaxial testing of the Portsea beach sand varying numbers, i.e. three or more, of specimens in each of a number of orientation groups have been used. One group consists of vertical cylindrical specimens, where the azimuth of the seaward direction has been marked on each individual specimen. Other groups consist of horizontal, cylindrical specimens enclosing angles of 0°, 30°, 60° and 90° respectively with the coastline, and where, in addition, the position of the bedding plane in each of the specimens is also known.

The most striking observations resulting from these tests are the following:

(i) the different but persistent failure patterns in the vertically oriented and in the horizontally oriented specimens,

(ii) the characteristic appearance of the stress-strain curves referring to all the tests on vertically and horizontally oriented specimens (unpublished data), and

(iii) the statistically significant differences in the magnitude of selected mechanical properties between vertically and horizontally oriented specimens.

In the present paper only the first and the last aspects will be discussed more thoroughly.

It appears now that almost all specimens show persistently* two inclined, intersecting, and practically plane failure surfaces. There are two specimens where there is only one plane failure surface, corresponding to either the one or the other failure plane in the other specimens. The difference between the vertical and horizontal cylinders, however, is due to the striking fact that these failure surfaces show consistently a completely different orientation with regard to the bedding and imbrication planes (Fig. 6). It will be noted that the intersection of the bedding and the imbrication planes is necessarily a horizontal straight line parallel to the coastline. In the group of horizontal cylinders perpendicular to the coastline the intersection of the two failure planes coincides with the intersection of the bedding and the imbrication planes, i.e. both lines of intersection are horizontal and parallel to the coastline. On the other hand, in the vertical cylinders and in the horizontal cylinders parallel to the coastline the intersection of the two failure planes is horizontal but *perpendicular* to the coastline. In all three instances, however, the presence of a single vertical symmetry plane, perpendicular to the coastline, is obvious. In other words, the deformation or failure pattern of the particular sand in the undisturbed or natural condition is also characterized by a *monoclinic symmetry, corresponding with the identical symmetry of the pre-testing geometrical fabric features.*

* It should be noted that to obtain this persistency in behaviour, a very careful sampling technique and a near-perfect polyethylene-glycol impregnation are required.

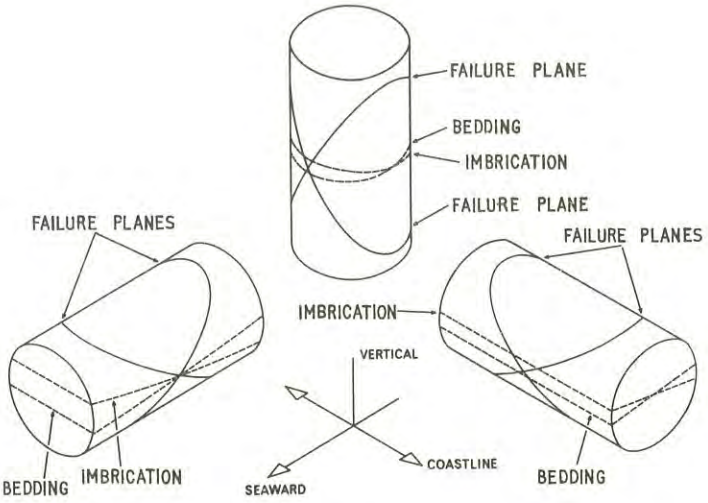


Fig. 6.- Perspective view of the failure pattern (schematically) in a vertical and two horizontal cylinders of undisturbed Portsea beach sand. Note that the bedding and imbrication planes in the three cylinders are oriented in the same manner. (Ref. 13)

The features just discussed are shown in stereographic projection in Fig. 7. In the diagram representing the vertical cylinders the intersection of the two failure planes is represented by the vertical diameter of the primitive circle, and the intersection of the bedding and the imbrication planes, as well as the coastline, are represented by the horizontal diameter. The same arrangement will be observed in the diagram representing the horizontal cylinders parallel to the coastline. In the diagram representing the horizontal cylinders perpendicular to the coastline the two intersections and the coastline are coincidental and represented by the horizontal diameter. Obviously the trace of the (vertical) symmetry plane is in all three instances given by the vertical circle diameter.

From the stress-strain data supplied by triaxial loading tests on vertical and horizontal cylinders the secant modulus has been determined in the conventional manner (Ref. 19). The mean secant moduli and their standard deviations for the five orientation groups are as follows.

1. Vertical cylinders; mean = $5.54 \times 10^2$ kg cm$^{-2}$, standard deviation = $\pm 0.28 \times 10^2$ kg cm$^{-2}$.
2. Horizontal cylinders, parallel with coastline; mean = $4.10 \times 10^2$ kg cm$^{-2}$, standard deviation = $\pm 0.24 \times 10^2$ kg cm$^{-2}$.
3. Horizontal cylinders, 30° with coastline; mean = $3.93 \times 10^2$ kg cm$^{-2}$, standard deviation = $\pm 0.18 \times 10^2$ kg cm$^{-2}$.
4. Horizontal cylinders, 60° with coastline; mean = $3.84 \times 10^2$ kg cm$^{-2}$,

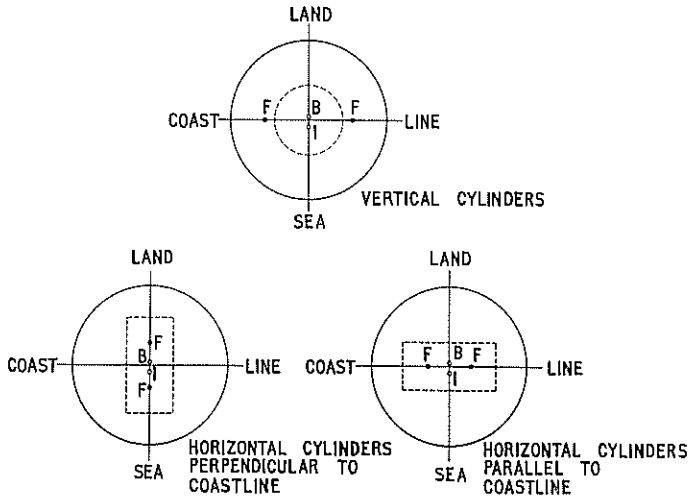


Fig. 7.- Failure planes in undisturbed Portsea beach sand specimens in stereographic projection. Horizontal projection plane, poles in lower hemisphere; F = failure planes, B = bedding plane, I = imbrication plane. The broken line figures indicate the orientation of the test cylinders. (Ref. 13)

standard deviation = ± 0.23 x $10^2$ kg $cm^{-2}$.

5. Horizontal cylinders, perpendicular to coastline; mean = 3.62 x $10^2$ kg $cm^{-2}$, standard deviation = ± 0.54 x $10^2$ kg $cm^{-2}$.

It has been stated elsewhere (Ref. 13) that:

(i) the mean secant modulus for the vertical cylinders is statistically significantly different at the 5 per cent confidence level from those for the horizontal cylinders.

(ii) the *simplest* 'best-fitting' curve to represent the data on the directional variation of the modulus in the horizontal plane is not a circle but an ellipse, where the major ellipse axis is parallel to the coastline, and the minor ellipse axis is parallel to the symmetry plane of the pre-testing geometrical fabric.

In other words, as far as the secant modulus is concerned *the Portsea beach sand does not possess a horizontal plane of isotropy*. Furthermore, the symmetry of the secant modulus distribution in the horizontal plane shows a logical and very simple relationship with the monoclinic symmetry of the original geometrical fabric pattern.

(c) Test Results of Silvan Krasnozem Silty Clay

In the triaxial loading tests on the Silvan krasnozem silty clay varying numbers (three or more) of specimens in each of three orientation groups have been used. The three orientation groups comprise one set of oriented, vertical cylinders, one set of oriented, horizontal cylinders where the major cylinder axis runs north-south, and, finally, one set of oriented, horizontal cylinders with the major cylinder axis running east-west.

As mentioned earlier, all triaxial loading tests on the particular soil have been performed with a standard type triaxial machine. Since there was some doubt initially about the possible influence of the type of endplates on strength and on deformation patterns, about half of the tests on *vertical* cylinders have been carried out with standard ('high-friction') ceramic endplates. The others were tested using highly polished ('low-friction') brass endplates that were lubricated and covered with a thin rubber membrane. The differences of the mean strengths and of the mean secant moduli, using 'high-friction' as compared with 'low-friction' endplates are clearly statistically insignificant at the 5 per cent confidence level. Consequently, as far as strength or secant modulus is concerned, the type of endplates used seems to be irrelevant.

A similar irrelevance of the types of endplates, used in testing, is suggested by the deformation patterns of loaded krasnozem cylinders of various orientations, shown in Fig. 8, 9, 10 and 11. It will be noted that the discontinuity or planar pore patterns in the four specimens are basically the same, irrespective of their orientation and the types of endplates used. All four specimens show a major 'horizontal' discontinuity perpendicular to the major axis of the cylinder, and dividing this axis into two approximately equal parts. This major discontinuity, in a number of instances, approaches a plane surface; in other cases (Fig. 11) it may be somewhat curved. In addition to this major feature, other less evident discontinuities parallel to the edges of the cylinders may be present. The development of one or two intersecting failure planes inclined to the axis of the cylinder, like the Portsea beach sand, has *not* been observed to occur in the particular Silvan krasnozem silty clay. The discontinuity patterns demonstrated in Fig. 8 to 11 (inclusive) or observed in any other of the triaxially tested specimens of the particular soil *do not show any clear evidence of a monoclinic symmetry*. It could possibly even be argued that, in this particular instance, the discontinuity patterns seem to reflect the 'higher' symmetry of the triaxial test itself. As there are no radial strain measurements available for the tested specimens, there is presently no evidence either to support or to invalidate the hypothesis of *monoclinic symmetry of the deformation process* available from the discontinuity patterns. The results of the corresponding secant modulus determinations to be discussed later, however, do support the hypothesis of monoclinic symmetry of the mechanical properties of the particular soil.

Apart from mutual differences in deviator stress, the stress-strain curves of the triaxially tested undisturbed krasnozem specimens do not show any unusual features (Fig. 12): the curves commence approximately linear with varying steepness, and, onwards from about 5 to 10 per cent axial strain tend to run horizontally or nearly so.

The stress-strain curves shown in Fig. 12 suggest in themselves differences in mechanical properties, e.g., peak strength, secant modulus, for the three orientation groups. Such differences, however, could possibly also result from significant differences in void ratio and/or moisture content in the original test specimens. To examine this possibility, data on both void ratio and moisture content have been arranged according to the three orientation groups with the following results.

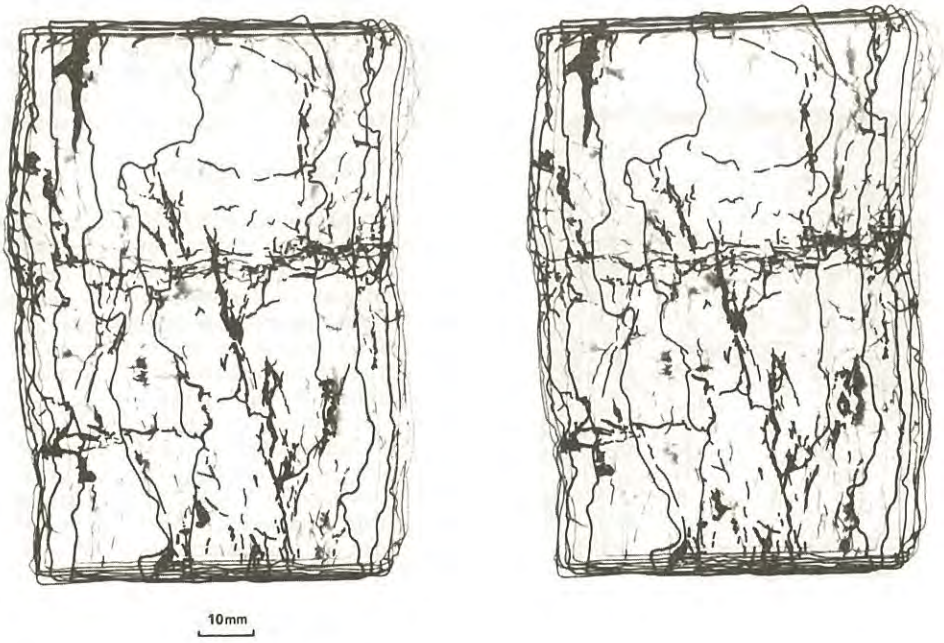


Fig. 8.- Stereopair of photographs of a transparent model showing the discontinuity pattern in a triaxially loaded vertical cylinder of Silvan krasnozem silty clay. Low-friction endplates, 20% axial strain. The original dimensions of the cylinder are 75 x 150 mm.

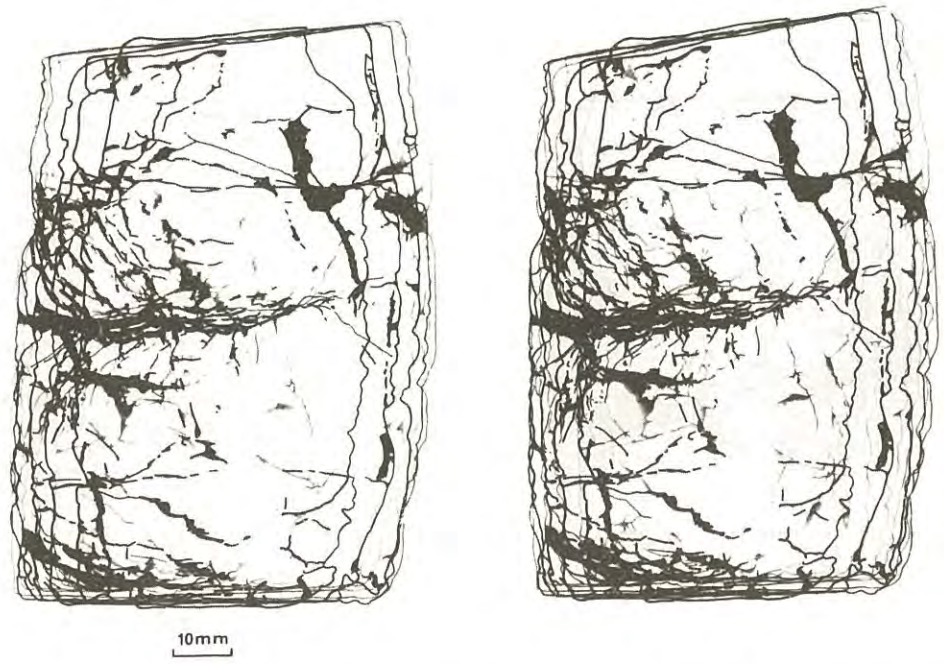


Fig. 9.- Stereopair of photographs of a transparent model showing the discontinuity pattern in a triaxially loaded vertical cylinder of Silvan krasnozem silty clay. High-friction (standard) endplates, 20% axial strain. The original dimensions of the cylinder are 75 x 150 mm.

Void Ratio:

1. Vertical cylinders: mean = 1.21, standard deviation = ± 0.029.
2. Horizontal NS-cylinders: mean = 1.30, standard deviation = ± 0.085.
3. Horizontal EW-cylinders: mean = 1.41, standard deviation = ± 0.050.

Moisture Content:

1. Vertical cylinders: mean = 38.8%, standard deviation = 0.70%.
2. Horizontal NS-cylinders: mean = 38.0%, standard deviation = ± 3.25%.
3. Horizontal EW-cylinders: mean = 39.7%, standard deviation = ± 2.94%.

Formal analysis of variance indicates that, for both void ratio and moisture content, the between-sample and within-sample variances for the three groups of specimens do not differ significantly at the 5 per cent confidence level. *All* samples can be considered to have been drawn from the one population. If, however, the secant modulus is determined from the test data, the results are as follows.

Secant Modulus:

1. Vertical cylinders: mean = $0.97 \times 10^2$ kg cm$^{-2}$, standard deviation = $\pm 0.25 \times 10^2$ kg cm$^{-2}$.
2. Horizontal NS-cylinders: mean = $0.73 \times 10^2$ kg cm$^{-2}$, standard deviation = $\pm 0.11 \times 10^2$ kg cm$^{-2}$.
3. Horizontal EW-cylinders: mean = $0.44 \times 10^2$ kg cm$^{-2}$, standard deviation = $\pm 0.07 \times 10^2$ kg cm$^{-2}$.

In this instance it appears that the difference between-sample and within-sample variances is *statistically significant* at the 5 per cent confidence level. Or, as far as the secant modulus is concerned, the values obtained from the three orientation groups can be considered as drawn from *different* populations. The most striking feature at present is the fact that the horizontal secant modulus in the N.S. direction is statistically significantly different at the


Fig. 10.- Stereopair of photographs of a transparent model showing the discontinuity pattern in a triaxially loaded horizontal cylinder, orientation N.S. of Silvan krasnozem silty clay. Low-friction endplates, 20% axial strain. The original dimensions of the cylinder are 75 x 150 mm.

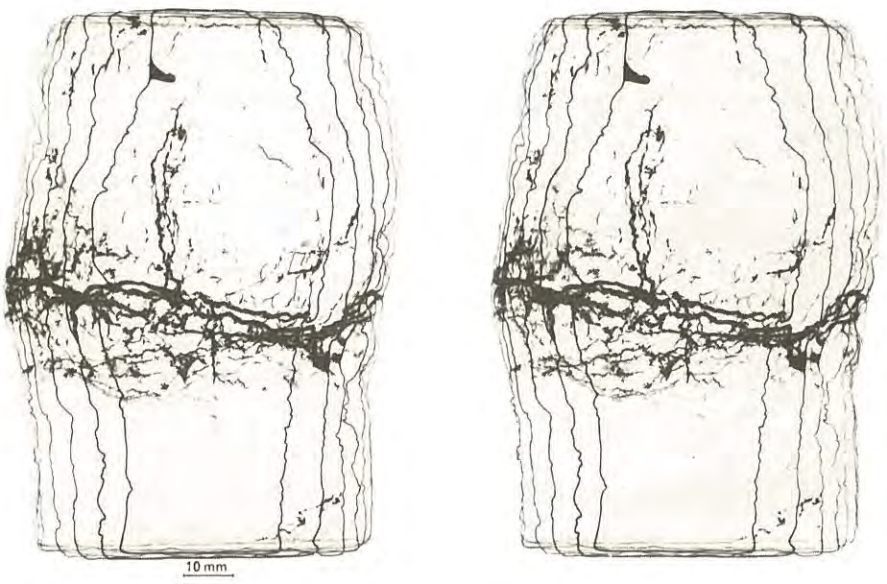


Fig. 11.- Stereopair of photographs of a transparent model showing the discontinuity pattern in a triaxially loaded horizontal cylinder, orientation E.W. of Silvan krasnozem silty clay. Low-friction endplates, 20% axial strain. The original dimensions of the cylinder are 75 x 150 mm.

5 per cent confidence level from that in the E.W. direction, i.e. this particular Silvan krasnozem silty clay *does not possess a horizontal plane of isotropy or a vertical* n-fold *axis of symmetry* (n = ∞) *in the particular soil as far as the secant modulus is concerned.*

## IV.- CONCLUDING REMARKS

It has been pointed out in this paper that the anisotropy concept in modern soil mechanics has been restricted in general to one particular case where the anisotropy is solely a result of gravitationally controlled consolidation and compaction. These conditions lead then to the well-known concept of 'cross-anisotropy', where a vertical or near-vertical n-fold axis of symmetry (n = ∞) and a plane of isotropy perpendicular to this axis are the only symmetry elements of the physical system.

The evidence obtained from the two natural soils discussed in the present paper, however, indicates that:

(i) Both soils lack a vertical n-fold axis of symmetry (n = ∞) or horizontal plane of isotropy in their original, pre-testing geometrical or morphological fabric, but they do possess a single vertical plane of symmetry (= monoclinic symmetry) containing the horizontal transportation component.

(ii) The beach sand shows in its deformation pattern a strong control by the original monoclinic fabric symmetry. There is not sufficient experimental evidence at this stage, however, to demonstrate a similar fabric control for the deformation of the silty clay.

(iii) Both soils show differences in secant modulus between horizontal specimens sampled in variously oriented directions, i.e. they seem to lack a horizontal plane of isotropy or a vertical n-fold axis of symmetry (n = ∞) as far as this mechanical property is concerned.

(iv) The (presently hypothetical) symmetry elements of the three-dimensional secant modulus distribution can be related in a simple and logical manner with those of the original, pre-testing

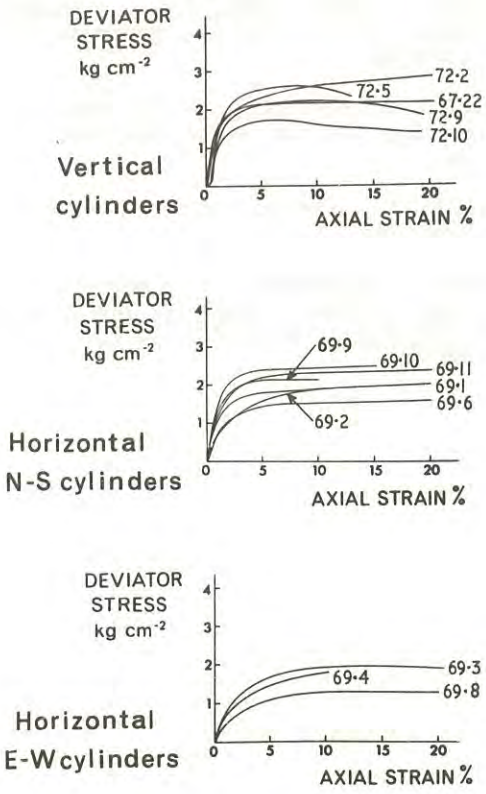


Fig. 12.- Typical stress-strain curves of triaxially loaded vertical and horizontal cylindrical specimens of undisturbed krasnozem silty clay, Silvan, Victoria. (Ref. 10)

morphological fabric of the two soils (see also Ref. 13).

(v) In both instances the 'micro-fabric' can be related in a simple manner to major terrain features, such as the direction of the coastline or the orientation of the natural terrain slope.

It is possible that in some soils the influence of gravitationally controlled consolidation and compaction on their mechanical behaviour is very substantially stronger than that of their primary structures. There is no sufficient reason, however, to exclude or ignore the influence of the structure *a priori*. It is believed that a thorough reconsideration of the anisotropy concept in soil mechanics is well overdue. Such reconsideration will have to include a clarification or redefinition of concepts such as $K_o$ (Ref. 20) and the anisotropy index or anisotropy coefficient (Ref. 21).

## V. ACKNOWLEDGEMENTS

The authors wish to acknowledge the very substantial assistance given by Mr. J.D. Walsh and Miss J. Hollingsworth in the field sampling, preparation, and testing of the soil specimens discussed in this study.

## REFERENCES

1. TERZAGHI, K. - Erdbaumechanik auf bodenphysikalischer Grundlage. Deuticke, Leipzig/Vienna, 1925, 399 pp.

2. BISHOP, A.W. - The Strength of Soils as Engineering Materials. Géotechnique, Vol. 16, No. 2, 1966, pp. 91-130.

3. LAFEBER, D. - The Graphical Representation of Planar Pore Patterns in Soils. Aust. J. Soil Res. Vol. 3, No. 2, 1965, pp. 143-164.

4. LAFEBER, D. - The Optical Determination of Spatial (Three-Dimensional) Orientation of Platy Clay Minerals in Soil Thin-Sections. Geoderma, Vol. 1, No. 3, 4, 1967, pp. 359-369.

5. LAFEBER, D. - Micromorphometric Techniques in Engineering Soil Fabric Analysis. Proc. 3rd Intern. Working Meeting Soil Micromorphology, Wroclaw, Poland, 1969, in press.

6. WILLOUGHBY, D.R. - The Geometrical Description of Linear and Simple Planar Features in Soils. Aust. J. Soil Research, Vol. 5, 1967, pp. 21-36.

7. WALSH, J.D. and HOLLINGSWORTH, J. - Sampling and Preparation of Natural Soils for Quantitative Three-Dimensional Fabric Analysis. Div. Soil Mech. CSIRO, Melbourne, Vic., Tech. Rep. No. 7, 1968, 10 pp.

8. WILLOUGHBY, D.R. and WALSH, J.D. - Preparation of Large Thin-Sections from Polyethylene-Glycol Impregnated Soil Samples. Proc. 3rd Intern. Working Meeting Soil Micromorphology, Wroclaw, Poland, 1969, in press.

9. LAFEBER, D. - Soil Structural Concepts. Eng. Geol., Vol. 1, No. 4, 1966, pp. 261-290.

10. LAFEBER, D. - Soil Anisotropy and Soil Sampling. In 'Soil Mechanics Aspects of Soil Sampling' Ed. AITCHISON, G.D. Proc. Specialty Session No. 1, 7th Intern. Conf. Soil Mech. Found. Engg., Mexico, D.F., IGOSS, Melbourne, pp. 32-39.

11. INGLES, O.G. and LAFEBER, D. - The Initiation and Development of Crack and Joint Systems in Granular Masses. Proc. Symp. Stress and Failure around Underground Openings, Dept. Min. Engg, University Sydney, N.S.W., No. 7, 1967, pp. 1-7.

12. LAFEBER, D. and WILLOUGHBY, D.R. - Geometrical Anisotropy and Triaxial Failure in Soils. Proc. 3rd Asian Reg. Conf. Soil Mech. Found. Engg, Haifa, Israel, Vol. 2, 1967, pp. 186-192.

13. LAFEBER, D. and WILLOUGHBY, D.R. - Morphological and Mechanical Anisotropy of a Recent Beach Sand. Proc. Symp. Foundations on Interbedded Sands, Perth, 1970.

14. SANDER, B. - Gefügekunde der Gesteine. Springer Vienna, 1930, 352 pp.

15. SANDER, B. - Einführung in die Gefügekunde der geologischen Körper (Allgemeine Gefügekunde). Springer, Vienna, 1948, 215 pp.

16. SANDER, B. - An Introduction to the Study of Fabrics of Geological Bodies. Perg. Press, 1970, 641 pp.

17. PHILLIPS, F.C. - The Use of the Stereographic Projection in Structural Geology. Arnold, London, 1963, 86 pp.

18. KENNEY, J.F. and KEEPING, E.S. - Mathematics of Statistics, Vol. 1, 3rd ed., Nostrand, Princeton, N.J., 348 pp.

19. TERZAGHI, K. and PECK, R. - Soil Mechanics in Engineering Practice, Wiley, New York, 1948, 566 pp.

20. TERZAGHI, K. - Theoretical Soil Mechanics. Wiley, New York, 1943, 510 pp.

21. LIVNEH, M. and KOMORNIK, A. - Anisotropic Strength of Compacted Clays. Proc. 3rd Reg. Conf. Soil Mech. Fdn Engng, Haifa, Israel, Vol. 1, 1967, pp. 298-304.

# Estimating the Strength of Jointed Soils

By
P. Lumb, M.Sc. (Eng.)
(Reader in Civil Engineering, University of Hong Kong)

SUMMARY.- The shear strength of jointed soils can be estimated from laboratory tests which measure the matrix and joint strength parameters, provided that the form of the probability distribution of joint plane orientation and spacing is known. The influence of joint plane orientation can be treated statistically by assuming a combination of Uniform, Spherical Normal, and Girdle Distributions, whose parameters are estimated from the results of a joint survey. The influence of joint spacing can be treated crudely by assuming that the spacings follow a Poisson Distribution. The strength distribution of the soil in the field will inevitably be bimodal. At present there is no satisfactory way of selecting a single-valued design strength to characterize the bimodal distribution.

## 1.-INTRODUCTION

Many natural soils contain planar discontinuities along which the soil strength is less than in the soil matrix. In residual soils these discontinuities are formed by the joints of the parent rock and the in-situ strength would be expected to be strongly influenced by the dip, bearing, and spacing of these joints. Some theoretical aspects of the strength of jointed soils will be outlined, for the case where both frictional and cohesive components of strength need to be considered. For illustrative purposes reference will be made to two types of residual soil in Hong Kong (Ref.1), decomposed granite and decomposed rhyolite, both of which contain abundant joints.

## II.-HONG KONG RESIDUAL SOILS

Decomposed granite is essentially a silty coarse sand, free-draining and generally unsaturated above permanent water-table. Its drained strength shows high friction angle ($\phi$=30 to 45 degrees) and low cohesion (c=0 to 50 kN/m$^2$). The joints are widely spaced, giving a massive structure.

Decomposed rhyolite is a sandy silt to clayey silt, unsaturated in general, with a low friction angle ($\phi$=25 to 35 degrees) and a high cohesion (c=20 to 70 kN/m$^2$ ). The joints are closely spaced, giving a blocky structure.

The joint planes were formed prior to decomposition, and along some, but not all, joint surfaces a thin coating of iron oxides has subsequently been formed.

Although no systematic measurements of strength along the joints have yet been made, it may be assumed that the friction angle along uncoated joints is about the same order as for the matrix, while along the coated joints the friction angle will be appreciably smaller. The cohesion along the joints will be assumed to range from zero to one half of the matrix cohesion.

Both friction angle and cohesion are variable quantities and for illustrative purposes the following parameters (average values ± standard deviation) will be used.

| | Matrix, and Uncoated Joint $\phi^o$ | Coated Joint $\phi^o$ | Matrix c kN/m$^2$ |
|---|---|---|---|
| Decomposed granite | 35±2 | 25±2 | 25±5 |
| Decomposed rhyolite | 30±2 | 22½±2 | 50±10 |

## III.-STRENGTH OF SOIL SPECIMEN

Considering a triaxial test specimen under a lateral confining pressure $\sigma_3$ and vertical pressure $\sigma_1$ ($\sigma_1>\sigma_3$) in which there is a single joint plane dipping at $\beta$ to the horizontal, the shear strength $q = \frac{1}{2}(\sigma_1-\sigma_3)$ will be the smallest of either the matrix strength $q_0$ or the joint strength $q_\beta$ . It is easy to show (Ref.2, p.128) that $q_\beta$ will be the smallest strength if $\beta$ is inside the critical range $\beta_0$ to $\beta_1$ , where

$$\beta_0 = \tfrac{1}{2}\phi_j + \tfrac{1}{2}\arcsin\left\{\frac{\sin\phi_j}{\sin\phi_m}\left[1-\frac{H_m-H_j}{p+H_m}\right]\right\} \qquad (1)$$

$$\beta_1 = \tfrac{1}{2}\pi + \phi_j - \beta_0$$

where $\phi_j$, $c_j$, are the joint strength parameters; $\phi_m$, $c_m$, the matrix parameters; $H=c.\cot\phi$ , and $p=\frac{1}{2}(\sigma_1+\sigma_3)$

The shear strength is given by

$$q=q_0=\frac{\sigma_3\sin\phi_m + c_m\cos\phi_m}{1-\sin\phi_m} \quad ; \quad \begin{matrix}\beta<\beta_0\\ \beta>\beta_1\end{matrix} \qquad (2)$$

$$q=q_\beta=\frac{\sigma_3\sin\phi_j + c_j\cos\phi_j}{\sin(2\beta-\phi_j)-\sin\phi_j} \quad ; \quad \beta_0<\beta<\beta_1 \qquad (3)$$

Fig.1 shows the relative importance of the various factors in the form of a polar plot of $q/q_0$ radially versus $\beta$, for the two soils with coated and uncoated joints; $c_j/c_m$ zero and one half; tested at low stress level ($\sigma_3 = 70$ kN/m$^2$) and high stress level ($\sigma_3 = 400$kN/m$^2$). It will be clear that while all factors influence the strength the dominant factors are $\beta$ and $\phi_j/\phi_m$.

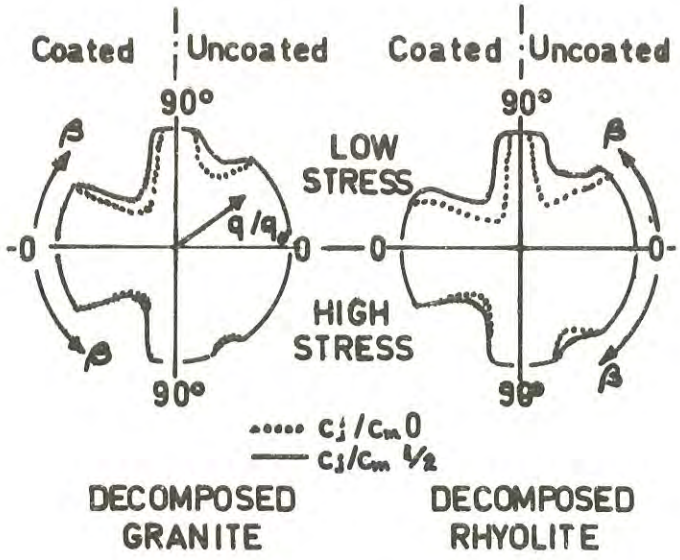


Fig.1. Strength versus Dip Angle.

## IV.-STRENGTH PARAMETER VARIABILITY

Taking account of the innate variability of cohesion and friction angle, the coefficient of variation (ratio of standard deviation to mean value) of the shear strength can be calculated approximately as

| | | Matrix | Joint |
|---|---|---|---|
| Decomposed Granite | Low stress | 7% | 5% |
| | High stress | 2% | 1% |
| Decomposed Rhyolite | Low stress | 11% | 8% |
| | High stress | 4% | 2% |

In order to estimate the mean strength to within ±10%, about 10 tests at a low stress level and 5 at a high stress level would be required for each particular value of dip angle $\beta$. In practice the maximum amount of testing would probably be limited to about 15 tests on intact jointless specimens to measure matrix strength and another 15 tests on jointed specimens, all with the same dip angle, to measure joint strength. The strength at other dip angles would be calculated from Eq.3. Since $q_\beta$ is least sensitive to errors in $\beta$ at around the minimum strength ($\beta = \frac{1}{4}\pi + \frac{1}{2}\phi_j$) the best choice for $\beta$ would be between 50 and 60 degrees.

## V.-DIP ANGLE VARIABILITY

Figs.2A and 3A show the results of measurements of dip angle $\beta$ and bearing angle $\alpha$ (measured from North through East) at two locations in Hong Kong.

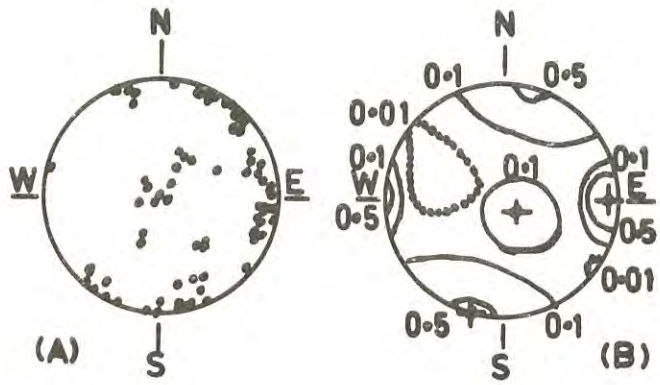


Fig.2. Joint Orientation in Decomposed Granite (A) Observations (B) Probability Density Function Contours.

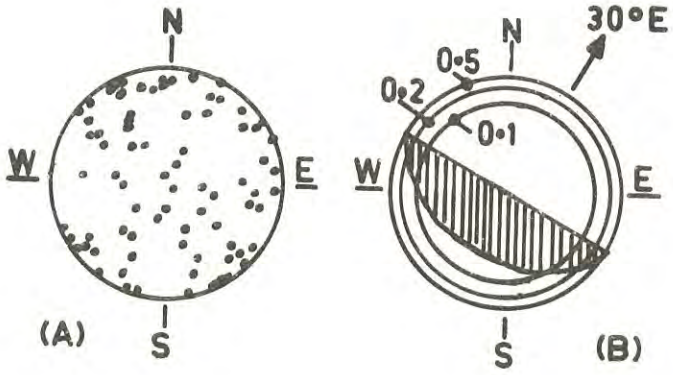


Fig.3. Joint Orientation in Decomposed Rhyolite (A) Observations (B) Probability Density Function Contours.

The points are the directions of the poles of the joints plotted on an equiareal, polar, lower hemisphere projection. Point diagrams are merely descriptive and are not sufficiently accurate for quantitative work (Ref.3) and it is preferable to use some estimated theoretical distribution of $\beta$ and $\alpha$. Three simple distributions which are often sufficient will now be described briefly.

(a) Distributions on a Sphere.

The locations of the joint plane poles can be regarded as following a three-dimensional distribution in spherical co-ordinates $\beta$, $\alpha$, and unit radius. If the poles are clustered about a particular value $\beta_o$, $\alpha_o$ then the spherical analogue of the one-dimensional Normal distribution may give good agreement. Writing $\theta'$ and $\psi$ as the dip and bearing measured from $\beta_o$ $\alpha_o$ as origin, the probability of $\theta'$ being less than a particular value $\theta$ at a given value of $\psi$, $P(\theta, \psi)$ is

$$P(\theta,\psi) \propto \int_{\theta=0}^{\theta} \exp(k.\cos\theta')\,dA \qquad \begin{matrix} 0< \theta< \pi \\ 0< \psi< 2\pi \end{matrix} \qquad (4)$$

where $dA = \sin\theta' d\theta' d\psi$

Here k is a measure of the concentration of values around the origin, a large value of k representing a tight clustering and a small k a more dispersed distribution.

Eq.4 defines what will be called the Spherical Normal Distribution, and it will be written in terms of its parameters as

$$P(\theta,\psi) = S(\beta_o,\alpha_o:k;p)$$

in general, where p is the proportion of the whole population of joints following this particular distribution.

If the concentration factor k is zero then the joints are distributed uniformly over the whole sphere and, since only one hemi-sphere need be considered,

$$\frac{dP(\beta,\alpha)}{d\alpha} = \frac{dP(\theta,\psi)}{d\psi} = \frac{1-\cos\beta}{2\pi} \qquad (5)$$

$$0<\beta< \tfrac{1}{2}\pi \quad , \quad 0<\alpha< 2\pi$$

Since the only parameter is the proportion p, this Uniform Distribution will be written

$$P(\beta,\alpha) = U(p)$$

If the dip angles are not concentrated about a point but spread about a great circle of the unit sphere then, measuring $\theta'$ and $\psi$ from $\beta_1,\alpha_1$, the pole of this great circle, the Girdle Distribution can be defined by

$$P(\theta,\psi) \propto \int_{o}^{\theta} \exp(-m.\cos\theta')\,dA \qquad \begin{matrix} 0<\theta < \tfrac{1}{2}\pi \\ 0<\psi < 2\pi \end{matrix} \qquad (6)$$

where m is again a concentration factor, and large values of m represent a tight clustering about the great circle. This Girdle Distribution will be written

$$P(\theta,\psi) = G(\beta_1,\alpha_1:m;p)$$

The estimation of the parameters $\beta_0,\alpha_0;\beta_1,\alpha_1;k$ and m, and tests for significance, are described in Refs.4,5, 6,&7. The following results summarize the analysis of the two examples of Figs.2A and 3A.

(b) Decomposed Granite.

The joints are clustered but there are three distinct clusters, two with high dips and one with a low dip. A satisfactory distribution is a combination of three Spherical Normal Distributions with parameters

$S_1(90,16 :7;0.5)$

$S_2(79,270:35;0.3)$

$S_3(16,315:7:0.2)$

Fig.2B shows the probability density function contours of the combined distribution $S_1+S_2+S_3$ on an equiareal projection. The three cluster centres (marked with crosses) are almost orthogonal. A chi-squared test of goodness of fit of $S_1+S_2+S_3$ compared with the observations of Fig.2A gave $\chi^2=13.7$ with 11 degrees of freedom, thus $\text{Prob}(\chi^2 > 13.7)=24\%$, indicating an excellent agreement.

(c) Decomposed Rhyolite.

Fig.3A shows a more dispersed pattern than for the decomposed granite but with some clustering at high dips. A satisfactory distribution is a combination of a Uniform and an equatorial Girdle Distribution with parameters.

$U(0.5)$

$G(0,0 :7;0.5)$

The combined probability density contours are shown on Fig.3B. The goodness of fit test gave $\chi^2=11.3$ with 7 degrees of freedom, $\text{Prob}(\chi^2 > 11.3)=10\%$, again indicating excellent agreement.

VI.-STRENGTH DISTRIBUTION FOR JOINTED SPECIMEN

Knowing the distribution of dip angle and the variability of the strength components it is relatively simple to calculate the distribution of shear strength q, for a specimen containing a single joint plane. Two cases need distinguishing, the triaxial test specimen where failure will occur on the joint if $\beta_0<\beta<\beta_1$ irrespective of bearing angle $\alpha$, and the plane-strain specimen where the orientation of the specimen might influence the occurrence of failure.

(a) Triaxial Strength.

The strength will be controlled by the marginal distribution of dip angle $P(\beta)=\int P(\beta,\alpha)d\alpha$, since failure can occur on any dip plane at any bearing. The expected distribution of strength, the marginal distribution P(q) obtained by numerical integration, is shown by the solid lines of Figs.4 & 5 for coated joints with zero joint cohesion, at low and high stress levels. The distributions are, of course, bimodal with the two modes at the average strengths for matrix and most critical joint dip respectively.

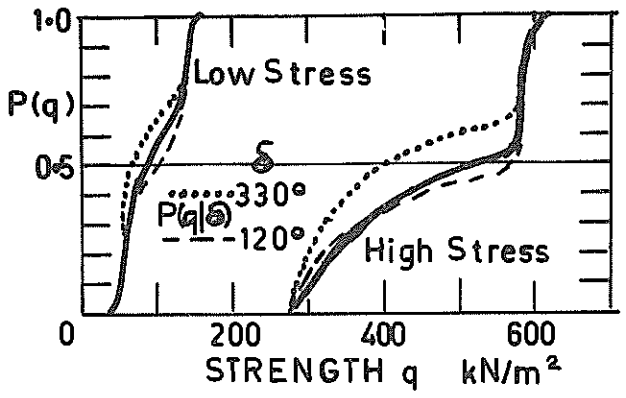


Fig.4. Distribution of Strength, Decomposed Granite.

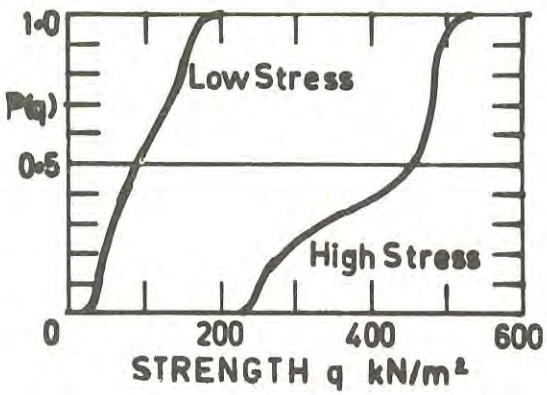


Fig.5. Distribution of Strength, Decomposed Rhyolite.

(b) Plane-Strain Strength.

Here, bearing angle has relevance to strength, but the pertinent dip angle distribution is a little complicated. For a specimen cut with its long axis normal to a bearing angle $\delta$ a joint plane bearing at $(\delta+\psi)$ will be a potential failure surface if the apparent dip $\beta'$ in the direction $\delta$ is within the critical range $\beta_0$ to $\beta_1$. If the true dip at bearing $(\delta+\psi)$ is $\theta$ the apparent dip is given by

$$\beta' = \arctan(\cos\psi . \tan\theta)$$

and planes of true dip $\theta > \beta_1$ may be critical planes.

The probability of apparent dip being less than $\beta$ is the conditional probability

$$P(\beta|\delta) = \int_A P(\theta,\psi)dA \Big/ \int_A dA$$

where the region of integration is that portion A of the sphere for which $\cos\psi \tan\theta < \tan\beta$. The region A is indicated on Fig.3B by the shaded area for the case $\beta=45^o$, and $\delta=30^oF$.

For the decomposed granite $P(\beta|\delta)$ is strongly influenced by orientation and consequently the strength distribution $P(q|\delta)$ depends on $\delta$. Fig.4 shows the two extreme distributions for $\delta=120^o$ and $330^o$ as dotted lines, compared with the axially symmetric marginal distribution P(q). Again, the strength is bimodal.

For the decomposed rhyolite there is comparitively little difference between $P(\beta|\delta)$ and $P(\beta)$ and the conditional and marginal distributions $P(q|\delta)$ and P(q) are indistinguishable to the scale of Fig.5.

## VII.-EFFECT OF JOINT SPACING ON STRENGTH MEASUREMENTS

The strength distributions of Figs.4 & 5 are for specimens containing a single joint plane, and quite clearly the probability of finding a joint in the specimen will depend on the size of the specimen and the spacing of the joints. For very large specimens and close spacings there is a strong likelyhood of multiple joints but, since failure will be controlled by the most critical of these joints and not by all of them, the final strength distribution will not differ greatly from the distribution for singly-jointed specimens.

For very small specimens of the size commonly used for strength measurements there will be an appreciable probability of no joint being found at all, and thus strength tests on samples obtained from routine site investigations will give a distribution biased towards the upper mode of matrix strength.

The influence of joint spacing can be treated very roughly on the basis of average joint density n, the average number of joints per unit length. For a length L, area $L^2$, or volume $L^3$, the expected number of joints would be nL, so the expected probability of no joints in the volume $L^3$ is $p_o = \exp(-nL)$, from the Poisson Distribution, and the corresponding probability of one or more joints is $(1-p_o)$. Thus the distribution of strength will be a combination of the distribution of matrix strength $P(q_o)$ and of singly-jointed strength P(q) or $P(q|\delta)$, and hence for a size L the probability of a particular strength q is P(q,L) where

$$P(q,L) = p_o P(q_o) + (1-p_o)P(q) \qquad (7)$$

for the triaxial strength.

For the two locations of Figs.2 & 3 the average joint densities n are 0.91 per metre and 5.4 per metre for decomposed granite and rhyolite respectively, and the approximate probabilities of finding no joint plane in small specimens (40mm dia. by 150mm) and large specimens (100mm dia. by 450mm) are

| | Small | Large |
|---|---|---|
| Decomposed granite | 87% | 66% |
| Decomposed rhyolite | 45% | 9% |

The probability of finding a joint inclined at about the optimum dip for joint-strength measurement $(50^o<\beta<60^o)$ in any sample is

| | Small | Large |
|---|---|---|
| Decomposed granite | 0.8% | 2.7% |
| Decomposed rhyolite | 4.6% | 7.5% |

Routine borehole site investigations are clearly inefficient for estimating joint strength parameters $c_j, \phi_j$, unless the joint spacing is very small. The efficiency can be improved somewhat by cutting inclined test specimens from large samples at angles of $50^o$ to $60^o$ to any joint plane, neglecting any effects of matrix strength anisotropy, but the best method is systematic sampling from trial pits or exposures, after actual inspection of the joint planes.

Eq.7 can be used to obtain an expression for the change in average strength with specimen size. As size L decreases $p_o$ increases and the strength distribution becomes less skew, finally approaching the unimodal distribution of matrix strength. Very roughly, if $q_L$ is the average strength of a specimen of size L, $q_\infty$ the average strength of a very large

site, and $q_m$ the average matrix strength then

$$q_L = q_\infty + (q_m - q_\infty)\exp(-nL)$$

The large site average strength $q_\infty = pq' + (1-p)q_m$ with $q'$ the average value of $q_\beta$ ($\beta_0<\beta<\beta_1$) and $p$ the Prob($\beta_0<\beta<\beta_1$), and writing $r = q'/q_m$ the expression reduces to

$$q_L/q_m = 1-(1-r)p\{1-\exp(-nL)\} \qquad (8)$$

VIII.-CONTINUITY OF JOINTS

The most important design problem associated with soils containing discontinuities is of course the stability of cuttings. The controlling factor is not really the distribution of strength in the whole volume influenced by the cutting, but the possibility of a critical joint plane extending over a large enough area to cause a major slide.

If the joints dividing the soil mass into numerous irregular blocks terminate on contacting each other, then the probability of a series of adjacent joints linking up to form a potential slip surface can be calculated. For N adjoining regions each of size L, assuming independence between regions, if the probability of a dip angle $\beta \pm \frac{1}{2}d\beta$ for one region is $p_\beta$ the resulting probability of a continuous plane would be

$$\text{Prob(Continuous)} = (p_\beta)^N$$

For large N this probability would be very small.

If the joints do not terminate but extend continuously over large areas the probability of a potential failure plane would be simply $p_\beta$, and this would be fairly large.

These two extremes, discrete and continuous joint patterns, give upper and lower limits to the probability, but unfortunately the limits are too wide apart to be of much practical use. The true joint pattern will be a combination of discrete and continuous patterns and the distributions of each component ought to be estimated separately. This topic will not be pursued here, but it is worth mentioning that the observed behaviour of deep cuttings in Hong Kong is more in agreement with the discrete than the continuous pattern probability. Major slips due to joint plane failure are extremely rare for both soils.

IX.-DISCUSSION

The main conclusion is the rather obvious one that routine site investigations cannot be expected to give any useful information on the strength of jointed soils, and that special investigations with trial pits are essential.

Provided that a precise joint-pattern survey has been made, the strength distribution can be calculated numerically from the matrix and joint strength parameters. The distribution of dip and bearing angles needed for the calculations is best found by smoothing the observations, and the uniform, spherical normal, and girdle distributions described here will generally be sufficiently flexible for this purpose. The accuracy of the estimated probabilities will be proportional to the number of observations for each group of clustered joints. For tight clusters (large k or m) perhaps about 20 observations would suffice, but for disperse distributions 50 or more may be necessary.

With regard to joint spacings there is at present no really satisfactory statistical method of describing naturally occurring patterns, and much more work needs to be done on this aspect.

The large-site strength distributions, such as illustrated in Figs.4 & 5, are inevitably bimodal, and just how this information is to be incorporated into a design remains an open question. An average strength such as given by Eq.8 has little relevance, while the use of the lower mode (minimum $q_\beta$) is unduly conservative and the upper mode (matrix strength) is too risky. Some sort of probabilistic treatment appears unavoidable, but at present there is no clear-cut answer.

REFERENCES


1. LUMB, P.-The Residual Soils of Hong Kong, Geotechnique, Vol.15, 1965, pp. 180-194.

2. SOKOLOVSKI, V.V.-Statics of Soil Media. London, Butterworth, 1960, 237pp.

3. VISTELIUS, A.B.-Structural Diagrams. Oxford, Pergamon, 1966, 178pp.

4. FISHER, R.A.-Dispersion on a Sphere, Proc. Royal Soc. Vol.217, Series A, 1953, pp. 295-305.

5. SELBY, B.-Girdle Distributions on a Sphere, Biometrika, Vol.51, 1964, pp. 381-392.

6. STEPHENS, M.A.-Statistics Connected with the Uniform Distribution: Percentage Points and Application to Testing for Randomness of Directions, Biometrika, Vol.53, 1966, pp. 235-240.

7. STEPHENS, M.A.-Tests for the Dispersion and for the Modal Vector of a Distribution on a Sphere, Biometrika, Vol.54, 1967, pp. 211-223.

# The Use of In-situ Tests in a Study of the Effects of Fissures on the Properties of Stiff Clays

By

A. Marsland, M.Sc.

(Principal Scientific Officer, Building Research Station, United Kingdom)

SUMMARY. - The large variations in the shear strengths and modulii measured in triaxial tests on standard 76 mm long x 38 mm diameter specimens of stiff fissured clay has led to the use of large in-situ tests to measure these properties. The undrained properties have been measured by means of loading tests on plates with diameters of up to 865 mm at various depths in boreholes and effective strength parameters have been determined by in-situ tests using a 610 mm square shear box.

A detailed study has been made of the effects of plate diameter, fissure spacing, degree of confinement of the borehole immediately above the test level, the method of preparing the test surface and the interval of time between excavation and loading the plate.

Effective strength tests have been made in the large shear box using effective normal stresses between 17.5 and 100 $kN/m^2$ which is the range of particular interest in many engineering applications. In some of the tests pore pressure measurements were made on the plane of shear to check that the rate of shear was sufficiently slow to ensure that the pore pressure remained zero.

Large in-situ tests have provided a better measure of strength and deformation parameters applicable to full-scale conditions for two highly fissured clays. By comparing the results obtained from both field and laboratory tests of various sizes a better understanding of the influence of fissures on the properties of stiff fissured clays has been obtained.

The paper describes these tests, gives typical results to illustrate the influence of fissures and compares the results with laboratory tests. The use and limitations of in-situ tests for determining the full-scale strength applicable to a particular problem are discussed.

## I. - INTRODUCTION

The difficulties of sampling and the wide scatter of results obtained from laboratory tests on small samples of stiff fissured clays has raised severe doubts as to the value of present procedures for obtaining the mechanical properties of these clays. During detailed investigations of the London Clay in a deep shaft at Ashford Common (Refs 1 and 2) large variations in strength were measured in triaxial tests on 76 mm high and 38 mm diameter specimens even though the specimens were carefully prepared from hand excavated block samples. These large variations made it almost impossible to decide which values were representative of the large scale strengths of the clay. In-situ loading tests on a 152 mm diameter plate and on a 38 mm diameter cone penetrometer made at various levels in the deep shaft from which the block samples were obtained showed that the shear strength of the clay that was mobilized depended on the size of the test in relation to the spacing of the fissures in the clay. They also suggested that the lower strengths obtained in the laboratory tests on small specimens were more representative of the large-scale strengths than were the average values. The conclusions drawn from this investigation have led to an increased use of in-situ plate loading tests to estimate the undrained strength of fissured London Clay (Ref 3) for use in the design of piled foundations (Ref 4). These tests, together with loading tests on instrumented piles (Ref 5) confirmed that the large-scale strengths of the fissured London Clay were appreciably lower than the average values given by tests on small specimens. Tests on different sized specimens of London Clay, and Barton Clay which is also highly fissured, showed that the measured strength decreased as the size of the specimen was increased (Refs 6, 7 and 8). As a consequence of these findings the author initiated a study of in-situ tests using different sizes and types of equipment in conjunction with laboratory tests on specimens of various sizes prepared and sampled by the best available techniques. Loading tests on a 865 mm diameter plate installed at various levels in boreholes and in-situ shear tests

using a 610 mm sq shear box formed an important part of the investigations. The present paper describes these tests and gives some typical results and comparisons with the results of laboratory tests. The use and limitations of both in-situ and laboratory tests for determining the strengths applicable to particular problems are discussed.

## II. - THE USE OF IN-SITU LOADING TESTS FOR MEASURING THE UNDRAINED PROPERTIES OF STIFF FISSURED CLAYS

### (a) Factors Which May Affect the Undrained Properties of Stiff Fissured Clay Estimated From In-Situ Loading Tests

The undrained properties of stiff fissured clay determined from in-situ plate loading tests may be influenced by the following factors:

i) The mineralogical composition, strength, and the type of discontinuities present in the clay. Stiff clays contain numerous discontinuities in the form of bedding surfaces, joints, shear dislocations, and fissures. Even in clays with similar mineralogical properties the discontinuities can vary in size, continuity, inclination and surface roughness with both depth and location.

ii) The forces and restraints imposed on the ground around the test levels by different arrangements adopted for the tests.

iii) Dimensions of the test equipment and in particular the relative dimensions of the loaded plate and the spacing of the fissures in the clay.

iv) The reduction in stress and the accompanying strains which occur in the clay during drilling and insertion of the test equipment.

v) The interval of time between drilling the hole and loading the plate.

vi) The rate of penetration during loading.

The effects of the type of clay and the different structural weaknesses will only become apparent when comparable results are available from tests in a number of clays with widely differing properties.

The effect of forces or restraints imposed on the ground near the test level may vary with the type and structure of the clay. Model studies of deep in-situ loading tests in soft unfissured clay made by the author (Ref 9) showed that the maximum bearing pressure which could be applied to a plate installed in a borehole having a diameter equal to that of the plate was the same for tests made in unlined and lined boreholes irrespective of whether the liner remained stationary or moved down at the same speed as the plate. However, the maximum bearing capacities measured on a plate of a given size decreased rapidly as the ratio of the hole to plate diameter increased from 1.0 to 1.5. At present there is only limited data available from tests in stiff fissured clays. In-situ loading tests in fissured London Clay at Wraysbury near London Airport using 292 mm diameter plates in cased and uncased boreholes gave almost identical results. At another site in London Clay a few tests made on a 292 mm diameter plate pushed from inside a thick, very tight fitting liner gave ultimate bearing pressures of up to 10 to 15 per cent greater than loading tests on plates at the same levels in unlined boreholes.

Loading tests on 38 mm diameter probes and on a 152 mm diameter plate at Ashford Common (Ref 2) clearly showed the importance of the size of the test equipment in relation to the spacing of the fissures. The large scatter obtained from loading tests in London Clay on plates with diameters less than 200 mm (Ref 3) also showed the importance of the size of the test equipment. The main purpose of the large-diameter plate tests described in the next section of this paper was to provide a reliable basis for evaluating the results of both smaller in-situ tests and laboratory tests on various sizes of specimens.

Very little data is available on the influence of the interval of time between excavation and loading the clay, but deformation moduli determined from plate loading tests made in the base of the Ashford Common shaft at time intervals from $\frac{1}{2}$ hour to $2\frac{1}{2}$ days after completion of excavation showed an appreciable decrease with time.

No exhaustive series of tests have yet been made to study the effect of the rate of penetration during loading on either the load-settlement curves or the ultimate bearing pressures measured on plates. The limited data available from plate and pile loading tests where rates of loading several times lower and higher than the rate of 2.5 mm/min used in our loading tests were employed suggests that this is a minor factor at these rates of loading. Further investigations are however required, particularly in those clays which expand rapidly when unloaded.

### (b) Loading Tests on a 865 mm Diameter Plate in 900 mm Diameter Boreholes

Loading tests on a 865 mm diameter plate in 900 mm diameter boreholes have been made for the purpose of evaluating the reliability of the undrained properties of stiff fissured clay as measured by in-situ and laboratory tests. One of the principle aims was to keep the interval of time between drilling and testing as short as possible. The tests were made in unlined boreholes apart from the short lengths of

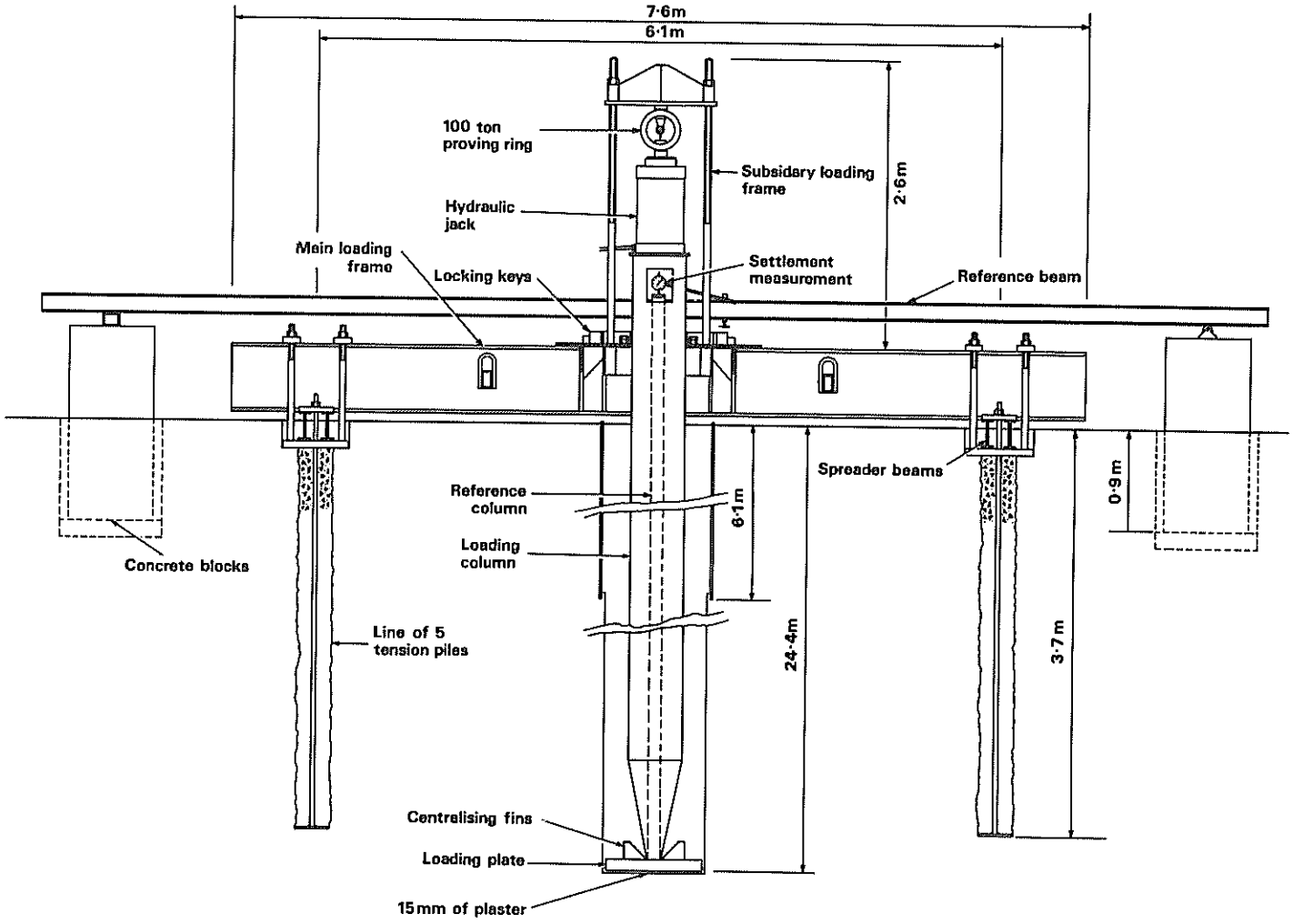


Fig 1 Vertical section through the plate loading test equipment

lining provided at the top of the boreholes to ensure the safety and efficiency of the operations. A crane-mounted drilling rig of the type used for constructing large bored piles was used to drill the boreholes and to erect the test equipment. A vertical section through the plate loading equipment is shown in Fig 1. The loading frame was designed so that the major part of it could be left in place during drilling and erection of the test equipment. In the particular application illustrated in Fig 1 the reaction was provided by 10 small tension piles which were pulled out by a crane after completion of the tests, but the arrangement is sufficiently flexible to permit other tension pile arrangements. The main reaction frame consisted of two 7 m long 610 mm x 320 mm I-section steel girders spaced 1200 mm apart with a fabricated centre table having a 1200 mm diameter hole. The frame was fixed at ground level to spreader beams connected across the tops of the tension piles. A helical flight auger was used to drill the 900 mm diameter borehole to within about 600 mm of the test level, and a flat-bottomed bucket auger was used to take out the remainder so as to produce a flat-bottomed hole. Loose and protruding clay was removed from the bottom of the hole by hand for all the tests and for some of the tests additional clay was removed from the bottom using a sharp spade and a hand scraper.

Operations in the bottom of the borehole were carried out from a safety cage fitted with a removable base to allow a man to alight at the bottom of the borehole and work under the protection of the cage. A continuous clean air supply was also provided down the borehole and the operations were generally in accordance with the requirements of British Standard CP 2011:1969.

As soon as the removal of spoil from the base of the borehole was completed, a quantity of high strength gypsum plaster was taken down in the safety cage and spread on the bottom of the borehole to form a layer 15-20 mm thick. The plaster mix used consisted of $2\frac{1}{2}$ parts by weight of Crystacal EN plaster

to 1 part of a 1 per cent $K_2SO_4$ solution. This gave a mix which could be easily poured up to about 10 minutes after mixing, remained fairly plastic for a further 5 minutes, but reached a strength of about 3000 kN/m$^2$ in 30 minutes. The loading plate was lowered into the hole by suspending it below the safety cage from where it was guided into position and carefully centralised in the bottom of the borehole. During the lowering operation three guides consisting of steel strip were fixed to the plate to prevent it scraping clay from the side of the borehole, but these were removed when the plate was in position.

The loading column was built up from 1.5 m lengths of screwed 460 mm diameter casing tube and was lowered into the borehole in 6 and 12 m lengths. Each 6 m length was provided with handling lungs that engaged in slots in a small frame supported on the main reaction frame, thus eliminating the need for clamping devices during the fixing of additional 6 m lengths. The bottom end of the loading column was tapered in order to minimise eccentricity of the load transferred to the plate. During the final stages of lowering the column was guided into a central position on the plate by a conical cup welded to the top of the plate.

The settlement of the plate was measured on an independent axial column built up from lengths of 100 mm diameter tube which were fitted with handling lugs and pinned spigot joints to speed erection. With the reference column in position the loading column was capped by a special section incorporating a window giving access to the head of the internal reference column and with a horizontal top plate

Fig 2 Subsidiary loading frame being lowered into position

to carry the jack. A subsidiary loading frame fitted with rollers to keep the top end of the loading column central was then lifted into position, as shown in Fig 2. The loading jack and 100 tonne proving ring were incorporated in this loading frame and arranged to be self-centering on the top of the loading column. The loading frame was held down on to the main frame by four steel locking keys, sliding into key-ways attached to both frames. The complete loading system was designed to provide loads on the plates of up to 150 tonnes.

The dial gauge to measure the settlement of the reference column was attached to a rod which passed through the window of the loading column and was clamped to a 12 m long reference beam. The ends of the reference beam rested on rollers cast into concrete blocks which in turn rested on concrete pad foundations, well removed from the tension piles and the test borehole. This reference beam was left in position throughout all the tests in a particular borehole.

The whole of the arrangements were devised with the intention of keeping the time taken to erect the loading and settlement measuring system to a minimum. The average time between the completion of machine boring and the commencement of a loading test was 140 minutes for the tests in which the loose material only was removed by hand from the test level and 180 minutes where an additional depth of clay was removed from the bottom of the borehole by hand digging, but times as low as 60 minutes were achieved.

During the loading test the jack was extended at a constant rate of 2.5 mm per minute using a multi-speed hydraulic pumping unit which ensured a very smooth penetration, free from pressure pulses.

(c) Typical Results From Loading Tests on 865 mm Diameter Plates and Comparison with Laboratory Tests

Bearing pressure - settlement curves obtained on 865 mm diameter plates using this equipment in unlined boreholes in London Clay at Hendon are compared in Fig 3 with similar tests on 292 mm diameter plates in 300 mm diameter boreholes. The tests on the 865 mm diameter plate gave load settlement curves with reasonably well-defined maximas while the tests on the smaller plates seldom attained maximum values. The large plate tests did not show any obvious bedding errors that were common in the smaller tests made in boreholes that were too small to permit access for cleaning the test surface by hand. In the large tests, where additional clay was dug from the base of the borehole by hand, there was no sign of initial concavity in the load settlement curve commonly recorded in plate tests of all diameters and usually attributed to the closing up of surface fissures in the clay caused by the

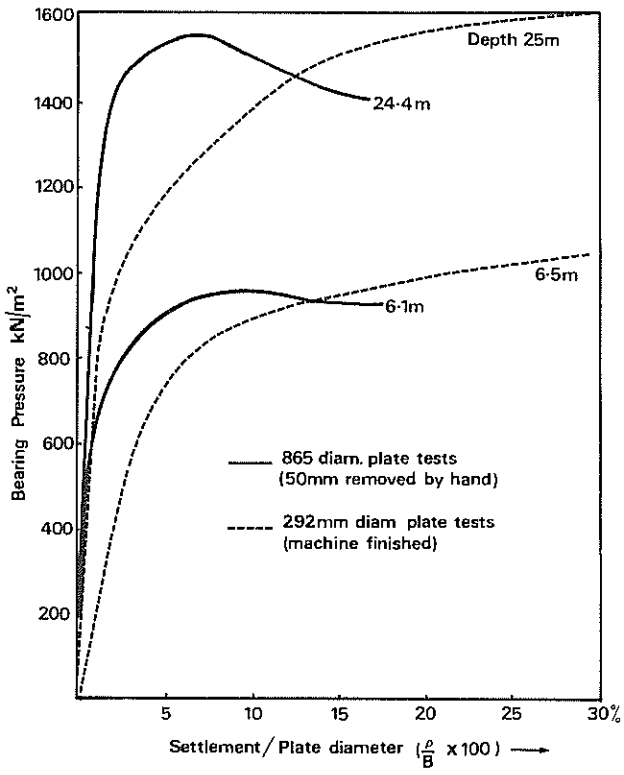


Fig 3 Typical load settlement curves obtained from loading tests on 292 and 865 mm diameter plates in London Clay at Hendon

tearing action of the auger. Initial concavity in the load settlement curves did however occur in a few of the large diameter tests in which only the loose clay was removed from the base of the borehole prior to setting the plate on plaster.

Shear strengths calculated from the 865 mm diameter plate tests in London Clay using a bearing capacity factor $N_c$ of 9.25 (which value is based on results of model tests by the author (Ref 9) and on plasticity theory (Ref 10) have given very reproducible results, see Fig 2 of reference 11). The shear strength of London Clay calculated from 865 mm diameter plate tests made in London Clay at Chelsea are compared in Fig 4 with triaxial tests on 38 mm and 98 mm diameter specimens and with laboratory penetration tests in which a 5.5 mm loading plate was used. At this particular site the average spacing of the fissures increased from about 15 mm at a depth of 4 m to about 100 mm at a depth of 15 m. The surface of many of the fissures were very curved and the lumps of clay between the fissures were interlocked to a considerable extent. Some idea of the extent of the interlocking can be obtained from the fact that it was safe to work in a deep unlined borehole for at least 9 days as against a maximum of 2-3 days at other sites in fissured London Clay. This pronounced interlocking of the clay probably accounted for the high strength measured on both 38 and 98 mm diameter specimens as compared with the strengths calculated from the plate tests. At this site the strength measured on both the 38 and 98 mm diameter specimens from a depth of about 15 m were about 1.75 times those calculated from the plate tests. Comparable figures from tests at a similar depth made at another site in London Clay (briefly reported in Ref 11) were 1.1 for tests on the 98 mm diameter specimens and 1.35 for tests on 38 mm diameter specimens.

The results of the 5.5 mm diameter penetration tests provided an approximate measure of the strength of the 'intact' clay within the lumps between the fissures. At the site in Chelsea the shear strengths calculated from the penetrometer tests increased from about twice to more than four times the large-scale strength of the clay as determined by the large in-situ test between depths of 5 and 15 m. The large difference between the laboratory and the large-scale in-situ strength values have clearly shown the fallacy of using strengths from laboratory tests on small specimens for design purposes.

Load tests on 140 mm, 292 mm and 865 mm diameter plates in London Clay at Hendon showed that the bearing pressures on 292 mm diameter plates at a settlement equal to 15 per cent of the plate diameter were in reasonable agreement with the maxima measured on the 865 mm diameter plates. Tests on 140 mm diameter plates gave very erratic results which could not be satisfactorily interpreted.

In addition to providing better measures of the large-scale strengths of fissured clays the large in-situ plate tests also gave moduli nearer the values deduced from movements of foundations and excavations. The values of the secant moduli at half the ultimate load calculated from the load settlement curves obtained in tests on 865 mm diameter plates in which 50 to 75 mm of clay was removed by hand digging were appreciably greater than values measured in triaxial tests on specimens obtained by carefully pushing in the thin-walled sampling tubes. Values of E calculated from smaller plate tests, where it was not possible to prepare the test surface by hand, were appreciably lower than those calculated from the large tests.

## III.- LARGE IN-SITU SHEAR BOX TESTS TO DETERMINE THE EFFECTIVE STRESS PARAMETERS OF STIFF FISSURED CLAYS

In order to investigate the stability of excavations and earth retaining structures reliable shear strength parameters in terms of effective stresses are required. The results from large in-situ plate tests given in the first part of this paper have

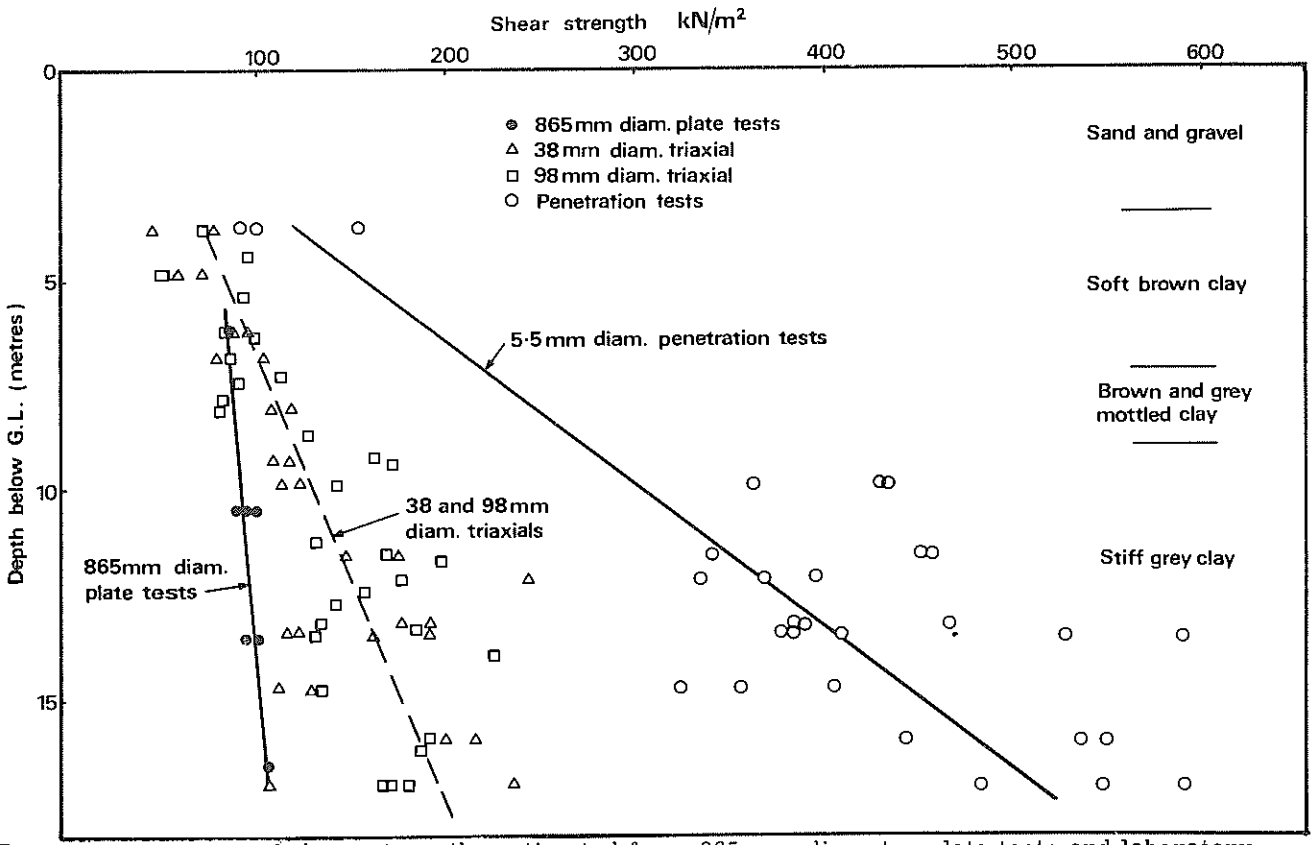


Fig 4 Comparison of shear strengths estimated from 865 mm diameter plate tests and laboratory tests on 38 mm and 98 mm diameter specimens in London Clay at Chelsea

shown that laboratory tests on small samples gave higher undrained shear strengths than those determined by large in-situ plate tests. Since this difference was largely attributed to the fact that the proportion of the shear planes which passed through hard intact clay between the fissures was larger in the laboratory than in the field tests it followed that effective stress parameters determined from tests on small laboratory specimens were also suspect. During the early stages of construction of a large power station at Fawley, Hampshire, tests on 150 mm high x 75 mm diameter specimens of stiff fissured Barton Clay gave an effective strength envelope which was appreciably lower than the envelope from tests on 76 mm high x 38 mm diameter specimens carried out as part of the original site investigation. In order to check this discrepancy and obtain more reliable stress parameters a number of large in-situ shear tests using a 610 mm square shear box were made.

(a) Details of Large In-Situ Shear Box and Method of Test

A diagrammatic section through the shear box and loading arrangements are shown in Fig 5. In plan the shear box was square with sides having an internal length of 610 mm. It was constructed in two halves, each suitably reinforced to form rigid units which could be bolted together to facilitate installation. The lower half of the box was made of perforated sheet steel, fitted at the lower end with a sharpened cutting edge. When making a test a level surface was prepared by hand digging in undisturbed clay 75 to 100 mm above the proposed level of shear. An outline of the box was marked on the prepared surface and a shallow trench about 100 mm deep was carefully dug from around the outside leaving an undisturbed pedestal of clay a little larger than the inside dimensions of the box. The box was then placed centrally over the pedestal of undisturbed clay and pushed down evenly using a heavy concrete block suspended from a crane. The trench around the box was deepened in small stages and the box was pushed down each time until the horizontal joint between the two halves of the box was 75 to 100 mm below the level of the prepared surface. The trench around the lower half of the box was filled with a gravel filter up to the top of the lower half of the box to provide drainage during the consolidation and shearing stages. The area around the shear box was kept flooded up to the level of the shear plane throughout the test. A porous concrete block and piston were placed on the clay surface in the top half of the box. A ballast tank was used to apply a vertical load to the piston through a ball-seating fixed to the centre of the piston and the clay inside the shear box was allowed to come to equilibrium under each applied load. When consolidation or expansion was complete, the bolts connecting the two halves of the box were

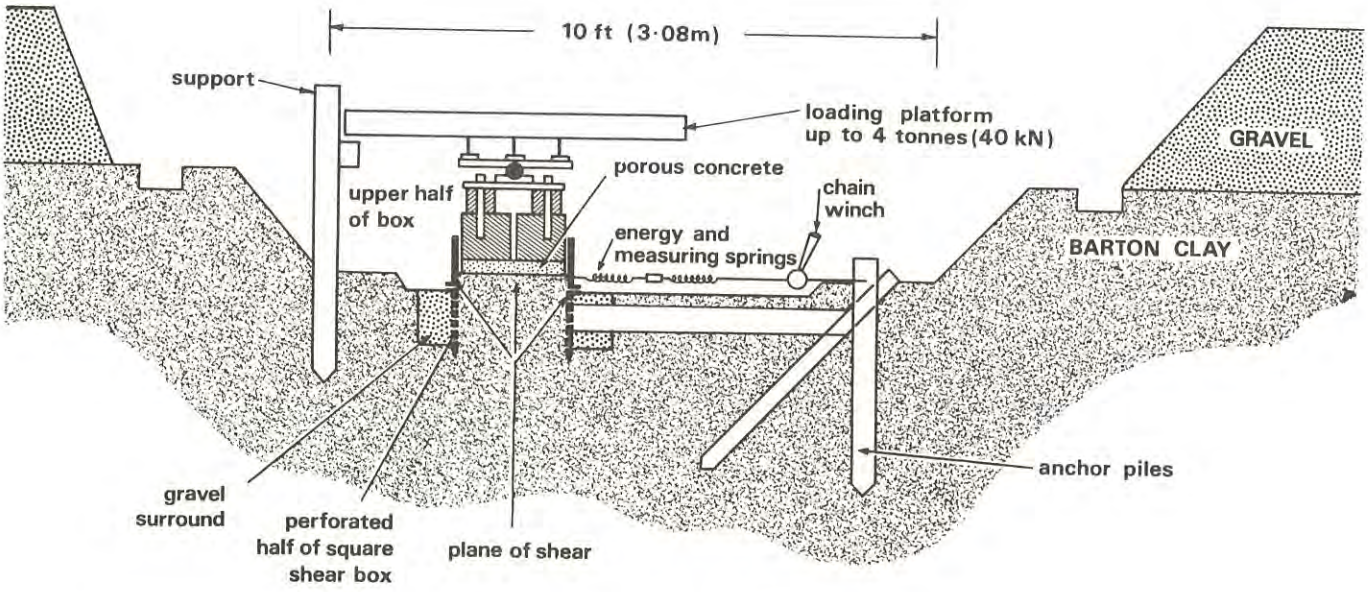


Fig 5 Diagrammatic section of in-situ shear box and loading arrangements

removed and the top half of the box lifted, relative to the clay and the lower half of the box, by means of jacking screws to give a gap of 1 to 2 mm. Horizontal shear loads were applied to the clay between the two halves of the box by means of a winch used in conjunction with calibrated springs. By adjusting the winch 2 to 3 times a day it was possible to maintain horizontal loads to within 0.1 tonnes. The vertical settlement of the piston was measured relative to an external reference frame and horizontal displacements between the two halves of the box were measured directly on targets fastened to the two halves. In order to check that the application of the shear load was sufficiently slow to enable drainage to take place within the clay, pore water pressure measurements were made in some of the tests using small piezometers installed in the centre of the pedestal of clay on the plane of separation of the two halves of the box. The use of hydraulic equipment to provide a constant rate of strain was considered but the test arrangement described above was chosen because of its simplicity, robust nature, and the need for easy recording by site personnel.

(b) Typical Results Obtained from Large In-Situ Shear Box Tests

Tests using this equipment were made in highly fissured Barton Clay at Fawley near Southampton (Ref 8). The tests were made in the upper 1.5 to 3 m of the unweathered clay, 14 to 17 m below ground level. At this level the clay contained about 70 per cent of particles less than 2 $\mu$ and had average liquid and plastic limits of 80 and 32 per cent respectively. When excavated the hard highly fissured clay fell apart into separate irregular shaped lumps that had dimensions of from 10 to 100 mm; those shown in Fig 6 being typical. The moisture content of the clay in the centre of the lumps was approximately equal to the plastic limit, while the moisture content near the surface of the lumps was 1 to 2 per cent higher. Comparison of the results of small laboratory penetration tests and undrained triaxial tests on 125 mm diameter specimens indicated that the strength of the intact clay within the lumps was about 4 times the bulk strength of the clay in-situ.

Six tests were made using different vertical loads to give normal effective pressures between 17 and 100 kN/m$^2$. Prior to shearing, the clay was allowed to come to equilibrium under the selected vertical load for about 7 days by which time the rate of vertical movement had become negligible. The horizontal shear load was then applied in small increments at regular intervals so that in test No 1, 2 and 6 the peak stress was reached in 5 to 8 days. In order to check any possible effects of the rate of application of the load, the rate of shearing in test No 3 was much slower, so that the maximum shear stress was reached in 39 days. Additional confirmation that the rate of shearing was sufficiently slow to allow almost complete drainage in the fissures was provided by pore water pressure measurements made at the centre of the clay under test on the plane of separation of the two halves of the box in test 5(a) and in a duplicate test 5(b) in which


Fig 6 Typical intact lumps of Barton Clay from shear box test No 3

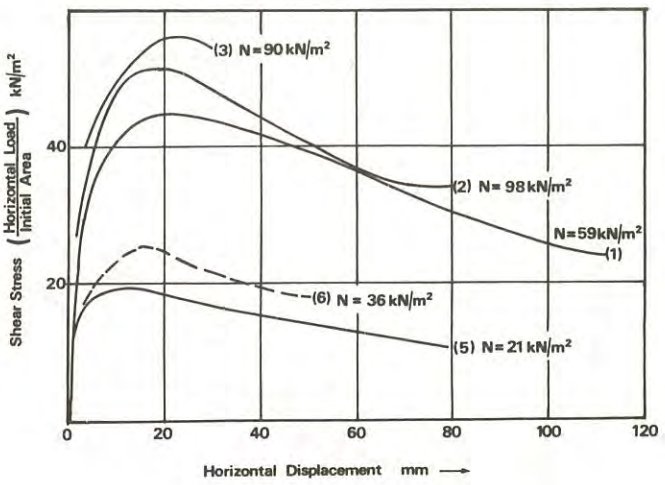


Fig 7 Shear stress - displacement curves obtained from tests on Barton Clay using the large in-situ shear box

the sample was sheared at a much faster rate, the maximum shear stress being reached in 4 hours. In both these tests the pore water pressure increased as the shear load was applied until half the maximum shear stress was reached and then dropped steadily to give pore water pressures around zero at the maximum shear stress and pore suctions after failure. In the quick test the pore water pressure reached a maximum of 11 per cent of the shear load as against 8 per cent for the test loaded at the standard rate. The most significant difference between the two tests occurred after the maximum shear stress had been reached and by the end of the test the pore water suction in the quick test exceeded the shear stress while in the standard test it was only about 11 per cent of the shear stress. Shear stress-displacement curves obtained using the large in-situ shear box are shown in Fig 7. The peak and minimum post-peak values from these tests are plotted in Fig 8 together with the upper and lower limits of the peak strengths on 75 to 125 mm diameter specimens and residual strengths obtained by reversal tests in 60 mm square shear boxes. The peak shear strength measured by the in-situ shear box lies within the range of those measured in triaxial tests on 75 and 125 mm diameter specimens. However, under the lowest normal effective stresses the maximums obtained from the in-situ shear tests tend to the lower limit of those measured in the triaxial tests. The most significant feature of the results obtained from large in-situ shear tests was the very small cohesion intercept and the relatively large angle of internal friction under low stresses. In the case of the Barton Clay the peak values lay close to a straight line giving a c' of 8.3 kN/m$^2$ and angle of internal friction of $\phi'$ of 27°. The results of these large in-situ shear tests show that under low effective stresses fissured clays behave like a granular material composed of interlocking lumps of clay which have an intact strength of 4 to 5 times the strength of the clay in the mass.

## IV.- CONCLUSIONS AND GENERAL OBSERVATIONS ON THE USE AND LIMITATIONS OF IN-SITU TESTS FOR MEASURING THE PROPERTIES OF STIFF FISSURED CLAYS

Large in-situ tests of the type described in this paper have shown the important influence which fissures have on the properties of fissured clays. They have led to a better understanding of the behaviour of these clays and have provided strength and deformation parameters more applicable to engineering design than those measured in laboratory tests on 'undisturbed' samples.

Comparison of the results of large in-situ plate tests and laboratory tests have shown that even in the same type of clay the relationships between various tests vary with depth, location, and differences in the fissure structure. They have shown the fallacy and dangers of applying correction factors of the type suggested in References 5 and 12, to results of laboratory tests in order to predict the large-scale behaviour of stiff fissured clays. The same conclusions apply to small in-situ tests such as the Dutch cone (Ref 13), which in general provide a measure of the strength of the clay in the intact lumps between the fissures and the use of these tests to predict the large-scale strength is not recommended.

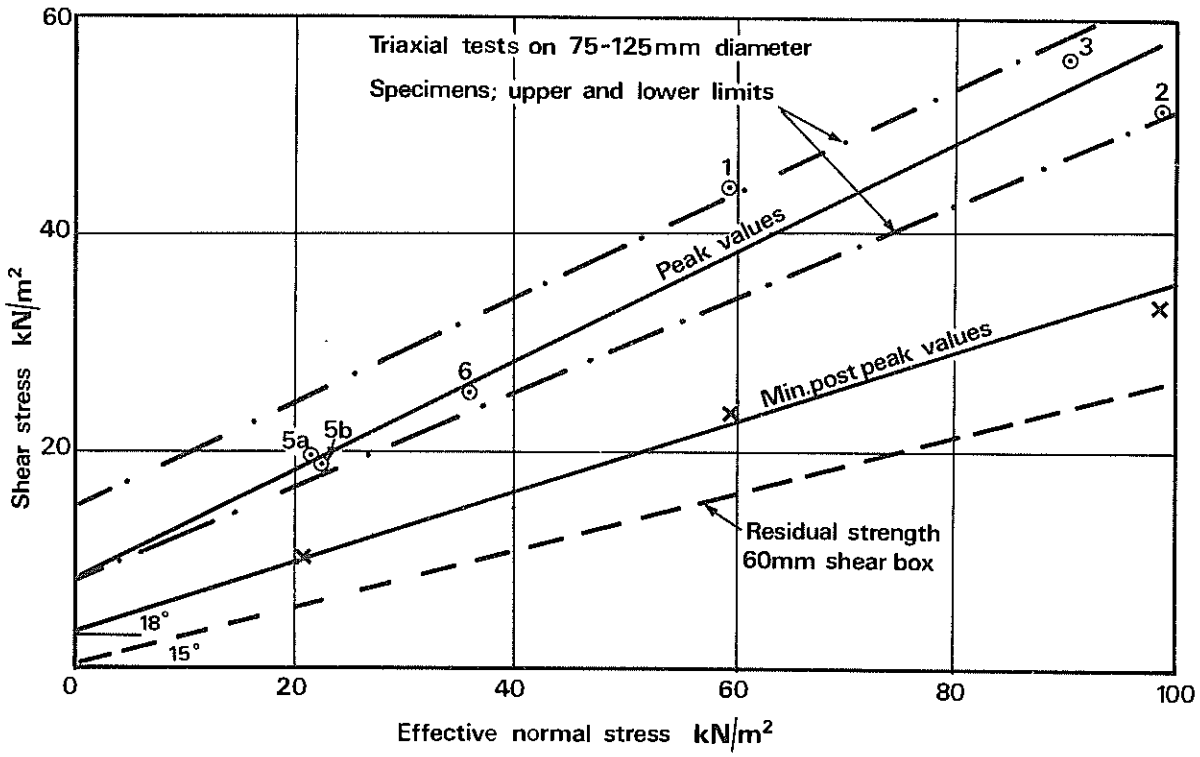


Fig 8 Results of in-situ shear tests expressed in terms of effective stresses

To obtain reproducible and reliable estimates of the modulii of stiff fissured clays it is necessary to make loading tests in boreholes which are sufficiently large to enable a man to remove loosened clay from the test level. The effects of drilling the boreholes and the interval of time between excavation and testing require further investigation. Even though in the present tests this interval has been reduced to a few hours some reduction of the modulii and to a smaller extent of the shear strength due to the opening of the fissures in the clay was inevitable. This effect was probably greatest in tests made at the deeper levels and may have accounted for the very small increase in both strength and modulii with depth which was obtained from the tests below about 20 m. More tests are required in which different periods of time are allowed between excavation and testing, and in which strains are measured in the clay below the loaded area. Ideally such tests should include measurements of strains occurring during excavation or drilling.

The complex nature and variability of fissured clays make it necessary to consider each clay individually. New problems are bound to arise when the techniques described in this paper are used to measure the properties of harder clays than those already tested, but even so they should provide a more reasonable measure of the large-scale properties than laboratory or small in-situ tests.

REFERENCES

1. MARSLAND, A. - Discussion 5th Int Conf Soil Mech & Found Engg, vol III, 1961, pp 179-180.

2. WARD, W H, A. MARSLAND and S.G. SAMUELS Properties of the London Clay at the Ashford Common shaft: In-situ and undrained strength tests. Geotechnique, vol 15 (Dec) 1965, pp 321-44.

3. HOOPER, J.A. and F.G. BUTLER - Some numerical results concerning the shear strength of London Clay. Geotechnique, vol XVI, No 4 (Dec) 1966, pp 282-304.

4. BURLAND, J.B., F.G. BUTLER and P DUNICAN The behaviour and design of large diameter bored piles in stiff clay. Proc Symp on Large Bored Piles, Instn Civ Engrs, 1966, pp 51-71.

5. WHITAKER, T. and R.W. COOKE - An investigation of the shaft and base resistances of large bored piles in London Clay. Building Research Station, Current Papers, Engineering Series 31, 1966, 49 p.

6. AGARWAL, K.B. - The influence of size and orientation of samples on the strength of London Clay. Theses (PhD) University of London, 1967.

7. MARSLAND, A. - Discussion: Session 2 - Shear strength of stiff clay. Proc Geotech Conf Oslo, 1967, pp 160-161.

8. MARSLAND, A. and MURIEL E BUTLER - Strength measurements on stiff fissured Barton Clay from Fawley, Hampshire. Proc Geotech Conf Oslo, 1967, vol 1, pp 139-146.

9. MARSLAND, A. - Model studies of deep in-situ loading tests. 1971 (Tech Note in preparation for publication in Geotechnique).

10. MEYERHOF, G.G. - The ultimate bearing capacity of wedge-shaped foundations. Proc 5th Int Conf Soil Mech & Found Engg, vol 2, 1961, pp 105-109.

11. MARSLAND, A. - The shear strength of stiff fissured clays. Paper presented to the Roscoe Memorial Symposium, Cambridge March 1971 (see also Building Research Station, Current Papers 21/71, 14 p).

12. SKEMPTON, A.W. - Summing up. Proc Symp on Large Bored Piles, Instn Civ Engrs, 1966, pp 155-157.

13. THOMAS, D. - Static penetration tests in London Clay. Geotechnique, 15(2), 1965, pp 174-179.

# The Role of Porosimetry in Geomechanics

By
B. Shackel, B.E., M.Eng.Sc.
(Lecturer, School of Highway Engineering, The University of New South Wales)
AND
A. F. S. Nettleton, B.Sc., B.E., M.E., D.I.C., M.I.E.Aust.
(Associate Professor, School of Civil Engineering, The University of New South Wales)

SUMMARY - The most fundamental parameters used to characterise soils and rocks are those that are functions of the porosity. To date engineers have, of necessity, used gross porosity as the only practical measure. However, the application of the techniques of porosimetry enable the complete distributions of pore sizes and pore volumes to be determined.

The theory and techniques of mercury intrusion porosimetry are described and the errors and limitations of the method are discussed. It is then shown that, by using porosimetry, it becomes possible to obtain information on soil properties which has not hitherto been available. Moreover, it is demonstrated that it becomes possible to define several new parameters which can usefully supplement conventional measurements based on gross porosity.

Finally, the role of porosimetry in investigating a well known engineering problem is discussed and typical experimental data is presented.

## I.- INTRODUCTION

The materials of geomechanics differ from most other engineering materials in that an appreciable proportion of their volume comprises void spaces. It is convenient to regard these voids as defects in the material since failure normally initiates within them. Consequently the porosity, and closely related units such as the dry density and voids ratio,provide the most significant parameters for describing soil or rock structure. To date, engineers have concentrated on two aspects of porosity in soils and rocks. The first of these is the gross porosity, and its relation to strength, deformation and failure. The second aspect which has received wide investigation concerns the permeability. The authors believe that porosimetry, a technique new to geomechanics, provides a powerful new tool to explore both of these research areas.

In the past, the only practical measure of soil and rock fabric was the gross volume of the voids although limited information on the distribution of pore sizes could be obtained from the water retention curves of certain soils. However by using porosimetry, the complete distributions of equivalent pore sizes and pore volumes can be determined. It then becomes possible to employ a new set of parameters, which are functions of the pore size and volume distributions, to supplement conventional measurements based on the gross porosity.

## II.- NOTATION

$e$ = void ratio

$n$ = porosity

$p$ = pressure

$R$ = equivalent circular pore radius

$R_{60}$ = 60th percentile pore radius

$R_{50}$ = 50th percentile pore radius

$R_{10}$ = 10th percentile pore radius

$S_r$ = degree of saturation

$T$ = surface tension

$\gamma_d$ = dry density

$\theta$ = contact angle

## III.- THE MEASUREMENT OF PORE CHARACTERISTICS

In order to fully describe a pore system three characteristics must be considered. These are -

a) The volume of the pores

b) The size of the pores

c) The geometry of the pores

Historically, most engineering measurements have been exclusively concerned with the gross volume of the pores. Techniques for measuring pore sizes and pore geometry are a comparatively recent innovation e.g.(Refs.1,2) and,in general, do not provide information in a form that is suitable for engineering application.

The various techniques for measuring pore sizes have been summarised elsewhere (Ref.3). Only one of these has received general application in the study of soil and rock fabric. This is the technique by which thin sections of the material are optically observed under high magnifications (e.g.Ref.1). Such

methods can provide fundamental information on the size and geometry of both the pores and the components of the mineral skeleton but suffer the disadvantages of being complex and time consuming and of sampling only a small part of the total pore system. By contrast the techniques of mercury intrusion porosimetry provide a rapid means of measuring pore sizes and pore volumes in which a relatively large proportion of the pore system is sampled.

In common with all other methods, porosimetry does not measure all three of the characteristics needed to describe a pore system. Whilst detailed information on pore sizes and pore volumes is provided the shape and geometry of the pores is ignored. Thus in order to completely describe a pore system it would be necessary to combine the porosimetry data with measurements made using one of the optical techniques. Nevertheless it is believed that parameters which are derived solely by porosimetry may receive the same engineering application as such conventional parameters as the porosity and voids ratio.

To date the application of porosimetry to soils and rocks has been limited to

a) The study of petroleum reservoir rocks (Refs.4,5)

b) Studies of clay minerals (Ref.6)

c) The measurement of intrinsic permeability (Refs.4,7)

## IV.- THE PRINCIPLES OF INTRUSION POROSIMETRY

When a non-wetting liquid, such as mercury is placed in contact with a porous material it will not freely enter the interstices in the material unless sufficient external pressure is applied to overcome the surface tension forces. The magnitude of the pressure required to cause intrusion of any given pore is a function of the ratio of the perimeter to the cross-sectional area of the pore. For cylindrically shaped pores the relationship between the minimum pore size intruded and the applied pressure can be written (Ref.8) as

$$R = \frac{-2\ T \cos\theta}{P} \qquad (1)$$

where

R = equivalent pore radius (cm.)

P = applied pressure (dynes/cm$^2$)

T = surface tension (dynes/cm)

$\theta$ = contact angle (degrees)

In an intrusion test, a sample of the porous material is placed in a dilatometer and submerged in mercury. Pressure is then applied to the surface of the mercury causing it to intrude the sample. For a given change in pressure, the volume intruded can be determined by observing the change in level of the mercury in the dilatometer. Thus the test data comprise the volumes of mercury that penetrate the sample for known increments of pressure. By using a simple, idealised model in which the real,irregularly shaped pores are replaced by circular pores of equivalent radius, Eq.1 may be solved to determine the pore radius corresponding to any given pressure. The distributions of pore volumes and pore sizes in the model may then be derived.

## V.- LIMITATIONS OF THE MERCURY INTRUSION METHOD

Three factors limit the valid application of mercury intrusion techniques. In order of importance these are

a) Specimen characteristics

b) Test procedures

c) Methods used to interpret the experimental data

### (a) Specimen Characteristics

Most porosimeters are only capable of testing small amounts of material (usually less than 20g.). It is seldom possible, therefore, to examine more than a few fragments of material taken from either core samples or compacted specimens. The surface areas, weights and shapes of the fragments are thought to have a negligible influence on intrusion measurements (Ref.4) although the experimental evidence concerning the effects of these factors is inconclusive. Since only small specimens can be examined it is essential to use standard sampling procedures such as quartering to select representative test material.

Having obtained a representative sample, it is customary to remove all traces of pore water before intrusion with mercury. Rock samples are normally solvent extracted and then oven dried (Refs.4,5). The preparation of soil samples is more difficult. Often oven drying will result in particle reorientation and a change in the gross porosity due to shrinkage. For clays compacted dry of optimum moisture content the shrinkage is not normally sufficient to impede the interpretation of intrusion data (Ref.6). However, for clays close to full saturation, oven drying characteristically results in sufficient shrinkage to cause serious errors in the determination of equivalent pore sizes. It has been suggested (Ref.6) that, in such cases, freeze drying, or drying at elevated pressures and temperatures, offer more suitable methods of sample preparation.

A first evacuation of the sample may occur during the drying process and the air permeabilities of wet soils are generally much lower than the corresponding water permeabilities (Ref.9). It is therefore necessary to evacuate soil specimens at a sufficiently slow rate to ensure equalisation of pore air pressures. Without equalisation of air pressures there is a risk that the structure of the micropores may be disturbed.

### (b) Test Procedures

After evacuation of pore air the specimen is immersed in clean mercury. The pressure is then slowly increased from 0 to a maximum of about 1,000 atmospheres. At any stage during the test the effective stress in those regions of the specimen that have not been fully intruded does not remain constant and some disturbance of the soil structure may occur. As the applied pressure is raised the volume of voids fully

penetrated by mercury increases. Thus as the effective stress in the unintruded material increases it acts within a steadily diminishing volume. It is therefore probable that any disturbance of the pore geometry will be confined to the finer pores in the material. Although it does not appear possible to experimentally assess the extent to which mercury intrusion may modify pore structure, it is unlikely that the disturbance would be any more severe than that associated with most alternative methods of measuring pore sizes.

It is normally impossible to evacuate all traces of pore air when preparing a sample for intrusion. Thus, as the pressure is increased during a test there will be an apparent change in volume due to compression of the residual air. It is therefore necessary to make corrections, based on Boyle's law, for this effect. The application of pressure also produces changes in the volumes of the dilatometer, the mercury and the soil skeleton as the result of hydrostatic compression. Corrections, based on observations of volume changes in the apparatus in the absence of a sample, can be made for changes in the volume of the dilatometer and the mercury it contains. However, volume changes in the mineral skeleton of a soil or rock specimen cannot be readily assessed and may give rise to small errors in the determination of pore volumes.

One other source of error arising from the test procedures needs to be considered. This is the effect of a change in temperature. When mercury is compressed its temperature increases causing a change in the surface tension. Thus the rate at which the pressure is increased should be kept sufficiently low to permit the temperature of the mercury to continually equalise with that of the laboratory which itself should be maintained constant.

(c) Interpretative Procedures

It is customary to drastically simplify the problem of interpreting the test data by making the assumption that the pores have circular cross-sections. Eq.1 may then be used to determine the equivalent circular pore radius, R, corresponding to any value of the applied pressure,p. However, before Eq.1 may be solved it is necessary to assign values to the surface tension, T, and the contact angle, $\theta$. Although T is a constant for a particular temperature, reported values vary widely. Values of T varying from 473 dynes/cm to 484 dynes/cm (Ref.6) have been used in investigations of soils and rocks. The contact angle, $\theta$, depends on the nature of the material under examination. The only values so far reported that are applicable to soils are for clay minerals (Ref.6). These range from a mean value of $139^{\circ}$ for bentonites and montmorillonites to $147^{\circ}$ for kaolinites and illites. Thus at present it is often necessary to assume values for $\theta$ which are not supported by experimental evidence. However, the error in determining the equivalent pore radius assuming an erroneous contact angle is probably less than that incurred by assuming that the pores are cylindrical (Ref.10).

The need to employ some mathematically tractable model of pore geometry such as that represented by Eq.1, places a restriction on the interpretation of intrusion data. Whilst the effects of this restriction can be minimised by the development of more realistic models, it should be recognised that the intrusion method imposes a fundamental limitation on all models of pore geometry. This concerns the manner in which the pores are interconnected. Where entry to a pore is constricted it will not be penetrated by mercury until the applied pressure is sufficiently high to cause intrusion of the narrowest portion of the entrance to the pore. Consequently the entire volume of a pore will be assigned to a pore size equivalent to the smallest dimension of the pore entrance rather than to the mean or predominant size of the pore.

VI.- PARAMETERS USED TO CHARACTERISE POROSIMETER DATA

The data obtained by intrusion porosimetry comprise the frequency distributions of equivalent pore radii and of pore volumes. From the limited evidence available (Ref.5) including that presented below it appears that the distributions will often be multimodal. It is then necessary to derive suitable parameters from these distributions to enable different pore systems to be compared. Essentially the problem is to select established statistical parameters for this purpose. These include measures of location such as the mean, median and mode, measures of dispersion, i.e.moments measured about the mean and other arbitrary origins and measurement of kurtosis.

The selection and manipulation of suitable parameters is neither an obvious nor a simple decision. In view of the exploratory nature of the experimental work reported here it was decided only to use measures of location and dispersion which were expected to be comparatively insensitive to changes in the frequency distributions. It was thought that if a change in these simple parameters was observed it would reflect a significant change in the frequency distributions. The measures selected were the 10th, 50th (median) and 60th percentile pore radii, but it is not suggested that these were necessarily the most suitable parameters. However, it will be shown later that these measures provided a useful if limited basis for comparing different pore systems.

VII.- THE EXPERIMENTAL WORK

In this section an experiment, which investigated the concept of optimum moisture content in the compaction of soils, is described. This serves as an illustration of a particular application of intrusion porosimetry to a well known, if hitherto intractable, problem in Geomechanics.

(a) The Problem

The gross porosity, n, of a compacted soil is an inverse function of the energy expended during compaction. It has long been known (e.g. Ref.11) that for most soils the minimum porosity is attained when the degree of saturation, $S_r$, lies within an optimum range of approximately 0.85 to 0.90. Although simple conceptual models, based on considerations of soil structure, have been proposed to explain the characteristic peaked relation between dry density and moisture content (e.g. Ref.12,13), such models are generally restricted to clay soils. Thus it ought to be recognised that, where changes in the structure of soils, other than clays are involved, the mechanisms of compaction are still not fully understood. It was therefore decided to examine whether it was possible to relate changes in the pore system of a soil to its compaction characteristics.

(b) Preparation of Test Specimens

It was decided to examine a soil exhibiting both frictional and cohesive components of shear strength with neither property dominating the soil response. In order to minimise the effects of extraneous variables such as soil composition, mineraology and grading, samples of an artificial soil, whose properties could be controlled and reproduced whenever necessary, were used. The soil comprised a sand-clay composed of 60% Botany sand and 40% commercial kaolinite by weight. The properties of the soil are given in Table I and the compaction characteristics are shown in Figure 1.

Table I. Properties of the Soil

| | | |
|---|---|---|
| Liquid limit | $w_I$ | 26.0% |
| Plastic limit | $w_P$ | 17.6% |
| Plasticity Index | $I_P$ | 8.4% |
| Shrinkage limit | $w_S$ | 14.9% |
| Linear shrinkage | | 6.0% |

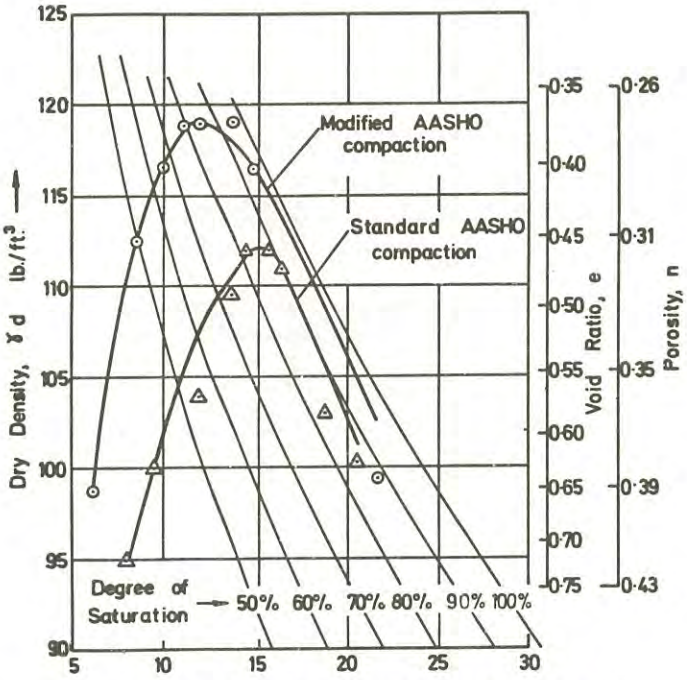


Fig.1 Compaction Characteristics of the soil.

The soil was mechanically mixed and then compacted at 20°C to designated values of dry density and degree of saturation by Floating Mould Compaction; a variant of static compaction known to give specimens of exceptional uniformity (Ref.14). The specimens were prepared to dry densities, $\gamma_d$, of 112, 115.75 and 119.5 lb/ft$^3$ (corresponding to gross porosities, n, of 0.31, 0.29 and 0.27) at saturations, $S_r$, ranging from 0.75 to 0.95. These porosities and saturations were chosen as being typical of many compacted soils. After compaction the specimens were cured for 24 hours and then air dried at 20°C. Residual pore water was removed by drying at 45°C under a vacuum of 74 cm of mercury. Representative samples were then extracted from the dried compacted specimens and determinations of the distributions of equivalent pore sizes in the dried soil were made using the equipment described in the next section.

(c) The Apparatus and Experimental Techniques

The determination of the distributions of pore volumes and pore sizes was made in two stages. First the macropores (pores having radii greater than 75,000 A°) were measured manually. Following this the micropores were measured using the automated equipment.

The distribution of the macropores was determined using the apparatus shown schematically in Figure 2. The first function of this apparatus was to evacuate air from the dilatometer containing the sample. Mercury was then permitted to fill the dilatometer. By opening a needle valve the pressure applied to the mercury could be gradually increased to that of the atmosphere thereby causing the macropores to be intruded. The pressure applied to the mercury was measured by means of a mercury manometer. The volume of the pore space intruded for each increment of pressure was calculated from observations, made with a cathetometer, of the movement of the mercury along a capillary tube of known, constant cross-section which formed the neck of the dilatometer.

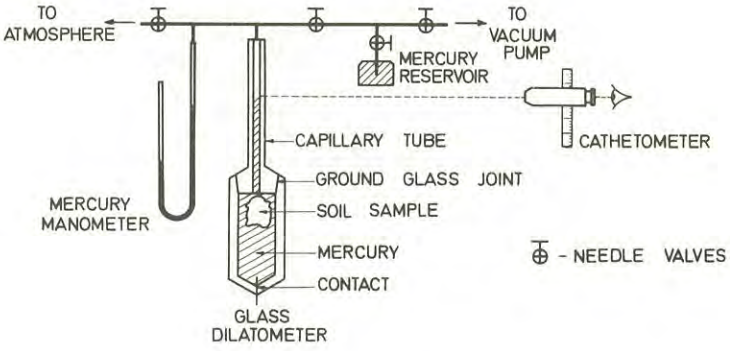


Fig.2. Equipment for measuring macropores

The smallest equivalent pore radius that could be measured using this apparatus was approximately $7 \times 10^4$ A°. The pressure experienced by the sample represented the combined effects of the pressure applied to the mercury and the mercury head. Thus the height of mercury in the capillary tube limited the maximum equivalent pore size that could be measured to approximately $5 \times 10^5$ A°. This restriction on the greatest pore size that can be measured can be largely overcome by filling the dilatometer while in a horizontal position thereby reducing the mercury head to almost zero (Ref.5). Unfortunately the design of the authors' apparatus did not permit this refinement. Consequently macropores with radii in excess of $5 \times 10^5$ A° could not be examined and for many soils the distribution of macropores obtained with the apparatus would be incomplete.

A more serious flaw in the macropore equipment, however, arose from the design of the dilatometers. In order to permit a sample to be loaded into a dilatometer the capillary neck could be removed by breaking

a ground glass joint (Fig.2). The presence of this joint provided a second porous space for the mercury to penetrate during a test. Attempts to entirely eliminate this source of error by calibration failed. Consequently some of the intruded volumes, attributed to the sample, actually arose from a movement of mercury into the joint. Tests indicated that the joint was completely intruded at a pressure corresponding to an equivalent pore radius of approximately $6 \times 10^4$ A°. It is possible to remove this source of error by using one piece dilatometers into which the sample may be introduced through an opening which may be subsequently sealed by fusing the glass walls of the opening together (Ref.10). This requires the use of a fresh dilatometer for each test. The high initial cost of the dilatometers used by the authors prohibited this solution.

From the literature it appears that most of the reported pore size distributions of soils and rocks have been obtained using dilatometers sealed by ground glass joints. It is probable therefore that these distributions may be in error in the macropore range.

In order to determine the distribution of the micropores smaller than 75,000 A° the dilatometer was transferred to the apparatus shown schematically in figure 3. Here the dilatometer was placed in a high pressure bomb which was then filled with alcohol. The alcohol was connected to the high pressure side of a pressure multiplier. By pumping oil into the low pressure side of the multiplier, pressures of up to 1,000 atmospheres could be developed in the alcohol. The position of the mercury in the capillary of the dilatometer was sensed by a steel follower driven by a motor to maintain electrical contact with the mercury. Signals representing the applied pressure and the movement of the follower were fed to a chart recorder which kept a continuous record. The equipment was fully automatic and could complete a test in about 1½ to 2 hours. The range of equivalent pore sizes that could be measured using this equipment was 75 A° to 75,000 A°.

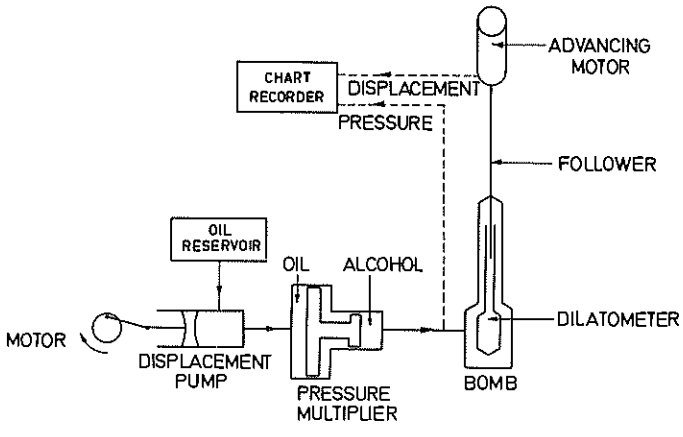


Fig.3 Equipment for measuring micropores

It was observed that on releasing the pressure at the end of a test a small volume of the mercury tended to remain in the sample. Visual examination of specimens at the completion of a test revealed that the soil matrix was invariably stained a grey colour by the mercury retained in it. Thus mercury intrusion is not a fully reversible process.

(d) The Results of the Experiment

The test data were interpreted using the simple model represented by equation 1. Here values of the surface tension, T, of 480 dynes/cm and of the contact angle, $\theta$, of 141.3° were assumed.

A typical frequency distribution of equivalent pore sizes in the soil is shown in figure 4. It will be seen that the frequency distribution is multimodal and in this respect is similar to the distributions observed elsewhere for highly indurated rocks (Ref.5). The cumulative frequency distribution is shown in figure 5.

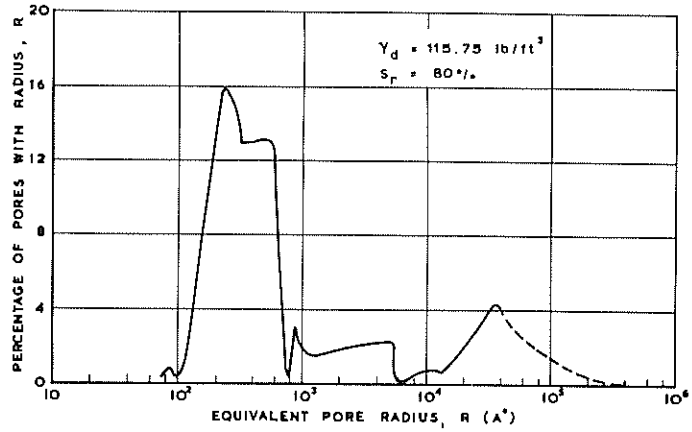


Fig.4 Typical frequency distribution of equivalent pore radii

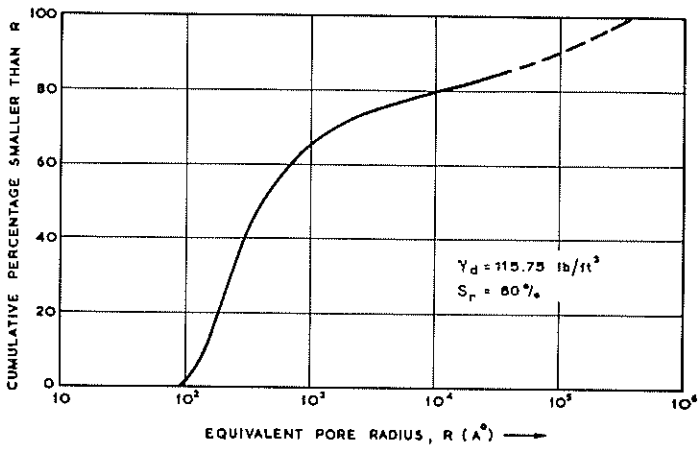


Fig.5 Cumulative frequency distribution of equivalent pore radii

In view of the uncertainties introduced by the presence of the ground glass joint of the dilatometer and in the method used to measure the macropores, it was decided to restrict further analysis to equivalent pore radii lying between 75 A° and 37,500 A°. It was

believed that the results obtained in this range of sizes was relatively free of errors arising from defects in the apparatus.

Two parameters were used to characterise the distributions of pore sizes. These were the median pore radius, $R_{50}$, and a uniformity coefficient, $R_{60}/R_{10}$. As shown in figures 6 and 7, for particular porosities, these parameters were found to be functions of the initial degree of saturation, i.e. the degree of saturation existing immediately after compaction. It can be seen that the median pore sizes and uniformity coefficients converged to single values at saturations of 0.855 and 0.865 respectively.

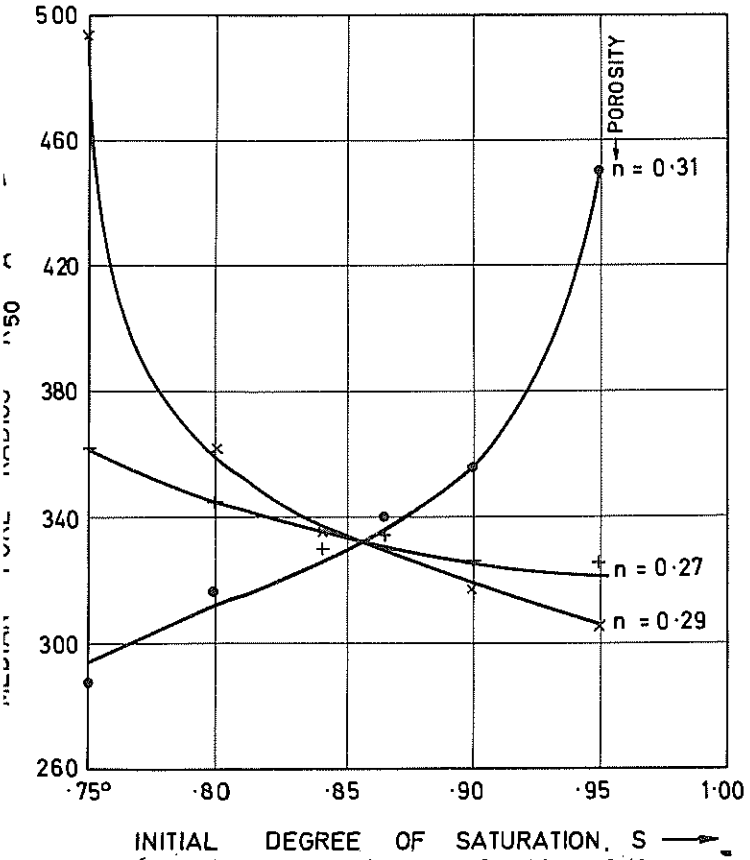


Fig.6 Median pore radius as a function of the initial saturation

In fig.8, the total volumes of pores, in unit dry weight of the soil, having equivalent radii of up to 37,500 A° are plotted as a function of the initial saturation for various porosities. It was established that, for a given gross porosity, the effect of a change in saturation was to vary the total volume of the pores falling within the prescribed range of equivalent pore radii. Moreover the pore volumes were a maximum when the initial saturation was 0.865, i.e. samples compacted at this saturation exhibited a greater proportion of the pore volume made up of small pores than exhibited by samples compacted on either side of this optimum saturation.

Thus within the small range of saturations from 0.855 to 0.865, both the median pore sizes and uniformity coefficients appeared to be single valued, and the pore volumes were a maximum. This range of saturation closely corresponded to that known to give

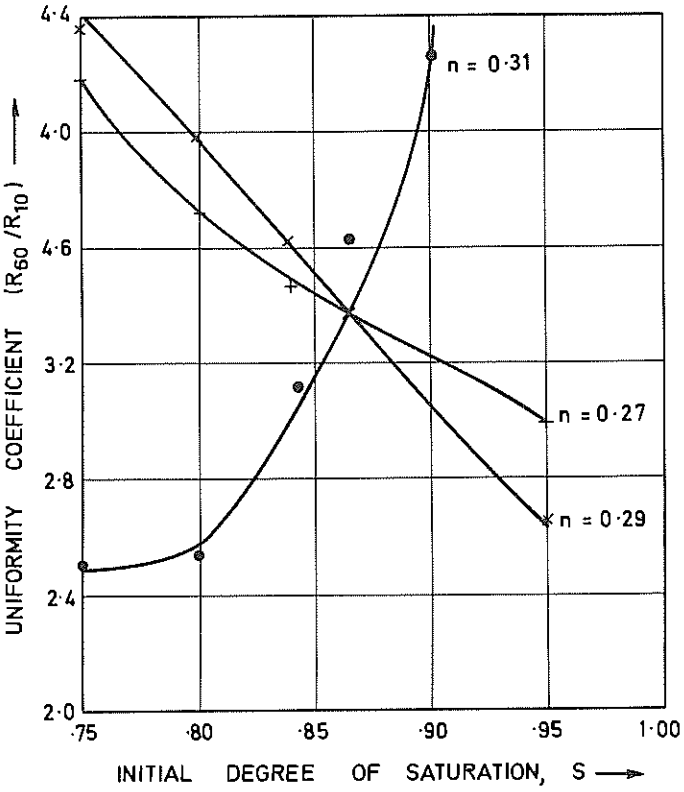


Fig.7 Uniformity Coefficient as a function of the initial saturation

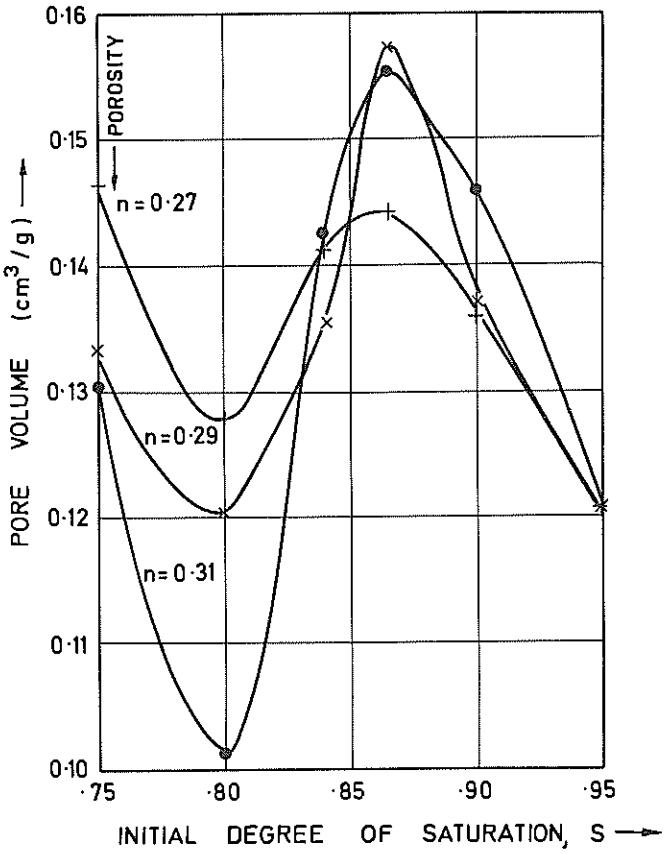


Fig.8 Total pore volume as a function of initial saturation

the minimum gross porosity for any designated energy input. Within this range, the median pore sizes and coefficients of uniformity were independent of the two parameters most commonly employed to characterise the compaction of soils, namely the gross porosity and thus the energy dissipated in compaction. It is concluded that two hitherto unsuspected factors strongly influence the compaction characteristics of soils. These are the total pore volume and the distribution of pore sizes. Moreover, it appears that for soils compacted at optimum moisture content the pore structure is such that it would promote the widest possible distribution of capillary moisture throughout the solid phase.

## VIII.- CONCLUSION

From these initial, exploratory investigations it became clearly evident that the correct explanation of the behaviour of compacted and natural soils should be sought in terms of the behaviour of the pore void phase.

## IX.- ACKNOWLEDGEMENTS

The authors wish to acknowledge the contribution of funds by the Water Research Foundation of Australia Ltd., which made possible the purchase of the porosimeter used in the experimental work.

Some of the work reported here forms part of a PhD research project conducted by B. Shackel under the supervision of Professor D.F. Orchard, Professor of Highway Engineering, University of New South Wales.

## REFERENCES

1. LAFEBER, D. - Soil Structural Concepts Eng.Geol.,Vol.1, No.4, 1966,pp.261-290

2. WINDISCH, S.J. and SOULIE, M. - Technique for Study of Granular Materials. Journal ASCE Vol.96, No.SM4, 1970, pp.1113-1126.

3. ORR, C. and DALLAVALLE, J.M. - Fine Particle Measurement. Macmillan N.Y. 1960.

4. BURDINE, N.T., GOURNAY, L.S. and REICHERTZ,P.P.- Pore Size Distribution of Petroleum Reservoir Rocks. Trans.Am.Inst.Mining Met.Engrs., Vol.189, No.196,1950.

5. SHERWOOD, W.C. and HUANG, J.H. - Pore Studies of Highly Indurated Appalachian Rocks - Bull.Am. Assoc.Petrol.Geol., Vol.53/10,Pt.1, 1969, pp.2161-2170.

6. DIAMOND, S. - Pore Size Distribution in Clays. Clays and Clay Minerals, Vol.18, 1970, pp.7-23.

7. KLOCK, G.O., BOERSMA, L. and DeBACKER, L.W. - Pore Size Distributions as Measured by the Mercury Intrusion Method and their Use in Predicting Permeability. Proc. Soil Sci.Soc. America, Vol.33, No.1,1969, pp.12-15.

8. WASHBURN, E.W. - Note on a Method of Determining the Distribution of Pore Sizes in a Porous Material. Proc.Nat.Acad.Sci.U.S. Vol.7, 1921, pp.115-116.

9. MATYAS, E.L. - Air and Water Permeability of Compacted Soils. ASTM, STP417, 1967, pp.160-175.

10. RITTER, H.L. and DRAKE, L.C. - Pore Size Distribution in Porous Materials. Ind. Eng. Chem. Anal. Ed. 1945, pp.782-786.

11. WOODS, K.B. - Compaction of Earth Embankments Proc. HRB Vol.18(2), 1938.

12. LAMBE, T.W. - Soil Stabilisation Chapter 4 of Foundation Engineering - G.A.Leonards Ed. McGraw Hill, N.Y. 1962.

13. SEED, H.B. and CHAN, C.K. - Structure and Strength Characteristics of Compacted Clays. Journal ASCE, Vol.85, No.SM5, 1959.

14. SHACKEL, B. - The Compaction of Uniform Replicate Soil Specimens. Journal Aust.Rd.Res.Board,Vol.4, No.5, 1970, pp.12-31.

---

Pore symmetry.

Dilation

# The Influences of Structure on the Dilatation of Clay

By

J. D. Nelson, M.S., Ph.D.

(Associate Professor of Civil Engineering, Asian Institute of Technology, Thailand)

AND

K. L. Siu, M.Eng.

(Assistant Lecturer, Hong Kong Baptist College)

SUMMARY.- The dilatation characteristics of clays during shear are presented for several soils with different structures. The dilatation is considered to be caused by the release of strain energy that had been stored in diagenetic bonds during consolidation and unloading. An increase in the overconsolidation ratio increased the amount of strain energy stored in the bonds. Consequently, the dilatation increased. Soils with greater amounts of recoverable strain energy could exhibit either a greater or smaller amount of dilatation depending on the strength of the bonds, and their ability to store strain energy without failing during overconsolidation.

## I.- INTRODUCTION

One of the most significant characteristics of overconsolidated clay is the dilatation which occurs during shear. In dense sand dilatation is caused by interlocking between particles and its magnitude depends primarily on the initial void ratio. However, in clay it depends mainly on the overconsolidation ratio. In fact, for a particular maximum past pressure a soil having a higher overconsolidation ratio, and thus a higher initial void ratio, would exhibit a greater tendency to increase its volume during shear.

Many hypotheses have been proposed to explain this phenomenon. Rosenqvist (Ref. 1) suggested that it was due to reorientation of the particles. Hvorslev (Ref. 2, 3) considered that it was due to the liberation of swelling pressure which had been stored in some form of internal energy during consolidation. Lambe (Ref. 4) proposed that it was the result of changes in electrical forces caused by particle interference. Trollope and Chan (Ref. 5) suggested that dilatation was caused by physical interaction between hydrated ions. Scott (Ref. 6) explained the volume change mechanism using a bar magnet-spring model. Rowe, et al. (Ref. 7) concluded that the volume change of clay was similar to that of sand.

The above concepts do not explain fully the complicated mechanism of dilatation. In a study of overconsolidated clay, Bjerrum (Ref. 8) considered that during consolidation, diagenetic bonds would form at points of close proximity of the mineral surfaces or points of very high stress. These bonds were considered to be capable of storing strain energy when the consolidation load was removed. When the clay was subjected to shear, the failure of the diagenetic bonds would have released some recoverable strain energy which in turn would induce an increase in volume. Nelson and Hengchaovanich (Ref. 9) found this concept to be adequate to explain the observed behavior of an undisturbed stiff marine clay.

In accordance with this concept, clays with different structures should exhibit different degrees of dilatation during shear. Consequently, the investigation reported herein was conducted to study the dilatation characteristics of soils having different structures. In this text the term "structure" will be taken to include particle arrangement, interparticle forces and factors influencing the nature or magnitude of the interparticle forces. Also, dilatation will be considered to be an increase in volume of the soil.

Samples were prepared by sedimentation in sodium chloride solution. The soil was subsequently leached with distilled water to achieve various final salt concentrations in the pore fluid. In addition, one sample was prepared by sedimentation in sodium hexametaphosphate solution. Isotropically consolidated undrained triaxial tests with pore pressure measurement were performed on the samples.

It was observed that the tendency of soil to dilate depends on the stress history of the soil, the strength of the diagenetic bonds and the electrical interparticle forces. The tendency to dilate increased with an increase in strength of diagenetic bonds and overconsolidation ratio.

## II.- EXPERIMENTAL INVESTIGATION

### (a) Soil Description

The soil used in this study was a gray, slightly weathered clay taken from a test excavation at Rangsit, 42 km north of Bangkok, Thailand. The soil is an alluvial clay containing montmorillonite with lesser amounts of illite and kaolinite (Ref. 10). Its general properties are shown in Table I.

### (b) Sample Preparation

Four different groups of samples were prepared. Three of these were prepared by sedimentation in salt water (NaCl) and they are referred to as flocculated soil. Of the three samples, two were

leached with distilled water to achieve different final salt concentrations in the pore fluid. The fourth sample was prepared in sodium hexametaphosphate solution and this is referred to as the dispersed soil. It is recognized that considerable flocculation probably existed in both samples, but as will be seen later, the dispersed soil appeared to exhibit a less random orientation than the flocculated soil.

TABLE I

GENERAL SOIL PROPERTIES

| Properties | Values |
|---|---|
| Natural water content | 63.5 - 66% |
| Liquid limit | 70 - 71.5% |
| Plastic limit | 32 - 34.5% |
| Specific gravity | 2.70 |
| Particle size distribution | |
| sand 2-0.074 mm | 4% |
| silt 0.074-0.005 mm | 38% |
| clay 0.005 mm | 58% |

The method of preparation was similar to that adopted by Bjerrum and Rosenqvist (Ref. 11) and is discussed briefly below. A more detailed discussion of the procedure is presented elsewhere (Ref. 12).

Sedimentation of the flocculated soil was accomplished by introducing a suspension into perspex cylinders in increments of about 550 grams. The soil suspension had a water content of 200 per cent and used 1.5 N sodium chloride solution as the pore fluid. For the samples that were subjected to leaching, distilled water was allowed to percolate through the soil until the salt concentration in the porefluid had reached 17 gm/l (0.3 N) in one sample and 6 gm/l (0.1 N) in the other. All samples were consolidated one-dimensionally in the cylinders under a pressure of 10 lb/in$^2$ prior to sampling. This pressure was equivalent to the in situ overburden pressure of the natural soil.

The dispersed sample was prepared in a similar manner except that the suspension was introduced in increments of about 150 grams and sodium hexametaphosphate solution was used as the pore fluid.

The soil samples were divided into four groups according to the conditions of sedimentation and leaching as described previously. Isotropically consolidated undrained triaxial tests with pore pressure measurement were performed on each sample. The samples were consolidated under a pressure of 120 lb/in$^2$ and then unloaded to obtain overconsolidation ratios of 24, 15, 8, 3, and 1.

All samples were tested by using conventional triaxial equipment and procedures. A loading rate of 0.00156 in/min was used throughout.

## III.- RESULTS AND DISCUSSION

### (a) General Soil Properties

Table II summarizes the properties of the artifically sedimented soils used in this study. Of particular interest is the fact that although the horizontal shrinkage of the dispersed sample is only slightly greater than that of the flocculated samples, the vertical shrinkage is considerably more. This suggests a more orderly particle arrangement in the dispersed sample. If the orientation were random the shrinkage should have been the same in all directions as was nearly true for the flocculated soil.

### (b) Consolidation Characteristics

Fig. 1 shows the isotropic consolidation characteristics of the various samples. For the flocculated soil the compressibility was unaffected by leaching. However, the unleached soil expanded less than the leached soil when unloaded. When the pressure had decreased to less than about 15 lb/in$^2$ the rebound curve for the unleached soil approached the curves for the leached soils.

At small strains, the compressibility of the soil depended primarily on the geometric arrangement of the particles (Ref. 13). Since the particle arrangement was not influenced appreciably by the leaching process, the compression portions of the curves for all flocculated samples coincided.

The difference between the rebound curves reflects the difference in the amount of strain energy that was stored in the soils. As the soil was loaded, strain occurred by deformation of the particles and by changes in the particle spacing so as to produce electrical interparticle forces and interparticle contact forces of a magnitude that would be in equilibrium with the externally applied forces. During loading, diagenetic bonds were formed between the particles (Ref. 8). When the soil was unloaded these diagenetic bonds prevented the particles from returning to the spacing to which they would have returned if the bonds had not existed. Therefore, some of the recoverable strain energy of the soil was stored in the diagenetic bonds (Ref. 9). The stress induced in the bonds was a function of the imbalance between the interparticle forces and the externally applied forces. Thus, for any particular soil the greater the OCR was, the greater should have been the stress induced in the bonds, i.e. the amount of stored strain energy.

The exact nature of these diagenetic bonds is not clear but they are believed to be the result of extremely high stresses and very close contact between particles at points of "contact". Another contributing factor to these bonds may have been a bridging type of bonding resulting from a higher concentration of adsorbed ions at points of close proximity between particles (Ref. 14). The decrease in salt concentration during leaching would decrease the strength of this type of bond. The effect of leaching on other factors influencing bond strength is not clearly known, but it appeared that the net effect of leaching was to decrease the bond strength.

Leaching would also have increased the electrical repulsion forces between particles. This could result in the interparticle forces changing from a net attraction force to a net repulsion force at certain interparticle spacings.

During unloading more bonds failed in the leached soil than in the unleached soil because of

TABLE II

PROPERTIES OF SOIL AFTER SEDIMENTATION

| Soil Property | Flocculated Soil | | | Dispersed Soil |
|---|---|---|---|---|
| | Unleached | Leached | Leached | |
| Soluble salt content[1] | 84 gm/l (1.5 N) | 17 gm/l (0.3 N) | 6 gm/l (0.1 N) | |
| Liquid limit | 68 - 70% | 68 - 71% | 69 - 70% | 74 - 76% |
| Plastic limit | 32 - 33% | 31 - 33% | 33 - 34% | 37 - 38% |
| Sensitivity[2] | 3.4 | 4.7 | 5.3 | 5.4 |
| Vertical shrinkage[3] | 1.19-1.23 | 1.18-1.28 | 1.19-1.24 | 1.30-1.32 |
| Horizontal shrinkage[3] | 1.16 | 1.16 | 1.16 | 1.19 |
| Effective cohesion intercept | 3.3 lb/in$^2$ | 2.7 lb/in$^2$ | 2.2 lb/in$^2$ | 4.2 lb/in$^2$ |
| Effective angle of friction | 24.1° | 22.3° | 22.3° | 18.1° |

1 From measurement of the conductivity of the solution
2 From unconfined compression tests
3 Ratio of linear dimension of undisturbed soil to that of oven dry soil

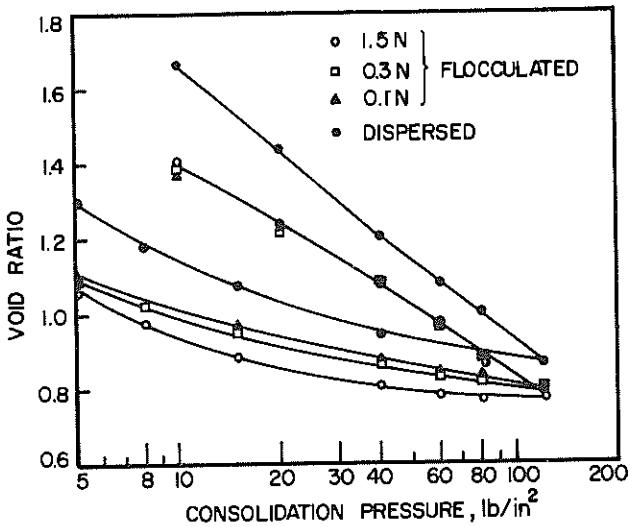


Fig. 1 Isotropic Consolidation Characteristics

the weaker bonds and the greater stresses induced in them by the larger repulsion forces. Thus, during rebound more strain energy was stored in the unleached soil. Also, it is seen from Fig. 1 that the amount of strain energy stored in the soil was inversely proportional to the amount of leaching.

At high values of OCR, the imbalance between internal and external forces was great enough to cause failure of an increased number of bonds in the unleached soil. Hence, the rebound curves for all three flocculated soils tended to converge at low pressures. Nevertheless, the amount of strain energy stored in the various flocculated soils at all pressures was inversely proportional to the degree of leaching.

Because of the difference in initial water contents, the consolidation curve of the dispersed soil is displaced considerably from those of the flocculated soils. Also, the dispersed soil was more compressible than the flocculated soil. This was because the dispersed soil had a comparatively thicker double layer, a more parallel particle arrangement and less actual particle contact. Because of the less random particle arrangement the dispersed soil had fewer interparticle contact points at which diagenetic bonds could form during consolidation. In addition the different electrolyte may have resulted in weaker diagenetic bonds in the dispersed soil. Consequently, the dispersed soil rebounded more than the flocculated soil and considerably less recoverable strain energy was stored in the dispersed soil during unloading.

(c) Stress-Strain Relationships

Fig. 2 through Fig. 5 show the normalized deviator stress as a function of strain for the various samples. Stresses were normalized by dividing by the value of the consolidation pressure prior to shear.

By comparison of the various curves it can be seen that the maximum deviator stresses of the normally consolidated samples did not differ significantly from each other. Along the loading portion of the consolidation curve no stresses were induced in the diagenetic bonds other than what could normally be carried just by contact between particles, with the exception of possibly some small sliding or shear stresses. Thus, these bonds contributed little or no strength to the normally consolidated samples.

For overconsolidation ratios greater than unity, the normalized deviator stress decreased with an increase in the amount of leaching. The increase in normalized deviator stress with OCR is caused by the stored strain energy in the diagenetic bonds. Thus, the bonds caused the internal stress in the soil to be greater than what would have existed if the bonds had not stored energy. The increase in internal stress resulted in a strength greater than what the soil would have had at that consolidation pressure if it was normally consolidated. Furthermore, the relative increase in strength was greater at higher overconsolidation ratios because of the greater imbalance between internal and external stresses.

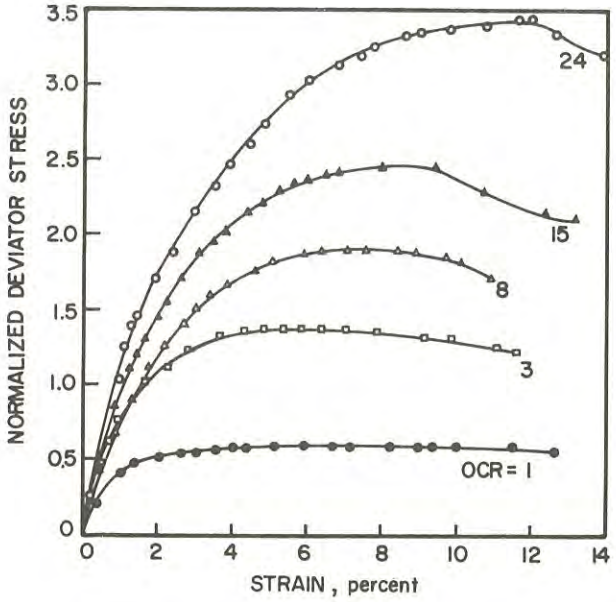


Fig. 2 Normalized Deviator Stress vs Strain Unleached Flocculated Soil (1.5N NaCl)

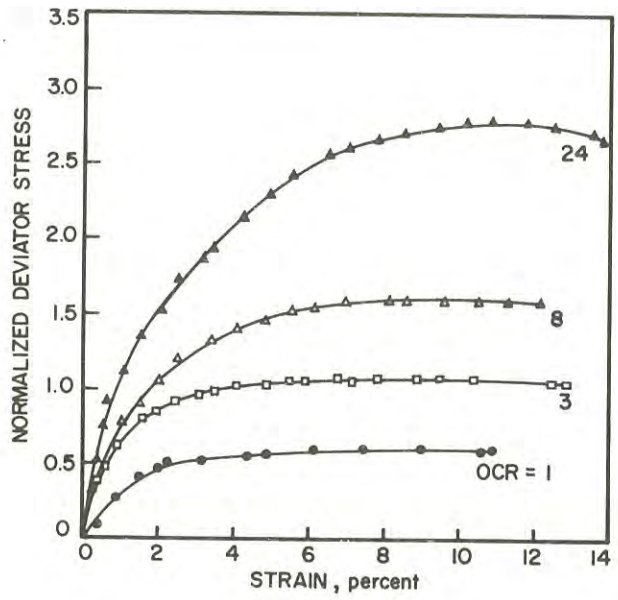


Fig. 4 Normalized Deviator Stress vs Strain Leached Flocculated Soil (0.1N NaCl)

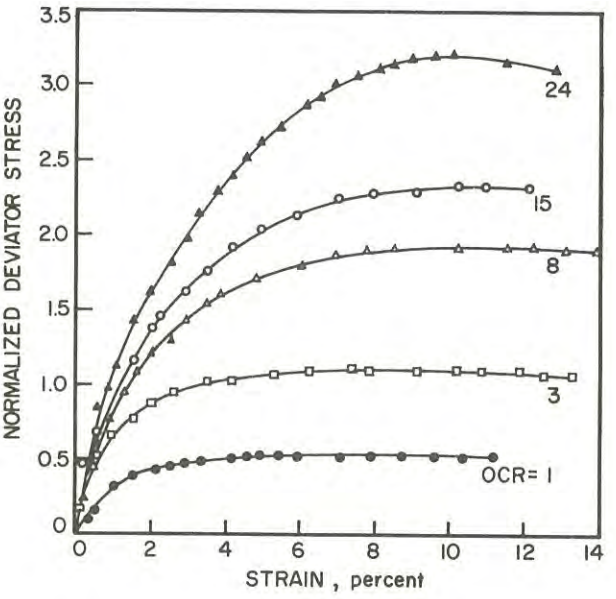


Fig. 3 Normalized Deviator Stress vs Strain Leached Flocculated Soil (0.3N NaCl)

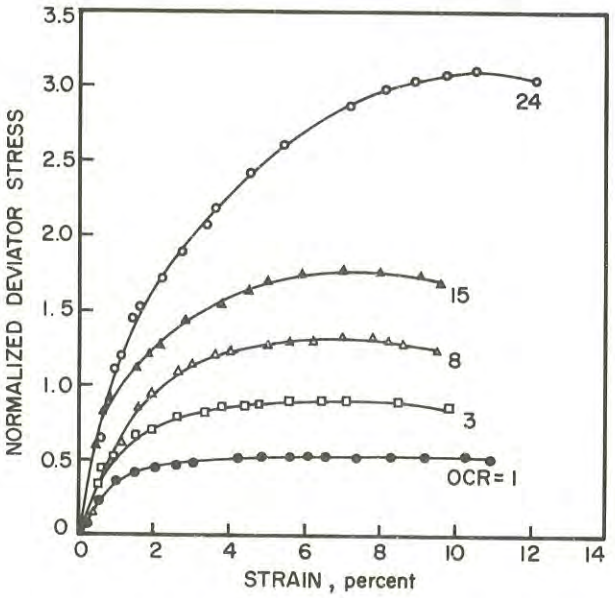


Fig. 5 Normalized Deviator Stress vs Strain Dispersed Soil

The relative increase in strength would also depend on the strength of the bonds. Thus, the decrease in maximum normalized deviator stress as the leaching increased indicates a decrease in the strength of the bonds.

In this regard it is interesting to note that the unleached soil exhibited somewhat more of a peak in the stress-strain curve than the leached soil did. If this peak is caused by a decrease in strength when the bonds were broken, the soil with the stronger bonds should have exhibited the more pronounced peak. Although the maximum strains to which the samples were subjected were not large enough to show the actual ultimate strength, the general trends indicated in Fig. 2 through 4 are in agreement with the hypothesis that the leaching decreased the strength of the diagenetic bonds.

In general, the maximum normalized deviator stress in the dispersed soil was lower than in the flocculated soil. This also indicates weaker interparticle bonding in the dispersed soil. The less random particle arrangement may also have contributed

to the lower shear resistance. An exception was for the dispersed sample with an OCR of 24. This exception was due to a relatively large negative excess pore pressure in the soil just prior to testing. This was caused by the low permeability and greater swelling in the dispersed soil.

(d) Mechanism of Dilatation

The pore pressure parameter, A, and the normalized pore pressure are shown as functions of strain for unleached flocculated soil in Fig. 6 and 7. The same general trends of behavior were exhibited in all soils but are not presented for the sake of brevity. Only the general shapes of the curves are necessary to discuss the mechanism of dilatation.

When the overconsolidated soils were sheared, the pore pressure parameter and the normalized pore pressure increased initially, but after that they decreased as the strain increased. This decrease in pore pressure and parameter A indicates a tendency of the sample to dilate. If the sample had been allowed to drain during shear it would have dilated.

As discussed previously, the diagenetic bonds that formed during consolidation prevented the soil from rebounding fully when it was unloaded. Thus, the internal repulsion forces were greater than what was required for equilibrium with the external forces and the difference between the external forces and the interparticle forces was resisted by the diagenetic bonds. When the sample was sheared the diagenetic bonds were broken and no longer resisted the difference in forces. Consequently, a negative pore pressure (or a decrease in positive pore pressure) was necessary in order to maintain equilibrium (Ref. 9 and 12). In a drained sample the particles would have attained a larger spacing (i.e. dilatation) to decrease the interparticle repulsion forces.

It follows that the amount of dilatation that will take place depends upon the amount of strain energy stored in the diagenetic bonds. The greater the overconsolidation ratio is, the greater should be the amount of strain energy stored in the soil. Consequently, highly overconsolidated clays exhibit a greater tendency to dilate than do slightly overconsolidated clays. Furthermore, the diagenetic bonds in normally consolidated soil do not store energy, and hence, normally consolidated soils do not exhibit a tendency to dilate. This explains why the dilatancy of clay depends primarily on OCR and not void ratio as is the case in sands.

In Fig. 6 and 7 it can be seen that at a strain of about 0.01 the pore pressure parameter began to decrease but the pore water pressure continued to increase. This indicates that some of the weaker bonds had begun to fail but the amount of energy released was not sufficient to cause dilatation to occur. At larger strain more strain energy was released as more and stronger bonds failed and the soil tended to dilate.

(e) Influence of Soil Structure on Dilation

Fig. 8 shows the pore pressure parameter at failure, $A_f$, as a function of overconsolidation ratio, OCR. Since the pore pressure parameter is a

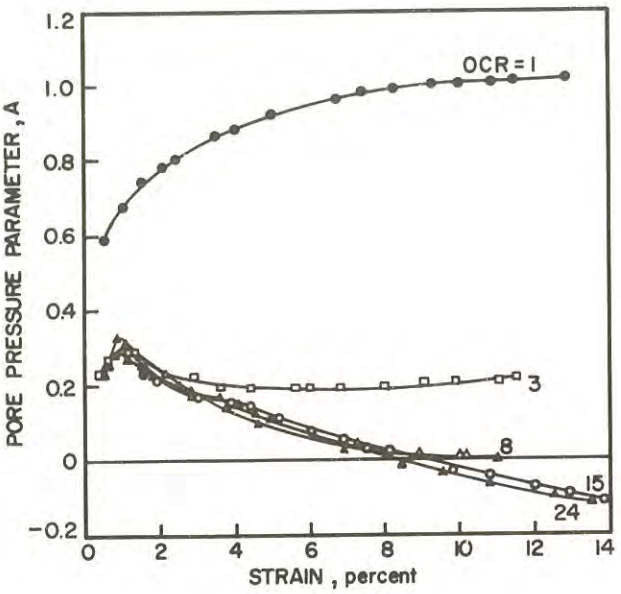


Fig. 6 Pore Pressure Parameter, A, vs Strain Unleached Flocculated Soil

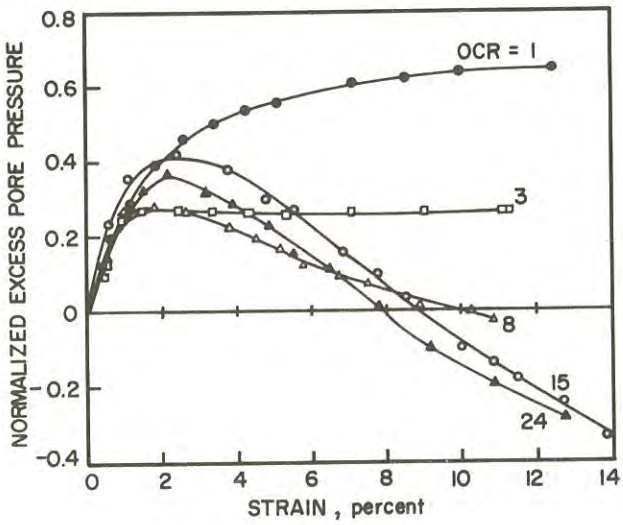


Fig. 7 Normalized Excess Pore Pressure vs Strain Unleached Flocculated Soil

function of the change in pore pressure and applied shear stress, low values of $A_f$ indicate a tendency for the soil to dilate.

In general, the pore pressure parameter increased as the final salt concentration in the pore fluid decreased. The dispersed sample exhibited the least tendency for dilatation. The curves converge at an OCR of unity and at high values of OCR. However, at intermediate values of OCR a considerable difference exists. It should be noted that the curves in Fig. 8 are very similar to the rebound curves in Fig. 1 in regard to their relative positions and the spacing between curves at different

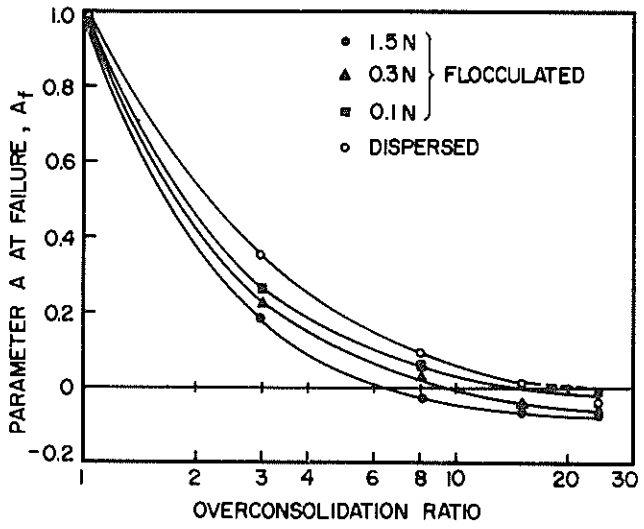


Fig. 8 Effect of OCR on $A_f$

values of OCR.

The particle arrangement of the flocculated soils was probably similar to a "card-house" type of arrangement and a considerable amount of interparticle contact probably existed. As was pointed out by Bjerrum (Ref. 8), deformation of the particles may contribute greatly to the recoverable strain energy. Thus, in the flocculated soil even if the net electrical force was attraction the resultant interparticle force would be repulsion. The repulsion force then induced stress in the diagenetic bonds in all soils during unloading of the soil.

However, if the leaching increased the repulsion forces and if a sufficient amount of electrical interaction existed in the flocculated soils this would have had the effect of increasing the stresses induced in the bonds in the leached soil. If the greater stress was sufficient to cause failure of more diagenetic bonds this would explain, in part, why the leached soil stored less strain energy during rebound. Considerably more research is necessary, however, to explain fully the reasons why the various soils stored different amounts of strain energy.

It was seen from Fig. 1 that the unleached soil appeared to store the greatest amount of strain energy. As seen from Fig. 8 it also exhibited the greatest tendency to dilate. Similarly, a greater amount of leaching decreased the amount of strain energy stored in the bonds, and hence, decreased the tendency of the soil to dilate.

In Fig. 1 it is seen that the dispersed soil exhibited the greatest amount of rebound and in Fig. 8 it showed the least tendency to dilate. The anomalous point at an OCR of 24 in Fig. 8 is believed to be due to the residual pore pressure in this soil after rebound, as discussed previously. In view of the expected greater electrical interaction between particles and the less random orientation of particles this soil should have contained more recoverable strain energy than the flocculated samples. However, formation of diagenetic bonds would have occurred mainly at points of high interparticle stresses and close proximity between mineral surfaces, i.e. points of edge to face contact (Ref. 8). Because of the less random particle orientation fewer such points existed in the dispersed soil and fewer diagenetic bonds were formed in this soil. Consequently, a relatively small amount of strain energy was stored in the soil, and it exhibited a relatively small tendency to dilate.

Finally, it was stated previously that under normally consolidated conditions little or no strain energy was stored in the diagenetic bonds. Thus, dilatation did not occur in the normally consolidated clay samples.

## IV.- CONCLUSION

A mechanism for the dilatation of clays has been put forth. According to this hypothesis it was considered that during consolidation, diagenetic bonds were formed in the soil. When the consolidation pressure was reduced, these bonds carried some of the internal stress, and hence, recoverable strain energy was stored in the bonds. When the soil was sheared, the bonds were broken and the consequent release of strain energy resulted in dilatation.

It was seen that the amount of recoverable strain energy stored in the bonds, and hence, the amount of dilatation that the soil exhibited depended on 1) the stress history of the soil 2) the strength of the diagenetic bonds and 3) the amount of recoverable strain energy in the soil.

As the OCR increased, the amount of strain energy stored in the bonds increased. Thus, the dilatation increased as the OCR increased.

The stronger the diagenetic bonds were the greater was the ability of the soil to store strain energy. If the bonds were too weak, they failed during rebound of the soil after consolidation. Hence, soils with weak bonds were not capable of storing as much strain energy as soils with stronger bonds, and the dilatation decreased as the strength of the bonds decreased.

Soils with a small amount of recoverable strain energy would not induce much stress (i.e. strain energy) in the diagenetic bonds. Hence, not much dilatation would occur in such soils.

In normally consolidated clays, diagenetic bonds may have been formed, but there was little or no recoverable strain energy stored in them. Consequently, dilatation did not occur when these soils were sheared.

## REFERENCES

1. ROSENQVIST, I.Th. - Physical-Chemical Properties of Soils; Soil Water Systems. Jour. Soil Mech. Found. Engg. Div., Proc. ASCE, Vol. 85, No. SM2, 1959, pp. 31-53.

2. HVORSLEV, M.J. - Discussion on Soil Properties. Proc. Third Int. Conf. Soil Mech. Found. Engg., Zurich, Vol. 3, 1953, pp. 122-124.

3. HVORSLEV, M.J. - Physical Component of the Shear Strength of Saturated Clays. Research Conf. on Shear Strength of Cohesive Soils, Proc. ASCE, 1960, p. 169.

4. LAMBE, T.W. - A Mechanistic Picture of Shear Strength in Clay. Research Conf. on Shear Strength of Cohesive Soils, Proc. ASCE. p. 437.

5. TROLLOPE, D.E. and CHAN, C.K. - Soil Structure and the Step-Strain Phenomenon. Jour. Soil Mech. Found. Engg. Div., Proc. ASCE, Vol. 85, No. SM2, 1959, pp. 1-39.

6. SCOTT, R.F. - Principles of Soil Mechanics. Addison - Wesley, 1963, 550 pp.

7. ROWE, P.W., OATES, D.B. and SKERMER, N.A. - The Stress-Dilatancy Performance of Two Clays. ASTM Lab. Shear Testing of Soil, 1963, pp. 134-143.

8. BJERRUM, L. - Progressive Failure in Slopes of Overconsolidated Plastic Clay and Clay Shales. Jour. Soil Mech. Found. Engg., Proc. ASCE, Vol. 23, No. SM5, 1967, pp. 1-49.

9. NELSON, J.D. and HENGCHAOVANICH, D. - Effect of Overconsolidation on the Shear Strength Characteristics of a Marine Clay. Proc. Second South East Asian Conf. Soil Mech. Found. Engg., Singapore, 1970, pp. 1-9.

10. HALEY & ALDRICH INC. - Report on Soil and Foundation Investigations in Bangkok and Thonburi, For Camp, Dresser and McKee, Consulting Engineers, 1968.

11. BJERRUM, L. and ROSENQVIST, I.Th. - Some Experiments with Artificially Sedimented Clays. Geotechnique, Vol. 6, No. 3, 1956.

12. SIU, K.L. - Effect of Soil Structure on Dilatation. Thesis (M.Eng.), Asian Institute of Technology, 1970.

13. BJERRUM, L. and KENNEY, T.C. - Effect of Structure on the Shear Behaviour of Normally Consolidated Quick Clays. Proc. Geotechnical Conf. Oslo, Vol. 2, 1967.

14. NELSON, J.D. and VEY, E. - Relative Cleanliness as a Measure of Lunar Soil Strength. Journal of Geophysical Research, Vol. 73, No. 12, 1968, pp. 3747-3764.

# The Collapse of Clastic Aggregates

By
D. H. Trollope, M.Sc., Ph.D., D.Eng., F.I.E.Aust.
(Professor of Civil Engineering, James Cook University of North Queensland)

SUMMARY.- Analysis of the failure conditions of an ideal systone has been applied to the failure of granular materials. Both theory and experiment suggest that the plane strain strength of such materials is significantly greater than that in triaxial compression. An approximate theory relating these two strengths is presented.

## I.- INTRODUCTION

Traditional analyses of the behaviour of natural materials are based on the assumption of an element, which in itself, represents the macro behaviour of the material at large. This element may conveniently be described as the Cartesian Molecule (Figure 1) which satisfies the requirements of reproducible regularity and physical continuity. Since the 1930's it has been evident that the fundamental atomic element of matter is quasi-spherical rather than parallelipipedic. Aggregates of the fundamental units are therefore anisotropic and physical isotropy, or anisotropic regularity, can only be achieved by the concept of random arrangements of the aggregate (or clastic) unit (Ref. 1).

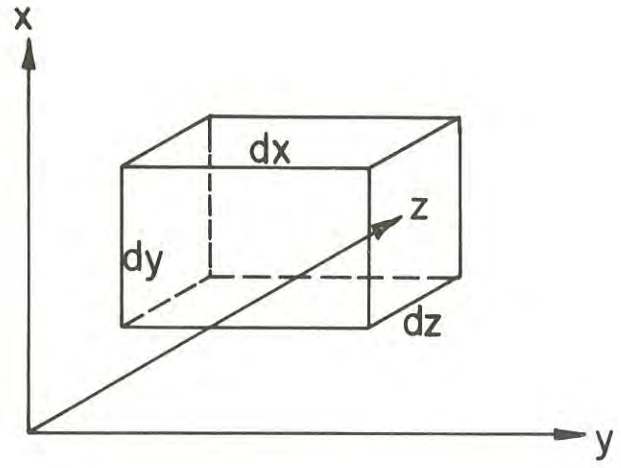


The 'Cartesian' Molecule

Fig. 1.

It is pertinent, therefore, to examine the properties of a clastic element as a sub-unit of the Cartesian Molecule. From the point of view of collapse of such an element, the first successful treatment is due to Rennie (Ref. 2) who regarded a clastic unit as a close-packed assembly of mono-sized spheres (a systone, Ref. 1) and defined collapse as incipient gap formation (or negative displacement) at an opposite pair of contacts.

The purpose of this paper is to examine the properties of the systone, firstly in its simplified two dimensional (disc) form and then to apply this information to the strength of natural aggregates such as sand.

## II.- THE IDEAL ELEMENT

The simulation of an isotropic element necessitates a random arrangement of systones. It is interesting to realise that Osborne Reynolds (Ref. 3) had a similar concept although it lacked mathematical expression. Quoting from Reynold's paper "a model consisting of equal spheres is the most general and presents least difficulty" and further, "practically when the boundaries (of systones) are not plane, or when the grains are of various sizes or shapes, such media consist of more or less crystalline groups having their axes in different directions, so that their mean condition is amorphorous" (or isotropic)*. The ideal "element" therefore consists of a random array of systones as shown in two-dimensional form in Figure 2.

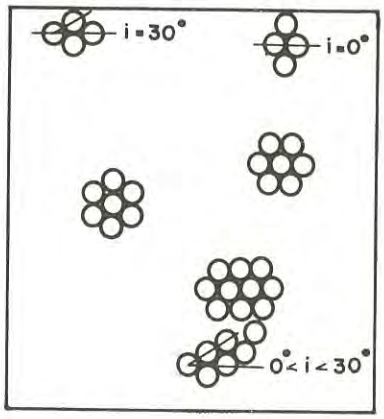


The Ideal Element -
A Random Array of Systones

Fig. 2.

*Author's Note

III.- THE COLLAPSE OF AN IDEAL ELEMENT

It is assumed that, in a typical element each systone is subjected to an average stress condition, fully defined, in two-dimensions, by the principal stresses $\sigma_1$, $\sigma_3$ and the angle i.

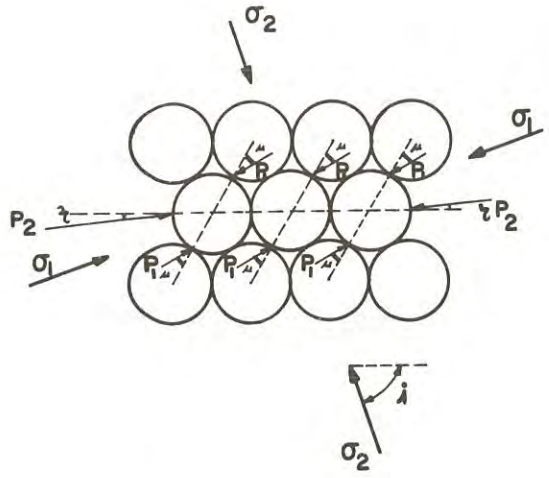


General Two-Dimensional Model

Fig. 3.

Figure 3 illustrates this condition and it may be shown that at incipient collapse when one pair of contact forces vanishes then, on an incipient plane of failure

$$\sigma_n = P_1 \sin(90-\theta-\phi_\mu)$$

$$\tau = P \cos(90-\theta-\phi_\mu)$$

where $\theta$ is the distribution angle (Ref. 1) (= $30^o$ for discs), $\phi_\mu$ is the angle of contact friction.

Recognising that the geometry of the systone may be related to the orientation of the principal stress system through the angle 'i', equations 3.1 may be expressed as

$$\frac{\sigma_n}{\tau} = \tan(90-\theta-\phi_\mu) = \frac{\sigma_{1_f} + \sigma_{3_f}}{\sigma_{1_f} - \sigma_{3_f}} \operatorname{cosec} 2i + \cot 2i \qquad ...3.2$$

or

$$\frac{\sigma_{1_f}}{\sigma_{3_f}} = \frac{\cos(90-\theta+2i-\phi_\mu) - \cos(90-\theta-\phi_\mu)}{\cos(90-\theta+2i-\phi_\mu) + \cos(90-\theta-\phi_\mu)} \qquad ...3.3$$

where $\sigma_{1_f}$= major principal stress at collapse
$\sigma_{3_f}$= minor principal stress at collapse.

Figure 4 shows a plot of equation 3.3 in terms of the inclination variable (i) and it is evident that the family of solutions to equation 3.3 have minima of

$$\frac{\sigma_{1_f}}{\sigma_{3_f}} = \tan^2(90-\theta+\frac{\phi_\mu}{2}) \qquad ...3.4$$

occurring when

$$i = \frac{1}{2}[(n-\tfrac{1}{3})\ \pi + \phi_\mu] \qquad ...3.5$$

Conventionally the failure, or collapse, condition is defined as ···

$$\frac{\sigma_{1_f}}{\sigma_{3_f}} = \tan^2(45 + \phi/2) \qquad ...3.6$$

where $\phi$ is the so-called angle of internal friction.

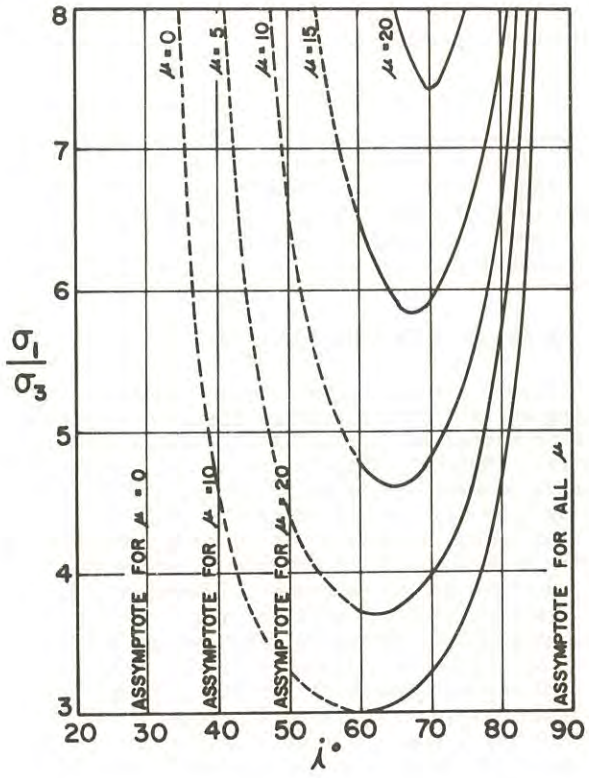


General Strength Solution in Two Dimensions

Fig. 4.

Comparing equations 3.3, 3.4, 3.5 and 3.6 it is clear that if the failure of a granular medium is to be described in clastic terms then, in general the value of $\phi$ depends upon

- $\theta$ - the distribution angle which defines the rotundity (Ref. 4) of the particles.
- i - the orientation of the systone, i.e. the packing geometry.
- $\phi_\mu$ - the angle of contact friction between particles.

Equation 3.3 shows that the orientation in space of the systone (i) is an important variable.

IV.- THE FAILURE OF AN IDEAL ELEMENT

Rennie (Ref. 2) originally implied that failure would automatically follow as soon as equation 3.4 was satisfied i.e., as soon as the weakest systone reached its maximum strength. If this were true then, assuming that a granular medium such as sand could be represented by the ideal disc systone, we would have that

$$\frac{\sigma_{1_f}}{\sigma_{3_f}} = \tan^2(60 + \frac{\phi_\mu}{2}) = \tan^2(45 + \phi/2) \qquad ...4.1$$

or

$$\phi = \phi_\mu + 30^o \qquad ...4.2$$

In an ideal isotropic element however, all values of 'i' are equally possible and the maximum possible strength at failure is

$$\frac{\sigma_{1_f}}{\sigma_{3_f}} \rightarrow \infty \qquad ...4.3$$

The maximum strength must therefore lie between the values given by equations 4.1 and 4.3. It is to be noted that, in the ideal situation, a given systone may be reduced from infinite strength to the minimum value merely by rotation with respect to the principal stress directions through an angle of $i = (30 - \phi_\mu/2)$.

## V.- THE STRONG SYSTONE HYPOTHESIS

Consider a random array of disc systones representing an isotropic element. If a line - representing a potential failure plane - is drawn through such an array, then all orientations of the systone have an equal probability of being found on this line, including some systones of, theoretically, infinite strength (equation 4.3). In contrast with the simple tension mechanism, which depends on its weakest element, a shear mechanism cannot be propagated until the strongest systones collapse and, ideally, the shear strength is therefore dependent on the stability of the strongest systone - which in the case of the simple disc systone is infinite. Clearly, in a practical situation infinite strength is unattainable because, apart from the fact that the discs themselves cannot be infinitely strong, inevitable geometrical imperfections will mitigate against this situation. Nevertheless it is important to recognise that the maximum strength in shear is governed by the stability of the strongest systone(s). Once the strength of the strongest systone(s) is reached it will fail by the process of gap formation which involves dilation. The systone dilation cannot continue indefinitely as the discs will come into contact with new neighbours giving a new systone with orientation differing from the original critical value. It should be noted that the new systone orientation can be developed without involving a body rotation of the original systone. The limit of this process occurs when, along the failure 'line' a uniform orientation, corresponding with the appropriate minimum (principal) stress ratio in Figure 4, is reached.

In practical terms, the strength of the strongest systone(s) is identified with the peak strength of a material such as dense sand while the stable uniform orientation is associated with the ultimate or residual value. The physical model resembles the behaviour of slender columns, where the ideal infinite strength of a theoretical centrally loaded strut cannot be achieved practically because of the limitations of material strength and the influence of imperfections in loading and strut geometry.

Figure 5 illustrates the application of the above hypothesis to a typical stress-strain diagram for a dense sand.

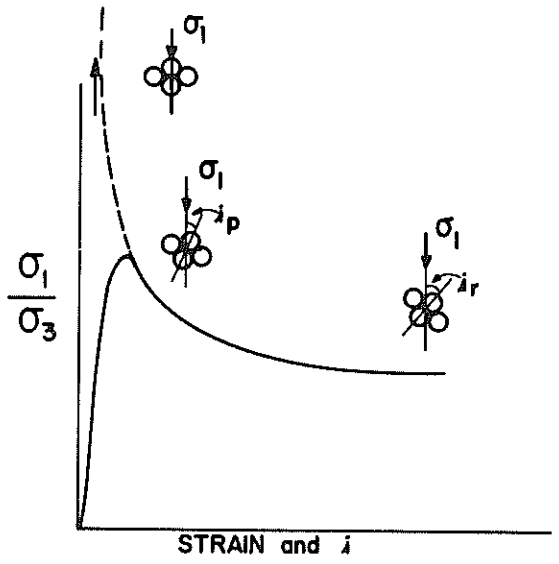


Systone Orientation and the Stress/Strain Behaviour of Dense Sand

Fig. 5.

There are a number of factors which preclude theoretical prediction of the orientation of the strongest systone(s). Thus further means of predicting the peak strength must be sought.

## VI.- THE SPHERE SYSTONE

The simple disc systone is not adequate to describe fully the phenomenon of collapse of granular materials. When a three-dimensional systone of spheres is considered, the intermediate principal stress is found to have a significant influence on the collapse conditions.

Rennie presented a general analysis of this problem, taking into account the orientation of the systone. He showed that for the minimum strength condition, i.e. when the systone is orientated in its least favourable direction, equivalent to the lowest points of troughs in Figure 4, the principal stress ratio at collapse could be expressed as

$$\frac{\sigma_1}{\sigma_3} = 2+2\sqrt{6}\tan\phi_\mu+7\tan^2\phi_\mu - \frac{8}{9}\sqrt{6}\tan^3\phi_\mu \qquad ...6.1$$

Scott (Ref. 5) has pointed out that this equation is identical with that he produced from the earlier work of Thurston and Deresiewicz viz:

$$\frac{\sigma_1}{\sigma_3} = \frac{3\sqrt{3+4\tan^2\phi_\mu} + (\sqrt{3+4\sqrt{2}\tan\phi_\mu})}{3\sqrt{3+4\tan^2\phi_\mu} - (\sqrt{3+4\sqrt{2}\tan\phi_\mu})} \qquad ...6.2$$

which in turn can be expressed as

$$\tan\phi = \frac{\sqrt{3} + 4\sqrt{2}\tan\phi_\mu}{2(\sqrt{6}-\tan\phi_\mu)} \qquad ...6.3$$

where $\tan\phi$ is the Coulomb friction parameter.

Subsequently, using the method developed by Rennie, Parkin (Refs. 6,7) has shown that an essential

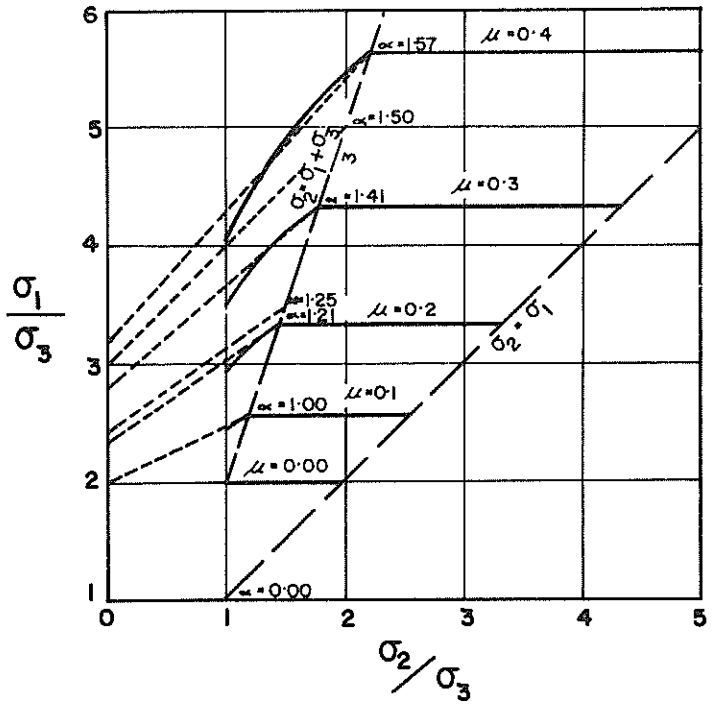


Critical Strength of Sphere Model

Fig. 6.

requirement for equations 6.1 to 6.3 to be valid is that

$$\sigma_2 \geq \frac{\sigma_1 + \sigma_3}{3} \qquad \ldots 6.4$$

Thus, in particular, these results are not applicable to the conventional triaxial test condition.

The solutions obtained by Parkin for the values of $\sigma_2$ outside those covered by equation 6.4 are shown in Figure 6.

It should be emphasised that in applying the results of equations 6.1 to 6.3 to test results on materials such as sand they are only applicable to the ultimate or residual condition.

As the orientation of the strongest systone corresponding to the peak condition is again indeterminate it is not possible to predict directly the peak strength ratio.

Nevertheless it may be inferred from the analysis that the shape of diagrams showing the principal stress relationships at peak is similar to that for the residual condition. Evidence in support of this is given in Figures 7 and 8. (Kirkpatrick Ref. 8, Bell Ref. 9 and Ko Ref. 10). Similar results were obtained by Sutherland and Mesdary (Ref. 11).

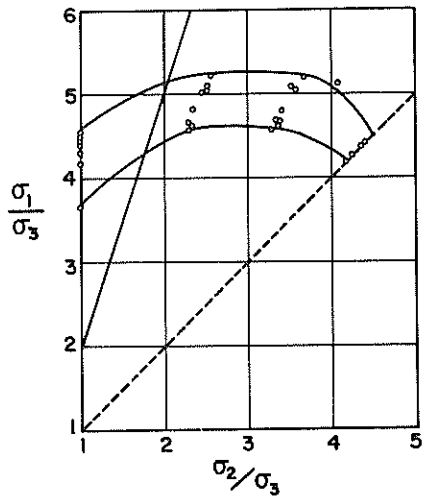


Thick Cylinder Tests (Kirkpatrick 1957)

Fig. 7.

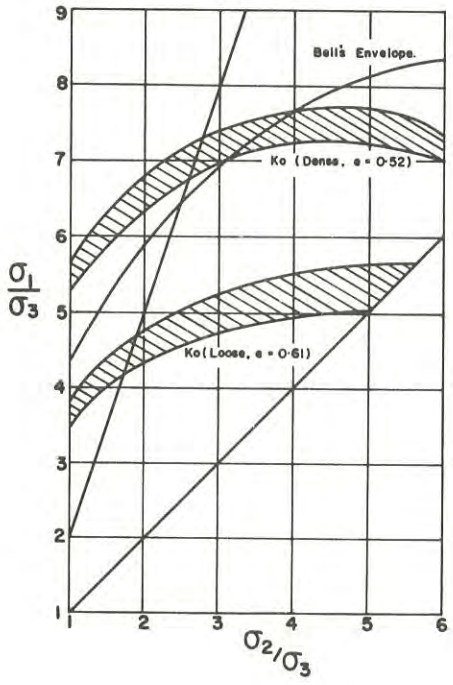


Cube Tests. (Bell 1965; Ko 1966)

Fig. 8.

One feature of these experimental results is the fact that extension results appear to agree with those obtained in triaxial compression. There is some evidence that this may be a product of testing techniques as more recently, Green and Bishop (Ref. 12) and Procter and Barden (Ref. 13) have produced experimental results which follow remarkably well the trends predicted in Figure 9.

Of particular interest also are the results of plane strain tests reported by Cornforth (Ref. 14). Figure 10 shows typical examples. In both cases it will be observed that the peak and subsequent values of the principal stress ratio fall on or very close to the line given by $\sigma_2 = \frac{\sigma_1+\sigma_3}{2}$. This suggests that this relationship may be used to define the plane strain failure condition.

## VII.- PREDICTION OF THE PLANE STRAIN FAILURE CRITERION

One way of predicting plane strain strength is to use equations of the type given in 6.1 to 6.3 to relate the strength to the coefficient of interparticle friction. A polynomial expression of the type

$$\frac{\sigma_1}{\sigma_3} = A + B \tan \phi_\mu + C \tan \phi_\mu^2 + D \tan^3 \phi_\mu \quad \ldots 7.1$$

could be used with the coefficients A, B, C and D determined empirically according to whether peak or residual values were required. Such an approach is however primarily of academic interest as the necessary testing procedures may be used to determine directly the strengths concerned.

A more pertinent practical aim is to attempt to use the theory to estimate likely differences between triaxial compression and plane strain conditions and also to evaluate testing techniques.

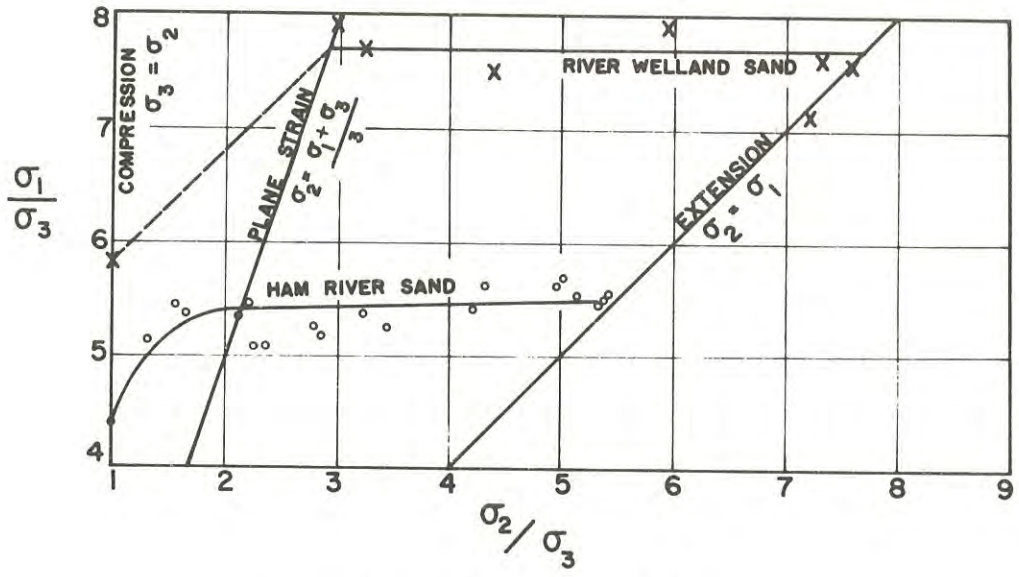


Tests on Dense Sand. (Refs. 12, 13)

Fig. 9.

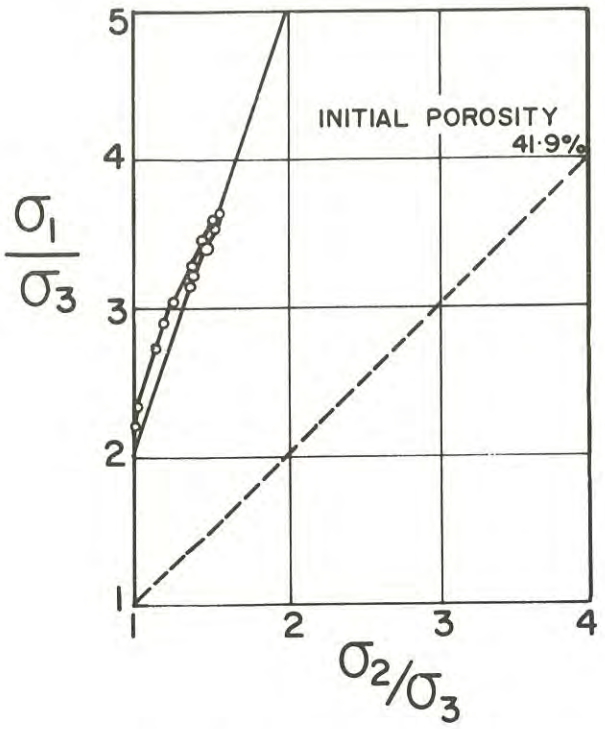


Brasted Sand (Cornforth 1961)

Fig. 10a.

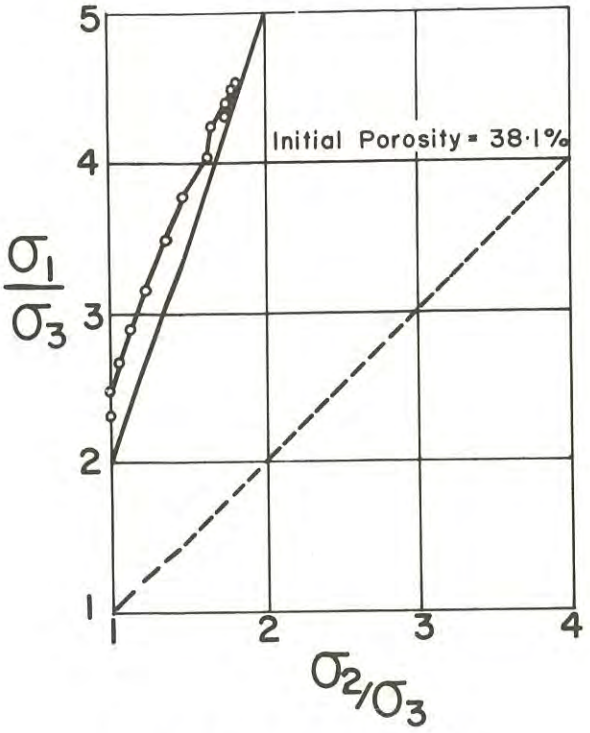


Brasted Sand (Cornforth 1961)

($\sigma_3$ decreased to failure)

Fig. 10b.

In this context it is convenient to introduce a linear approximation for the strength relationships in the range

$$\sigma_3 \leq \sigma_2 \leq \frac{\sigma_1+2\sigma_3}{3} \qquad \ldots 7.2$$

Such an approximation is shown in Figure 7. The dotted lines are described by the relationship

$$\sigma_1 - \sigma_3 = \alpha\, \sigma_{oct} \qquad \ldots 7.3$$

where $\alpha$ is a constant and $\sigma_{oct}$ is the octahedral normal stress. Thus,

$$\sigma_1 - \sigma_3 = \frac{2}{3}(\sigma_1+\sigma_2+\sigma_3) \qquad \ldots 7.4$$

which can be expressed as

$$\sigma_1 - \sigma_3 = \alpha^1 I \qquad \ldots 7.5$$

where $I = \sigma_1+\sigma_2+\sigma_3$ is the first invariant of the stress tensor.

The particular conditions of equation 7.3 which are of interest are

*triaxial compression* $\sigma_2 = \sigma_3$

when

$$\left(\frac{\sigma_{1f}}{\sigma_{3f}}\right)_t = \frac{2\alpha + 3}{3-\alpha} \qquad \ldots 7.6$$

and

*plane strain* $\sigma_2 = \frac{\sigma_1+2\sigma_2}{3}$

when

$$\left(\frac{\sigma_{1f}}{\sigma_{3f}}\right)_p = \frac{4\alpha + 9}{9 - 4\alpha}$$

By comparison with equation 3.3 it will be seen that the value of $\alpha$ for a real granular material is dependent on the parameters $\theta$, i and $\phi_\mu$. For a given material the average rotundity of the particles may be taken as constant and the evidence of Figure 9 suggests that an equivalent friction coefficient $\mu^1$ may be used which includes the effects of both i and $\phi_\mu$.

From Figure 7 it will be seen that for $\mu^1 = 0.1$ $\alpha = 1$ and the predicted plane strain strength is only 4% in excess of the triaxial compression value.

For $\mu^1 = 0.4$ however $\alpha = 1.57$ and the excess increases to 31% which is a significant value. These estimates are conservative because the approximate theory overestimates the triaxial compression strength.

## VIII.- THE INFLUENCE OF TEST CONDITIONS

It is always vital to examine laboratory test conditions in relation to field circumstances. In this context it is of interest to consider the possible influence of the boundary conditions applied to a laboratory sample. It has been hypothesized in Section 5 that the peak strength is largely dependent on the strength of the strongest systone(s). As the stresses are applied to a sample the point will be reached where the weakest systones will tend to fail.

Because of the restraint of stronger neighbouring systones however they cannot develop failure at this stage. The effect of these neighbouring systones on the weaker ones is analogous to the increased strengths developed in a multi-stage triaxial compression test. As the stresses are increased further towards failure of the sample as a whole the stronger systones being also stiffer will attract a greater proportion of the applied loads. If stiff end platens are used the load concentrations on the stiffer systones will be amplified. This suggests that stress controlled boundary tests in which the loads are all applied through flexible membranes should show higher peak strengths than deformation controlled boundary tests in which some or all of the loads are applied through stiff platens.

The stress controlled tests reported by Ko and Scott (Ref. 15) have been criticised by a number of authors (Ref. 11) because of the influence of corner restraints on the test results and the relatively high strengths observed have been attributed to this influence. The present argument suggests however that this may not be the sole or critical factor in producing these higher strengths.

If this argument is correct it also follows that the real values of the plane strain and triaxial compression results should be higher than those shown in Figure 9.

## IX.- ACKNOWLEDGEMENT

Much of the work described in this paper was carried out in the University of Melbourne by Dr. A.K. Parkin; then a graduate student under the author's supervision. Subsequently the author has benefited greatly through discussion and correspondence with Dr. Parkin. The views expressed in this paper must, of necessity however, be the responsibility of the author.

## REFERENCES

1. TROLLOPE, D.H. (1969) - The Mechanics of Discontinua or Clastic Mechanics in Rock Problems, Chapter 9 in "Rock Mechanics in Engineering Practice", Ed. Stagg and Zienkiewicz. Wiley.

2. RENNIE, B.C. (1959) - On the Strength of Sand. Journ. Aust. Math. Soc., Vol.1, p.71.

3. REYNOLDS, O. (1885) - On the Dilatancy of Media Composed of Rigid Particles in Contact. Phil. Mag. (Series 5). 20:469.

4. HORNE, M.R. (1965) - The Behaviour of an Assembly of Routund, Rigid, Cohesionless Particles. Proc. Roy. Soc. A286, 62 (Parts I and II).

5. SCOTT, R.F. (1963b) - Private Communication.

6. PARKIN, A.K. (1964) - The Application of Discrete Unit Models to Studies of the Shear Strength of Granular Materials. Ph.D. Thesis. University of Melbourne.

7. PARKIN, A.K. (1965) - On the Strength of Packed Spheres. Journ. Aust. Math. Soc., Vol.5, Pt.4, p.443.

8. KIRKPATRICK, W.M. (1954) - The Behaviour of Sands under Three-Dimensional Stress Systems. Ph.D. Thesis, University of Glasgow.

9. BELL, J.M. (1965) - Stress Strain Characteristics of Cohesionless Granular Materials. Ph.D. Thesis, Cal. Inst. of Tech.

10. KO, H.Y. (1966) - Static Stress-Deformation Characteristics of Sand. Ph.D. Thesis, Cal. Inst. of Tech.

11. SUTHERLAND, H.B. and MESDARY, M.S. (1969) - The Influence of the Intermediate Principal Stress on the Strength of Sand. Proc. 7th Int. Conf. Soil Mech. & Found. Eng., Mexico. 1:391-399.

12. GREEN, G.E. and BISHOP, A.W. (1969) - A Note on the Drained Strength of Sand under Generalized Strain Conditions. Geotechnique. Vol.19, No.3, p.424.

13. PROCTER, D.C. and BARDEN, L. (1969) - Correspondence on Reference 12. Geotechnique. Vol.19, No.3, p.424.

14. CORNFORTH, D.H. (1961) - Some Experiments on the Influence of Strain Conditions on the Strength of Sand. Ph.D. Thesis, University of London.

15. KO, H.Y. and SCOTT, R.F. - A New Soil Testing Apparatus. Geotechnique. Vol.17, No.1, p.40.

# Application of Oriented Drill Core in Structural Geology at Mount Isa

By

M. C. Bridges, B.Sc. (Hons.), S.Aus.I.M.M.

(Geologist, Mount Isa Mines Limited)

AND

E. J. Best, B.Sc., D.I.C.

(Senior Lecturer in Geology, Canberra College of Advanced Education and was formerly Senior Geologist, Mount Isa Mines Limited)

SUMMARY.- Orientation and properties of bedding, foliation and fractures in rock, with respect to operating or planned mining, are important for an assessment of stability and economics of underground stopes and open cuts. All core from Rock Mechanics diamond drilling at Mount Isa is oriented to permit these features to be studied in detail.

Three core orienting procedures are used

(a) CRAELIUS device with NMLC triple tube drilling for other than vertical holes,

(b) paint dribble on down hole stub of core for 4 inch diameter horizontal holes, using a single tube core barrel, and

(c) a uniform marker of known orientation such as bedding.

For planar and linear features on core, the dip direction, dip and depth are recorded, together with a description of surfaces of breaks. Orientation data are rotated to their true position, corrected for biased sampling, then analysed to delineate orientation groups. Analysis within each orientation group is for spacing, sliding friction properties, continuity of natural planes, relative strength across fractures or bedding breaks, relationship of structure with rock types or areas, and other statistical treatment of data.

The principal advantages of oriented drill core are that a true orientation can be found for core features, and where core is not intact, it can provide a link between adjacent sections of core. Without a true orientation for planar and linear features, where core can be fitted together, orientation groups can only be delineated relative to each other which means that only little subsequent analysis is possible.

## I.- INTRODUCTION

The objective of structural geologists in the Rock Mechanics group at Mount Isa Mine is to find and describe distribution of rock types, major zones of dislocation, fracture systems, and any other geologic structures of the rock which may have relevance to mining. Structural features such as orientation and description of bedding, foliation and fractures in rock, with respect to operating or planned mining, are important for an assessment of stability and economics of underground stopes and open cuts. All core from Rock Mechanics diamond drilling at Mount Isa is oriented to permit these features to be studied in detail.

## II.- NOTATION

(a) Reference Line

A straight, continuous line drawn on drill core that can be fitted together. This line is on the true top of core if the core is oriented, otherwise it is in an arbitary position.

(b) Dip Direction ($\beta$)

Assuming core to be vertical, with the reference line to north, it is the direction of dip of a planar feature on core. This is the direction of the downward major axis of an elliptical trace of a planar feature on the core. It is the angle between the reference line and the point on the ellipse furthest down the core, measured clockwise looking down core, in a plane normal to the core.

(c) Dip ($\alpha$)

Angle of feature with core axis measured in the dip direction. Actual dip is $90^{\circ}$ minus this measured angle for core assumed to be vertical.

(d) Continuity Index

(i) For drill core it is the number of natural fractures continuous across core divided by the number discontinuous across core.

(ii) For an underground rock exposure it is the number of fractures continuing more than 10 feet by 10 feet divided by the number continuing less than 10 feet by 10 feet.

(e) Cohesion Index

The number of drilling induced breaks (on weakness planes) divided by the number of natural breaks continuous across core.

(f) Relative Number

The number of fractures of an orientation group divided by the total number for all groups. It is an inverse measure of average spacing between fractures of a group.

Note: All numbers are corrected for biased sampling.

III.- DRILL CORE ORIENTING DEVICES

At Mount Isa Mine two drill core orienting devices are used, depending on size and inclination of the hole.

(a) CRAELIUS device with NMLC and NQ triple tube drilling for other than vertical holes (Fig. 1). This purely mechanical device,

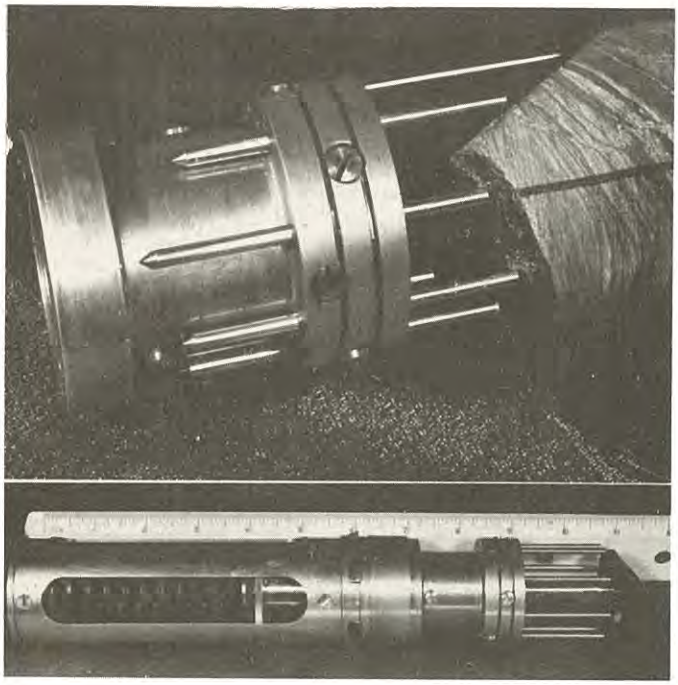

Fig. 1 CRAELIUS core orienting device for NMLC triple tube core barrel.

which initially fits in the front of a core barrel, does not interfere with or markedly handicap drilling. The principle of its operation is a free moving ball bearing in a cylinder where the ball bearing is always at the cylinder's gravitational bottom. As the device is lowered in the core barrel against the down hole face, retractable pins at the front of the device adjust to the rock profile. Also, this cylinder is compressed until the ball bearing comes against its ends, one hardened steel, the other aluminium, indenting the aluminium end at its gravitational bottom (Fig. 2).

With the bottom indentation and face profile taken, the device retracts back up the core barrel and drilling proceeds as usual. Later matching of core with the pins allows top or bottom of core to be found from the aluminium disc indentation.

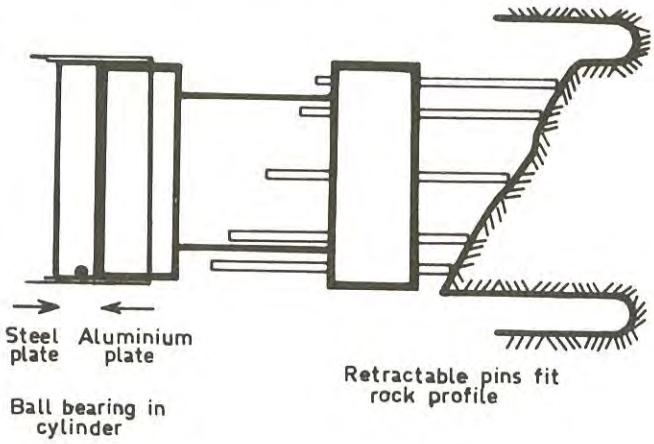


Fig. 2 Diagrammatic section of part of CRAELIUS core orienting device showing principles of its operation.

(b) Paint dribble on down hole stub of core for 4 inch diameter horizontal holes, using a single tube core barrel (Fig. 3). This device is separate from the actual drilling barrel. A small light bulb, partly filled with yellow enamel paint, is axially mounted on the front of a core barrel. This bulb is broken against the down hole rock face and paint dribbles down. Top or bottom of core can then be easily determined.

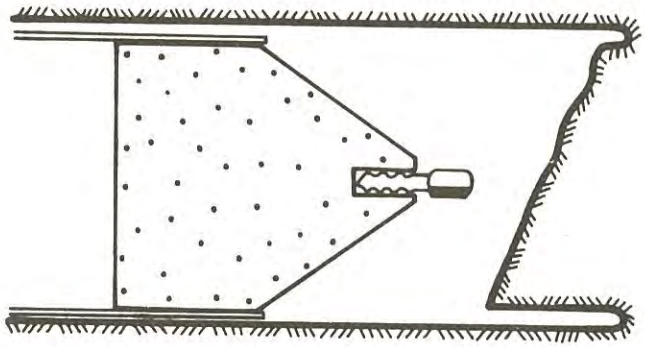

Fig. 3 Orienting device for 4 inch diameter horizontal drill holes.

IV.- DRILL CORE LOGGING PROCEDURE

Drill core is laid out in V-section rails and fitted together. Core recovery at Mount Isa is aimed at 100% so that most core can be fitted together, but where it cannot the orientation of core may provide a connection between adjacent sections. A reference line is drawn on either top of core or, where there is a uniform planar

marker in the rock such as bedding, the line which connects all points on the planes furthest down core. If the true orientation of this uniform marker is known then the core is effectively oriented (Ref. 1). If core is not oriented then an arbitrary reference line is drawn. For planar and linear features on core the dip direction, dip and depth are measured (Fig. 4), together with a description of surfaces of breaks. For purposes of logging, so that drill core information is compatible with exposure mapping, core is assumed to be vertical with the reference line to north. All data is recorded on standard sheets from which punch cards are taken so that data can be processed by computer.

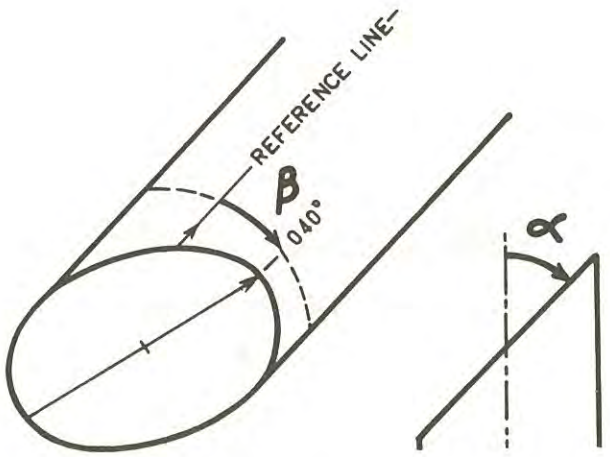


Fig. 4 Measurements of angles of dip ($\alpha$) and dip direction ($\beta$) of planar features on drill core.

V.- ANALYSIS OF DATA

There are essentially two approaches to the analysis of data: one approach subdivides core features by type and considers orientation distribution between and within each type (stereograms); the other takes each orientation group and considers the relative types within each group (tables).

(a) Orientation data are rotated to their true position, corrected for biased sampling and, by using the method of stereographic projection (Refs. 2, 3), groups of orientation data can be delineated. Data may be subdivided on the basis of:

(i) fractures against bedding breaks,

(ii) by continuity of features across core,

(iii) by relative cohesion, that is, natural breaks against drilling induced breaks (on weakness planes),

(iv) by rock type,

(v) by areas, or

(vi) by zones of apparent uniformity of structure.

Each feature of the core is assigned to a particular group, (or groups) and a separate stereogram prepared for each group.

(b) Analysis within each orientation group can be for:

(i) spacing between successive planes of that group,

(ii) sliding friction properties,

(iii) continuity of natural planes,

(iv) relative strength across fractures or bedding breaks,

(v) relationship of structure with rock type or areas, and

(vi) any other statistical treatment of data.

VI.- EXAMPLES OF USE OF ORIENTED DRILL CORE

(a) Proposed Underground Crusher Excavations

A total of 585 feet (not all oriented) of 4 inch diameter horizontal holes were drilled into an area of proposed underground crusher excavations to investigate any structure of the rock which might affect excavation or long term stability of these openings. Besides this drilling, about 500 feet of exposure was mapped near these proposed excavations. Drill core features, while being logged, were subdivided on the basis of fractures against bedding plane breaks, breaks continuous or discontinuous across core, natural against drilling breaks (on weakness planes), and veins.

(i) Analysis by core feature type

Orientation data were rotated to their true position using a computer (Ref. 1), separated into groups, then each group plotted on separate stereograms (Fig. 5). It can be seen that the majority of poles to planes of natural fractures continuous across core plot to the south and north, whereas those not continuous across core plot near centre and west. Drilling induced breaks plot near west with discontinuous natural fractures, and veins plot centre and west with discontinuous and drilling induced breaks (veins not shown in diagram). Bedding plane breaks plot to the east.

(ii) Analysis by orientation groups

By combining all data for fractures, five orientation groups or sets can be recognized, (Fig. 7) along with one set of bedding breaks (Fig. 5). Table 1, which has a breakdown of information for each orientation set, shows that fracture sets 1 and 11 have the greatest number of readings, are mainly continuous fractures (across 4 inch core), and have low cohesion; many of set 1 are shear fractures. Set III are mainly discontinuous drilling breaks, as are sets IV and V. From set I to set III, which are all normal to bedding, there is a gradation of properties: relative number decreases (average spacing increases), continuity decreases, and cohesion increases. Data on spacing between fractures within each set were taken from drill core and further analysed.

These results from oriented drill core can be compared with those from exposure mapping (Fig. 6). The main difference between these two sources of data are that, for exposures, fractures which continue more than 10 feet by 10 feet are separated from those continuing less than 10 by 10, and that fractures smaller than 2 feet by 2 feet are not measured. The three orientation sets for fractures from exposure mapping are the same as sets I, II and III from drill core (Fig. 7).

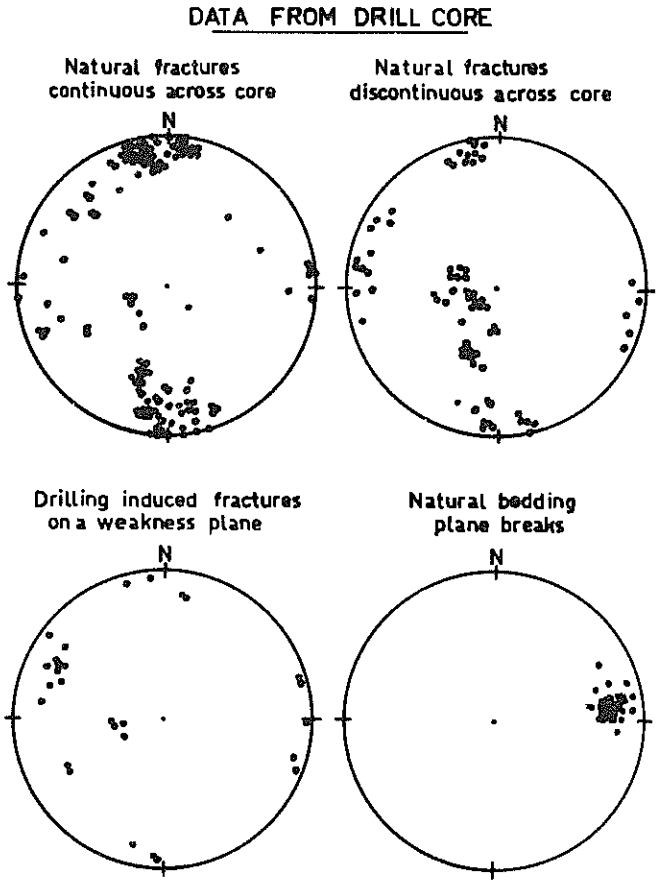


Fig. 5 Data from diamond drill core for proposed underground crusher excavations. Plots of poles to planes on lower hemisphere stereographic projection.

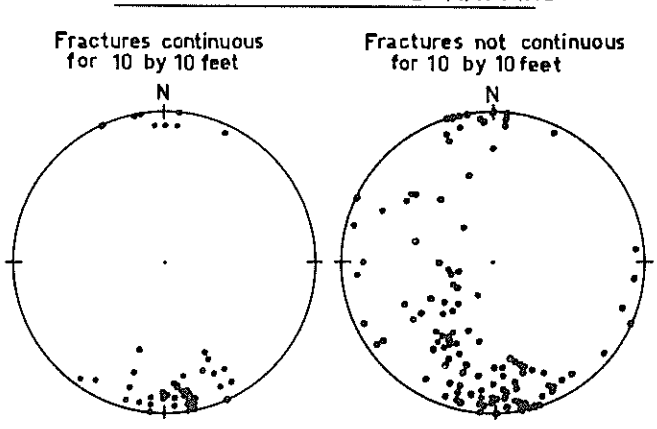


Fig. 6 Data from underground mapping for proposed underground crusher excavations. Plots of poles to planes on lower hemisphere stereographic projection.

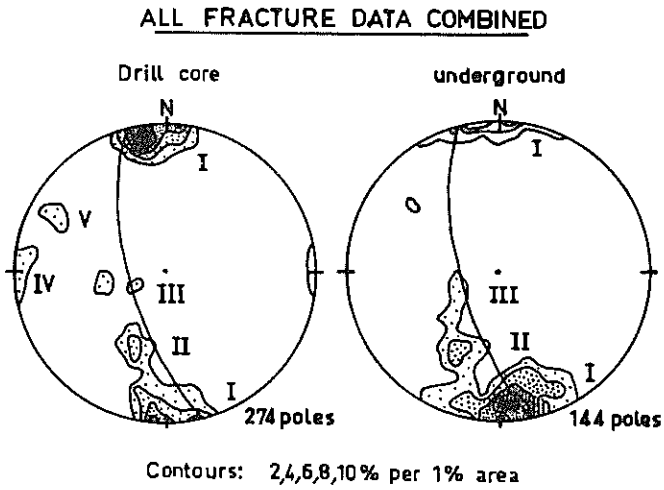


Fig. 7 All fracture data combined for proposed underground crusher excavations. Plots of poles to planes on lower hemisphere stereographic projection.

Table I shows that for exposure mapping many of set I and some of set II continue more than 10 feet by 10 feet, but that set III are all less continuous. Many of set I are shear fractures.

TABLE I

RELATIVE PROPERTIES OF SETS OF FRACTURES AND BEDDING PLANE BREAKS

| Fracture set | I | II | III | IV | V |
|---|---|---|---|---|---|
| Drill core data | | | | | |
| Relative number | 64% | 13% | 8% | 9% | 6% |
| Relative number | 75% | 15% | 10% (only sets I-III) | | |
| Continuity index | 3.1 | 1.4 | 0.25 | 1.0 | 0.67 |
| Cohesion index | 0.08 | - | 1 | 1 | 1.3 |
| Exposure mapping data | | | | | |
| Relative number | 79% | 15% | 6% | | |
| Continuity index | 0.58 | 0.20 | 0 | | |
| Bedding plane breaks, from drill core | | | | | |
| Continuity index | 5.1 | | | | |
| Cohesion index | 0.41 | | | | |

By considering data from both sources, weighing

up all factors relevant to stability of underground openings, it is concluded that set I, and to a lesser extent set II fractures, together with bedding plane breaks, will be of prime importance for any excavations in the area explored. It is encouraging that both sources of data lead to similar conclusions, though they tend to supplement each other rather than cover common ground. Confidence can be placed in this type of data from oriented drill core.

(b) Structure of Hanging Wall Area of Proposed Underground Stope

The first NMLC drill hole in which a CRAELUIS core orienter was used at Mount Isa provided an excellent example of the detailed structural information which can be obtained from oriented core. The hole, which was 220 feet long and horizontal, was drilled to test hanging wall conditions of a proposed large open stope in one of the lead-zinc orebodies (dip about 65°).

The first step in analysing the data was to divide the hole into zones of uniform structure. In this instance, structure was not consistent throughout the hole because of folding of strata, and it was necessary to divide the data into four zones for detailed analysis:-

Zone 1 - the attitude of bedding is different from the remainder of the hole due to folding;

Zone 2 - on the opposite limb of the fold to Zone 1;

Zone 3 - bedding plane joints prominently developed;

Zone 4 - a set of closely-spaced chloritic joints prominently developed.

As the four zones were obvious from visual inspection of the core, orientation data from core logging were plotted directly onto four pairs of stereograms (one bedding stereogram and one jointing stereogram for each zone).

(i) Analysis of bedding

Attitudes of all bedding plane joints and breaks were recorded, then plotted on the appropriate stereogram. In addition, the attitude of bedding on solid core was measured every 12 inches, or even closer in tightly folded zones, then plotted. The summary contour plot of poles to all bedding measurements for the entire hole is shown in Fig. 8. This shows two concentrations of bedding attitudes, representing the limbs of the main fold, with a scatter of measurements between them representing the core of the fold. Bedding poles lie on a great circle, the pole of which represents the attitude of a fold axis (plunging 36° in direction 343°M).

One significant fact to emerge from the analysis of bedding in zones 1 and 2 was that all bedding plane joints are parallel to one of the two limbs of the fold; in the transition zone between the limbs of both major and minor folds, joints are not developed along bedding planes. Cores of these folds are, therefore, composed of relatively unjointed rock, and the continuity of bedding plane joints is restricted by them.

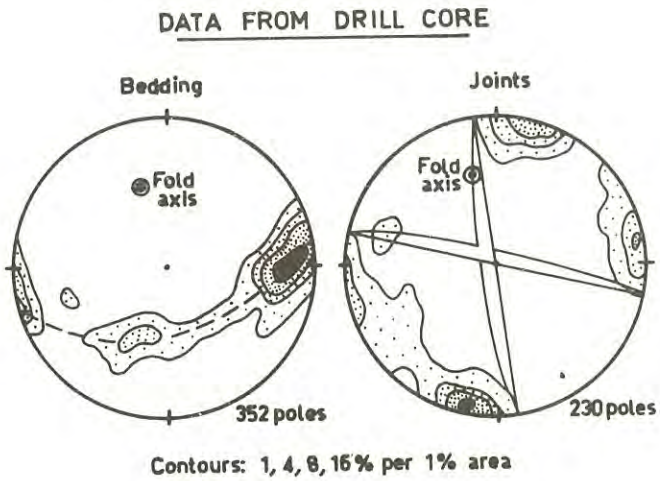


Fig. 8 Summary contoured plots of bedding and jointing for entire drill hole. Plots of poles to planes on lower hemisphere stereographic projection.

Further detailed analysis of bedding measurements on stereographic projections provided valuable information on the sytle and geometry of folding; as this has no direct significance for a rock mechanics analysis, details are not given here.

(ii) Analysis of jointing

Joints and breaks along weakness planes were plotted on four separate stereograms representing each "homogeneous zone" of the drill core. Two distinct joint sets were represented on each stereogram - these are shown in the summary contour plot of poles to all joints and weakness planes recorded in the drill log (Fig. 8). One set dips at 80° in direction 015°M, while the other set dips at 80° in direction 260°M. The north-dipping joints represent a joint set which is developed throughout the mine area, but the west-dipping joints are not commonly-developed in the mine. The planes representing these sets are shown in Fig. 8, and the fold axis is also plotted: it can be seen that the fold axis lies in the plane of the west-dipping joint set, and it is concluded that this set represents an axial plane cleavage related to this folding.

(iii) Relative physical properties of joint sets

From bedding and joint stereograms for each of the four zones of the drill core, values were calculated for relative numbers, cohesion index and continuity index for each joint set; the results are shown in Table II.

The following conclusions are drawn from the information in the table:-

TABLE II

RELATIVE FREQUENCY, COHESION AND CONTINUITY OF JOINT SETS DEDUCED FROM DRILL CORE LOGGING DATA

| Zone of drill hole and joint set | Relative number | Cohesion index | Continuity index |
|---|---|---|---|
| Bedding joints | | | |
| 1 (0 - 58') | 31% | 0.8 | 7.0 |
| 2 (58' - 87') | 41% | 0.7 | 6.5 |
| 3 (87' - 160') | 74% | 1.6 | 2.9 |
| 4 (160' - 222') | 16% | 1.3 | 1.3 |
| North-dipping joints | | | |
| 1 | 34% | 2.0 | 2.4 |
| 2 | 41% | 0.5 | 2.0 |
| 3 | 15% | 0.3 | 1.5 |
| 4 | 80% | 0.1 | 2.2 |
| West-dipping joints | | | |
| 1 | 35% | 10.0 | 11.0 |
| 2 | 18% | 2.5 | 10.0 |
| 3 | 11% | 2.5 | 0.9 |
| 4 | 4% | 1.4 | 0.8 |

1. The predominance of bedding plane joints in Zone 3 and north-dipping joints in Zone 4 is shown by the relative number values.

2. The relative number of west-dipping joints progressively decreases from Zone 1 to Zone 4. This supports the conclusion that this set represents axial plane joints, which would become less well-developed away from the core of the fold (Zone 1).

3. The cohesion index shows that the west-dipping joints are much stronger than the other two joint sets.

4. In Zones 3 and 4, north-dipping joints have very low cohesion; this is due to the chlorite coatings present on these joints.

5. The continuity index of both bedding and west-dipping joint sets decreases from Zone 1 to Zone 4, showing that continuity decreases away from the core of the fold. The continuity index of the north-dipping joints, which are independent of folding, remains relatively constant throughout the hole.

Considering the relative values of average spacing, cohesion and continuity for the three joint sets as represented in Table II the relative importance of the joint sets are assessed for each zone of drill core in turn; the results, in decreasing order of significance, are as follows:-

Zone 1 - bedding; west-dipping; north-dipping

Zone 2 - bedding; north-dipping; west-dipping

Zone 3 - bedding; north-dipping; west-dipping

Zone 4 - north dipping; bedding; west-dipping

The proposed hanging wall of the stope under investigation is within zone 4, where closely-spaced, low cohesion north-dipping joints are the most prominent rock defects. Bedding joints, by comparison, are more widely-spaced, less persistent and have higher cohesion, while the west-dipping joints are virtually insignificant.

This example of structural analysis of oriented core illustrates the detailed information which can be obtained by careful logging of good quality drill core. It also demonstrates the necessity for probing the rock mass under analysis rather than only mapping nearby development and assuming rock conditions will be the same. In this instance the distribution of defects in the rock mass changes markedly four times within 220 feet.

## VII.- CONCLUSIONS

These examples clearly show the practical advantage of diamond drill core, particularly oriented core, for the investigation of structure of rock. Some particular points for the collection and analysis of data are illustrated by these examples.

(a) Complete recovery of good quality core is essential.

(b) Natural and drilling induced breaks must be distinguished.

(c) Section of core being analysed must be structurally homogeneous.

(d) Data must be separated into groups, such as orientation or continuity, and each group analysed separately.

(e) Exposure mapping supplements drill core data.

(f) Data is still not as quantitative as desired but meaningful comparisons can be made between groups of data.

The principal advantages of oriented drill core are that a true orientation can be found for core features, and where core is not intact, it can provide a link between adjacent sections of core. Without a true orientation for planar and linear features, where core can be fitted together, orientation groups can only be delineated relative to each other which means that only little subsequent analysis is possible.

## VIII.- ACKNOWLEDGEMENTS

The idea of classifying core features for relative continuity and cohesion was originally put forward by Dr. K.J. Rosengren. We thank Mount Isa Mines Limited for allowing us to present this paper.

## REFERENCES

1. ROSENGREN, K.J. - Rock Mechanics of the Black Star Open Cut, Mount Isa. Thesis (Ph.D.), Australian National University, 1968.

2. BADGLEY, P.C. - Structural Methods for the Exploration Geologist. Harper and Brothers, New York, 1959, pp. 187-242.

3. PHILLIPS, F.C. - The Use of Stereographic Projection in Structural Geology. Edward Arnold (publishers) Ltd., London, 1954.

# Damage Induced in a Smooth Work Piece by a Sliding Diamond —an Approach to Hard Rock Drilling

By
J. Graham, M.Sc., Ph.D.
(Principal Research Scientist, Division of Mineralogy, C.S.I.R.O.)

SUMMARY.- Optical methods were used to evaluate the early stages of damage caused by a loaded spherical diamond moving over a smooth surface, as a function of speed, radius, load and lubrication, for several homogeneous materials. New types of cracking patterns and abraded tracks have been observed. The statistical variation from track to track, and even within one track, is so great that quantitative conclusions are not possible at this stage, although some general effects of the variables are noted. Application to hard rock drilling is not straightforward and will probably have to await an evaluation of material removed.

## I.- INTRODUCTION

It is surprising how little is known concerning the theoretical aspects of diamond drilling. One area in which a limited amount of work is being done concerns the mode of action of a single diamond point on a smooth work-piece. The problem has been approached from two different aspects; in one, the forces on the diamond are measured by dynamometer, and this approach was attempted by Mr D. A. Davies in a careful study in the Western Australian Laboratory of the Division of Mineralogy. In common with other workers (including those whose main interest is in the machining of metals) he found that the dynamometer signals were incredibly complex, and that their interpretation posed a very formidable task. Even when the situation was simplified by reducing load and speed, no satisfactory interpretation was achieved.

The second approach is to study the so-called chatter cracks which appear when an indenter is passed over the surface of a brittle material. If the work-piece is transparent, the scratches can be studied optically in fair detail. It has often been assumed that such cracks are in effect the rear portion of the ring cracks which form under Hertzian stresses when the indenter is stationary, the forward portion of the cracks having been prevented from forming when the indenter is moving, due to the compression of the surface in the direction of motion. These cracks do in fact form, but in our experience are associated with rather special conditions. They have been fitfully studied experimentally and theoretically with stationary and moving diamonds for some years (Refs 1-6). H. H. Schlössin of the University of Witwatersrand (Ref. 7) has studied cracking patterns in quartz due to a diamond indenter of radius 1 mm at a wide variety of speeds and a limited number of loads. He also sectioned some of the scratches to check on the cracking at depth. It seemed desirable to extend Schlössin's work to determine the effect of various lubricants or films, of different diamond radius, and of different loads.

## II.- APPARATUS

The apparatus (fig. 1) consists of a rigid yoke,

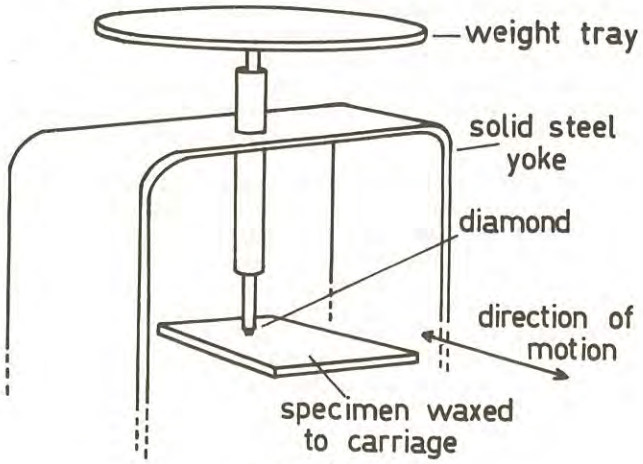


Fig. 1

Schematic diagram of the diamond scratching apparatus. The work-piece is moved under the diamond by a hydraulic drive.

bearing a vertical steel shaft which slides freely in teflon guides. The diamond is soldered to the bottom of the shaft, and a platform for weights attached to the top. The work-piece is attached to a slider operating at speeds from 0.01 cm/sec to 10 cm/sec. Uniform motion is provided by a hydraulic drive. The diamonds were ground to the required radius and polished on a cloth lap; no asperities could be detected in profile at a magnification of 100 x, but on glass and quartz the passage of the diamond left a plastic deformation track consisting of a number of parallel lines which were presumably due to surface irregularities. On silica glass this track was only visible for the smaller radius diamond. Plastic deformation of glass, while somewhat surprising, has been noted previously (Refs 8,9).

## III.- GENERAL OBSERVATIONS

The vertical loads required to scratch glass, silica glass, and quartz, were very comparable in magnitude and were of the order of 1 kg for the diamond of radius 0.5 mm and 7 kg for the 1.0 mm radius diamond. This would result in an average pressure of $\sim 50{,}000$ kg/cm$^2$ over the area of contact, though the actual pressure at the centre would be much higher. A precise calculation is not possible without making some assumptions about the degree of plastic deformation. The formation of the "chatter cracks" seems to be a statistical process, and the threshold load is not easy to determine. Many of the light-load tracks, for instance, may have only one or two Hertzian cracks along their entire length; others may show a great length of regular cracking, followed for no apparent reason by an equally great length in which there is no cracking at all - merely the plastically deformed track. The cracking patterns may be "developed" by etching in dilute solutions of HF.

The effects of lubrication and other variables cannot be evaluated quantitatively because of the qualitative changes which often occur in the cracking pattern. We used water, a 10% solution of soluble oil, a 10% solution of teepol detergent, a 10% bentonite suspension, and machine oil as lubricants or cutting fluids. In addition some surfaces were prepared by vibratory polishing and some by polishing on a rotary lap. In the case of quartz, some plates were cut with the c axis normal to the surface, and some with c parallel with the surface. In the latter case, scratching was carried out both parallel to the axis and across it.

In almost all cases, the least cracking occurred with a dry surface, or when the surface was lubricated with machine oil. The greatest damage was caused when the surface was flooded with the bentonite slurry or the detergent solution. There were some exceptions to these generalizations, e.g. when scratching occurred parallel to the c axis on quartz, the lubrication by machine oil became less effective, and considerable cracking occurred. Another peculiarity of the machine oil scratches was the large amount of residual stress in the substrate after cracking. With other cutting fluids such stresses were not observed (compare Dalladay (Ref.10)). The residual stress with oil may be due to adsorption of an oil film within the cracks, but it could not be removed by washing in detergent solution. Some relief of the strain could be effected by further sub-surface cracking when the specimen was etched. Other effects due to the cutting fluid are small, although in some cases it is apparent that the bentonite slurry and detergent solution cause surface abrasion in preference to deeper longitudinal cracking.

The radius of the diamond affects the width of track and the load required to induce cracking, but does not greatly affect the cracking pattern. The frequency of longitudinal cracks is much greater with the small than the large radius diamond.

The substrate itself is the variable that affects most the appearance of the cracking patterns, but the amount of damage for a given load and speed does not vary greatly between soda glass, silica glass, and quartz. The patterns in soda glass were usually much closer to the simple Hertzian geometry than in the silica compositions. Cracks in crystalline quartz tended to follow particular crystallographic directions, but never intersected to form a sharp angle like those on diamond (Ref. 3). For plates cut parallel to the c axis, scratches across the axis produced much less damage than those parallel to it. The latter were comparable with those on the basal plane. An interesting effect of the method of surface preparation occurs with the small radius diamond and with bentonite slurry or detergent solution; the tendency to surface abrasion already mentioned is much greater in the vibratory polished specimens where the surface layer of disordered material is probably less. The abrasion is accompanied by finely spaced reverse cracking as shown in fig. 2.

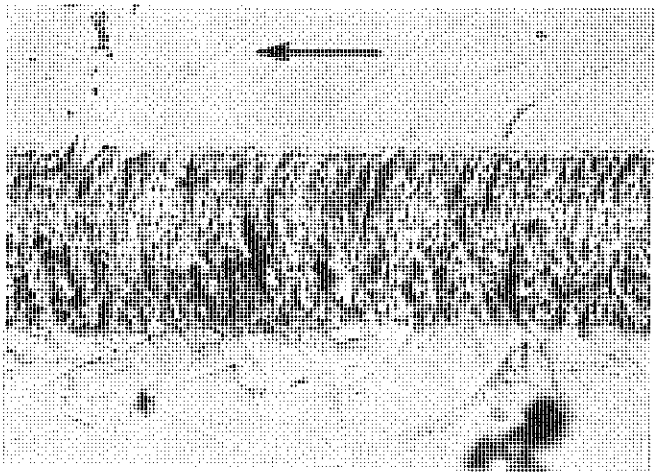

Fig. 2

Closely spaced reverse cracking and surface abrasion associated with bentonite slurry and detergent solution. Arrow shows apparent direction of motion of the diamond.

## IV.- DETAILED CRACK STRUCTURE

Some interesting features can be observed by microscopy at magnifications up to 500 times. The cracking patterns on glass are the simplest, and for both large and small diamonds suggest the usual regular sequence of Hertzian cracks radiating outwards and downwards from the surface at an angle of 40-50° (fig. 3a). Closer examination usually shows

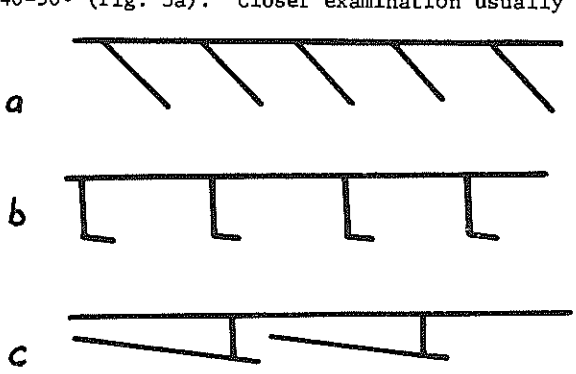

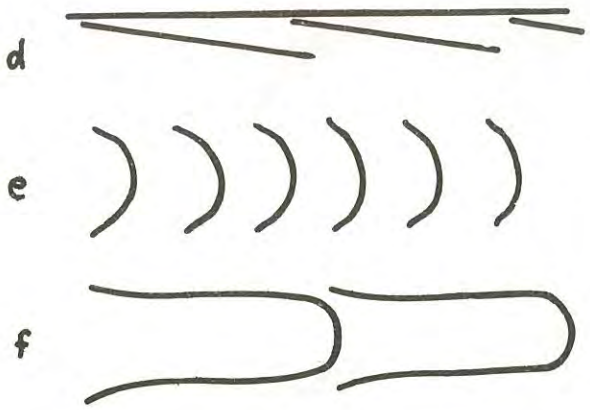


Fig. 3

Diagrammatic representation of scratches in glass. *a* - *d* longitudinal sections, *e* and *f* plans. *a*. Ideal Hertzian cracking behind indenter. *b*. Section of semi-circular crack with flange. *c*. Off-centre section of *b*. *d*. Section of scalloped edge cracking such as Fig. 6. *e*. Almost ideal Hertzian cracks produced by fast movement. Effective direction of movement of the diamond from right to left.

that the cracks are more nearly vertical to a depth of about 7-8 μ, and then break away nearly horizontally (fig. 3b and fig. 4). Sometimes entire circular cracks (complete with flanges) may occur

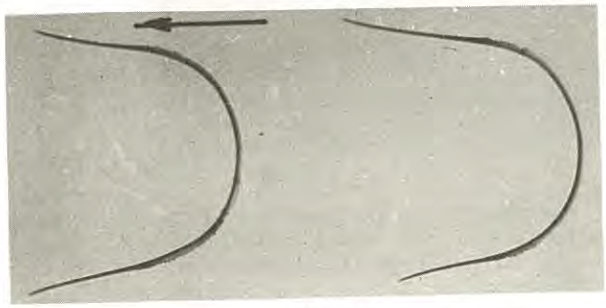

Fig. 4

Regular sequence of Hertzian cracks on glass, showing flanges.

(fig. 3c and fig. 5): the flanges are always tilted

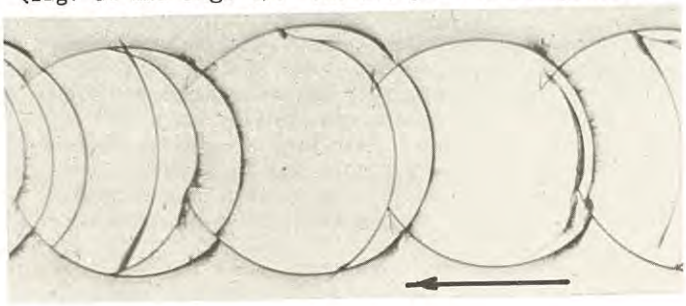

Fig. 5

Almost complete circular cracking pattern.

upwards so that the front of the flange is very close to the surface. When the loads are not much above those to initiate cracking, the diamond often leaves a track consisting only of longitudinal edge cracks, which may be featureless and near vertical, or may sometimes be rather beautifully scalloped (fig. 6).

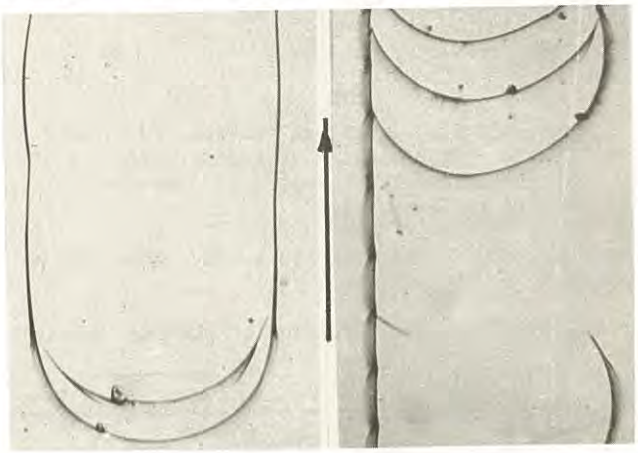

Fig. 6

The two types of edge cracks *a*. Shallow near vertical cracks. *b*. scalloped edge cracking shown in section in fig. 3d.

Examination under high power shows that cracks of the latter type are not continuous, but consist of the side flanges of the type of cracks shown in fig. 3c. A section view is shown in fig. 3d. Intersecting cracks are rare under these conditions, and when apparent intersections are viewed under higher power, it is observed that the two cracks occur on different levels. It thus appears that this kind of cracking is not very damaging.

Variations in these patterns with radius of diamond, speed and lubrication are all quite small, although slight deviations from sphericity of the diamond contact surface result in marked asymmetry of cracking. Contrary to the work of Schlössin[11] on quartz, we found the spacing of the cracks to be fairly unpredictable. Thus with the 0.5 mm radius diamond and a 2.5 kg load, a fast traverse generally gives longer distances between cracks, compared to a slow traverse, whereas with a 1.5 kg load the reverse is true. The longer spacings are compensated for by an extension of the ends of the crack, which in the limit may form complete sides to the track (fig. 3e, f). Similarly, an increase in the load may not necessarily decrease the spacing.

On three of the tracks on glass, widely spaced reverse cracks were noticed. These have the crack curvature convex in the direction of motion, and it is thus suspected that they are formed *ahead* of the diamond, in the compression zone. On all substrates it is observed that deep cracking occurs mainly when reverse cracks are present, although the closely spaced reverse cracking shown in fig. 2 is not very damaging. Where the reverse cracks are well separated, extensive networks of deep cracks have been observed in glass at pressures not much above that required to initiate cracking. There may be three levels of circular cracks similar to those observed at the surface; they are usually linked by

sloping cracks of Hertzian geometry, but these have different characteristics depending on their position in the hierarchy (fig. 7). The deepest cracks so far

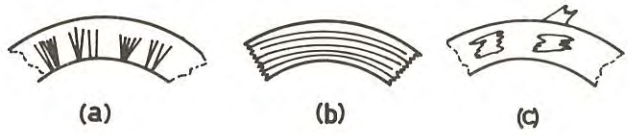


Fig. 7

Types of fine structure observed on sloping cracks. Plan view. *a*. Radial ridges (r). *b*. circumferential steps (c). *c*. clean smooth surfaces (s).

observed reach to 216 μ before surface material is removed.

Figure 8 is a cross-section of one such network

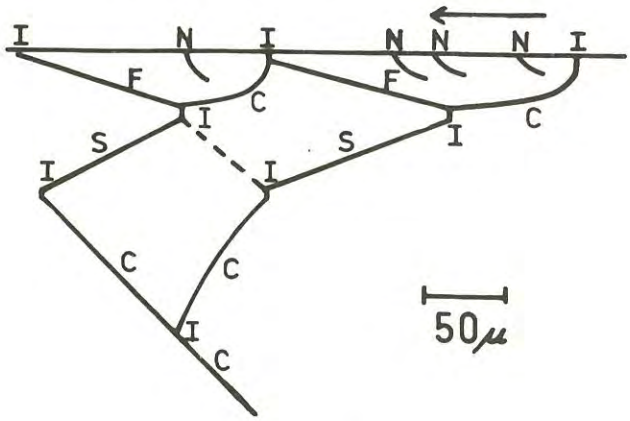


Fig. 8

"Honeycomb" network of deep cracking indicating the complexity of the cracking pattern. Letters refer to the crack types of fig. 7. In addition, I is a reverse crack and N a normal Hertzian type crack.

in which the vertical and horizontal scales are the same. It was obtained by plotting the coordinates of various points, read from the vertical traverse and mechanical stage of the microscope. Figure 9

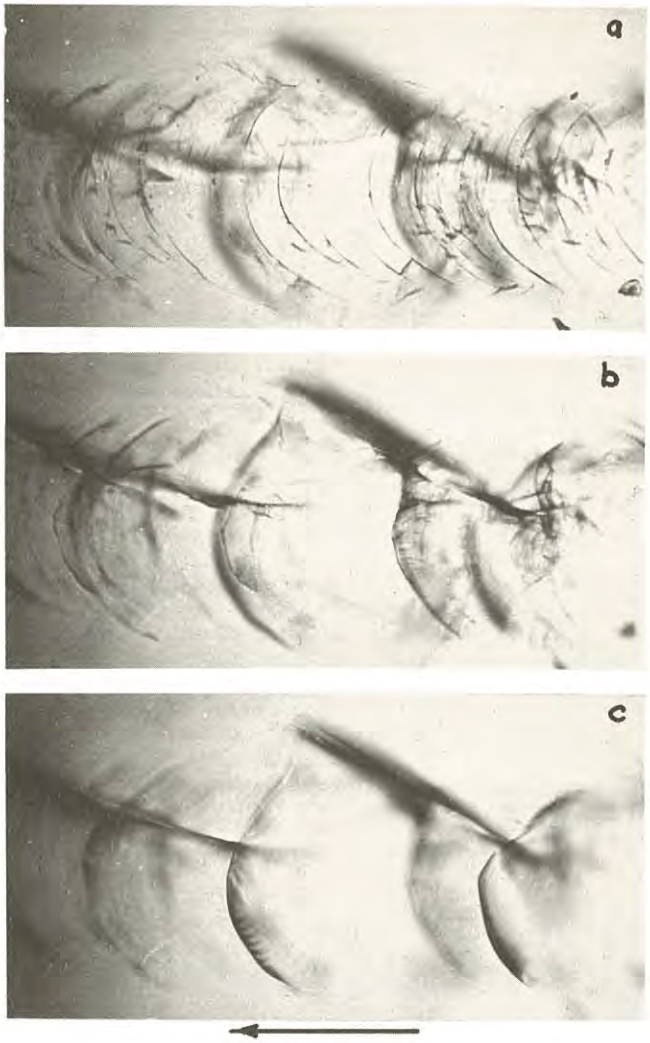


Fig. 9

Micrographs of the same portion of track focussed at different depths, showing the different cracking characteristics at different levels. *a*. surface cracking. *b*. about 40 μ deep. *c*. about 100 μ deep.

shows the appearance of the pattern at various depths; each picture shows a different level of cracking at the same point in the track.

In silica glass and quartz longitudinal cracks of varying severity occur. Especially with the small radius diamond, they may be continuous along the length of the track, and usually have an irregular wavy trace. Sometimes a regular sequence of deep semi-circular cracks can be linked by straight longitudinal cracks to form a repeated pattern. Figure 9 is a portion of such a pattern.

This may not be obviously linked to the surface cracking pattern. Occasionally with the small radius diamond horizontal cracking occurs similar to that observed by Schlössin (see fig. 10). However, the horizontal

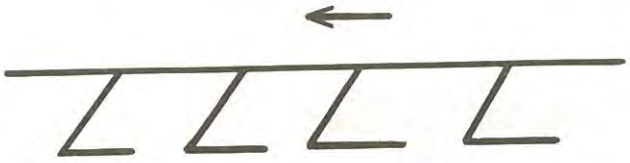

Fig. 10

Horizontal cracking extending back under the indenter from the edge of "reverse cracks".

portion may not be associated with a Hertzian crack, and in some cases isolated horizontal cracks occur at many depths up to 50 μ.

Material may be removed in at least three ways. The small radius diamond on silica glass abraded the surface, leaving a track roughened over a proportion of the area of contact. The material removed seems to have been shattered to a random fine powder, and the track is up to 7 μ deep under a load of 2.5 kg. The large diamond on silica glass and quartz resulted in a series of intersecting vertical cracks, and occasionally where these completely surrounded a small triangular or lens-shaped area the enclosed material could sometimes chip right out. The depth of these chips was of the order of 5-10 μ, corresponding to the depth of the horizontal part of the "rear" Hertzian type cracks. Under certain conditions large chips could be removed, bounded by the ladder-like regular cracks and with a large proportion of the under surface bounded by either horizontal or sloping sections of the deep cracking network. These have been noted to a depth of about 16 μ, but would be expected to be deeper for higher loads. It is also possible that a small amount of material is removed plastically, after the manner of a metal cutting tool, and some thread-like coils of glass have been observed.

## V.- CONCLUSIONS

Although the present work has not established any broad generalizations on the mode of action of a single diamond point in producing cracking, it has been shown that the situation even with a smooth surface of glass or a single crystal is much more complex than previously supposed, and that the simple Hertzian-type chatter cracks are only produced under very special conditions. There is a possibility that further work will enable the effects of the variables to be better separated, but this will probably prove to be far removed from the effects observed in actual drilling operations, where a heterogeneous polycrystalline aggregate is being abraded. A study of chip removal on a polycrystalline surface could easily turn out to be more readily applicable in practice, and preliminary experiments are being carried out along these lines.

## VI.- ACKNOWLEDGEMENTS

It is a pleasure to acknowledge the technical assistance of Messrs R. Couper and S. Baggott, and some advice on optical matters from Dr I. D. Martin, all of the Division of Mineralogy, CSIRO, Perth. I am indebted to Mr D. A. Davies for the initial motivation to the work.

## REFERENCES

1. FRANK, F.C., and LAWN, B.R.- On the Theory of Hertzian Fracture. Proc. Roy. Soc. A. Vol. 299, pp. 291-306.

2. FRANK, F.C., LAWN, B.R., LANG, A.R., and WILKS, E.M.- Strains in Abraded Diamond Surfaces. Proc. Roy. Soc. A. Vol. 301, 1967, pp. 239-52.

3. LAWN, B.R.- Partial Cone Crack Formation in a Brittle Material Loaded with a Sliding Spherical Indenter. Proc. Roy. Soc. A. Vol. 299, 1967, pp. 307-316.

4. LAWN, B.R., and KOMATSU, M.- The Nature of Deformation Around Pressure Cracks on Diamond. Phil. Mag. Vol. 14, 1966, pp. 689-99.

5. SEAL, M.- The Abrasion of Diamond. Proc. Roy. Soc. A. Vol. 248, 1958, pp. 379-93.

6. SEAL, M.- Industrial Diamond Review, Vol. 25, 1965, p. 111

7. SCHLÖSSIN, H.H.- Crack-Slip in the Abrasion of Quartz by Diamond, Reports No. 14, 18 and 30 of the Department of Physics, University of Witwatersrand, 1962, 1963 and 1968.

8. CUSTERS, J.F.H.- Plastic Deformation in Optical Glass During Scratching. Nature (Lond.) Vol. 164, 1949, p.627.

9. MARSH, D.M.- Plastic Flow in Glass. Proc. Roy. Soc. A. Vol. 279, 1964, pp. 420-435

10. DALLADAY, A.J., and TWYMAN, F.- The Stress Conditions Surrounding a Diamond Cut in Glass. Trans. Opt. Soc. (Lond.) Vol. 23, 1921, pp. 165-169.

# Some Basic Aspects of Diamond Drilling

By

D. Rowlands, B.Sc. (Hons.), M.E., Dip.Met.Min., M.Aus.I.M.M.

(Senior Lecturer in Mining Engineering, University of Queensland)

SUMMARY.- A theoretical model of the fracture pattern associated with the penetration of a diamond into brittle rock is presented. Diamond bit design is discussed in terms of this model and the physical properties of the rock. The operating variables associated with diamond drilling are discussed, and some laboratory results are given together with details of instrumentation and methods used to normalize results.

## I.- INTRODUCTION

At this date it would be correct to talk about the "state of the art" when discussing the operation of diamond drilling. Very little basic information is available regarding this rather costly operation, and that which can be obtained is rather subjective in nature. The work described in this paper arises from the initial part of a programme of diamond drilling research aimed at obtaining basic data, based upon measurement, from which it is hoped to establish a more scientific understanding of the operation.

## II.- THEORETICAL MODEL OF THE CUTTING ACTION OF A DIAMOND BIT

The cutting action of the diamond bit depends upon two basic mechanisms, the axial penetration of the diamond into the material being drilled, and the rotary "shearing" action of the applied torque. These may be modified by the physical properties of the rock.

### (a) Axial Penetration

Consider the penetration of a single diamond octahedron into a homogeneous isotropic brittle rock. Fig. 1.

Hoek (Ref. 4) has shown that in a brittle rock under the action of a compressive force, tension cracks develop in the direction of the applied major stress. Thus in Fig. 1 tension cracks would be expected to develop at the apex of the octahedron, and normal to the cleavage face of the diamond. In addition, due to the lateral displacement associated with the wedge penetration, shear stresses and shear cracks develop as illustrated. Penetration would be associated with the initial closing of open "Griffith" cracks followed by elastic deformation up to the point of brittle crack initiation. Plastic yield then occurs as cracks develop (both tensile and shear) until final fracturing develops. Tensile cracks may locate and initiate later shear failure.

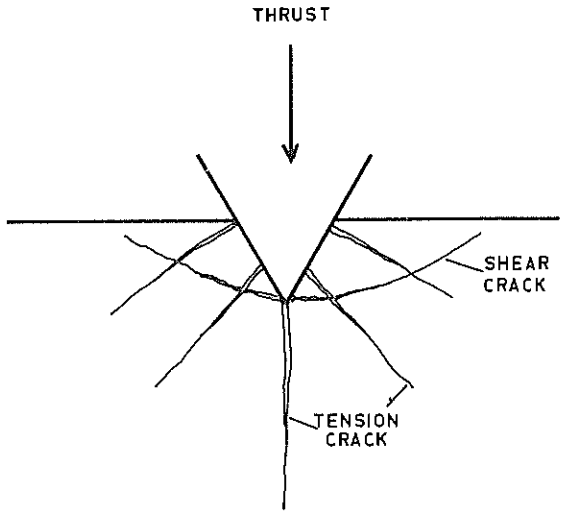


Fig. 1. Penetration of diamond into brittle rock.

### (b) Rotational Cutting

In addition to the thrust that results in axial penetration, the diamond is also subjected to a torque which develops a rotary cutting or shearing action. The torque force will cause shearing along the shear cracks illustrated in Fig. 1, while additional shear planes may also be developed. The transition from elastic straining to sudden failure of the rock, under the action of the shearing torque force, accounts for the vibration associated with diamond drilling.

Adjacent diamonds tracking on differing radii tend to develop furrows with intervening ridges. These ridges should shear towards the initial furrow if the diamond spacing and exposure are correctly designed.

(c) Modifications Due to Physical Properties of Rock

Because actual rock types do not conform to the idealized specifications considered in section (a), modifications to the theoretical model can be expected in practice. Such modifications are brought about by variations in the grain size of the constituent minerals and their physical properties, together with the cementing properties of the rock matrices. Some minerals are more easily sheared because they contain pronounced cleavage planes. Where the rock matrix is easily sheared, the properties of the mineral grains may be neglected. Such variations were observed by Pfleider and Blake (Ref. 7) during microscopic examination of diamond drill holes bored in granite, trap rock, taconite, marble, limestone and sandstone.

III.- DIAMOND BIT DESIGN

Based upon the theoretical model outlined in the previous section and the physical properties of diamonds, it is possible to examine some of the basic factors that should be considered in diamond bit design.

(a) Types of Diamond Bits

Two types of diamond bits are in general use, surface set bits and impregnated bits. Surface set bits have diamonds, usually octahedral crystals, set in a metallic matrix on the surface of the diamond crown. Impregnated diamond bits contain very small diamonds or crushed diamond material, sintered throughout the matrix. Diamond salvage is normal with surface set bits but is not practicable with impregnated bits. Impregnated bits are drilled to destruction or loss of gauge.

(b) Diamond Orientation

It is possible with surface set bits to orientate the diamond stones in such a manner as to provide the maximum resistance to wear (Ref. 5 and 8). Barrett (Ref. 1) indicated that oriented impregnated bits had a bit cost of $0.82 per foot compared with a normal surface set bit cost of $4.80 per foot. In spite of these claims Marx (Ref. 6, p. 15) states that because of the increased cost in setting the diamonds in the hard vector direction the method has not found wide acceptance.

(c) Diamond Exposure and Size

The exposure of the diamond i.e. the height it protrudes above the surrounding matrix, varies with the size of diamond and the physical properties of the matrix, diamond size and matrix properties being dictated by the nature of the material to be drilled. Marx (Ref. 6, p. 11) indicates that the exposure of the diamond is 1/8 to 1/3 of the diamond diameter with a best tolerance of some 0.001 mm. Considering a bit set with stones 40 per carat, i.e. 1.5 mm nominal diameter, the maximum exposure would be approximately 0.5 mm, and would indicate the maximum possible size of cuttings.

Surface set diamonds normally vary from 10-125 stones per carat equivalent to nominal diameters in the range of 2.1 - 1.0 mm respectively. Thus the maximum size of cuttings expected would range from 0.7 mm - 0.3 mm approximately. With impregnated bits the cuttings would obviously be much smaller.

(d) Diamond Spacing

There are two measures of diamond spacing, the radial spacing between adjacent rings, and the circumferential spacing between diamonds set at the same radial distance.

Considering the rounded face of a coring bit with equally exposed diamonds, it is evident that one ring of diamonds on the crest would be required to make the pilot cut. The work required to make this pilot cut, and the associated diamond wear, would be greater than that for adjacent cuts, because side shearing into the pilot cut is possible. Thus one would expect a heavy concentration and reduced circumferential spacing for diamonds in the pilot cutting ring. The number of diamonds would depend upon rock to be drilled and the bit life expected.

The radial spacing between diamond rings should be fixed by the width of the ridge of rock that can be side-sheared for a designed diamond penetration. This will obviously vary with rock type and diamond size. The number of diamonds in the ring should be a function of the expected wear life of the bit and the radial distance, since wear is a function of distance travelled.

(e) Matrix Properties

The matrix is designed to hold the diamond firmly in the crown. It is usually specified by its hardness, the following ranges being normal

| | | |
|---|---|---|
| Standard | Rockwell C | 20-30 |
| Hard | Rockwell C | 30-40 |
| Extra Hard | Rockwell C | 40-50 |

Marx (Ref. 6, p. 10) states that wear resistance of the matrix is a much more important factor in drilling than hardness, but an acceptable standard is not available. He recommends the standard matrix where erosion is not a problem, the hard matrix for moderate erosion or as an initial choice, and the extra hard matrix in badly broken formations where erosion is severe.

Other desirable properties of the matrix include good heat conductivity, a melting temperature low enough not to affect the diamonds during setting operations, and the capability of being chemically broken down for diamond recovery.

The various matrices tend to be trade secrets formed by powder metallurgical processes. Craelius (Ref. 2, Lecture V, p. 3) indicates that tungsten carbide is generally used as the base metal powder for the matrix, with additives such as cobalt, nickel, beryllium, iron, bronze, copper etc. Custers, Elliot and Young (Ref. 3) describe the various alloys used

and their application.

(f) Waterways

Waterways are provided across the cutting surface of the diamond bit to allow a free flow of drilling fluid. The drilling fluid is necessary to cool the diamonds and matrix and also to remove rock cuttings. The drilling fluid may contain additives such as rock hardness reducers which are designed to break down the intermolecular cohesive bonding in the rock, and thus reduce the specific energy of drilling. Hence the waterways must be designed to give a continuous flow of fluid across the full cutting face of the bit, and at the same time provide a passage for the removal of rock cuttings.

Various waterways have been designed by different bit manufacturers some of which originated from recommendations made by practicing diamond drillers. Some of the factors that influence the number and size of waterways are, the size of diamonds, spacing of the diamonds, the cutting surface area, the designed penetration rate and maximum size of rock particle liberated. These factors together with hole depth and annular area will in turn govern the quantity and pressure of the drilling fluid. It should be noted that the provision of waterways reduces the abrasive erosion of the matrix around the diamonds, and thus may increase bit life where matrix wear is a dominant feature.

IV.- OPERATING VARIABLES IN DIAMOND DRILLING

The operating variables associated with diamond drilling can be divided into two groups; the independent variables and the dependent variables.

(a) Independent Variables

The independent variables are, drilling bit thrust, rotary speed, and drilling fluid flow.

(i) Bit thrust

In section I(a) it was shown that sufficient thrust has to be exerted on each cutting diamond to overcome the yield stress of the rock being drilled.

The total thrust is calculated from the area of contact of the diamonds and the designed penetration of these diamonds. This is not a simple calculation, since the diamonds are not of regular shape and due to wear they do not present a constant area of contact. As wear develops and the diamond faces become rounded it is necessary to increase the thrust to maintain the designed penetration rate. Maximum thrust is limited by a number of factors which include, maximum diamond penetration when the matrix makes contact with solid rock face, the yield stress of the matrix securing the diamonds, and the mechanical strength of the drill stem.

There is also a lower limit of thrust, below which deformation of the rock is purely elastic and fully recovered when the thrust is removed. At thrusts of this order of magnitude polishing of the diamonds and rock take place and no useful penetration or rock removal is achieved.

(ii) Rotary Speed

The penetration rate of a diamond bit is, theoretically, directly proportional to the rotary speed if it is assumed that diamond penetration remains constant. Thus as the speed increases, the quantity of rock cuttings is increased which in turn should require an increased drilling fluid flow rate.

Increasing the rotary speed increases the time-rate of wear since more work is done in a given time. It may not however increase the depth-rate of wear, since there may be an optimum speed at which bit chatter or erosion wear are at a minimum.

(iii) Drilling fluid flow

The drilling fluid flow rate should be a function of the volume of material removed by the bit, and the size of the maximum rock particle liberated. As the penetration rate increases, extra drilling fluid is required to remove the increased volume of rock cuttings and dissipate the increased heat generated.

Drilling fluid flow may also be calculated from the stand point of heat dissipation and cooling of the diamonds and matrix. In this regard Marx (Ref. 6, p. 21) indicates that the amount of fluid required to cool the bit is greater than that required to transport the cuttings in the annulus. Nevertheless, he then calculates the minimum flushing water velocity in the annulus between drill rod and rock, based upon an average rock particle size of 1 mm, to be in the range 0.3-0.6 meters/second.

(b) Dependent Variables

The dependent variables are, penetration rate, torque and drilling fluid pressure.

(i) Penetration rate

The penetration rate is affected by all the independent variables and is additionally affected by the design of the diamond bit and size of diamonds used.

For a constant diamond penetration, the penetration rate will increase with rotary speed. Up to the theoretical limit, when diamond penetration equals diamond exposure, penetration rate increases with thrust. This theoretical limit may never be reached however, due to failure of the matrix or drill rod.

In addition, since it appears that a high percentage of the energy supplied to a diamond bit is consumed in reducing the size of liberated rock cuttings, the more rapidly the cuttings are removed, the smaller the amount of useful energy consumed. Under these conditions more energy is available for cutting which should result in an increased penetration rate. Rock cuttings are removed by the flushing fluid, hence an increase in the flushing fluid flow rate should increase the penetration rate. Sasaki and Yamakado (Ref. 9) found a linear relationship between penetration rate and water flow rate for a diamond coring bit producing a 46 mm core, as the flowrate was increased from 10-20 litres/min.

(ii) Torque

In shallow holes the torque acting upon the diamond bit results from the forces resisting the cutting and grinding action of the diamonds at the rock face. In deep deflected holes additional torque is required to overcome friction between the drill rods and the rock, and also the shearing force between the drill rods and the flushing fluid.

Considering shallow vertical holes, torque should increase with diamond penetration and thrust. Torque would also be expected to reduce with increased water flow rate; because less grinding of liberated particles should take place for a given penetration rate. Sasaki and Yamakado (Ref. 9) found that torque was independent of rotary speed but directly dependent upon thrust.

(iii) Drilling fluid pressure

A pressure difference exists between the fluid descending within the drilling rods and that ascending the annulus outside the rods. This pressure is used to counteract the difference in fluid densities, due to suspended rock particles, and to overcome the frictional resistance to flow.

Increasing the penetration rate, either by increasing the thrust or the rotary speed, will increase the weight of suspended rock particles and hence the differential fluid pressure. However, in shallow laboratory test holes this effect can be neglected.

Measurable fluid pressure differences arise from changes in flow resistance at the bit face. As the diamond penetration increases the flow area at the face is reduced and the flow pressure is increased. This difference is at a theoretical maximum when all the water flows through the waterways. Increasing the flow rate also results in an increase in the pressure difference.

(c) Theoretical Relationships Between Drilling Variables

Let P = mean penetration of diamonds into rock mass, feet

R = penetration rate of diamond bit, feet per minute

T = axial thrust on bit, lbs. force

F = torque force, lbs. force

N = rotary speed of bit, r.p.m.

A = area of hole, square feet

r = operating radius of torque force, feet

e = specific energy of drilling ft. lbs. per cubic foot

The specific energy is defined as the work done per cubic foot of material removed.

The penetration rate R = PN ft. per minute 1.

$$\text{The specific energy} = \frac{2\Pi rFN}{RA} + \frac{TR}{RA} \qquad 2.$$

Since the second factor of equation 2, which represents the work done by the axial thrust, is found to be less than 1 percent of the first factor, it can be neglected.

$$\text{Thus } e = \frac{2\Pi rFN}{RA} \qquad 3.$$

For a particular diamond bit $\frac{2\Pi r}{A}$ is a constant,

$$\text{so } e = \frac{C_1 FN}{R} \qquad 4.$$

If F is found to be directly proportional to T, then for a constant thrust we have

$$e = \frac{C_2 N}{R} \qquad 5.$$

where $C_2$ is a constant.

If e is directly proportional to N, then the penetration rate R must be a constant. If R is directly proportional to N, the specific energy must be conconstant for the particular thrust.

IV.- SOME RESULTS OF LABORATORY TESTING

(a) Instrumentation

A laboratory diamond drilling test rig has been designed by the author around a two horse power, floor mounted, electric drilling machine. The machine is fitted with a six speed gear box covering the range 140-1,500 revolutions per minute.

The drilling bit is fed by a constant thrust arrangement using a pulley and suspended weight attached to the manual feed shaft. Variable drilling thrusts can be obtained by increasing or decreasing the suspended weights.

The thrust exerted by the drilling bit is measured by a load cell mounted beneath the rotary table which carries the rock specimen. The load cell is a simple fixed-end steel beam with electrical resistance strain gauges mounted on the upper and lower faces to form half of a wheatstone bridge circuit. Thrust is obtained by dead weight calibration.

The torque force developed by the bit while drilling is measured by means of electrical resistance strain gauges mounted upon a cantilever arm. This arm is actuated by a rod fitted to the underside of the rotary table. The table rotates on a tapered thrust bearing which is mounted in a steel shaft that actuates the previously described thrust cell. See Fig. 2. Rock specimens are secured on the rotary table by means of four thumb screws. The rotary table is aligned so that its axis of rotation coincides with the axis of rotation of the drill bit. This device allows the reactional torque force to be measured, as against the difficult problem of measuring the torque in the drill rod. By altering the thickness of the cantilever arm or the radius of the actuating rod, a range of sensitivities can be obtained.

Rotary speed is measured with the aid of a tachogenerator, driven by friction against the knurled collar of the drill feed shaft.

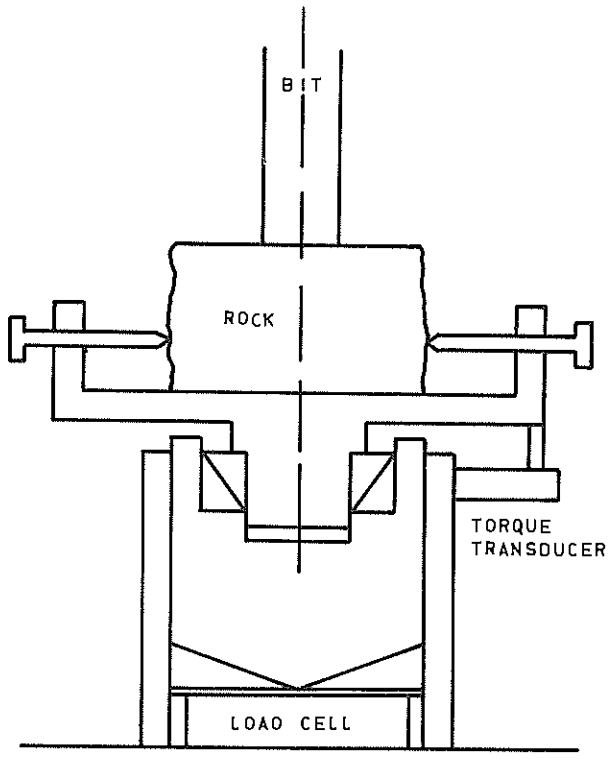


Fig. 2. Diagramatic illustration showing a section of drill rig.

Bit penetration is measured with an electrical displacement transducer fitted to the rotary swivel which carries the drilling bit.

Drilling fluid flow is obtained from an instrument designed about a mercury manometer which measures the differential pressure associated with the drilling fluid flowing through a restricted pipe. The mercury forms the variable plate of a capacitor which actuates a capacitance bridge as described by (Ref. 10).

The range and sensitivities of the various transducers under operating conditions are tabulated below. Table 1 lists the combined sensitivity of transducer and recorder, i.e. the minimum variation that can be clearly read on the recorder.

In order to make an adequate study of the interrelationships between the drilling variables, it was decided that continuous recording of all measuring transducers was essential. A six pen graphic recorder was chosen in preference to a magnetic tape recorder because of the recording speed range and the ability to visually follow the transducer outputs. Any malfunction of a transducer can be immediately observed and corrective action can be taken. In addition the recording of all variables on one chart greatly simplifies the problems of data correlation, storage and processing.

TABLE I

COMBINED TRANSDUCER AND RECORDER SENSITIVITY

| Variable | Sensitivity | Range |
|---|---|---|
| Torque | 0.5 lbs. | 0-70 lbs. |
| Thrust | 3.5 lbs. | 0-450 lbs. |
| Penetration | 0.016 ins. | ± 3 ins. |
| Rotary Speed | 10.0 r.p.m. | 2,000 r.p.m. |
| Water Flow | 0.0004 gall/min. | 0-0.15 gall/min. |
| | 0.003 gall/min. | 0-1.0 gall/min. |
| Water Pressure | 0.25 p.s.i. | 0-100 p.s.i. |

(b) Discussion of Results

The following results were obtained for an EX diamond coring bit cutting a hole of 1.459 inches diameter and yielding a core 0.839 inches diameter. Fig. 3 is a plot of torque force in lbs. against thrust in lbs. The results were obtained from measurements taken in four holes over a depth of approximately 12 inches, at various rotary speeds and thrust. Water flow was maintained constant at 0.124 galls per minute. The plot shows clearly that torque force is proportional to thrust for a given rock/bit combination, irrespective of the rotary speed. The conditions indicated are thus specified by equation 5.

$$e = \frac{C_2 N}{R} \qquad 5.$$

Fig. 4 is a plot of penetration rate in inches per minute against rotary speed in revolutions per minute at various thrusts. The figure shows that the penetration rate is proportional to the rotary speed for a constant thrust, and also that the penetration rate increases with thrust. Since the cut area of the hole is 1.119 square inches the range of nominal stresses varies from 160-390 pounds per square inch. Fig. 4 shows that R is proportional to N, which indicates that the specific energy is constant for a given thrust. Fig. 5 shows the relationship between specific energy and thrust. One plot at a constant speed has been reproduced since it was found that above a critical thrust of some 250 lbs., the specific energy did not vary with rotary speed, but was dependant upon thrust alone for a constant rate of drilling fluid flow. A possible explanation of this relationship is as follows. In drilling operations, energy is expended to bring about elastic deformation, plastic deformation and create new surface in the rock. The greater the penetration of the diamonds into the rock, the larger the particles produced, resulting in a reduction in the energy used in creating new surface area; this reduction being independant of the rotary speed of the drill.

Fig. 6 shows this relationship in another form. In this figure specific energy has been plotted against rotary speed at various bit thrusts.

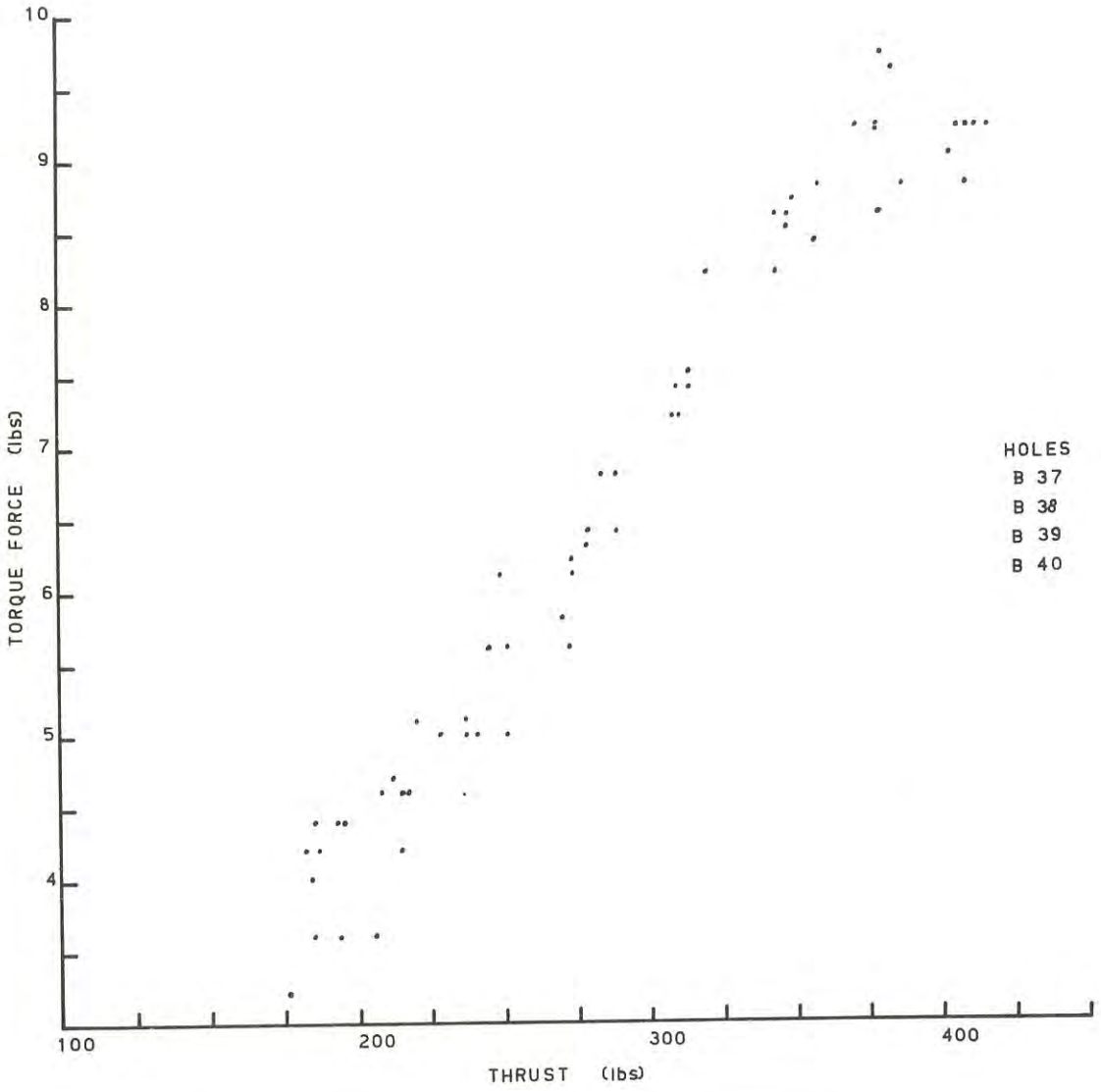


Fig. 3. Torque force and thrust relationships for an E.X. bit.

Considering the higher thrusts, it is seen that specific energy is independent of the rotary speed. As the thrust is reduced the scatter of the measured results increases, particularly at thrusts below 270 lbs. Below this level of thrust the bit is not cutting efficiently, a polishing action is developed with the diamonds removing asperities and creating very fine particles and a large surface area. The large scatter of results may be attributed to loss of bit contact and chatter at the rock surface.

## VI.- SOME BASIC PROBLEMS ASSOCIATED WITH DIAMOND DRILLING RESEARCH

Diamond drilling is an expensive operation normally undertaken by relatively small contracting organisations, hence the amount of research that has been undertaken to study the basic action of the diamond bit is very limited. Some of the results that have been published are of limited application because they have not been normalized to "new-bit" conditions.

### (a) Normalizing Drilling Data

When a drilling bit is new the diamonds have the maximum exposure and the minimum bearing area. As drilling proceeds the exposure is reduced due to wear and the bearing area of the diamonds increases. Thus under constant conditions of thrust and rotary speed the penetration rate decreases and the specific energy increases. In compiling data based upon laboratory measurements it becomes essential to take this wear into account and normalize the raw data back to

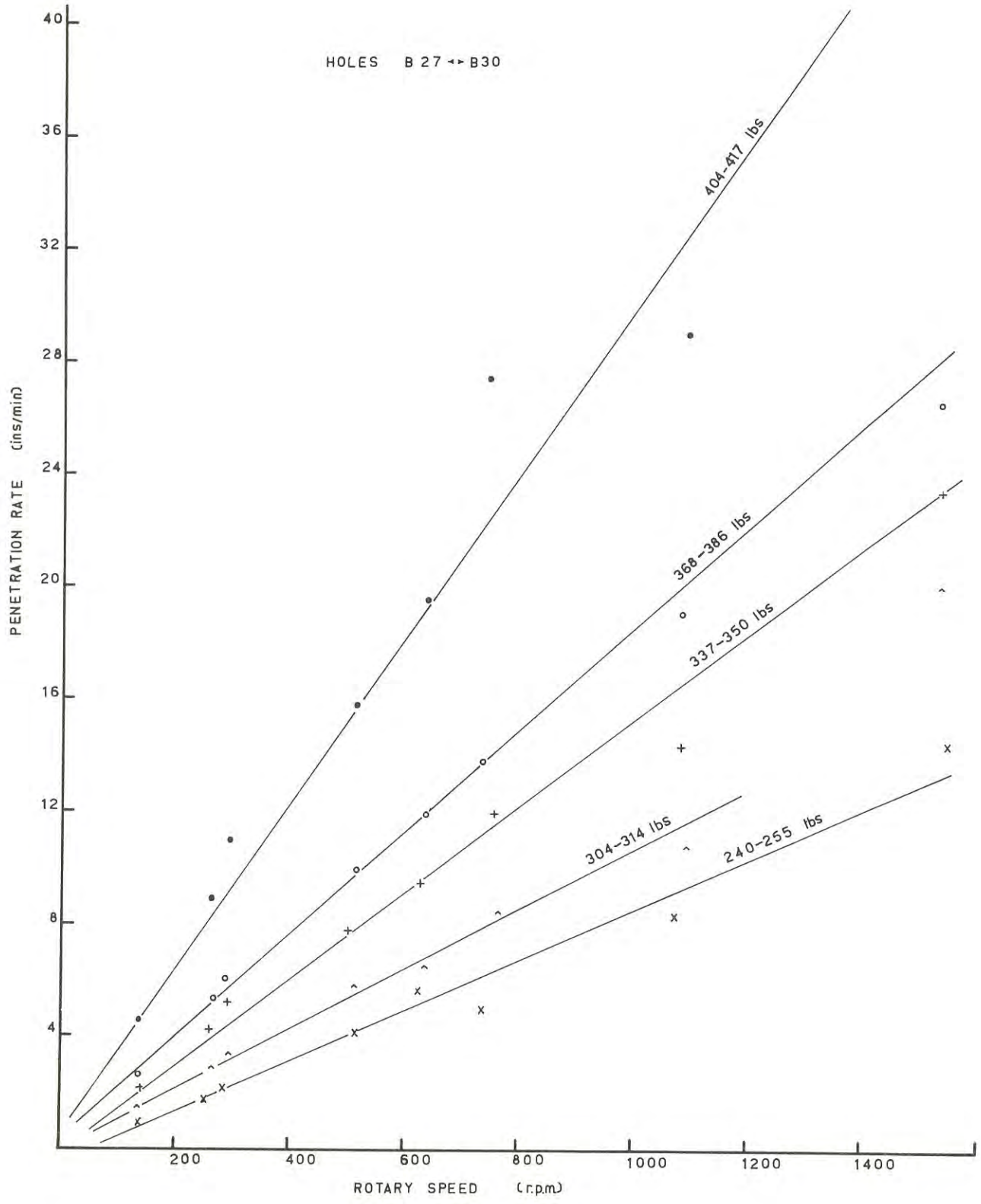


Fig. 4. Relationships between penetration rate and rotary speed of an E.X. bit at various thrusts.

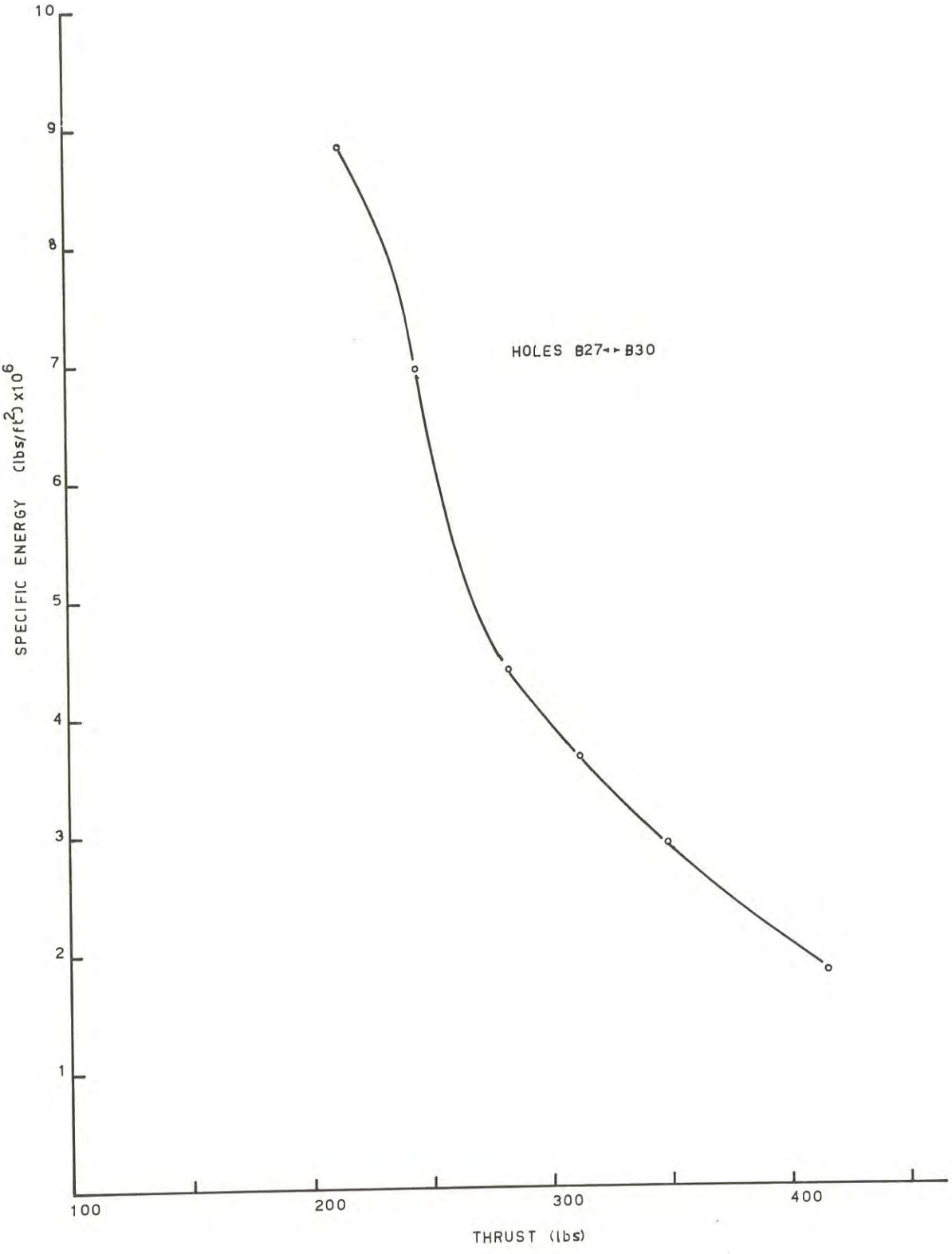


Fig. 5. Specific energy variation with bit thrust, E.X. bit.

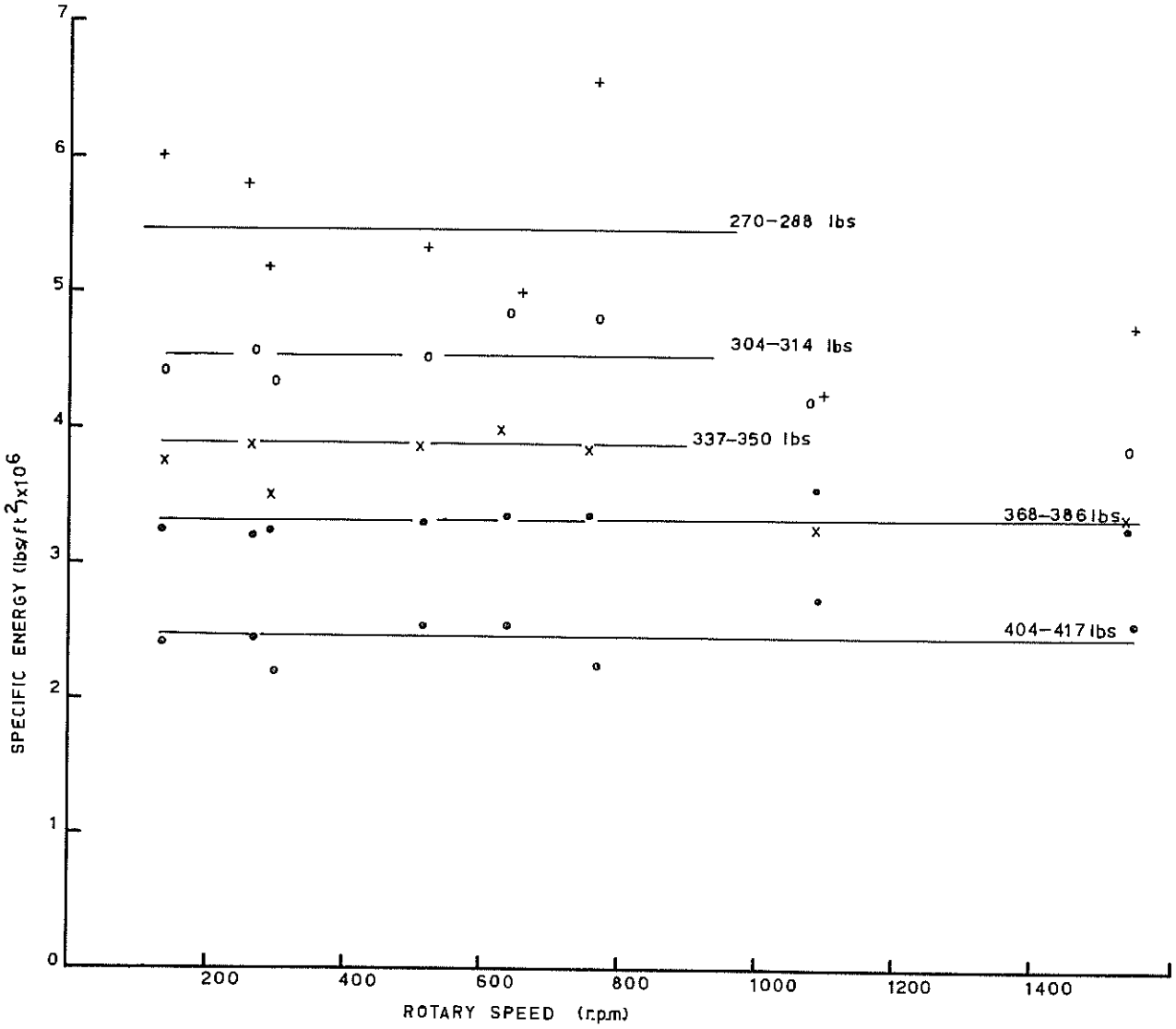


Fig. 6. Relationship between specific energy and rotary speed at various thrust.

"new-bit" conditions.

The data previously presented has been normalized to account for wear, the corrections being made as follows. For each new rock specimen, in which some 10-12 inches of drilling was undertaken, a small depth was drilled at standard conditions of thrust, rotary speed and water flow. The penetration rate and the specific energy for these standard conditions were then tabulated against the cumulative depth drilled. A least squares regression program was executed on the data with the aid of a digital computer to give the best fit relationship. The raw data was then corrected back to "new-bit" conditions by this normalizing curve.

For the data presented the general form of the normalizing curve is given by

$$R = a(\exp)^{-bD} \qquad 6.$$

So that $\log R = \log a - bD \log (\exp)$

where R = Penetration Rate (thousandth of an inch/minute)

D = cumulative depth (inches)

a and b are constants; a gives the initial drilling rate, while b depends upon the abrasitivity of the rock being drilled.

For the data presented the curve is specified by

$$R = 387.4(\exp)^{-0.0318D}$$

the correlation coefficient of this regression being 0.97419.

It immediately becomes obvious that to justify such a correction procedure for raw data, great care must be exercised to attain standard drilling conditions. The independent variables of thrust, rotary speed and fluid flow must be held constant and in addition the rock being drilled must be homogeneous and isotropic. The rock used in the above tests was a microsyenite obtained from the spillway of the Moogerah Dam near Ipswich, Queensland, its physical properties are as follows:

| | |
|---|---|
| Compressive Strength | 30,000 p.s.i. ± 5,000 |
| Vickers Hardness | 153-169 |
| Shore Hardness | 77-100 |
| Grain Size | 0.2-2.0 mm. |

## VII.- CONCLUSIONS

This paper presents a small amount of laboratory measured data in an area where very little factual information is available. Factorially designed tests at higher thrusts and water flows are necessary and are being executed to extend this data. Tests to show the effect of drill fluid flow, rotary speed and thrust upon wear and bit life are essential to indicate optimum drilling conditions. In addition the conflicting claims made regarding surface active hardness reducers need close examination.

## VIII.- ACKNOWLEDGEMENTS

The author wishes to thank the Australian Mineral Industries Research Association, the Queensland Mines Department and Universal Carborundum Australia Pty. (formerly Commonwealth Diamond Tools), for their financial support of this research project.

## REFERENCES

1. BARRETT, J.L. - Drilling research develops low-cost diamond bit, Qrty. Colorado Sch. Mines, Vol. 58, 4, Oct. 1963, pp. 259-273.

2. CRAELIUS, Svenska Diamantbergborrnings A.B., - Diamond Core Drilling (A Series of lectures) FACK, STOCKHOLM 1, SWEDEN, 2nd Ed. 1965.

3. CUSTERS, J.F.H., ELLIOTT, C.R. and YOUNG, R.S. - Fundamentals of diamond drilling, Jrnl. Chem. Met. Min. Soc. S. Africa, Vol. 52, No. 10, Part 2, April 1952, pp. 381-392.

4. HOEK, E. - Rock fracture under static stress conditions, Rep. Coun. Scient. Ind. Res. S. Afr., MEG 383, Oct. 1965, pp. 60-75.

5. LONG, A.E. - Diamond orientation in diamond bits, U.S. Bur. Mines. R.I. 4800, June, 1951.

6. MARX, C. - Diamond bits and their use in shallow holes, Christensen Diamond Products Co., English text rewritten by Kempe, W., 1967.

7. PFLEIDER, E.P. and BLAKE, R.L.- Research on the cutting action of the diamond bit, Trans. Amer. Inst. Min. and Met. Engrs., Vol. 196 (Mining), Feb. 1953, pp. 187-195.

8. PFLEIDER, E.P. - Orientation of cube diamonds in drill bits, Trans. Amer. Inst. Min. and Met. Engrs. Vol. 196 (Mining), Oct. 1953, pp. 998-1003.

9. SASAKI, K., and YAMAKADO, N. - Investigation of diamond core bit boring, Industrial Diamond Review, 1962, 22, pp. 178-186.

10. STACEY, F.D., RYNN, J.M.W., LITTLE, E.C. and CROSKELL, C. - Displacement and tilt transducers, Jrnl. Sci. Instrms. (Jrnl. Phys.), 1969, Series 2, Vol. 2, pp. 945-949.

# Reduced Soil Strength and Stiffness at the Top of Tube Samples

By

J. G. Lang, Dip.Civ.E., M.I.E.Aust.

(Experimental Officer, Division of Applied Geomechanics, C.S.I.R.O.)

SUMMARY.- An investigation is described designed to assess which part of a tube sample gives the more reliable estimate of the original soil properties in the ground. A decomposed granite and a decomposed mudstone were sampled with a 3 in. Auger Core Soil Sampler. In one set of tests at each site, each sample was long enough to permit an upper and lower test specimen to be cut, while in the other set the advance of the sampler was shorter, permitting only one test specimen per tube sample. Subsequently an immediate undrained triaxial compression test was made on the specimens in the laboratory.

Secant modulus values for the single specimens were found to match closely those for the lower specimens, even though the sampling forces required to obtain the latter were much higher. The influence of these forces, and of soil disturbance arising from the sampling procedures, on variations in tube sample properties is discussed. It is concluded that the lower part of a sample should give a more reliable indication of actual soil ground conditions than the upper part.

## I.- INTRODUCTION

Even though care is taken in obtaining intact soil samples, some disturbance is inevitable. While attempting to minimize disturbance to that acceptable for the proposed tests, a practical approach is to recognize that disturbance will occur, and to make allowance for its influence on the properties measured in the laboratories. Disturbance can be considered to be present when variations in the values of soil properties measured at points along the length of a sample exceed variations to be expected from natural causes. Experimental evidence of variations along the length of tube samples has been reported (Ref. 1, 2 and 3).

The author reported (Ref. 4) that when two test specimens were cut from the same tube sample, the lower specimen had significantly greater strength and stiffness than the upper specimen. The next question to be answered is which values give the better indication of the properties of the undisturbed material in place. For example, it could be argued that depressed values were obtained for upper specimens due to loosening of the sample during sampling, or alternatively that high values for the lower specimens were caused by compaction. Since in some cases, the forces applied to the sampler during the latter stages of the advance of the sampler were quite large, it was decided to investigate the significance of this factor.

## II.- BASIS OF EXPERIMENTATION

A method involving the comparison of two sampling procedures or patterns was used. Pattern A (Fig.1(a)) followed that used previously (Ref. 4), the advance of the sampler being sufficient to permit two test specimens (upper and lower) to be cut from each tube of sample obtained. In Pattern B (Fig. 1(b)) the possibility of large forces was reduced by limiting the length of sample taken with each advance of the

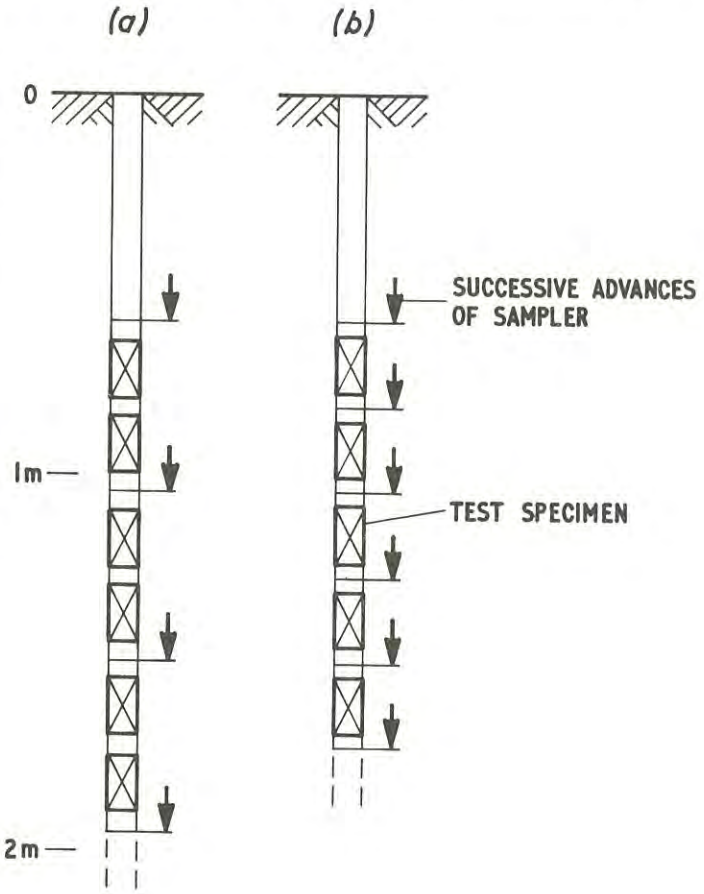


Fig. 1.- (a) Sampling Pattern A;
(b) Sampling Pattern B.

sampler. From these short samples only a single test specimen could be prepared.

The secant modulus of elasticity was adopted as the principal criterion for assessing variations of disturbance. The superiority of this variable over soil strength had been predicted (Ref. 1), and demonstrated experimentally (Ref. 4 and 5). The greater sensitivity of the modulus of elasticity is due to this property being related to that part of a test where little strain has occurred. The greater strain and distortion of the specimen before peak stress is reached will tend to mask any disturbance caused by the sampling operation.

## III.- TEST SITES

The soils at the two sites were residual, having been formed from decomposed granite at Greenvale and decomposed mudstone at Syndal. Features of the two sites are compared in Table I. The soil at Greenvale was chosen for test sampling because it was expected that any excessive sampling forces would tend to destroy the structure of the residual soil and that this would be readily apparent in laboratory test results. In contrast it is known that some soils can take a good deal of ill treatment without showing undue distress. Such soils are quite unsuitable for investigating sampling procedures as test results obtained will not show any difference between one sampling procedure and another.

The tests made at Syndal enabled comparison with earlier work done on this site.

## IV.- SAMPLING PROCEDURE

All sampling operations were carried out with a 3 in. Auger Core Soil Sampler (Ref. 6 and 7). In this sampler the sample tube does not rotate but is forced axially downward while the annular space outside the sample tube is cleared by cutters and auger flight fixed to the outer rotating barrel. The sampler was operated from a truck-mounted drill (Mobile B-40 Explorer) using hydraulic power for both feed and drill shaft rotation. For experimental purposes this machine is fitted with instruments developed to measure the principal parameters of the sampling operation, such as position, thrust, torque, rotational speed, and sample displacement. The instruments have been described elsewhere (Ref. 8).

TABLE I

TYPICAL PROPERTIES AT TEST SITES

| Site | GREENVALE | SYNDAL |
|---|---|---|
| Location (from City of Melbourne, Victoria) | 22 km (13 miles) NNE | 18 km (11 miles) ESE |
| Soil | Decomposed Granite | Decomposed Mudstone |
| Clay size, under 0.002 mm (%) | 15 | 35 |
| Silt size, 0.002 - 0.060 mm (%) | 20 | 35 |
| Sand size, 0.060 - 2.000 mm (%) | 50 | 30 |
| Gravel size, over 2.000 mm (%) | 15 | 0 |
| Dry Density ($kg/m^3$) | 1800 | 1730 |
| Moisture content (%) | 13 | 19 |
| Degree of saturation (%) | 72 | 91 |
| Strength ($\sigma_1-\sigma_3$ at $\sigma_3$ = 70)($kN/m^2$) | 360 | 390 |

In Pattern A the sampler was advanced 450 or 600 mm (1.5 ft or 2.0 ft), to obtain a sample long enough to cut two test specimens. Each sampling began from the depth to which the sampler had advanced previously, that is, the sampling was *continuous*. The machine was anchored to the ground and the designated advance of the sampler obtained, even though this meant that large forces had to be applied and that less than complete recoveries were obtained. Thus at Greenvale the axial forces applied to the sampler rose to the region of 16 kN (3500 lbf.), while the torque reached 270 Nm (200 lbf. ft). Gross recoveries for this pattern at Greenvale were low, generally about 70 per cent. Examination of record made showed that usually in these cases, the specific recovery ratio was 100 per cent for 70 per cent of the total advance; then jamming occurred quite suddenly and no further sample entered the tube. At Syndal forces were less and recoveries better, but still often less than 100 per cent.

In Pattern B the advance of the sampler was about 210 mm (0.70 ft). Again the sampling was *continuous* but with this pattern recovery ratios were generally 100 per cent while applied forces were a good deal less, averaging in the case of Greenvale about half the values of Pattern A. (This seems reasonable as the advances were approximately halved.)

At each site several bores were made spaced about 1 m apart. At Greenvale, samples were taken from four bores using Pattern A and two bores using Pattern B, while for Syndal there were seven bores using A and two bores using B. There was no free water in any of the bores.

## V.- LABORATORY TESTING

In the laboratory an immediate undrained triaxial compression test was made on specimens 6 in. (152.4 mm) long and the full 3 in. (76.2 mm) diameter as sampled. All tests reported were made at a lateral pressure of 70 $kN/m^2$ (10 p.s.i.). The secant modulus values are determined from the stress-strain origin (with the strain origin corrected if necessary for bedding-in effects) to a point where the stress is one-third of the peak value reached.

## VI. DISCUSSION OF RESULTS

For the Greenvale samples both peak deviator stress and secant modulus values obtained from the triaxial tests were generally higher for the lower specimens than for the upper specimens of pairs cut from the same tube sample (Fig. 2). Similar results were reported previously for a site at Syndal (Ref. 4). No explanation can be found for the one notable exception in Fig. 2(b).

Fig. 3 and 4 show for Greenvale and Syndal respectively, the peak deviator stress and secant modulus

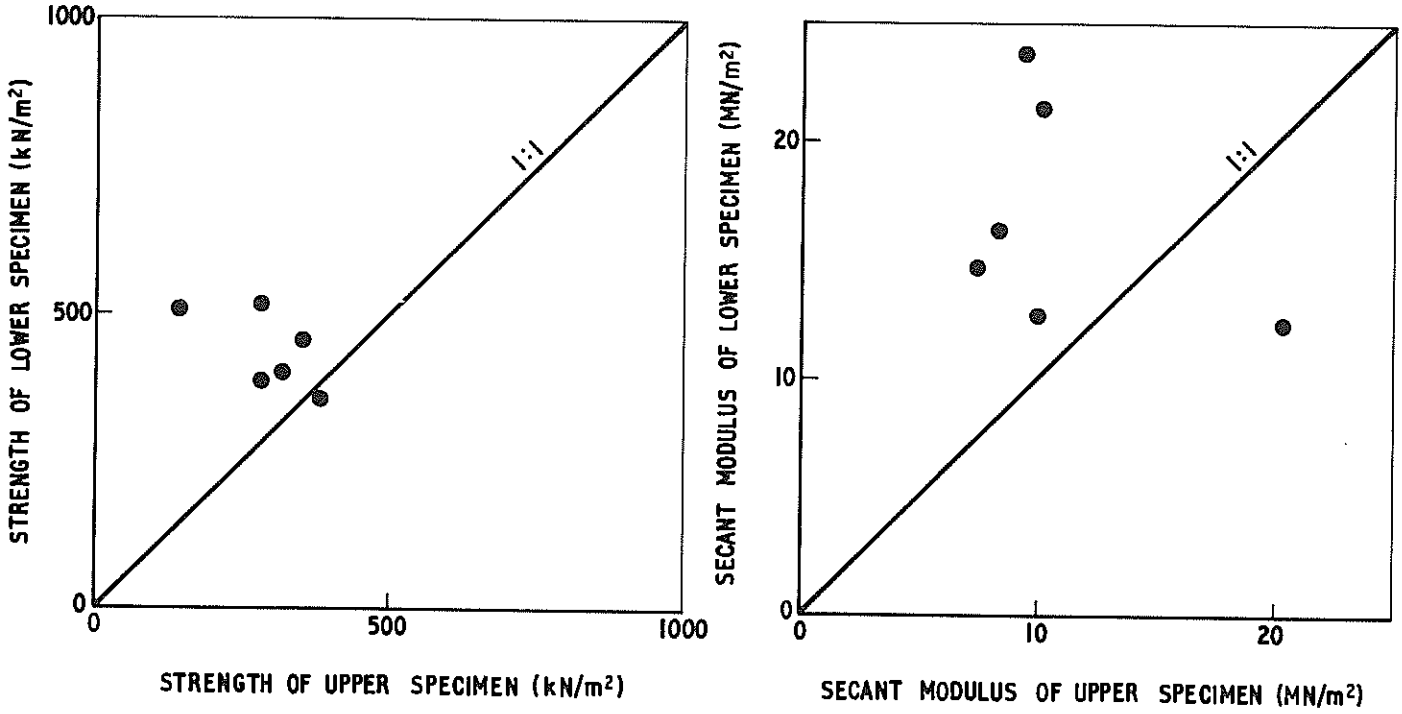


Fig. 2.- Greenvale Site: Comparison of peak deviator strength and secant modulus of elasticity for upper and lower specimens from same sample tube.

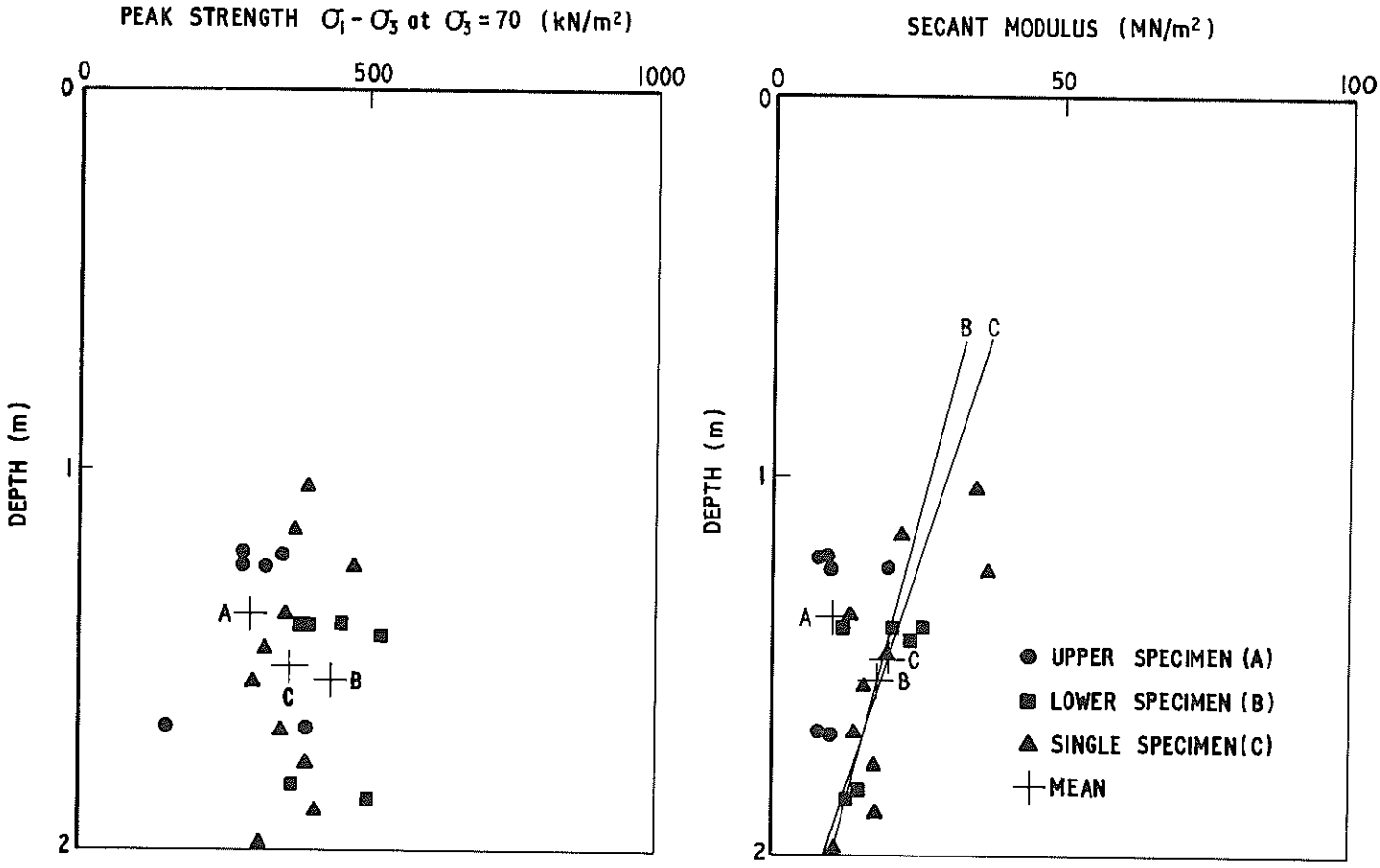


Fig. 3.- Greenvale Site: Peak strength and secant modulus of elasticity for different types of specimen against depth.

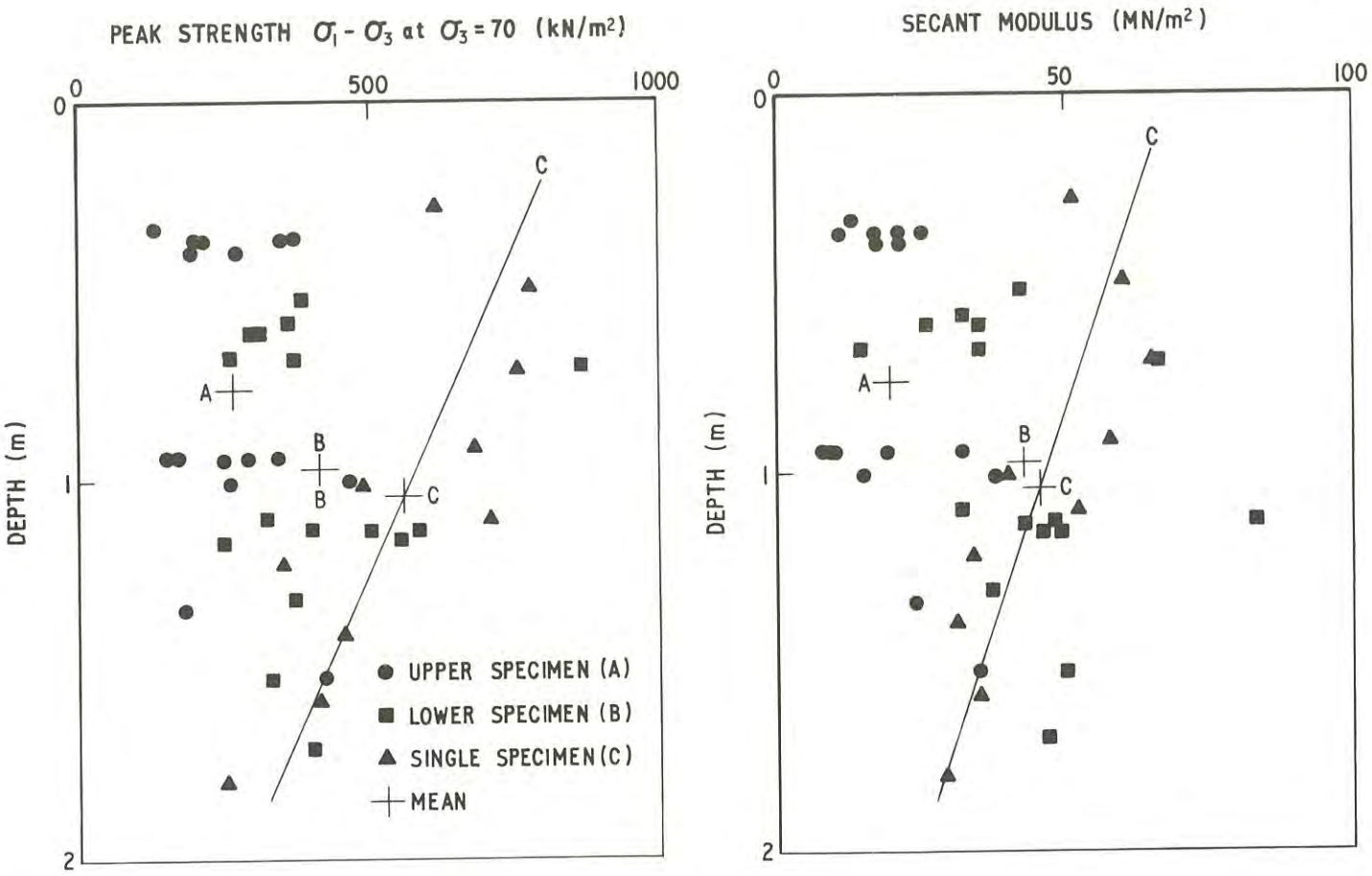


Fig. 4.- Syndal Site: Peak strength and secant modulus of elasticity for different types of specimen against depth.

plotted against depth. In these figures the points for the upper specimens, lower specimens or single specimens are differentiated. Mean points for each set are marked and when the correlation is statistically significant, the regression line for a set of values against depth is also shown.

From the records obtained during the sampling operations at Greenvale, the peak axial forces applied to the sampler during the intervals that the upper and lower parts of a sample were entering the sample tube have been determined. In Fig. 5 the secant modulus of test specimens is shown against the force applied while the sample was entering the sample tube. It is seen that there is no correlation between these variables. However, when the secant modulus is plotted, as in Fig. 6, against the force applied in the interval immediately before the sampling of the part of the sample being considered, then a significant, negative correlation is found, with the secant modulus decreasing as the force increases. Apparently, the application of high forces during the time that a particular part of a sample was being cut did not affect *that* part of the sample, but after a sample jammed in the sample tube the soil zone below the sampler was subjected to shear failure as the sampler was forced down to the designated sampling depth. Because the sampling was *continuous*, this shear failure zone would lie in the material from which the upper part of the next sample would be cut and would account for the lower values of the corresponding test specimens. Thus the variations within a tube sample were not influenced very much by what happened during the taking of a sample, but were influenced considerably by what had happened during the previous sampling operation. For sampling Pattern B (short samples), there would have been less prior disturbance of this nature because the forces applied were lower. While the possibility of this prior disturbance mechanism has been recognized previously (Ref. 1), this present experimental work provides some positive evidence of its significance.

The relationship of the single specimens to the pairs is not consistent for peak strength. For Syndal clay, the single specimen mean is higher than that of upper or lower specimens of pairs, but for Greenvale the single specimen mean lies about midway between the other two.

## VII.- CONCLUSION

The results of the experimental investigation are generalized and consolidated in Table II.

This table shows a negative association between secant modulus and force applied *prior* to sampling, but no association between secant modulus and force during sampling.

This result is contrary to initial expectation and suggests that prior disturbance of a soil sample was the dominant cause for the difference in values obtained for upper and lower specimens, particularly

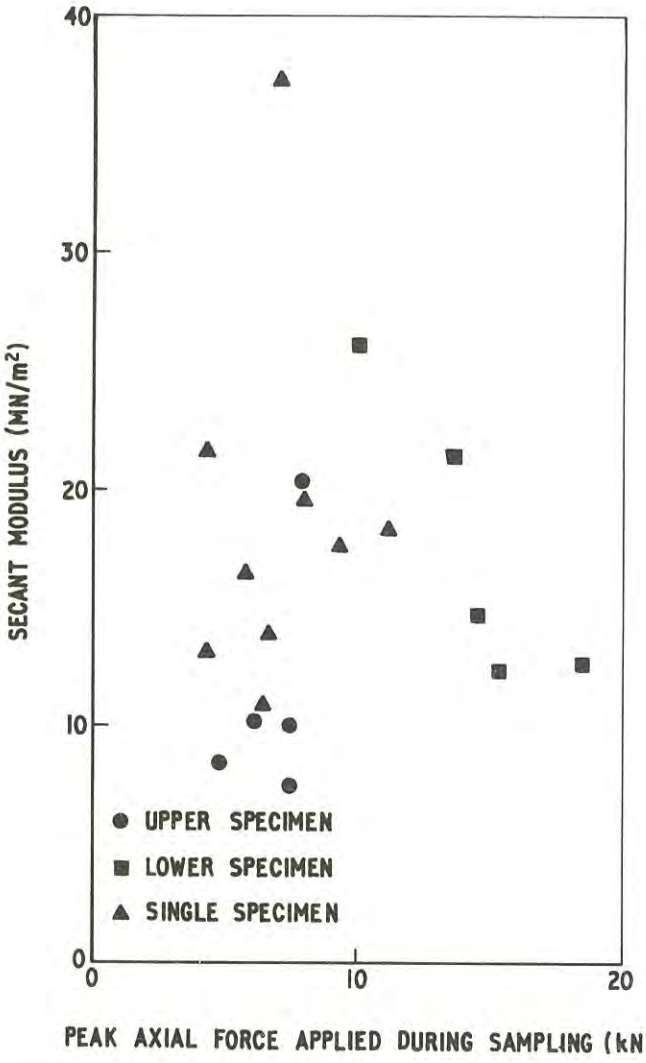


Fig. 5.- Influence of force applied during sampling on secant modulus of elasticity of specimens.

in view of the fact that *continuous* sampling was used in all the tests. Before a sample was taken, the upper zone of the depth to be sampled had already, in some cases, been disturbed by the final stages of the previous sampling operation.

TABLE II

CONSOLIDATION OF RESULTS

| Type of Specimen | Forces Applied to Sampler | | Secant Modulus |
|---|---|---|---|
| | During Sampling | Prior to Sampling | |
| A. Upper | Low | High | Low |
| B. Lower | High | Low | High |
| C. Single | Low | Low | High |

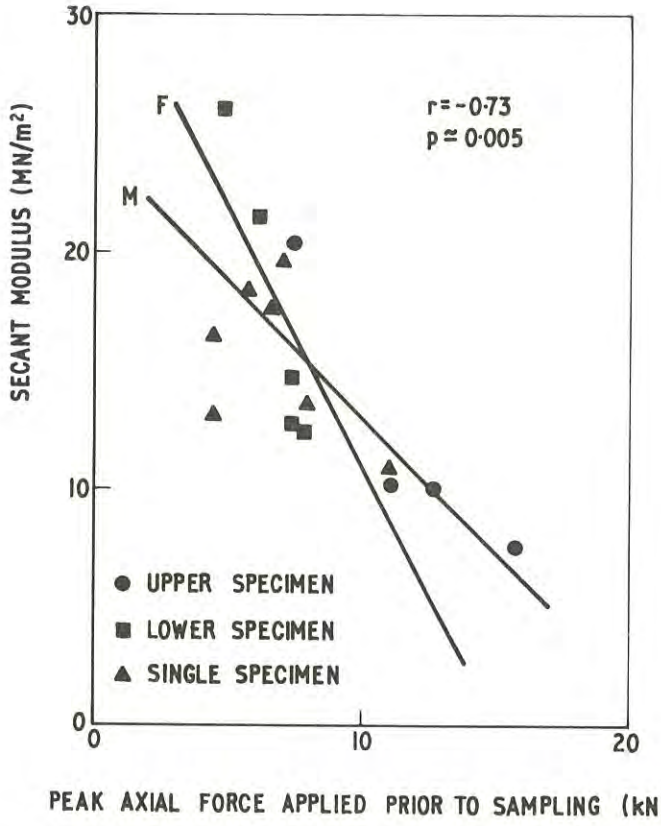


Fig. 6.- Influence of force applied prior to sampling on secant modulus of elasticity of specimens. (F is regression line for force, M for modulus.)

In the present work the influence of prior disturbance has not been investigated directly. A possible extension would be to use a pattern similar to Pattern A (long samples) but to space the samples and carefully remove the potentially disturbed material from below one sample before taking the next sample. This next sample would then be from ground not subjected to prior sampling forces.

On the basis of the results obtained, and the suggested cause, it follows that the test results from lower specimens of pairs, cut from the same tube sample, give a better indication of the true conditions in the ground, particularly when secant modulus of elasticity is the property being examined. For peak strength, the position has not been so well defined, but in the absence of other evidence, it is considered that the same conclusion may reasonably be applied for practical purposes.

VIII.- ACKNOWLEDGEMENT

The assistance of Mr. D.G. Blore in the field and laboratory work is gratefully acknowledged.

REFERENCES

1. HVORSLEV, M.J. - Subsurface Exploration and Sampling of Soils for Civil Engineering Purposes. Report on a Research Project of the Committee on Sampling and Testing, Soil Mech. and Found. Div., ASCE, printed by Waterways Experiment Station, Vicksburg, Miss., 1949, 521 p.

2. BARTLETT, A.H. and HOLDEN, J.C. - Sampling and *In Situ* Testing Equipment used by the Country Roads Board of Victoria for Evaluating the Foundations of Bridges and Embankments. Proc. 4th Conf. A.R.R.B., Melbourne, 1968, pp. 1723-1736.

3. DE LORY, F.A. and SALVAS, R.J. - Some Observations on the Undrained Shearing Strength used to Analyse a Failure. Canadian Geotechn. J., 1969, 6, pp. 97-110.

4. LANG, J.G. - Longitudinal Variation of Soil Disturbance within Tube Samples. Proc. 5th A.N.Z. Conf. on Soil Mech. and Found. Engng, Auckland, 1967, pp. 37-42.

5. WARD, W.H., SAMUELS, S.G. and BUTLER, Muriel E. - Further Studies on the Properties of London Clay, Geotechnique, 1959, Vol. 9, pp. 33-58.

6. AITCHISON, G.D. and LANG, J.G. - A basic Series of Samplers for Undisturbed Sampling of Soil. Techn. Rep. No. 2, Soil Mechanics Section, CSIRO, Melbourne, 1963.

7. AITCHISON, G.D. and LANG, J.G. - Undisturbed Soil Sampling in Australia and the Need for a Basic Series of Samplers. Proc. 4th A.N.Z. Conf. on Soil Mech. and Found. Engng, 1963, pp. 354-57.

8. LANG, J.G. - Instrumentation of Soil Sampling Operations. Proc. of Specialty Session No. 1, 7th Intern. Conf. on Soil Mech. and Found. Engng, Mexico, 29th August, 1969, pp. 77-83; published by Intern. Group on Soil Sampling, Melbourne, Australia.

# Model Studies of Fragmentation of Explosives

By

G. D. Just, B.E., Ph.D., A.M.Aus.I.M.M.

(Lecturer in Mining Engineering, University of Queensland)

AND

D. S. Henderson, B.E.

(Postgraduate Research Scholar, Department of Mining and Metallurgical Engineering, University of Queensland)

SUMMARY.- Measurement of the size distribution of rock particles produced by explosive charges should indicate the relative effectiveness of any blasting design. Such data, although commonly used to optimise rock breakage in mineral processing, has not apparently been used to optimise the explosive rock breakage process. The paper describes the results of investigations into the size distribution of particles produced by blasting in small scale models. Crater testing techniques were used with the charge located at varying distances from the surface. A method of analysis has been developed to describe the particle size distribution in terms of the geometry and size of the explosive charge. The significance of these results to full scale blasting operations is discussed in relation to the modelling parameters used in the experiments.

## I.-INTRODUCTION

The rock breaking process is an essential feature of most mineral extraction and processing operations. Fragmentation in primary and secondary breaking affects materials handling problems in mineral extraction, and crushing and grinding processes control the liberation of mineral particles in mineral processing. Although major technological advances have been made in the materials and power sources available to the mineral industry for rock breaking, the real efficiency of the rock breaking process remains very low. If the efficiency is to be increased, research is necessary to develop entirely new concepts.

Advanced research into the nature of rock breakage has not yet resulted in the development of a satisfactory theory to explain the observed phenomena in a rock mass subjected to impact loading. A rock breakage process cannot therefore be described using basic scientific principles. Initially an empirical approach must be made, followed by continuous improvements as the results of full scale applications become available until sufficient reliable data are obtained for a sound theory to be developed and tested. An example of this approach has been the development and application of rock breakage models in mineral processing. These models are based on size distribution analyses of the initial and final products. The application of this technique to rock breakage by explosives is restricted by a lack of knowledge of the size distribution of the material broken by blasting.

One major problem on the use of size distribution as a measure of blasting efficiency is the difficulty associated with the measurement of this parameter in full scale blasting operations. Attempts to overcome this problem by the use of photographic and sampling techniques have not yet been successful. However, further tests have been planned in which all material from a large-scale blast will be screened to obtain statistical information to improve sampling techniques. The main objective of the research programme on fragmentation in small scale blasting experiments, as described in this paper, was to develop a method of analysis which would indicate the nature of any relationship between size distribution and charge burden. This should reduce the amount of costly full-scale testing required to develop a practical mathematical model to optimise industrial rock breakage operations.

The current postgraduate research programme on rock fragmentation by explosives has been in progress since 1970. This paper describes the detailed results achieved during this period. A method of analysis to relate these results to full-scale operations is presented. Further large scale testing is planned to determine the significance of these model relationships. Because the available literature on this subject does not contain any reference to studies of this nature, detailed results have been presented in the Appendix to this paper.

## II.- CRATER TESTING THEORY

The most commonly used method of evaluating the performance characteristics of a particular explosive in a given material is a series of crater tests. This allows the determination of critical depth, strain energy factor and optimum depth ratio as defined by Livingston in 1956 (Ref.1). Also inherent in the Livingston Crater theory is a method of scaling, which allows larger scale blasts to be designed from testing on a small scale.

The Livingston theory has been successfully applied to large scale production blasts by Bauer in 1961 (Ref. 2) and Grant in 1964 (Ref. 3).

For a concentrated charge buried below a free face, Livingston defined four ranges of behaviour of the blast, depending upon the burden or distance from the charge to the free face. These were:-

(a) Strain Energy Range

(b) Shock Range

(c) Fragmentation Range

(d) Air Blast Range

The above ranges occur in the above order as the burden is decreased from infinity, for charges of constant weight.

(a) Strain Energy Range

In this range no crater occurs. The energy of the explosion is completely absorbed by the molecular structure of the rock. The depth where surface breakage just becomes evident is called the critical depth and this point indicates the upper limit of the strain-energy range. Livingston describes a relationship between the critical depth and the weight of the charge, in the form

$$N = E_s(W_c)^{1/3}$$

where N = critical depth

$W_c$ = weight of explosive charge

$E_s$ = strain energy factor

The strain energy is constant for a particular combination of explosive type and rock type.

(b) Shock Range

With further decrease in depth, slabbing occurs at the surface due to reflection of shock waves. As the burden is reduced, the amplitude of the wave which is reflected at the free face increases. This increased slabbing results in a larger crater volume. Eventually the resultant burden between the charge and the final free face, after slabbing is complete, will be small enough to allow the radial cracking due to gas pressure effects to extend and cause complete loosening of material. This is the point of maximum utilisation of explosive energy and corresponds to the optimum depth defined by Livingston, in the equation below:-

$$D = \Delta_o E_s(W_c)^{1/3}$$

where D = optimum depth

$\Delta_o$ = optimum depth ratio = $(\frac{D}{N})$

(c) Fragmentation Range

With a decrease in depth below the optimum depth, a combination of shock energy and gas expansion energy causes the rock breakage. The upper limit of this range occurs when the quantity of energy transferred to the atmosphere exceeds that transferred to the rock.

(d) Air Blast Range

When the explosive charge is placed adjacent to the free face, surface breakthrough occurs and the remaining energy of the explosion is vented to the atmosphere. The effect of charge weight and depth of burial on crater volume is illustrated in Fig. 1, for one of the series of tests carried out at the University of Queensland Experimental Mine.

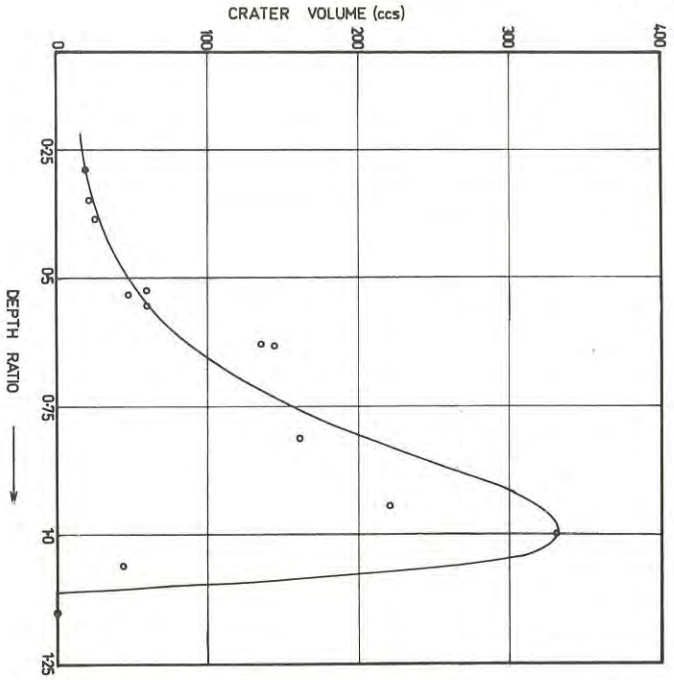


Fig. 1. Crater volumes (ccs) for various depth ratios (charge depth/optimum depth).

As the depth of a constant weight concentrated charge is increased from zero to the critical depth, the volume of the crater formed increases until the depth coincides with the optimum depth and then decreases in the shock range until it is zero at the critical depth.

The normal commercial production blast occurs in the fragmentation range defined by Livingston and design of large scale blasts involves investigation of this range of explosive behaviour. This research project involves determination of fragmentation for burdens varying from small values (corresponding to the air blast range) up to the optimum depth (the limit of the fragmentation range).

III.- EXPERIMENTAL TECHNIQUES

To obtain accurate relationships between fragmentation and burden, a large number of carefully controlled tests must be carried out. This is most easily accomplished by model testing. These cannot be relied upon to give results corresponding exactly to large scale applications, but they can give a good indication of the relationships involved. In order to determine the fragmentation characteristics for explosives in rock, it was decided to obtain these relationships for concentrated or point charges and for linear charges.

(a) Concentrated Charge Tests

The choice of explosive and rock type for this model was relatively simple. The rock had to be capable of being formed into required shapes with flat surfaces. It had to be homogeneous and isotropic with no fractures and planes of weakness. A cement mortar satisfied these conditions and concrete of proportions sand: cement: water of 2:1:0.5 was used. Tests were also carried out in sandstone.

The model explosive used had to be capable of complete detonation in very small quantities and small diameters. This necessitated the use of a high explosive such as P.E.T.N. For concentrated charges, detonators were used. Crater tests were carried out in concrete with No. 6 (0.24 gms. P.E.T.N.) and No. 8 star detonators (0.8 gms. P.E.T.N.) and in sandstone with No. 8 star detonators.

A block of concrete three feet square and 10 inches thick was large enough to carry out a series of 13 crater tests with No. 6 detonators. As each block was cast, cylindrical samples were taken so that strength and density tests could be carried out. The unconfined compressive strength and indirect tensile strength (Brazilian test) were calculated for each block before testing.

Holes were drilled from the bottom of the block using a masonary drill until the required burden remained at the top of the block. The detonator was placed in the hole and a cement slurry was used as a stemming agent. Electric instantaneous detonators were used because of their smaller size and minimum interference with the stemming material.

Each crater was fired upwards, using a plunger type exploder to initiate the detonator. The cratered particles were caught in a steel container lined with foam rubber and thick gasket rubber to minimise secondary particle breakage by collision.

After each test, the crater was completely cleaned of all broken material and the crater dimensions were measured. The rock broken by the blast was weighed and subjected to a screen size analysis to measure the degree of fragmentation.

(b) Linear Charge Tests

For linear charge testing the model materials used were concrete and sandstone. The model explosive was P.E.T.N. in the form of detonating fuse. As for crater testing, a block of concrete three feet square by ten inches thick was used. Holes were drilled in the small faces parallel to the large square faces of the block, which was the major free face. The burden was varied and accurately measured for each test. A constant length of hole was used for each series of tests.

The charge was initiated by a detonator attached to the end of the detonating fuse outside the hole. The concrete was shielded from the effects of the detonator by a steel plate with a central hole to permit passage of the detonating fuse. A large wooden box lined with rubber was used for collecting the fragmented particles after each test.

The broken material was collected for size analysis and the dimensions of the crater were measured.

## IV.- EXPERIMENTAL RESULTS

The experimental results for concentrated charges are tabulated in Appendix I. For each series of tests, the following information is given:

(a) Explosive type

(b) Rock type and relevant physical properties

(c) Crater dimension

(d) Fragmentation parameters.

This experimental data allows the calculation of a relationship between the fragmentation produced and the charge burden. This set of equations is given at the end of each series of results in Appendix I. Preliminary results for linear charge tests indicate similar relationships. Further tests are currently in progress to determine more accurate relationships for linear charges.

The crater information sets out the burden or depth of burial of the charge for each hole and the corresponding crater volume. This allows the optimum depth to be calculated, as shown in Fig. 1. The fragmentation results tabulated consist of the size distribution for each test expressed as the cumulative percent passing a given screen size.

To determine the nature of any relationship between size distribution and burden, it was necessary first to establish Y as a function of (x/D) where Y = 100y = cumulative percent passing a screen of aperture x and D = optimum depth. To enable scaling of results, the size of particles and depth of burial of the explosives were expressed as dimensionless ratios in terms of the optimum depth. Analysis of results indicates a linear relationship between log ln Y and log (x/D).

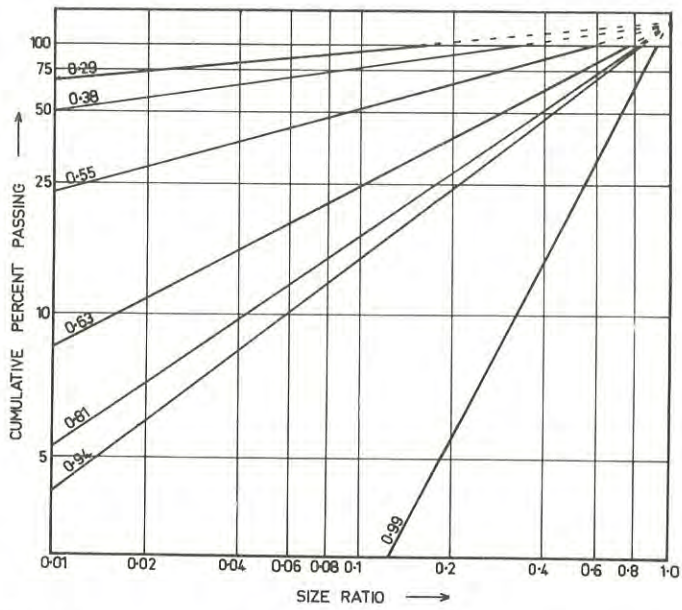


Fig. 2. Size distribution curves for different charge burden ratios.

$$\text{Size ratio} = \frac{\text{particle size}}{\text{optimum charge depth}}$$

$$\text{Burden ratio} = \frac{\text{charge burden}}{\text{optimum charge depth}}$$

Fig. 2 shows this relationship for a number of explosive burden ratios. This results in a relationship of the following form:

$$y = \frac{1}{100} \; e^{4.8(\frac{x}{D})^f}$$

where f is the gradient of fragmentation lines in Fig. 2. Since the gradient of these lines depends upon the burden ratio, a graph as illustrated in Fig. 3 was drawn to determine this relationship. In this graph log f is plotted against log $(\frac{d}{D})$, where d is the burden and D is the optimum depth.

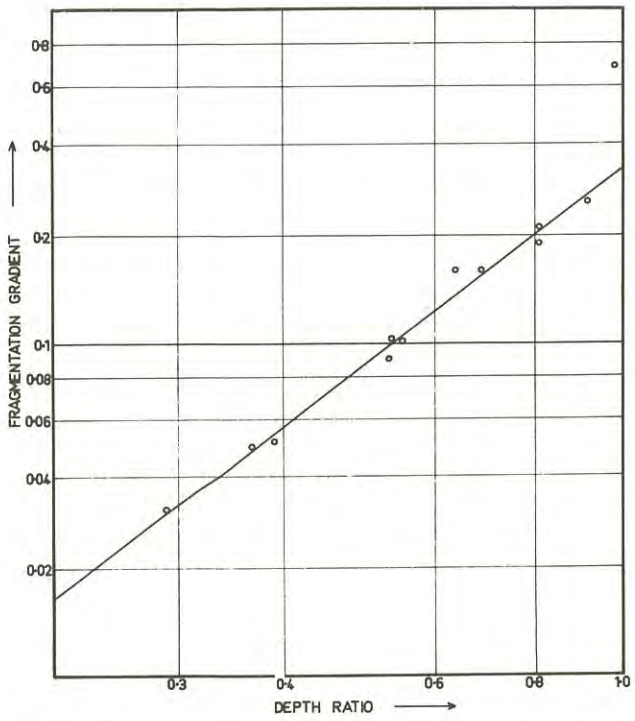


Fig. 3. Fragmentation gradient versus depth ratio $(\frac{\text{charge burden}}{\text{optimum depth}})$.

From Fig. 3, f is expressed as a function of $(\frac{d}{D})$ in the form

$$f = \frac{1}{E} (\frac{d}{D})^2$$

where E is a constant depending on the explosive type and material properties. Figs. 1, 2 and 3 show some of the results obtained from Block 2C, which resulted in a function of the form

$$y = \frac{1}{100} \; e^{4.8(\frac{x}{D})^f}$$

where $f = \frac{1}{3.11} (\frac{d}{D})^2$

Analysis of the results tabulated in Appendix I, and summarised in Table I shows that each set of a particular combination of rock and explosive type gives a similar relationship except for variations in the factor E. Thus a knowledge of this factor would immediately allow calculation of a certain size distribution for a certain burden ratio and would also allow estimation of the size of the largest particles.

## V.- CONCLUSION

One of the main objectives of primary rock breaking operations is to fragment the rock mass into blocks which can be economically transported to the primary crushing stage. The degree of fragmentation is therefore one basic measure of the relative efficiency of different blasting designs. The problems associated with measuring this parameter in full scale operations has discouraged the use of this technique as a measure of blasting efficiency. Small scale model tests have been conducted in order to determine the relationship between size distribution and charge burden. Analysis of the results obtained has shown that it is possible to predict the size distribution for a particular charge burden, if these dimensions are expressed as dimensionless ratios in terms of the optimum charge depth. The application of this method of analysis on an industrial scale cannot be justified until large scale tests have been carried out. The model test results have provided sufficient justification for the expenditure of funds on large scale testing. These tests are currently in progress.

TABLE I

SUMMARY OF CRATER TEST RESULTS USING CONCENTRATED CHARGES

| Block No. | Detonator Type (gms.P.E.T.N.) | Compressive Strength (p.s.i.) | Tensile Strength (p.s.i.) | Optimum Depth (cms.) | Critical Depth (cms) | Constant E Factor |
|---|---|---|---|---|---|---|
| 2A | No.6-0.24 gms. | 5730 | 425 | 3.32 | 4.00 | 5.63 |
| 2B | No.6-0.24 gms. | 5500 | 410 | 2.70 | 3.45 | 5.63 |
| 2C | No.6-0.24 gms. | 4300 | 210 | 3.45 | 3.65 | 3.11 |
| 1SS | No.8-0.8 gms. | 4600 | 187 | 6.60 | 7.30 | 3.30 |
| 2F and 2G | No.8-0.8 gms. | 3900 | 205 | 7.00 | 9.00 | 2.30 |

VI.- ACKNOWLEDGEMENTS

Thanks are expressed to the Companies who have made financial assistance available to support this work.

VII.- REFERENCES

1. LIVINGSTON, C.W. - Fundamental Concepts of Rock Failure. Quarterly, Colorado School of Mines, Vol. 51, Part 3, 1956.

2. BAUER, A. - Application of the Livingston Theory. Quarterly, Colorado School of Mines, Vol. 56, Part 1, 1961.

3. GRANT, C.H. - Simplified Explanation of Crater Method. Engineering and Mining Journal, Vol. 165, Nov. 1964.

VII.- APPENDIX

RESULTS OF CRATER TESTS - CONCENTRATED CHARGES

Block 2A - No. 6 detonators in mortar

CONCRETE - Sand/Cement/Water = 2:1:0.5

SAND - Coarse river sand

Compressive strength = 5730 psi

Tensile strength = 425 psi (Brazilian Test)

Specific gravity = 2.15

CRATER INFORMATION (2A)

| Hole No. | Burden Drilled (cms) | Burden to C/G of Charge (cms) | Crater Vol. (ccs) | Av. Crater Radius (cms) |
|---|---|---|---|---|
| 2A1 | 0 | 0.32 | 8.5 | 2.2 |
| 2A2 | 0.5 | 0.82 | 17 | 3.0 |
| 2A3 | 1 | 1.32 | 19.5 | 3.2 |
| 2A4 | 1 | 1.32 | 24 | 4.4 |
| 2A5 | 2 | 2.32 | 56 | 5.4 |
| 2A6 | 2 | 2.32 | 60 | 5.7 |
| 2A7 | 2.5 | 2.82 | 102 | 6.7 |
| 2A8 | 3 | 3.32 | 148 | 7.5 |
| 2A9 | 3.5 | 3.32 | 148 | 7.3 |
| 2A10 | 3.5 | 3.82 | 95 | 6.0 |
| 2A11 | 3.5 | 3.82 | Misfired | |
| 2A12 | 4 | 4.32 | Cracks occurred | |
| 2A13 | 4 | 4.32 | " | " |
| 2A14 | 4.5 | 4.82 | No effect | |

From Crater results,

Optimum depth (D) = 3.32 cm

Critical depth (CD) = 4.00 cm

$\therefore$ $\Delta = 0.83$

FRAGMENTATION INFORMATION (2A)

| Screen Size (x) (cms) | Cumulative % Passing (100Y) | | | | |
|---|---|---|---|---|---|
| | 2A1 | 2A2 | 2A3 | 2A4 | 2A5 |
| 2.69 | 100 | 100 | 100 | 100 | 100 |
| 1.885 | 100 | 100 | 100 | 83.52 | 95.4 |
| 1.33 | 100 | 100 | 100 | 63.26 | 84.26 |
| .9423 | 100 | 100 | 100 | 46.78 | 73.27 |
| .566 | 96.25 | 96.81 | 96.17 | 33.90 | 59.94 |
| .3327 | 91.25 | 90.10 | 89.39 | 25.94 | 47.70 |
| .1981 | 81.25 | 81.47 | 82.02 | 20.45 | 41.00 |
| .085 | 48.78 | 50.48 | 52.81 | 11.36 | 25.41 |
| 0 | 0 | 0 | 0 | 0 | 0 |

| Screen Size (x) (cms) | Cumulative % Passing (100Y) | | | | |
|---|---|---|---|---|---|
| | 2A6 | 2A7 | 2A8 | 2A9 | 2A10 |
| 2.69 | 100 | 100 | 100 | 93.46 | 4.84 |
| 1.885 | 90.55 | 86.35 | 83.48 | 80.91 | 4.84 |
| 1.33 | 72.41 | 70.78 | 63.22 | 58.58 | 4.84 |
| .9423 | 66.23 | 55.25 | 43.93 | 40.91 | 3.94 |
| .566 | 51.44 | 38.98 | 30.18 | 26.57 | 2.77 |
| .3327 | 39.65 | 31.15 | 20.48 | 18.99 | 1.33 |
| .1981 | 33.89 | 25.81 | 17.88 | 14.43 | .93 |
| .085 | 20.53 | 13.66 | 9.08 | 6.69 | .37 |
| 0 | 0 | 0 | 0 | 0 | 0 |

These results plotted in the form

$$\log \ln (100Y) \text{ vs. } \log \frac{x}{D}$$

give the relationship $Y = \frac{1}{100} e^{4.8(\frac{x}{D})^f}$

where $f = \frac{1}{5.63} (\frac{d}{D})^2$ i.e. $E = 5.63$

d = burden

D = optimum depth

BLOCK 2B - No. 6 detonators in mortar

CONCRETE - Sand/Cement/Water = 2:1:0.5

SAND - Coarse river sand

Compressive strength = 5,500 psi

Tensile strength = 410 psi (Brazilian Test)

Specific Gravity = 2.15

CRATER INFORMATION (2B)

| Hole No. | Burden Drilled (cms) | Burden to C/G of Charge (cms) | Crater Vol. (ccs) | Av. Crater Radius (cms) |
|---|---|---|---|---|
| 2B1 | 3.49 | 3.81 | Feint cracks on surface | |
| 2B2 | 3.45 | 3.77 | Larger cracks | |
| 2B3 | 3.02 | 3.34 | Very large cracks | |
| 2B4 | 3.02 | 3.34 | 51 | 6.03 |
| 2B5 | 2.5 | 2.82 | 102 | 6.69 |
| 2B6 | 2.38 | 2.70 | 127 | 6.69 |
| 2B7 | 1.94 | 2.26 | 59 | 5.72 |
| 2B8 | 2.02 | 2.34 | 82 | 6.35 |
| 2B9 | 1.51 | 1.83 | 51 | 4.92 |
| 2B10 | 1.47 | 1.79 | 36 | 4.76 |
| 2B11 | .87 | 1.19 | 16 | 3.02 |
| 2B12 | .87 | 1.19 | 17 | 3.02 |
| 2B13 | 4.13 | 4.45 | No visible effect | |

From Crater results,

Optimum depth (D) = 2.7 cms

Critical depth (CD) = 3.45 cms

$\therefore \Delta = 0.78$

FRAGMENTATION INFORMATION (2B)

| Screen Size (x) (cms) | Cumulative % Passing (100Y) | | | |
|---|---|---|---|---|
| | 2B4 | 2B5 | 2B6 | 2B7 |
| 2.69 | 2.86 | 93.77 | 93.16 | 100 |
| 1.88 | 5.86 | 85.08 | 90.48 | 86.67 |
| 1.33 | 5.86 | 75.72 | 71.5 | 82.69 |
| 0.9423 | 3.25 | 60.34 | 53.5 | 72.64 |
| 0.566 | 2.14 | 42.33 | 38.17 | 58.84 |
| 0.3327 | 1.35 | 32.29 | 28.98 | 46.84 |
| 0.1981 | 1.03 | 25.68 | 22.21 | 39.20 |
| 0.085 | .48 | 13.05 | 11.23 | 24.47 |
| 0 | 0 | 0 | 0 | 0 |

| Screen Size (x) (cms) | Cumulative % Passing (100Y) | | | |
|---|---|---|---|---|
| | 2B9 | 2B10 | 2B11 | 2B12 |
| 2.69 | 100 | 100 | 100 | 100 |
| 1.88 | 84.08 | 100 | 100 | 100 |
| 1.333 | 81.68 | 92.74 | 100 | 100 |
| 0.9423 | 76.50 | 79.96 | 100 | 96.19 |
| 0.566 | 64.52 | 73.69 | 97.86 | 93.65 |
| 0.3327 | 53.59 | 61.53 | 91.81 | 88.25 |
| 0.1981 | 45.25 | 52.13 | 84.34 | 81.27 |
| 0.085 | 27.8 | 32.83 | 55.16 | 53.97 |
| 0 | 0 | 0 | 0 | 0 |

From graphical representation of these results,

$$Y = \frac{1}{100} e^{4.8(\frac{x}{D})^f}$$

where $f = \frac{1}{5.63}(\frac{d}{D})^2$ i.e. E = 5.63

BLOCK 2C - No. 6 detonators in mortar

CONCRETE - Sand/Cement/Water = 2:1:0.5

SAND - Beach sand (fine)

Compressive strength = 4,300 psi

Tensile strength = 210 psi

Specific Gravity = 2.2

CRATER INFORMATION (2C)

| Hole No. | Burden Drilled (cms) | Burden to C/G of Charge (cms) | Crater Vol. (ccs) | Av. Crater Radius (cms) |
|---|---|---|---|---|
| 2C1 | .67 | .99 | 18 | 2.8 |
| 2C2 | .87 | 1.19 | 20 | 3.0 |
| 2C3 | 1.00 | 1.32 | 25 | 3.3 |
| 2C4 | 2.46 | 2.78 | 121 | 7.5 |
| 2C5 | 2.46 | 2.78 | 160 | 8.5 |
| 2C6 | 3.33 | 3.65 | 43 | 5.1 |
| 2C7 | 2.92 | 3.23 | 225 | 9.6 |
| 2C8 | 3.12 | 3.43 | 330 | 11.5 |
| 2C9 | 1.85 | 2.17 | 145 | 8.5 |
| 2C10 | 1.82 | 2.14 | 137 | 8.5 |
| 2C11 | 1.47 | 1.79 | 62 | 5.5 |
| 2C12 | 1.5 | 1.82 | 46 | 5.2 |
| 2C13 | 1.59 | 1.90 | 63 | 6.0 |

From Crater results,

Optimum depth (D) = 3.45 cms.

Critical depth (CD) = 3.65 cms.

$\therefore \Delta = 0.94$

FRAGMENTATION INFORMATION (2C)

| Screen Size (x) (cms) | Cumulative % Passing (100Y) | | | | | |
|---|---|---|---|---|---|---|
| | 2C1 | 2C2 | 2C3 | 2C4 | 2C5 | 2C6 |
| 2.69 | 100 | 100 | 100 | 87.4 | 92.2 | 8.9 |
| 1.88 | 100 | 100 | 100 | 84.3 | 75.9 | 8.9 |
| 1.33 | 100 | 100 | 100 | 65.3 | 56.0 | 8.9 |
| .9423 | 100 | 100 | 100 | 54.2 | 35.7 | 7.3 |
| .566 | 98.2 | 92.2 | 94.7 | 34.8 | 26.8 | 5.7 |
| .3327 | 92.9 | 85.0 | 83.7 | 22.4 | 17.5 | 3.3 |
| .1981 | 86.3 | 74.4 | 74.4 | 15.9 | 12.3 | 2.7 |
| .085 | 75.7 | 63.6 | 62.2 | 10.6 | 8.0 | 1.3 |
| 0 | 0 | 0 | 0 | 0 | 0 | 0 |

| Screen Size (x) (cms) | Cumulative % Passing (100Y) | | | | | | |
|---|---|---|---|---|---|---|---|
| | 2C7 | 2C8 | 2C9 | 2C10 | 2C11 | 2C12 | 2C13 |
| 2.69 | 85.3 | 37.4 | 84.1 | 82 | 90.6 | 100 | 100 |
| 1.88 | 71.9 | 21.8 | 65 | 58.4 | 74 | 100 | 100 |
| 1.33 | 50.3 | 11.4 | 59.6 | 49.6 | 68.6 | 96 | 90.7 |
| .9423 | 37.2 | 7.4 | 46.4 | 39.1 | 64.7 | 90.2 | 81.3 |
| .566 | 22.4 | 4.5 | 32.9 | 28.2 | 52.1 | 77.8 | 67.4 |
| .3327 | 14.2 | 2.5 | 23.8 | 20.4 | 43.3 | 62.6 | 50.2 |
| .1981 | 9.9 | 1.6 | 18.8 | 16.6 | 36.3 | 50.2 | 40.2 |
| .085 | 6.7 | 1.0 | 13.8 | 12.8 | 28.7 | 38.9 | 30.8 |
| 0 | 0 | 0 | 0 | 0 | 0 | 0 | 0 |

From graphical representation of these results,

$$Y = \frac{1}{100} e^{4.8(\frac{x}{D})^f}$$

where $f = \frac{1}{3.11}(\frac{d}{D})^2$ i.e. E = 3.11

BLOCK ISS - No. 8 detonators in sandstone

Compressive strength = 4600 psi

Tensile strength = 187 psi

Specific gravity = 2.3

CRATER INFORMATION (ISS)

| Hole No. | Burden Drilled (cms) | Burden to C/G of Charge (cms) | Crater Vol. (ccs) | Av.Crater Radius (cms) |
|---|---|---|---|---|
| ISS1 | 1.27 | 1.90 | 38 | 3.5 |
| ISS2 | 2.38 | 3.01 | 76 | 5.84 |
| ISS3 | 3.81 | 4.44 | 254 | 8.87 |
| ISS4 | 1.27 | 1.90 | 42 | 3.5 |
| ISS5 | 1.75 | 2.38 | 64 | 5.08 |
| ISS6 | 3.17 | 3.80 | 142 | 6.98 |
| ISS7 | 4.44 | 5.07 | 351 | 9.65 |
| ISS8 | 1.90 | 2.53 | 60 | 5.08 |
| ISS9 | 5.40 | 6.03 | 790 | 12.7 |
| ISS10 | 6.11 | 6.74 | 790 | 13.0 |
| ISS11 | 6.50 | 7.13 | 340 | 10.6 |

From Crater results,

Optimum Depth (D) = 6.6 cm

Critical Depth (CD) = 7.3 cms

$\therefore \quad \Delta = 0.9$

FRAGMENTATION INFORMATION (ISS)

| Screen Size (x) (cms) | Cumulative % Passing (100 Y) | | | | | |
|---|---|---|---|---|---|---|
| | ISS1 | ISS2 | ISS3 | ISS4 | ISS5 | ISS6 |
| 2.69 | 100 | 100 | 75.9 | 100 | 100 | 100 |
| 1.88 | 100 | 93.4 | 61.5 | 100 | 95.8 | 88.2 |
| 1.33 | 90.4 | 85.8 | 49.8 | 96.1 | 84.7 | 66.5 |
| .9423 | 86.0 | 82.5 | 39.1 | 85.2 | 76.9 | 54.3 |
| .566 | 80.9 | 71.9 | 26 | 75.5 | 66.8 | 36.8 |
| .3327 | 73.4 | 59.4 | 19.4 | 67.5 | 60.2 | 28.0 |
| .1981 | 67.3 | 53.3 | 15.9 | 61.3 | 54.8 | 22.9 |
| .085 | 56.1 | 44.3 | 11.1 | 50.1 | 45.8 | 16.2 |
| 0 | 0 | 0 | 0 | 0 | 0 | 0 |

| Screen Size (x) (cms) | Cumulative % Passing (100Y) | | | | |
|---|---|---|---|---|---|
| | ISS7 | ISS8 | ISS9 | ISS10 | ISS11 |
| 2.69 | 66.7 | 100 | 30.1 | 30.9 | 17.0 |
| 1.88 | 52.3 | 90.4 | 19.4 | 19.4 | 1.5 |
| 1.33 | 38.9 | 85.2 | 12.3 | 13.5 | 1.5 |
| .9423 | 30.2 | 80.2 | 8.0 | 9.0 | 1.5 |
| .566 | 20.3 | 68.8 | 5.6 | 6.2 | .9 |
| .3327 | 15.1 | 61.8 | 3.4 | 4.0 | .9 |
| .1981 | 12.3 | 56 | 3.0 | 3.5 | .9 |
| .085 | 8.6 | 46.2 | 2.6 | 2.9 | .7 |
| 0 | 0 | 0 | 0 | 0 | 0 |

From graphical representation of these results,

$$Y = \frac{1}{100} e^{4.8(\frac{x}{D})^f}$$

where $f = \frac{1}{3.3}(\frac{d}{D})^2$ i.e. E = 3.3

BLOCK 2F and 2G - No. 8 detonator in mortar

CONCRETE - Sand/Cement/Water = 2:1:0.5

SAND - Beach sand (fine)

Compressive strength = 3900 psi

Tensile strength = 205 psi

Specific gravity = 2.1

CRATER INFORMATION (2F & 2G)

| Hole No. | Burden Drilled (cms) | Crater Vol. (ccs) | Burden to C/G of Charge (cms) | Av. Crater Radius (cms) |
|---|---|---|---|---|
| 2F1 | .6 | 54 | 1.25 | 4.5 |
| 2F2 | .6 | 53 | 1.25 | 4.5 |
| 2F3 | | 54 | 1.9 | 4.8 |
| 2F4 | 1.25 | 65 | 1.9 | 5.2 |
| 2F5 | 1.9 | 102 | 2.5 | 6.3 |
| 2F6 | 1.9 | 104 | 2.5 | 6.2 |
| 2F7 | 2.5 | 212 | 3.2 | 9.0 |
| 2F8 | 2.5 | 192 | 3.2 | 8.6 |
| 2F9 | 3.75 | 700 | 4.45 | 14.5 |
| 2F10 | 3.75 | 440 | 4.45 | 11.9 |
| 2F11 | 5.1 | 1150 | 5.7 | 15.5 |
| 2G12 | 5.1 | Misfired | 5.7 | |
| 2G13 | 6.3 | 1709 | 7.0 | 16.6 |
| 2G15 | 7.6 | 1200 | 8.3 | 14.4 |

From Crater results,

Optimum Depth (D) = 7 cm

Critical Depth (CD) = 9 cm

$\therefore \Delta = 0.78$

$$Y = \frac{1}{100} e^{4.8(\frac{x}{D})^f}$$

$$f = \frac{1}{2.3} \times (\frac{d}{D})^2 \qquad \text{i.e. } E = 2.3$$

FRAGMENTATION INFORMATION (2F & 2G)

| Screen Size (x) (cms) | Cumulative % Passing (100Y) | | | | | |
|---|---|---|---|---|---|---|
| | 2F1 | 2F2 | 2F3 | 2F4 | 2F5 | 2F6 |
| 2.69 | 100 | 100 | 100 | 100 | 100 | 75.9 |
| 1.88 | 100 | 100 | 100 | 100 | 91.1 | 75.9 |
| 1.33 | 100 | 100 | 100 | 97.5 | 80.6 | 73.8 |
| .9423 | 97.1 | 98 | 100 | 96.2 | 76.6 | 67.8 |
| .566 | 88.6 | 88.6 | 91.6 | 91.6 | 67.9 | 60.7 |
| .3327 | 78.1 | 78.8 | 83.0 | 80.9 | 58.2 | 52.2 |
| .1981 | 68.9 | 71.2 | 76.2 | 72.4 | 50.6 | 45.5 |
| .085 | 58.9 | 62.1 | 67.3 | 62.1 | 42.7 | 38.2 |
| 0 | 0 | 0 | 0 | 0 | 0 | 0 |

| Screen Size (x) (cms) | Cumulative % Passing (100Y) | | | | | |
|---|---|---|---|---|---|---|
| | 2F7 | 2F8 | 2F9 | 2F10 | 2F11 | 2G13 |
| 2.69 | 100 | 93 | 83.6 | 97.1 | 51.1 | |
| 1.88 | 79.7 | 78.1 | 66.7 | 74.3 | 26.6 | |
| 1.33 | 66.2 | 69.7 | 51.5 | 58.4 | 15.5 | |
| .9423 | 59.7 | 59.2 | 38 | 43.1 | 11.0 | |
| .566 | 47.4 | 45.3 | 26.9 | 27.7 | 6.2 | |
| .3327 | 38.3 | 36.5 | 14.2 | 19.0 | 3.9 | |
| .1981 | 32.4 | 31.2 | 10.8 | 14.4 | 2.8 | |
| .085 | 26.3 | 26.2 | 7.5 | 10.2 | 2.0 | |
| 0 | 0 | 0 | 0 | 0 | 0 | |

From graphical representation of these results,

# An Analysis of Pile Loading Tests in a Stiff Clay

By

S. B. Bromham, B.Sc.

(Senior Scientific Officer, Country Roads Board, Victoria)

AND

J. R. Styles, Dip. C.E., B.E. (Civil), Grad.I.E.Aust.

(Lecturer in Civil Engineering, Preston Institute of Technology)

I.- SUMMARY - Results are presented for loading tests performed on two steel shell piles driven into the stiff clayey soil of the Dandenong Valley area - about 15 miles south-east of Melbourne. The observed behaviour is compared with predictions based on the parameters obtained from extensive sampling and laboratory testing, and from the results of in-situ testing, including S.P.T. and Friction Penetrometer soundings which provide a direct measurement of both end bearing and side friction for each soil type.

The effect of load duration on the settlement characteristics of a single pile was examined by using three distinct loading periods. The data obtained do not support the concept of a unique stress - strain relationship but indicate that the relationship is dependent of loading duration.

## II.- INTRODUCTION

One of the major projects currently being undertaken by the Country Roads Board of Victoria is the construction of the Mulgrave Bypass Road, which is a major freeway system linking the south-east of the Melbourne city area with Dandenong and the Princes Highway. It was proposed to use driven pile foundations for all pier and abutment positions at the Stud Road Overpass.

Consequently a series of pile driving and pile loading tests was performed to assist in evaluating the relative merits of various types of piling.

The alternative proposals were 18" diameter steel shell friction piles or 10" H. section steel piles driven into the bedrock. This paper contains an analysis of the predicted performance and presents the results of loading tests on the steel shell pile.

## III.- GEOLOGY OF THE AREA

The basement or "bedrock" underlying and forming the valley walls of this section of the Dandenong Creek is a monotonous sequence of broadly folded marine siltstones and laminated fine sandstones of Upper Silurian-Lower Devonian age.

In Pleistocene and recent times aggradation of the Dandenong Creek has buried the basement by the deposition of up to 90 feet of clay, sandy clay, clayey sands and minor sand horizons.

## IV.- SITE EXPLORATION

### (a) Standard Penetration Testing.

The initial site investigation of the area consisted of bores drilled at pier and abutment positions.

Standard Penetration Tests were conducted at 5ft intervals in each bore. The location of test sites is shown in Fig.1. From the test information a soil profile could be compiled and assessment made of any

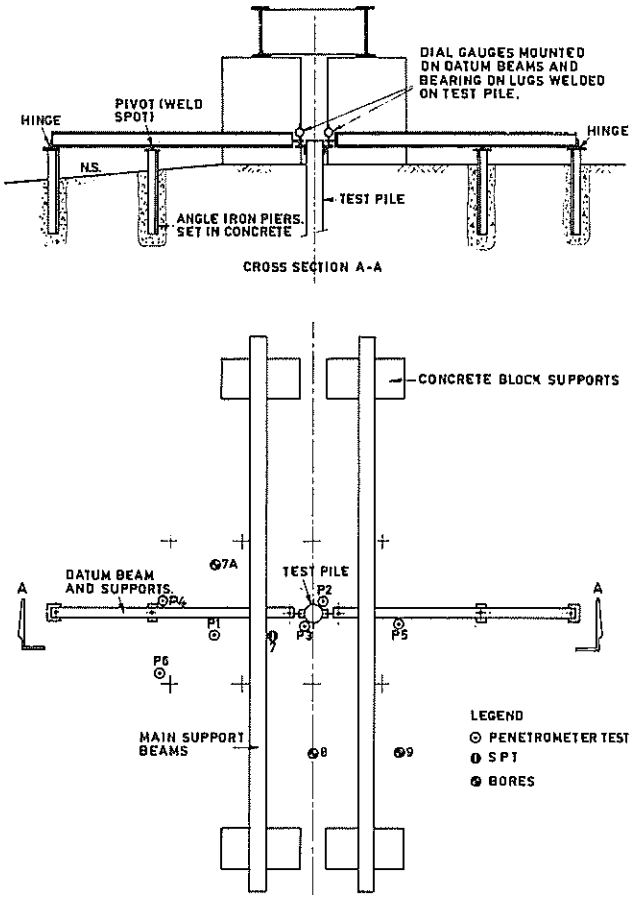


Figure 1. Pile Loading Test Arrangement and Location of Bores and Penetration Tests.

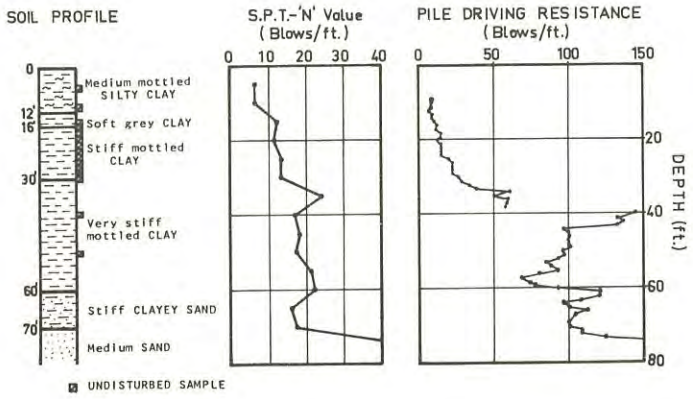


Figure 2. Penetration Tests.

areas requiring detailed investigation. A typical plot of blow count vs. depth is shown in Fig.2.

(b) Static Sounding.

To provide additional information on the soil profile static penetrometer soundings were conducted with a Friction Penetrometer at positions as shown in Fig.1. The Friction Penetrometer was designed and constructed by the Country Roads Board and is described by Styles (Ref.8). A feature of the design is the isolation of cone resistance measurement from the skin friction measuring system. The outputs from the cone and friction sleeve strain gauges are recorded on punched paper tape which is then processed by computer to give plots of cone and friction sleeve resistance vs. depth (see Fig.3). An estimate of the friction component of the total pile bearing capacity is obtained by integrating the area under the friction sleeve curve.

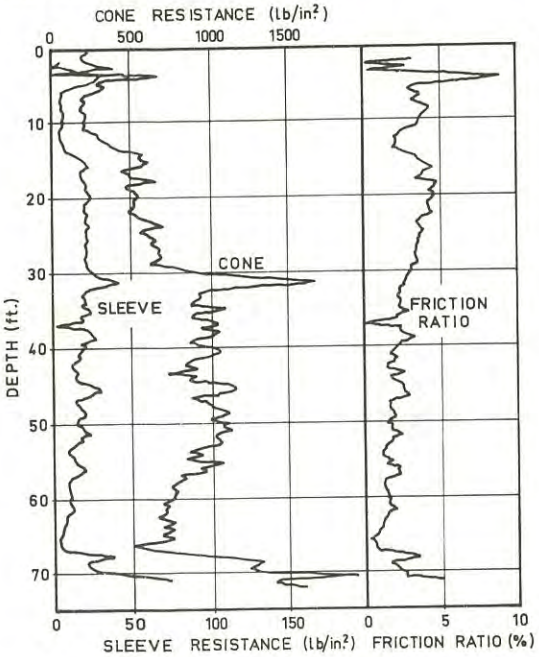


Figure 3. Friction Penetrometer Computer Plots - Site P4.

(c) Pile Driving Performance.

The test pile was an 18" diameter x 5/16" steel shell pile fitted with the Country Roads Board standard long tapered concrete toe section. The pile was driven to a depth of 38' and tested where the Hiley formula indicated a dynamic resistance of approximately 100 tons. After the static loading test was completed at this level the pile was extended and driven to 76' where a dynamic resistance of approximately 160 tons was obtained.

A 4 ton drop hammer was used in both driving tests, and the driving resistance is shown as a function of depth in Fig.2. The large discontinuity at 38' is obviously the result of 10 days delay which has produced considerable "set-up".

V.- LABORATORY TESTING

Laboratory testing was performed on undisturbed samples obtained from three bores as shown in Fig.1.

(a) Index and Classification Tests.

These tests were performed at the in-situ moisture content of the soil - the basic physical properties of each sample are shown in Fig.4. The classification is based only on the particle size analysis and is that used by the U.S. Engineer Department.

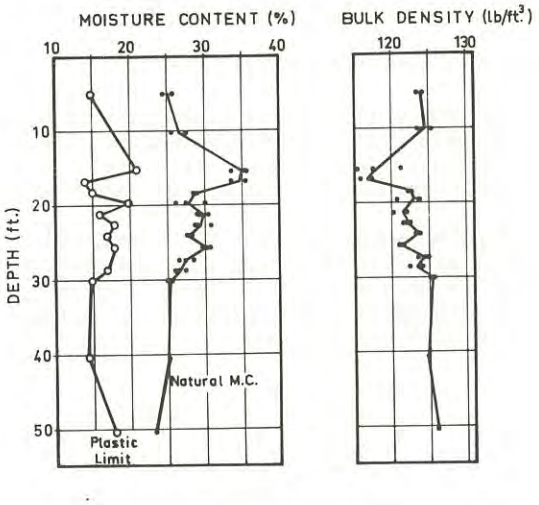


Figure 4. Soil Properties. Bore 7A

(b) Triaxial Shear Tests.

Three sample sizes were tested:
Series A: Immediate Undrained tests on 3 in. dia. x 3 in. high samples.
Series B: Undrained tests on -
(i) 4½ in. dia. x 4½ in. high.
(ii) 1½ in. dia. x 3 in. high specimens sub-sampled from the 4½ in. dia. sample.

The Series B tests were performed on samples which were re-consolidated to a stress equivalent to the in-situ anisotropic consolidation stress.

Stage testing (as outlined by Parry, Ref.5) was adopted for all tests. A check on the validity of stage testing was carried out in the testing of the 1½ in. dia. x 3 in high samples. (Three samples were cut from the 4½ in. dia. sample at one particular depth). For this series of tests the second stage cell pressure for the first sample was adopted as the cell pressure for the first stage on the second sample. A similar procedure was used in the testing of the third sample.

The shear strength parameters $c_u$ and $\emptyset_u$ obtained from total stress analyses of the triaxial results are presented in Table I.

VI.- PILE LOADING TESTS

(a) Description of Equipment.

(i) Reaction structure.

The reaction was provided by 300 tons of iron billets, railway lines and concrete blocks stacked on a platform constructed across two large universal beams which were supported on concrete blocks placed on the ground. (See Fig.1).

The top of the pile was ground flat and fitted with a 1" mild steel plate. The hydraulic jack was placed centrally on the loading plate and a piece of ½" particle board was inserted to ensure that there was a uniform distribution of load between the ram and the cross-beam of the loading frame.

(ii) Hydraulic jack and pumping unit.

The hydraulic jack was of single-action design with a load capacity of 1,000,000 lb at a hydraulic pressure of 10,000 lb/in$^2$. Two control units were used to supply and control these pressures.

1. Pump No.1 had an upper limit of 4,000 lb/in$^2$ and was used for Load Test No.1 and up to its limit for Load Test No.2. It was accurately calibrated up to 2,500 lb/in$^2$ and by extrapolation up to 4,000 lb/in$^2$.

2. Pump No.2 had an upper limit of 10,000 lb/in$^2$ and was used for the latter part of Load Test No.2. Accurate calibration was only possible to 2,500 lb/in$^2$, and an assumed calibration was used above this. This has probably produced some errors in absolute values of these higher loads, but unless there were any major inaccuracies in this equipment one would expect to obtain a reasonable relative performance.

(iii) Measurement of pile deflection.

The pile deflection was measured with dial gauges and displacement transducers attached to cantilevered reference beams which were supported on steel posts set in concrete to a depth of at least 5'. The outer end of the beam was fixed to the post with a simple hinge and was pivoted at the central support.

This system allows the beams to expand and contract with changes in ambient temperature without producing large movements in the dial gauges, which can be quite significant in long term tests where ambient temperature changes of up to 30°F were observed. There was still some movement of the beams observed (up to 0.005") with changes in temperature, and this is attributed to the existence of temperature gradients across the beams.

The arrangement of reference beams showing details of hinged supports is shown in Fig.1.

A set of three temporary bench marks was established approximately 40' from the pile and the level of the reference beams was checked regularly. A special staff with scale graduations of 0.02" was used and provided sight distances were kept down to 15 - 20' then it was possible to level to within ±0.01". It was established that the supports were outside the zone of influence of the pile settlement and consequently it was not necessary to adjust settlement records to compensate for any movement of the reference beams.

Two displacement recorders were used to measure

TABLE I. - TRIAXIAL TEST RESULTS

| Depth | 3" Samples | | | 4½" Samples | | | 1½" Samples | | |
|---|---|---|---|---|---|---|---|---|---|
| | $c_u$ lb/in$^2$ | $\emptyset_u$ degree | E lb/in$^2$ | $c_u$ lb/in$^2$ | $\emptyset_u$ degree | E lb/in$^2$ | $c_u$ lb/in$^2$ | $\emptyset_u$ degree | E lb/in$^2$ |
| 5' | 12 | 2 | 760 | | | | | | |
| 10' | | | | 8 | 5 | 1320 | | | |
| 15' | 6 | 2 | 845 | 13 | 4 | 1050 | 12 | 16 | - |
| 16' | 5 | 2 | 550 | 11 | 14 | 2060 | 20 | 5 | 1950 |
| 17' | 11 | 6 | 1990 | 11 | 10 | 2990 | 8 | 5 | 1520 |
| 19' | 12 | 6 | 1790 | 13 | 5 | 1810 | 12 | 3 | 1160 |
| 20' | 11 | 4 | 2100 | 16 | 4 | 2560 | 12 | 2 | 1275 |
| 22' | 9 | 7 | 1490 | 12 | 6 | 2120 | 8 | 4 | 535 |
| 23' | 5 | 8 | 690 | 12 | 4 | 2280 | 14 | 3 | 1160 |
| 25' | 3 | 14 | 550 | 11 | 6 | 1500 | 13 | 11 | 2160 |
| 28' | 5 | 15 | 2660 | | | | 7 | 4 | 530 |
| 30' | 10 | 11 | 3580 | | | | | | |
| 40' | 9 | 12 | 2380 | | | | | | |
| 50' | 7 | 16 | 750 | | | | | | |

pile deflection for the second test. These recorders were designed for the laboratory consolidation test and have a programmed print-out cycle at approximately 'square root of time' intervals which enabled accurate deflection readings to be obtained, especially during the early part of each loading cycle.

(b) Results of Loading Tests.

(i) Loading test No.1.

The shell pile was driven to a toe level of 38' below natural surface and the loading test was performed on the shell only. A basic load increment of 20,000 lb was used, and each load was maintained until it was estimated that primary settlement was completed. A deflection vs. log time curve for the 180,000 lb loading is shown in Fig.5 and this indicates that secondary consolidation effects begin after about 30 minutes. Results from other loadings yielded times of 30 - 100 minutes for the completion of the primary portion of the time-dependent deflection, and consequently most loadings were terminated at 100 - 200 minutes.

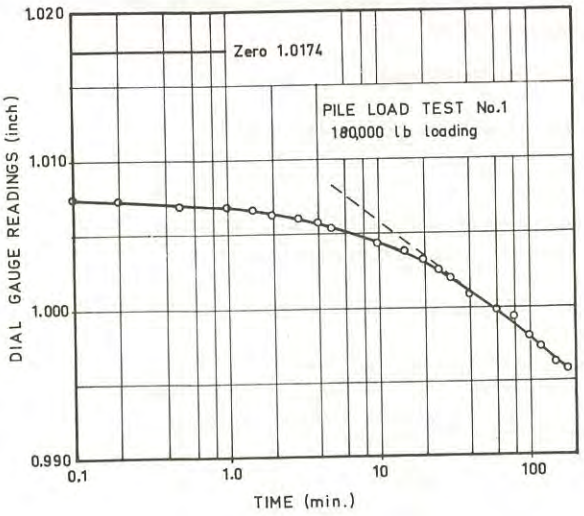


Figure 5. Deflection - log. Time Curve.

The load-deflection curve for this test is shown in Fig.6. This indicates that failure of this pile occurred at a load of approximately 300,000 lb. The two basic measurements of ultimate capacity are elastic limit and yield value. The elastic limit is defined as the load carried at a settlement equal to the total elastic settlement whereas the yield value is obtained by extrapolation of the terminal rates of settlement for each loading. The behaviour of this pile during unloading was not recorded and consequently no estimate of the elastic limit is possible. The yield value for this test was approximately 280,000 lb.

It is interesting to note that a smooth curve fits the majority of the points on the load deflection curve. The three points which are clearly above this curve correspond to the short term (50 minutes) loading periods and the two points which lie just below the curve are from the loadings which were

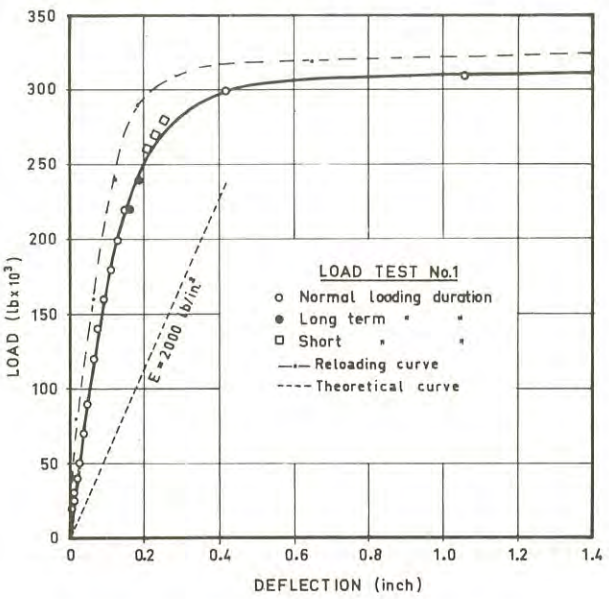


Figure 6. Load-Deflection Curve Test No.1.

maintained for a much longer period (6 - 7 hours). This observation suggests that the shape of the stress-strain curve may depend on the duration of the loading period and consequently it was proposed to check this supposition by using three distinct loading durations for the second loading test.

(ii) Loading test No.2.

After completion of the initial loading test the pile was extended and driven to 76' below N.S. A dynamic test at this level gave a satisfactory estimated capacity of 160 tons, so the shell was filled with concrete. The load was again applied in increments of 20,000 or 25,000 lb up to the capacity of the loading frame without producing failure. The pile was then unloaded in steps of 100,000 lb and the residual deflection was only about 0.10". The load deflection curve for this test is shown in Fig.7.

One of the objects of this second test was to examine the effect of loading duration on the load-deflection curve. Three different loading periods (30 min., 2 hrs. and 19 hrs.) were used with the 2 hour loading being considered as the base condition. The results (as shown in Fig. 7) certainly suggest that a family of stress-strain curves exists, each apparently similar in shape and displaced so that each curve represents a specific time of sustained loading. This is similar to the concept of delayed consolidation proposed by Bjerrum (Ref.1) when considering the settlement of buildings founded on a normally consolidated marine clay.

A series of simple shear tests on a saturated, normally consolidated kaolin was performed by Walker (Ref.11) when investigating secondary compression in the shear of clays. Part of his experimental program included tests specifically designed to check the effect of loading increment duration on the stress-strain curve and he concluded that "The equilibrium stress-strain curve is independent of load increment duration". This conclusion forms an

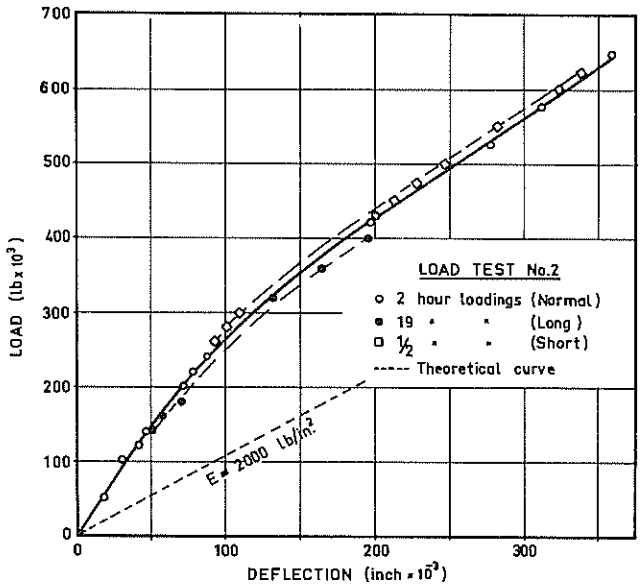


Figure 7. Load-Deflection Curve Test No.2

important step in the subsequent analysis of secondary compression, but the data obtained in this pile loading test do not support this concept. Evidence obtained from plate load tests, where the loading duration has been deliberately varied, also indicates that this concept does not appear to be valid, especially for field loading cases.

VII.- CALCULATION OF BEARING CAPACITY

The general equation for the bearing capacity of a pile, as given by Lee (Ref.3) is

$$W + Q_u = A_p c_u N'_c + N'_q \gamma A_p L + A_s c_a \qquad \ldots (1)$$

where $Q_u$ = ultimate bearing capacity

$W$ = weight of pile

$A_p$ = area of pile tip

$A_s$ = area of pile shaft

$c_u$ = apparent cohesion of soil

$c_a$ = average adhesion between soil and pile shaft

$N'_c$, $N'_q$ are general bearing capacity factors for deep footings

$\gamma$ = bulk density of soil

$L$ = length of pile

(a) Laboratory Tests

The values of $c_u$ have been determined from tests described as Series A and Series B, (see Table I). The resulting average shear strength for each of the layers is shown in Table II, and these values serve as a basis for estimating $c_a$. Information quoted by Lee (Ref.3) suggests that for a medium to stiff clay.

$$\frac{c_a}{c_u} \simeq 0.25 \qquad \ldots (2)$$

The values of the bearing capacity factors $N'_c$ and $N'_q$ for each of the layers has been estimated from the chart published by *Meyerhof (Ref.4) using the average values of $\phi_u$ for that layer. It must be noted that the value of $N'_c$ in particular varies greatly with small variation in the value of $\phi$. The analysis shown here uses a value of $\phi = 12^o$ which gives $N'_c = 29$, but if $\phi = 15^o$ is used then a value of $N'_c = 40$ is appropriate.

The initial series of laboratory testing (Series A) was on 3" diameter samples which were simply extruded from the sample tube and tested. Series B samples were restored to the estimated field conditions before testing and these are considered to give more reliable values of the shear strength parameters (See Table I). Average values of these parameters have been used for each layer and the calculations of side friction and end-bearing components of the pile capacity are shown in Table III.

The soil parameters at toe levels 38' and 76' are assumed to be -

$c_u = 2200$ lb/ft$^2$ $\qquad \phi_u = 12^o$

and thus from Meyerhof's chart -

$N'_c = 29$ $\qquad N'_q = 4$

The detailed calculations of total ultimate pile capacity are shown in Table III

TABLE II - PILE FRICTION VALUES

| Layer | Depth ft | $c_u$ lb/ft$^2$ | $\phi_u$ degree | $A_s$ ft$^2$ | $A_s c_a$ lb | $\Sigma A_s c_a$ lb |
|---|---|---|---|---|---|---|
| 0 -16' | 16' | 1150 | 4 | 76 | 21,800 | |
| 16'-35' | 35' | 1870 | 7 | 90 | 42,000 | |
| 35'-60' | 38' | 2200 | 12 | 14 | 7,700 | 71,500 |
| | 60' | 2200 | 12 | 104 | 57,200 | |
| 60'-78' | 78' | 2200 | 12 | 85 | 46,800 | 175,500 |

TABLE III - PILE CAPACITY CALCULATIONS

| Toe Level | $A_p c_u N'_c$ (lb) | $N'_q \gamma A_p L$ (lb) | $A_s c_a$ (lb) | $Q_u$ (ton) |
|---|---|---|---|---|
| 38' | 113,000 | 35,000 | 71,500 | 98 |
| 76' | 113,000 | 70,000 | 175,500 | 152 |

* Similar analyses have been presented by other workers (see Vesic, Ref.11). The values calculated by Meyerhof have been used in this paper since they provide an "average" figure for bearing capacity coefficients.

It must be realised that the assumptions implicit in the calculations are -

(i) $\frac{c_a}{c_u} = 0.25$

The range quoted by Lee (Ref.3) is from 0.25 to 0.4 for this type of material.

(ii) No undisturbed samples were taken near the lower toe level of 76' so that shear strength parameters obtained from samples at 40' and 50' have been assumed. In fact bore logs show that a medium sand horizon occurs here with a SPT value of 48 blows, which is considerably stronger. Thus the estimate of the end bearing component for the longer pile is likely to be very conservative.

It must be noted that the only shear strength parameters available from samples at 40' and 50' are those obtained from 3" specimens, which were not restored to field stress levels prior to testing, so the values used here are estimates based on the fact that this type of testing tends to give low values of $c_u$.

(b) Friction Penetrometer.

The Friction Penetrometer measures separately the end-bearing resistance and the side friction generated on the penetrometer during sounding. The capacity of a driven pile may then be calculated provided one assumes that the same, or some proportion of the measured unit end-bearing resistance and side friction can be applied. Van der Veen and Boersma (Ref.10) have suggested that the factor to be applied to the penetrometer results is 2.5.

i.e. Residual pile tip resistance =

$$\frac{\text{Penetrometer cone resistance}}{2.5}$$

This factor was derived from analysis of actual pile loads and loads predicted from the results of soundings with the Dutch Cone Penetrometer. We do not yet have sufficient data to be able to derive an arbitrary factor for the Friction Penetrometer, although the results of this test indicate that the total pile capacity has been over-estimated by a factor of about 2.

The end-bearing and friction components, which have been calculated using the penetrometer data from sites P3 and P4, are shown in Table IV. The estimated capacities for Test No.2 (toe depth 76') are only approximate as the penetrometer probe did not quite reach 76'.

TABLE IV - PILE CAPACITIES FROM FRICTION PENETROMETER RESULTS (TONS)

| Toe Level | Site | End Bearing | Friction | Total |
|---|---|---|---|---|
| 38' | P3 | 113 | 188 | 301 |
| 76' | P3 | 185 | 390 | 575 |
| 38' | P4 | 97 | 179 | 276 |
| 76' | P4 | 185 | 370 | 555 |

Unit pile end-bearing resistance was calculated by averaging the penetrometer resistance over a depth extending from four pile diameters above to one pile diameter below the pile level. This is the method adopted by Van der Veen and Boersma (Ref.10).

(c) SPT Results.

The capacities of a single pile can be estimated from the SPT results using the following expression - see Lee (Ref.3).

$$Q_u = 4 N A_p + \frac{\bar{N} A_s}{50} \quad \ldots(3)$$

where $N$ = SPT value at toe depth (average of readings immediately above and below actual toe depth).

$\bar{N}$ = average SPT value over whole length of pile.

$Q_u$ = ultimate capacity (short tons).

Inserting the appropriate values of N and $\bar{N}$ (See Fig.2) yields the following results.

Test No.1 $Q_u$ = 158 ton.

Test No.2 $Q_u$ = 320 ton.

It must be noted that this method of calculation is strictly only applicable to sands and silts, but is nevertheless widely used in cohesive soils. It has been included here to provide a comparison with the other methods.

Table V presents a summary of calculated pile capacities and the actual test values of ultimate capacity.

TABLE V - CALCULATED PILE CAPACITIES (TONS)

| | Loading Tests | Lab. Tests | Fric. Pen. | SPT Results | Hiley Formula |
|---|---|---|---|---|---|
| Test No.1 | 140 | 98 | 285 | 158 | 100<br>190* |
| Test No.2 | > 300 | 152 | 565 | 320 | 160 |

* after 3 weeks set

VIII.- CALCULATION OF SETTLEMENT

A comprehensive analysis of the deformation behaviour of loaded single piles has been published by Poulos & Davis (Ref.6). The displacement of a pile in a finite layer of ideal elastic soil is given by -

$$\rho = \frac{P}{LE} I_\rho \quad \ldots(4)$$

where $P$ = applied load

$L$ = length of pile

$E$ = Elastic modulus of the soil

$I_\rho$ = an influence factor dependent on the pile and layer geometries and on the elastic parameters of the soil.

If we consider a particular load for each pile test then -

$$\rho \propto \frac{1}{E} \qquad \ldots(5)$$

and the calculation of the displacement under that load depends only on the measurement of Elastic modulus of the soil. E has been calculated from the results of the triaxial shear tests, and to maintain a consistent method, the maximum slope of the stress-strain curve of the first stage of the test has been used throughout. The range of values for E is large which itself causes difficulties in selecting a value which will apply over the whole length of the pile. The range, and average values of E calculated from triaxial shear tests on the various sizes of samples from the uniform layer of clay (16' - 30') are shown in Table VI.

TABLE VI - VALUES OF E FROM TRIAXIAL TESTS

| Sample Diameter | E (lb/in$^2$) | |
|---|---|---|
| | Range | Average |
| 3" | 340 - 2900 | 1220 |
| 4½" | 1050 - 2990 | 2060 |
| 1½" | 530 - 4020 | 1650 |

The values obtained from the 4½" samples are the most consistent, and this is attributed to the larger volume of sample and also to the testing technique wherein each sample was restored to estimated field stress and moisture conditions prior to testing. The 1½" diameter specimens were sub-sampled from the 4½" tubes. They show a considerably lower value of E, which is probably caused by the added disturbance during the sub-sampling process, as an identical testing technique was used.

Using a value of 2,000 lb/in$^2$ for E yields load-displacement curves which are shown in Figs.6 and 7. Comparison with the actual loading curves indicates that this value of E is much too low, and that the value which fits the observed field behaviour lies between 5,000 and 6,000 lb/in$^2$. There is a considerable discrepancy here which emphasises the difficulty that exists in obtaining accurate and reliable values of the elastic parameters from laboratory tests.

Lang (Ref.2) has reported large differences in the value of E obtained from identical triaxial tests on two specimens from the same sample tube. The lower specimen always yielded a higher value (by factors up to 10) of E, and this was considered to reflect the variations in the amount of mechanical disturbance that occurs in a sample. If E is so sensitive to disturbance, then it is not unreasonable to expect that laboratory determinations could be much lower than the actual field values, as is apparently so in this case.

An attempt has been made by Poulos (Ref.7) to relate the values of E obtained from field loading tests to the undrained cohesion $c_u$. He obtains $200 < \frac{E}{c_u} < 500$ and a typical value for both normally consolidated and over-consolidated clays is about 250. In this case the average values are

$c_u$ = 13 lb/in$^2$ E = 5,000 lb/in$^2$

which gives a value of 380 for this ratio. This is within the range quoted and indicates that the field value of E is reasonably consistent with other observations.

## IX. - DISCUSSION

The various means of calculating pile capacities from both laboratory and field data have been presented, so this section will be restricted to a general discussion and critical comparison of the techniques used.

Results for the initial series of triaxial tests in the uniform layer of mottled clay showed failure strains ranging from 1% to 12%, and were consequently viewed with some suspicion. In some cases failure occurred along a near vertical plane, and this plane proved to be the interface between the two components of the mottled clay. These components were distinctly different in colour and appearance, although no significant difference could be measured in moisture content, grading, S.G. or plasticity.

In the second series of tests the samples were reconsolidated prior to shear and failure strains showed less variation and the typical semi-plastic failure mode predominated. This illustrates the difficulty in obtaining soil parameters that can be reliably applied to field calculations.

Table V shows that all methods, with the exception of the Friction Penetrometer, have yielded reasonable estimates of the ultimate pile capacity. The accuracy of computations using soil parameters depends to a large extent on the values assigned to various constants, and good agreement with the test loading may only be fortuitous. The end-bearing component, which contributes over 50% of the calculated capacities for the first test, depends on the selection of an appropriate bearing capacity factor, and the calculation of skin friction for both tests depends on the estimation of $c_a$. If $c_a/c_u = 0.4$, as is suggested by Poulos (Ref.7), had been used then an increase of over 50% in the skin friction component would result. Arguments can be produced which influence the selection of a bearing capacity factor, but the choice of the factor from which adhesion is calculated appears to be purely arbitrary (within a certain range).

What is obviously required is a means of directly measuring the skin friction. The Friction Penetrometer appears to over-estimate the skin friction component by a factor of at least two. The reason for this is not immediately evident but consideration in future investigations will be given to the following points:

1. The stress-strain behaviour of the soil - does the penetrometer measure the post-peak stress-strain behaviour?

2. Surface texture effects.

3. The influence of lateral soil pressure.

4. Strain rate differences.

5. Dynamic effects.

X.- CONCLUSIONS

1. The test loading gave the ultimate bearing capacity of this steel shell pile driven to 38', and indicated a lower limit for the capacity of the same pile driven to 76'. This allowed the merits of the two piling systems to be examined. The final design used H-section steel piles driven into the Silurian bedrock, and the choice was governed largely by economic considerations.

2. Good agreement was obtained between calculated and measured capacities, but it is realised that these calculations depend largely on the interpretation of soil parameters and on the selection of bearing capacity factors. We have used Meyerhof factors but other approaches would produce significantly different results.

3. The stress-strain characteristics of the soil mass, as measured by the load and deflection of the pile, indicate that no unique relationship exists and that the curve is dependent on the duration of the loading period.

4. Comparisons of predicted and measured settlements of this pile show that laboratory determinations of Elastic modulus are most unreliable. Two triaxial specimens from the same sample tube often produced widely disparate values of E, and the average values over the whole pile length were found to be lower by a factor of 2-3 than the value indicated by actual settlement behaviour.

XI.- ACKNOWLEDGEMENTS

The authors wish to thank Dr. J.C. Holden who organised and supervised the field loading tests and the staff of the Country Roads Board who assisted with both field and laboratory investigations.

This paper has been prepared and presented with the permission of Mr. I.J. O'Donnell, O.B.E., E.D., F.I.E.(Aust.), F.A.I.M., M.Inst.T., Chairman of the Country Roads Board, Victoria.

XII.- REFERENCES

1. BJERRUM, L. - Engineering Geology of Norwegian normally consolidated marine clays as related to Settlement of Buildings. Geotechnique 17:2 : pp. 81-118. 1967.

2. LANG, J.C. - Longitudinal Variations of Soil Disturbance within Sample Tubes. Proc. 5th A.N.Z. Conf. Soil Mech. and Found. Eng. Auckland 1967.

3. LEE, I.K. (Ed.) - Soil Mechanics - Selected Topics. Butterworths 1968. Chapter 9.

4. MEYERHOF, G.G. - Some Recent Research on the Bearing Capacity of Foundations. Canadian Geotech. J., Vol. 1, No.1, 1963.

5. PARRY, R.H.G. - Testing Small Undisturbed Samples. Proc. 4th A.N.Z. Conf. Soil Mech. and Found. Eng. Adelaide. 1963.

6. POULOS, H.G. and DAVIS, E.H. - The Settlement Behaviour of Single Axially Loaded Incompressible Piles and Piers. Geotechnique 18 : 351 - 371 1968

7. POULOS, H.G. - The Settlement of Single Floating Piles. Univ. of Sydney. School of Civ. Eng. Post grad. course on The Analysis and Settlement of Foundations 1969 Vol.1. Lecture 5.

8. STYLES, J.R. - A Study of a Friction Penetrometer. Uni. of Melb. School of Civ. Eng. Thesis submitted as partial requirement for M. Eng. Sc. 1970.

9. VAN DER VEEN, C. and BOERSMA, L. - The Bearing Capacity of a Pile Predetermined by a Cone Penetration Test. Proc. 4th Int. Conf. Soil Mech. London. 1957 Vol. 1.

10. VESIC, A.S. (Ed.) - Bearing Capacity and Settlement of Foundations. Duke University 1967. (Section on Ultimate Load and Settlement of Deep Foundations in Sand).

11. WALKER, L.K. - Secondary Compression in the Shear of Clays. ASCE. Vol. 95. No. SM.1. 1969.

# Model Tests on Piles in Clay

By
N. S. Mattes, B.E., Stud.I.E.Aust.
(Engineer, Docker and Smith, Sydney)
AND
H. G. Poulos, B.E., Ph.D., M.I.E.Aust.
(Senior Lecturer, School of Civil Engineering, University of Sydney)

SUMMARY.- A series of tests on model piles in Kaolin is described. Single floating piles and end-bearing piles, and floating pile groups have been tested. Using control piles to obtain the soil moduli, theoretical predictions of pile settlements, based on elastic theory have been made. The good agreement found between predicted and observed settlements indicates that elastic theory can be successfully used to predict the effects of pile length and compressibility and group action on settlements.

## I.- INTRODUCTION

Recent papers by Poulos and Davis (Ref. 1) Poulos (Ref. 2), Mattes and Poulos (Ref. 3), and Poulos and Mattes (Refs. 4 & 5), have described the use of elastic theory to predict the settlement behaviour of piles and pile groups in clay. In several instances good agreement has been found between the theoretical behaviour and that measured in tests reported in published literature, but some available comparisons are obscured by such practical complications as layering of the soil profile, anisotropy of the soil, and uncertainties involved in the effects of differing installation procedures. In addition, there is little reliable data available on the effects on settlement behaviour of such basic and important parameters as the relative length and stiffness of the pile.

In this paper, results of a series of carefully controlled tests on model piles are described. Most of the tests have been carried out on single floating piles to determine the effects of the length-to-diameter ratio and relative pile stiffness on the pile settlement behaviour. All the piles have been tested by dead-loading, after which many of the floating piles have been tested to failure under constant rate-of-penetration (C.R.P). Some tests have been carried out on single end-bearing piles, to measure the load transferred to the base, and on two floating pile groups to measure group settlements. The measured values have then been compared with values predicted from theoretical analyses of pile behaviour.

## II.- APPARATUS

The testing apparatus was basically similar to that used by Davis and Poulos (Ref. 1) for pad footing tests. However, because of the need to maintain extremely careful control over the model pile tests, it was necessary to make improvements to the apparatus.

The main piece of equipment was a pressure vessel which contained the clay and model piles and allowed the piles to be loaded while maintaining a constant overburden pressure on the soil. Ancillary apparatus consisted of pressurized water sources, loading devices, and pile displacement measuring equipment. The main features of the apparatus are shown in Fig. 1, and the major components are described below.

### (a) Pressure Vessel and Drains

The pressure vessel consisted of a steel base with a drainage tapping, one or more tubular steel body sections 12 inches in diameter, in which the soil and piles were placed, and a steel lid containing water which provided the consolidation pressure for the clay. O-rings and bolts were used to seal and connect the various sections of the vessel. A rubber membrane 0.017 inches thick separated the water in the top section from the clay. Holes in the lid allowed loading plungers to be located at the centre, and at four equally spaced positions around a 3 inch radius circle.

The loading plungers consisted of a hardened steel shaft, 3/8 inch in diameter, moving in a pair of precision ball bushings. The bushings were housed in a brass body which was bolted to the pressure vessel lid, and an O-ring located in a groove in the brass body provided an effective low-friction seal around the loading shaft.

Drainage was provided at the top and base of the clay, and at 4 vertical drains equally spaced around the sides of the central body of the vessel. Each drain consisted of a piece of 100 mesh gauze wrapped in 2 layers of filter paper; the top drain was connected to a sand pocket over a drainage outlet in the

A. Air Filter
B. Precision Pressure Regulator
C. Pressure Gauge
D. Air-Water Pressure Cylinder
E. Filter Paper-Gauze Drain
F. Sand Drainage Pocket
G. Model Piles
H. Soil Monitoring Target
J. Clay
K. Loading Plunger
L. Loading Hanger
M. Dial Gauge For Pile Movement
N. Dial Gauge For Soil Movement.
P. Mounting Beam
Q. Magnetic Clamp
R. O-Ring
S. Pressure Vessel Base
T. Pressure Vessel Body
U. Pressure Vessel Lid
V. Rubber Membrane

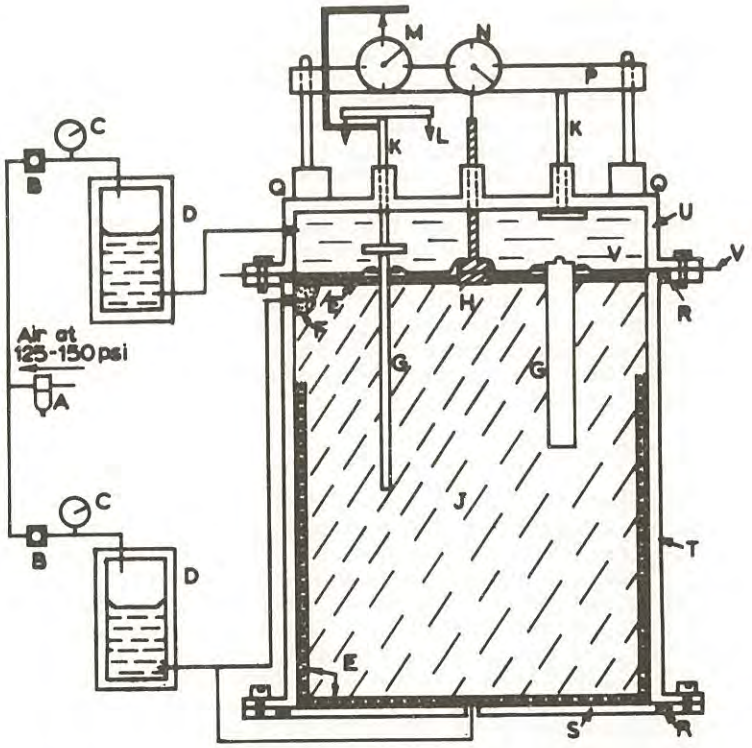


FIG.1. LAYOUT OF EXPERIMENTAL APPARATUS

body of the pressure vessel. The combination of radial and end drainage resulted in rapid and uniform consolidation of the soil.

(b) Pressure Supplies

Two separate sources of pressurized water were required; the first to provide consolidation pressure for the clay, the second to enable a 20 lb/sq.in. back pressure to be maintained in the pore-water, to minimize the amount of air within the clay. For each source, an accurate compressed air-water system was used. Precision regulators reduced the air pressure from the line pressure of 125-150 lb/sq.in. to the required pressure, with an accuracy of ± 0.02 lb/sq.in. The air, at the required pressure, was then fed into the top of a steel cylinder partially filled with water, and an outlet at the bottom of the cylinder was connected to the pressure vessel.

(c) Model Piles

Most of the piles were made from solid brass rod, the surface being roughened to promote pile-soil interaction. The piles had a domed top to ensure point contact with the loading plunger, and a narrow shoulder was provided about ½ inch below the top to enable the rubber membrane to be glued to the pile. To examine the effect of changes in relative pile length, piles of length 10, 25 and 40 diameters were tested. To enable pile compressibility effects to be observed, two piles were made from a plastic material with a relatively rough surface finish. The Young's Modulus of this material was 460,000 lb/sq.in., i.e. about 1/20 of that of brass.

For the tests on floating pile groups, ¼ inch diameter brass rod was threaded at the top, and screwed into drilled and tapped brass pile caps. A 3 x 3 group and a 6 x 1 group, with centre-to-centre spacings of ½ inch, were tested and in each case the piles were pushed through undersize holes in a reinforced rubber membrane so that a small gap remained between the membrane and the underside of the pile cap (i.e. the groups were free-standing).

For the end-bearing test, a pile was fabricated from 1 inch O.D. aluminium tube, 15 inches long and of wall thickness 0.035 inches. The tube was coated with epoxy glue and rolled in fine sand to give a rough protective coating. The bottom of the pile was glued to a steel base which was clamped into a recess in a special pressure vessel base. To measure the pile base load, two strain gauges were fixed diametrically opposed on the inside of the tube just above the base, with the connecting wires being led out through an axial hole in the steel base.

(d) Displacement Measurement

For the dead loading tests, pile displacements were measured with a 0.0001 inch dial gauge which was rigidly fixed to the pressure-vessel lid. For the constant rate of penetration tests, displacements were measured by a differential transformer, the amplified output of which was fed into an ultraviolet oscillograph. As the C.R.P. tests were carried out rapidly, the zero drift inherent in

this measuring system did not significantly affect the results.

Because of the small pile movements expected and the large depth of clay used, it was necessary to measure movement of the clay remote from the pile, to allow a correction to be made for consolidation and creep of the clay bed under the overburden pressure, and for transient effects such as temperature changes and slight pressure fluctuations. A 1 inch diameter brass footing attached to a loading shaft was placed under the central loading position of the lid. The overburden pressure held the footing firmly on the soil surface, and movements of the shaft were measured relative to the pressure vessel lid with a 0.0001 inch dial gauge.

## III.- TEST PROCEDURE

Powdered kaolin (LL 55, PL 33) was mixed to a moisture content of 53% and placed in the body of the pressure vessel, the side and base drains being already in place. A mechanical vibrator was used frequently to remove entrapped air. After installing the top drain and membrane, and bolting on the lid, which at this stage had blank pieces over the loading plunger positions, the cell pressure was increased in stages up to an effective pressure of 20 lb/sq.in. (i.e. a total cell pressure of 40 lb/sq.in. and a back pressure of 20 lb/sq.in.). When no further pore water was expelled, the drains were closed and the cell pressure was released. The top 4½ inch body section of the vessel was removed and the excess clay trimmed level with the rim of the remaining section.

In the tests on floating piles, four piles were installed vertically into the clay at predetermined positions by a constant rate of strain loading device. The soil monitoring target was glued to the membrane, which was in turn glued to the shoulders of the four piles, using a water-proof contact cement. The lid, fitted with loading plungers, was replaced, and the cell and back pressures were re-applied to give an effective overburden pressure of 30 lb/sq.in. Consolidation was allowed to proceed for at least 7 days after this stage. A loading hanger with a small seating load was then placed on one of the piles, and after a settling down period of about two hours the test load (approximately 1/3 of the estimated ultimate load) was added to the hanger. Time-settlement readings for the pile and the soil monitoring target were taken at frequent intervals. After completion of the load test, the procedure was repeated on the other piles in turn.

Constant rate of penetration (C.R.P.) tests were carried out on most piles after completion of all the dead-load tests, in order to compare the results with those obtained by dead loading, and to obtain load-settlement curves to failure. For these tests, loads were measured on a specially constructed load cell and displacements by a differential transformer, the outputs being recorded as two traces on an ultraviolet oscillograph.

The pile group tests were performed in an almost identical manner to the single pile tests. The two groups tested were placed under diametrically opposite loading positions, while single piles were placed and tested in the other two positions.

For the end-bearing pile tests, the soil was consolidated with the pile in position. Consolidation was carried out in stages, clay being added at each stage to maintain a flat surface close to the top of the pile. During the load test, the pile base load was measured on a direct reading strain bridge.

## IV.- RESULTS

### (a) Single Pile Tests

Typical time-settlement plots are shown in Figs. 2(a) and (b). To determine the immediate settlement, a settlement versus square root time curve was extrapolated to zero time. The end of primary consolidation, and hence the total final settlement, was determined on a log time - settlement plot as the position of the change in slope from the initial steep portion of the curve to the almost horizontal portion, as found by intersection of the appropriate tangents.

The results for the dead-loading tests are summarized in Table 1. As expected, settlements increase as pile length decreases or as the compressibility of the pile material increases.

Typical load-settlement plots for the C.R.P. tests are shown in Figs.3(a) and (b). Also shown are the immediate and final settlements measured from the prior dead-loading tests, and it will be seen that the agreement between C.R.P. and dead-load test settlements is quite close. The load-settlement curves for the brass piles are reasonably linear up to about 50% of the ultimate load, but the curves for the compressible plastic piles, as well as indicating considerably greater settlements, are non-linear over a larger range of load. This behaviour is consistent with the theoretical predictions of Mattes and Poulos (Ref. 3).

From the failure loads indicated by the C.R.P. tests, it has been calculated that the average undrained pile-soil adhesion $c_a$ is 4.0 lb/sq.in. for the brass piles, and 4.8 lb/sq.in. for the plastic piles. The undrained cohesion measured in several unconfined and triaxial compression tests was 12 lb/sq.in., so that the deduced adhesion factor $c_a/c_u$ was as follows:

brass piles: $c_a/c_u = 0.33$

plastic piles: $c_a/c_u = 0.40$

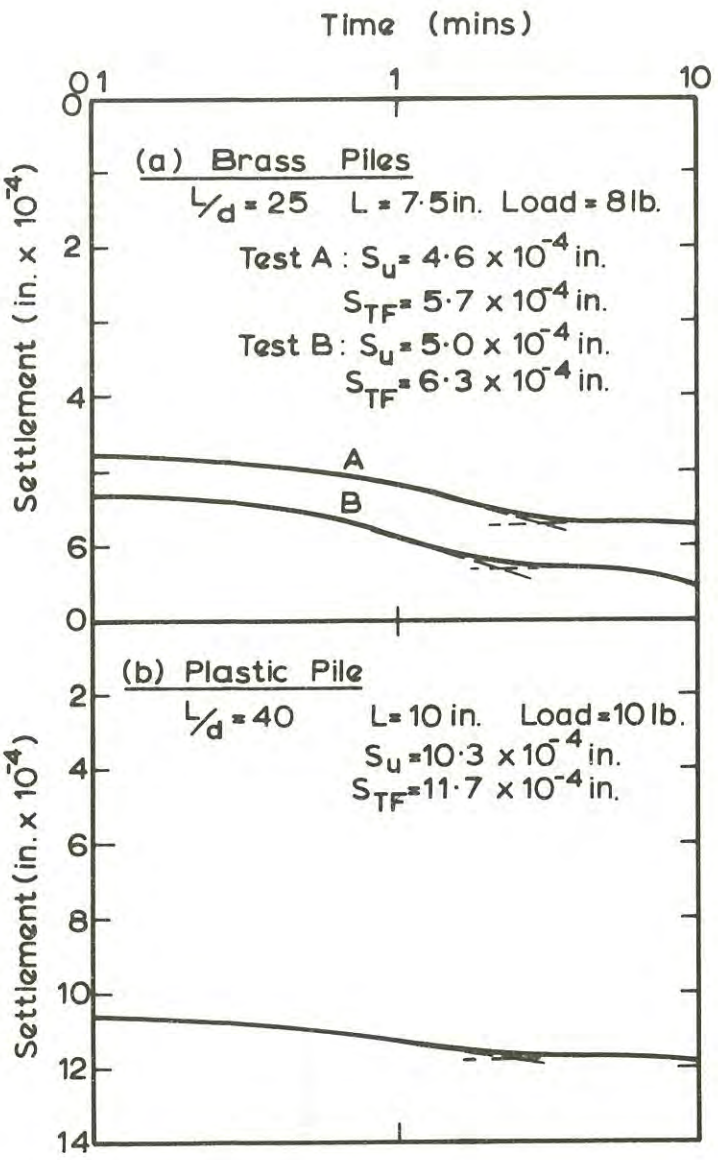


FIG.2. TYPICAL TIME-SETTLEMENT CURVES FOR MODEL PILES

(b) Comparisons with Theory

In comparing the behaviour of piles of different dimensions and elastic properties, it was decided to use the measured settlements for the piles of length 25 diameters as control piles to determine the undrained elastic modulus Eu and the drained elastic modulus $E_s'$ of the soil, and to use these moduli to calculate theoretical settlements of the other piles. The modulus values were calculated using the theoretical results of Mattes and Poulos (1969), taking the drained Poisson's ratio $\nu_s'$ of the soil to be 0.35, an average value obtained from several drained triaxial tests. The average values thus obtained were:

Eu = 4040 psi; standard deviation 418 psi.

$E_s'$ = 3120 psi; standard deviation 392 psi.

Using these moduli with the theoretical results of Mattes and Poulos (Ref. 3), the settlements of piles of different relative length and compressibility have been calculated, and are plotted in Fig. 4. In this figure the predicted settlements are expressed as a fraction of the settlements measured in model tests, and it will be seen that the agreement between measured and predicted settlements is reasonably good. Thus the theory predicts with adequate accuracy the effects of pile length and compressibility on settlement. In Fig. 5, the theoretical ratio of immediate to final settlement, calculated by the method of Mattes and Poulos (1969) are compared with the observed ratios for the brass piles, and again good agreement between theory and experiment is obtained. For the plastic piles, the observed ratios ranged between 0.79 and 0.94, with a mean value of 0.87, whereas the theory predicted a value of 0.78.

(c) Pile Group Tests

The results of the tests on floating pile groups are shown in Table 2. Using the values of Eu and $E_s'$ calculated from the control

TABLE 1

SUMMARY OF SINGLE PILE TESTS

| Length (inches) | Length/ Diameter | Young's Modulus of Pile (lb/sq.in.) | Applied Load (lb) | Immediate Settlement (inch x $10^{-4}$) | | Total Final Settlement (inch x $10^{-4}$) | | Number of Tests |
|---|---|---|---|---|---|---|---|---|
| | | | | Mean | Range | Mean | Range | |
| 7.5 | 10 | 10 x $10^6$ | 20 | 8.8 | 8.5 - 9.2 | 12.1 | 11.6 -12.6 | 2 |
| 7.5 | 25 | 10 x $10^6$ | 8 | 4.5 | 3.7 - 5.0 | 5.5 | 4.6 - 6.3 | 6 |
| 10 | 40 | 10 x $10^6$ | 10 | 4.5 | 3.8 - 5.7 | 6.0 | 4.6 - 7.2 | 6 |
| 10 | 40 | 0.46 x $10^6$ | 10 | 11.6 | 10.3 -13.7 | 13.4 | 11.7 -14.6 | 8 |

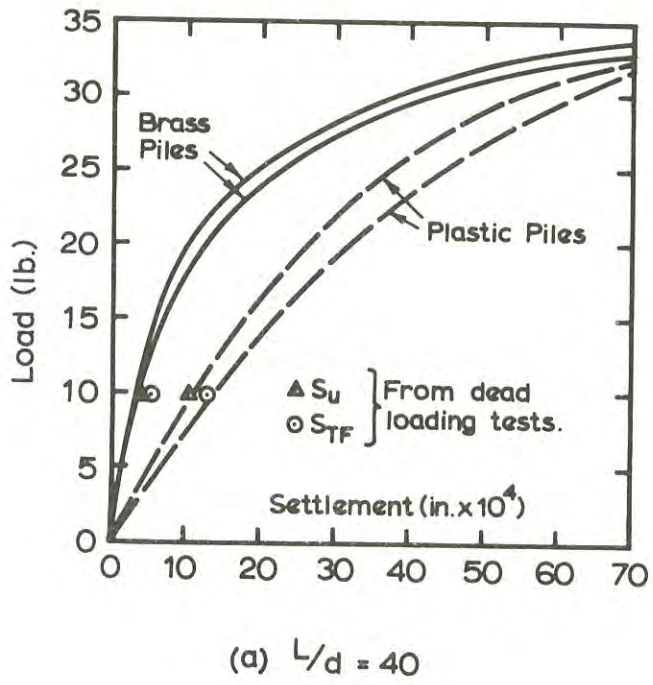


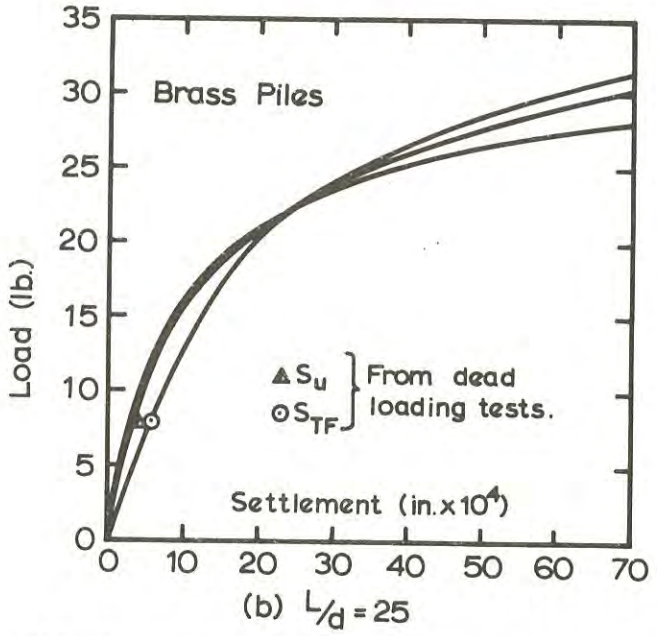


FIG. 3. TYPICAL LOAD-SETTLEMENT CURVES FROM C.R.P. TESTS

piles on single tests, the group settlements were calculated theoretically from the method described by Poulos and Mattes (1971), assuming the pile cap to be rigid. These values are also shown in Table 2, and it will be seen that there is good agreement between theory and experiment for both immediate and final settlement.

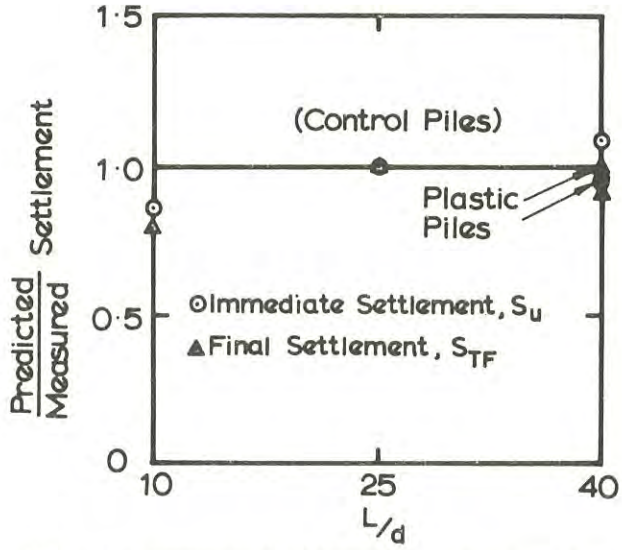


FIG. 4. COMPARISON BETWEEN MEASURED AND PREDICTED SETTLEMENTS

(d) End Bearing Pile Tests

Five tests were carried out, and the measured base loads of 70-80% of the applied load compared reasonably well with the theoretical base load of 82-88%, calculated from the analysis of Poulos and Mattes (1969). In these tests, the maximum base load was developed about 30 minutes after the application of load.

## V.- CONCLUSIONS

A number of carefully controlled tests on model piles have been carried out in a specially developed apparatus, and the measured settlements have been compared with theoretical predictions based on elastic theory. For the theoretical predictions the undrained and drained moduli of the soil have been determined from the settlements of a series of control piles.

The generally good agreement between theory and observation in these tests, together with other instances of agreement in reported field tests previously analysed, is further evidence that elastic theory, discretely used, can adequately predict the settlement of pile foundations.

## VI.- ACKNOWLEDGMENTS

The work described in this paper forms part of a general program of research into the settlement of all types of foundations being carried out at The University of Sydney under the general direction of Professor E.H. Davis, Professor of Civil Engineering (Soil Mechanics). The authors wish to acknowledge the assistance of J.L. Coppe and K. Larymore in the construction and assembly of the apparatus.

TABLE 2

MODEL GROUP TEST DATA

| Group | | 3x3 | 6x1 |
|---|---|---|---|
| Total group load (lb) | | 50 | 40 |
| Theoretical group settlement ratio $R_s$ | | 4.77 | 3.24 |
| Settlement of single pile at average pile load (predicted from average values of soil modulus) (in.x$10^{-4}$) | Immediate | 3.82 | 4.41 |
| | Final | 4.98 | 5.56 |
| Immediate Settlement of Group (in.x$10^{-4}$) | Predicted | 18.2 | 14.3 |
| | Observed | 15.3 | 15.0 |
| | Predicted / Observed | 1.19 | 0.95 |
| Final Settlement of Group (in.x$10^{-4}$) | Predicted | 23.8 | 18.0 |
| | Observed | 24.2 | 20.0 |
| | Predicted / Observed | 0.98 | 0.90 |

Group Settlement = $R_s$ x single pile settlement

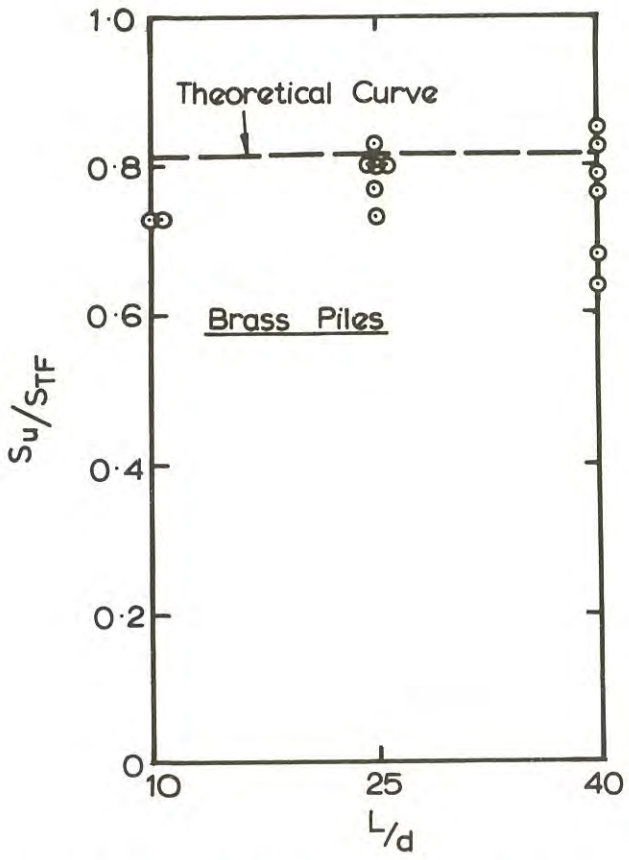


FIG. 5. COMPARISON BETWEEN OBSERVED AND PREDICTED RATIO $S_u/S_{TF}$

REFERENCES


1. POULOS, H.G. and DAVIS, E.H. (1968) - The Settlement Behaviour of Axially-Loaded Incompressible Piles and Piers. Geotechnique, 18: 351-371.

2. POULOS, H.G. (1968) - Analysis of the Settlement of Pile Groups. Geotechnique, 18: 449-471.

3. MATTES, N.S. and POULOS, H.G. (1969) - The Settlement of a Single Compressible Pile. Jnl Soil Mechs & Fndns Divn, Am.Soc. Civ.Engrs, Vol.95, No.SM1, pp.189-207.

4. POULOS, H.G. and MATTES, N.S. (1969) - The Behaviour of Axially-Loaded End Bearing Piles. Geotechnique, 19: No.2, pp.285-300.

5. POULOS, H.G. and MATTES, N.S. (1971) - Settlement and Load Distribution Analysis of Pile Groups. To be published in Australian Geomechanics Journal.

APPENDIX - NOTATION

| | |
|---|---|
| CRP | constant rate of penetration test |
| $E_u$ | undrained Young's modulus of soil |
| $E_s'$ | drained Young's modulus of soil |
| L | pile length |
| $R_s$ | group settlement ratio = ratio of settlement of group to settlement of single pile carrying same average load as a pile in the group |
| $S_u$ | immediate or undrained settlement |
| $S_{TF}$ | total final settlement |
| $c_a$ | undrained adhesion between pile and soil |
| $c_u$ | undrained cohesion of soil |
| d | pile diameter |
| $\nu_s'$ | drained Poisson's ratio of soil. |

# A High Capacity Load Test for Deep Bored Piles

By
J. D. Moss, B.E., F.I.E.Aust.
(Brickell, Moss and Partners, New Zealand)

SUMMARY.- The equipment and field procedures used in an end-bearing load test for bored piles founded at depths of from 30 to 50 feet in strong marine deposits are described. Good correlation was obtained between the calculated and actual intensities of applied bearing pressure at failure. Brief reference is made to secondary pull-out tests on the grouted cable anchors used as loading reactions in the pile test. The application of test results in the final design of piles is also described.

## I.- INTRODUCTION

The first stage of construction of the Downtown Redevelopment Scheme in Auckland, New Zealand, commenced in late 1968. The site covers two city blocks and approximately 10 acres; it adjoins the waterfront and includes the commercial area bounded by Queen, Quay and Hobson Streets and Customs Street West. The redevelopment is being undertaken in three stages by the international consortium of Mainline-Dillingham-Fletcher.

Buildings constructed in the first stage include the 21-storey Air New Zealand House, the 14-storey Auckland Travelodge motor-hotel, an extensive multi-storey carparking station for 1700 vehicles and a two-storey tourist centre. All buildings except the tourist centre have full or partial basements. Apart from the parking station which is generally of precast, prestressed shear-wall construction, the buildings are of conventional reinforced concrete construction. All structures were designed to the requirements of the New Zealand code for earthquake resistant construction. Column loads (for dead plus real live loading conditions) ranged from 400 to 2300 kips; these static loads were increased by up to 50 percent for superimposed seismic loadings.

A combination of weak surface soils and structural factors required that the buildings be supported on piles founded in the strong Waitemata series sedimentary deposits which underlie the site at depths of from 20 to 40 feet. Investigation studies had indicated that the three major buildings could be supported satisfactorily and most economically on 190 large diameter drilled-and-cast-in-place piles designed to derive their full capacity from end bearing. Side wall adhesion was neglected as piles in some areas were only expected to penetrate about 7 feet into the dense Waitemata series deposits. Depending on the intensity of applied loading, the piles could be either straight shafted or belled at their bases. The local code ordinance covering foundation design at that time required that applied end-bearing pressures in Waitemata series deposits could not exceed 12 tons per square foot. Accordingly, in view of the number of piles and high order of structural loading involved, it was decided to undertake a comprehensive load test to verify the indicated favourable pile capacities derived by engineering analyses based on laboratory testing results and to persuade the local authority to approve a variation of the code limitations.

## II.- DIMENSIONS

All dimensions of quantities are expressed in terms of feet - pounds - hours, or multiples thereof. "Tons" refer to long tons (2240 pounds). Pressures are quoted as tons per square foot (TSF) or pounds per square foot (PSF). Kips equal 1000 pounds.

## III.-SITE CONDITIONS

Prior to the settlement of Auckland in 1840, part of the site extended on to a flat tidal shelf bordering the original shoreline. The area was initially developed by several stages of reclamation between 1859 and 1923. Research has disclosed that old rock bunds, quay walls, piling and part of a former graving dock were filled over in successive reclamation stages.

Subsoil conditions at the site were explored in two investigations involving 30 borings of from 50 to 82 feet in depth. These studies proved that the site is consistently underlain by:-

(a) surface reclamation fills;

(b) recent marine sediments, and

(c) Waitemata series deposits

The surface fills vary from 14 to 23 feet in depth and consist of weak, poorly compacted intermixed soil, rock and harbour bed deposits. The fills generally overlie up to 20 feet of recent marine sediments comprising soft to moderately firm clays and silts which contain random lenses of sand. At depths of from 18 to 39 feet below present ground level, the surface fills or marine sediments are underlain by dense Waitemata series sediments which extend to the depths explored. These deposits comprise alternating strata of variably cemented sandstones and siltstones which have the appearance, texture and strength characteristics of weak rock. Approximately equal

volumes of sandstone and siltstone were encountered in the borings although their distribution tended to vary throughout the site.

Near-continuous cores were recovered from selected borings in the Waitemata series deposits. A large number of unconfined compression, triaxial and direct shear tests performed on samples of the Waitemata series sandstones and siltstones indicated their strength parameters, for purposes of design (Appendix), are of the following orders:-

sandstone: $c_u$ = 2600 PSF $\phi_u$ = 35°
siltstone: $c_u$ = 1000 PSF $\phi_u$ = 30°

The simplified log of a boring located adjacent to the load test is reproduced in figure 1 together with a summary of the unconfined compression tests performed on selected continuous core samples of the Waitemata series deposits recovered from this hole.

The ground water level, measured in numerous exploratory borings throughout the site, consistently stabilised at depths of from 7½ to 8 feet below the present surface. Although the site is within several

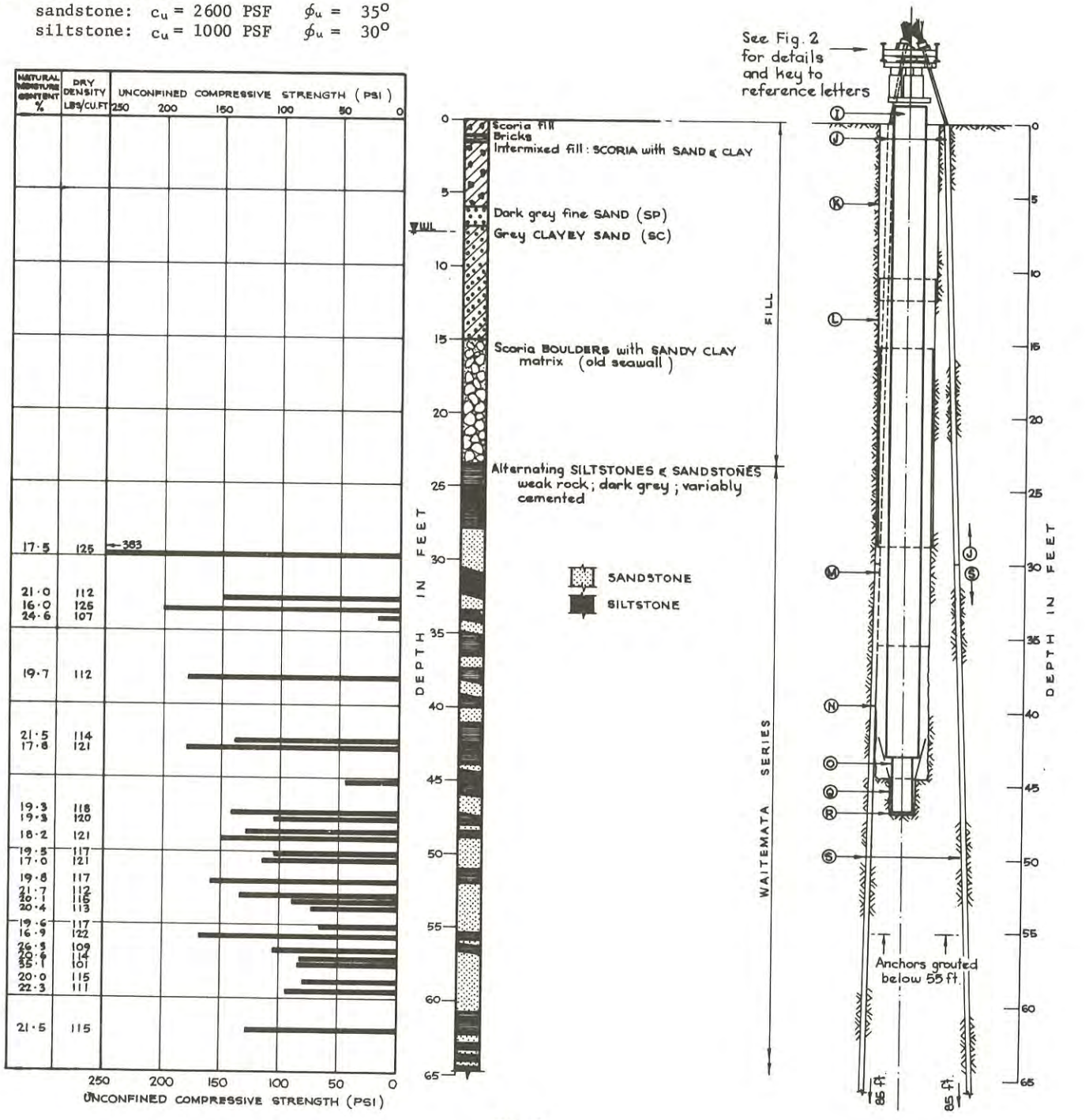


Fig.1

BORING LOG, TYPICAL STRENGTH DATA AND ELEVATION OF TEST PILE

hundred feet of the harbour, continuous ground water level observations over several tide cycles did not reveal any significant fluctuation of the ground water table due to tidal influence.

## IV.- PLANNED SCOPE OF TEST

The purpose and scope of the load test were to determine the following information for use in design and construction:-

(a) A basis for estimating the load-settlement performance of deep end-bearing drilled piles founded in Waitemata series deposits of average strength;

(b) The relationship between the apparent yield and ultimate bearing values of the Waitemata deposits, as applicable to drilled piles;

(c) Correlation between the theoretical and actual ultimate bearing capacity of an individual pile;

(d) Construction problems involved in drilling large diameter shafts through the variable fills and natural deposits at the site; and

(e) Ultimate capacities of grouted cable anchors in Waitemata series deposits.

## V.- THEORETICAL CAPACITY OF TEST PILE

In order to assure that base failure would occur under test loading, it was essential that the dimensions of the transfer pile and bearing plate be correctly proportioned and that adequate reaction capacity be provided. For these reasons, the theoretical ultimate capacities of various sizes of end-bearing piles were calculated prior to undertaking the load test. These calculations were based on the Terzaghi "General Shear Failure" formula and assumed strength parameters for the supporting Waitemata series deposits as determined from prior laboratory studies.

As described below, the test pile was founded at a depth of 47 feet in predominantly sandstone deposits and had an end-bearing area of 2.05 square feet. The ultimate capacity of this pile was calculated to be 370 tons; this capacity was equivalent to an end-bearing pressure of 181 TSF.

The approximate yield point strength of the Waitemata series sandstones was assessed from the results of a high-capacity consolidation test. A sample of cored sandstone recovered from a depth of 50 feet in the boring adjoining the load test site was loaded to pressures in excess of 500 TSF. The resulting plot of applied pressure against percentage consolidation gave straight line relationships from 4 to 64 TSF and from 128 to 512 TSF. The assumed yield occurred at 95 TSF corresponding to 5 percent vertical strain. It was concluded that between pressures of 64 and 128 TSF the natural cementing bonds progressively yielded and, at higher pressures, the sandstone acted as a non-cemented material. It was further concluded that apparent yielding of the founding materials could be expected to occur under applied test pressures of from 90 to 110 TSF.

## VI.- TEST PILE INSTALLATION

The load test assembly was selected from several alternatives on the basis that it appeared to satisfy all prime objectives of the study. The basic configuration was planned to determine the end-bearing capacity of a free-standing load transfer pile located within an oversized, partially cased shaft. Loading was applied at the ground surface by hydraulic jacking against a steel frame anchored by grouted cables. Details of the shaft, pile, loading frame, anchor cables and measuring equipment are illustrated in figures 1, 2, 3 and 4.

Supplementary comments on the assembly, including its sequence of installation, are as follows:-

Three symmetrically spaced, 4-inch diameter anchor holes were drilled on a 5-foot diameter circle centred on the selected test location. The holes were raked at an inclination of 1 horizontal to 30 vertical and extended to depths of approximately 85 feet. These holes were cased through the surface filling to a depth of 30 feet. On completion of drilling, the anchor holes were reamed and flushed clean, the cables were inserted and their lower 30 foot lengths were pressure grouted. Minor difficulties were experienced in cleaning the base of one hole due to seepage through the casing seal; in this case, the cable terminated 4 feet higher than those in the other anchor holes. The anchor cables consisted of twelve ½-inch diameter high tensile wire strands. In the grouted section of the cable, the individual strands were held symmetrically on a 3-inch diameter pitch circle by two types of spacers, located alternately at 3-foot intervals. The upper ends of the cables terminated in anchor grips at the surface load frame. The cables were installed and grouted 18 days prior to loading.

Following installation of the cable anchors, a partially cased, truly plumb shaft was drilled to a depth of 47 feet. As drilling proceeded, the uppermost section of the shaft was lined with a 12-foot length of 48-inch diameter casing. After this starter casing had been installed, the next section of shaft was advanced and lined with a prepared length of 46-inch diameter "core barrel" casing to a depth of 29 feet. The leading edge of this latter casing was tipped with tungsten steel cutting teeth to assist drilling through the basalt and scoria boulders encountered between depths of from 15 to 25 feet. The "core barrel" casing was advanced through the boulders by rotary drilling methods and had to be withdrawn periodically for dressing or replacing of the cutting teeth. A third section of 42-inch diameter casing was then inserted and advanced to a depth of 35½ feet, some 12 feet below the surface of the Waitemata series deposits, to ensure a seal against peripheral seepage. The shaft was then pumped dry and advanced to a depth of 44 feet by a combination of machine drilling and hand excavation. Although an effective seal was obtained at the base of the inner casing, a minor inflow of ground water occurred between the 42-inch and 46-inch diameter casings. Although attempts to seal the seepage between the casings were not fully effective, the inflow was reduced to less than several cubic feet per hour. Following completion of the main shaft, a concentric 20-inch diameter cased shaft was drilled from depths of 44 to 47 feet. The casing for this secondary shaft extended to within 9 inches

of the base. The bottom of the shaft was cleaned by hand trimming and then covered with a 1-inch thick layer of sand.

A special precast concrete pile was manufactured to serve as the load transfer unit. This member consisted of a standard 26-inch square, prestressed concrete pile with a 4-foot long, 16-inch diameter reinforced concrete extension cast monolithically at its base. A 19⅜ -inch diameter, 2-inch thick steel plate was bolted concentrically to the base of the pile extension. A number of small fillets were welded to the projecting upper face of the bearing plate to prevent binding of the pile with shaft casing during withdrawal.

The pile was installed by hoisting from two lifting lugs. The insertion of the base plate extension into the close-fitting base shaft was assisted by the provision of four steel guides welded to and projecting from the base shaft casing. The vertical alignment of the load transfer pile was established by

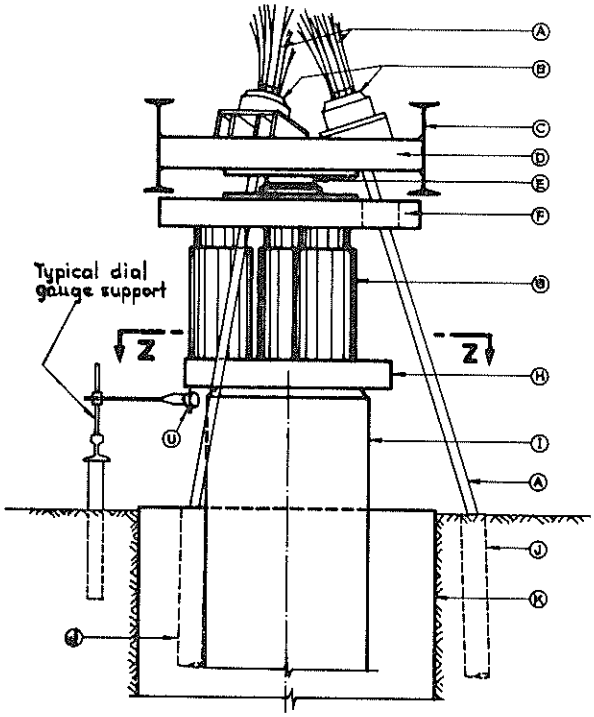


Fig. 2 : LOADING FRAME DETAILS

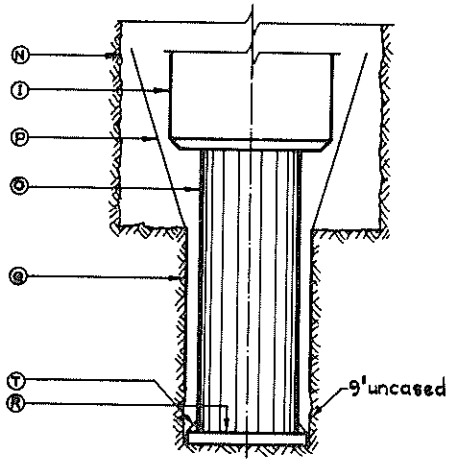


Fig.4 : PILE BASE DETAILS

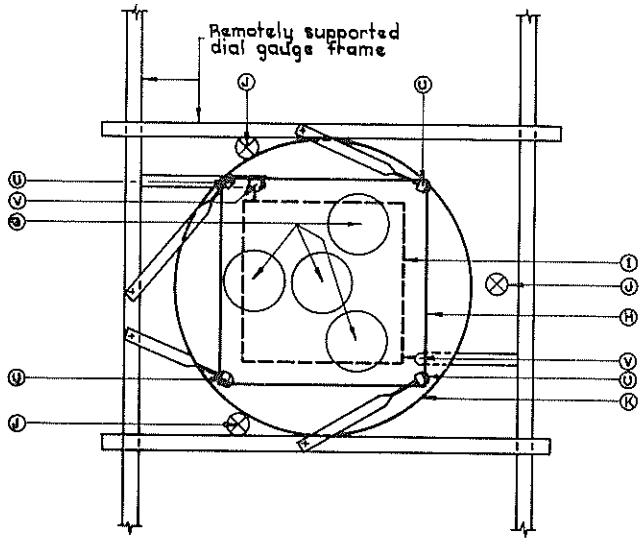


Fig. 3 : PLAN ON SECTION Z - Z

KEY TO FIGS 1, 2, 3 and 4:-

| | |
|---|---|
| A | Standard Freyssinet cables (12 nos ½" strands) |
| B | Cable anchor heads |
| C | Load frame support (15" x 5" x 42 lb RSJ$^{s}$) |
| D | 42" x 42" x 5" steel plate with aligned bearing plates for cable anchor heads |
| E | Hemispherical bearing |
| F | 42" x 42" x 4½" steel plate |
| G | 4 nos 100 ton hydraulic jacks |
| H | 33" x 33" x 4½" steel plate |
| I | 26" x 26" hollow-cone, pretensioned, prestressed concrete pile |
| J | 4" diam cased anchor cable holes |
| K | 48" diam cased shaft |
| L | 46" diam cased shaft |
| M | 42" diam cased shaft |
| N | 42" diam uncased shaft |
| O | 16" diam reinforced extension cast monolithically with pile |
| P | 4 nos steel angles to guide pile into shaft |
| Q | 20" diam cased shaft |
| R | 19⅜" - diam steel plate, 2" thick |
| S | 4" diam uncased anchor cable shafts |
| T | ¼" thick fillet plates |
| U | dial gauges to record vertical movement |
| V | dial gauges to measure horizontal movement |

Figs. 2, 3 and 4

TEST PILE DETAILS

plumbing down the central inspection core of the pile. A loading frame of the type detailed in figures 2 and 3 was installed between the load transfer pile and the cable anchorages. The four hydraulic jacks and concentric hemispherical seating were positioned by precise surveying. The jacks used were idential and had been specifically calibrated for this project. They were coupled to a common manifold. During erection, the load frame was supported by large greased timbers. A heavy timber frame (not illustrated) was erected to resist the horizontal reaction of the steeply-inclined anchors and to prevent contact between the cables and pile head assembly. The exposed sections of the anchor cables which extended through the load frame were sheathed as a safety precaution. Rigid, remotely-supported horizontal steel rails were erected in a square around the top of the test pile as a datum for determining its movement under test. Four dial gauges were installed to measure vertical deflections and two to determine lateral movements of the pile.

## VII.-LOADING SEQUENCE

The sequence of applied loading, determined after a review of selected published data relating to similar types of test (references 1 and 2), were planned to provide information on:-

(a) Settlement performance of an individual pile subjected to pressures equivalent to those imposed by future gravity loads;

(b) Yield-point bearing pressure of the deposits underlying the pile; and

(c) Ultimate bearing pressure intensity of the supporting foundation mass

The weight of the transfer pile and loading frame were calculated to impose a base pressure of 5½ TSF, or approximately 4 TSF in excess of the natural overburden pressure at the test depth. This initial net pressure has been neglected in all test results; thus "applied pressure" equals the actual load applied to the head of the pile divided by its base-end bearing area.

The initial stage of testing comprised a maintained load test to overcome seating problems and provide load-settlement data for future piles subjected to normal gravity loads. The applied pressure was increased in 4 TSF increments at 24 hour intervals. The pile was loaded to a maximum applied pressure of

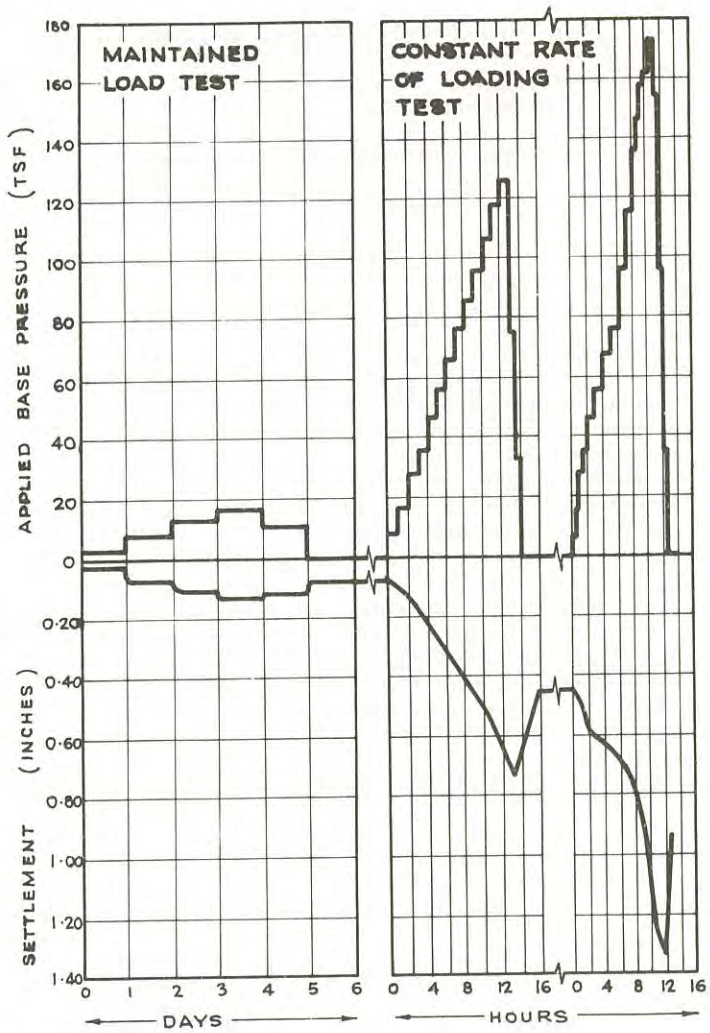


Fig. 5 : LOADING - SETTLEMENT HISTOGRAM

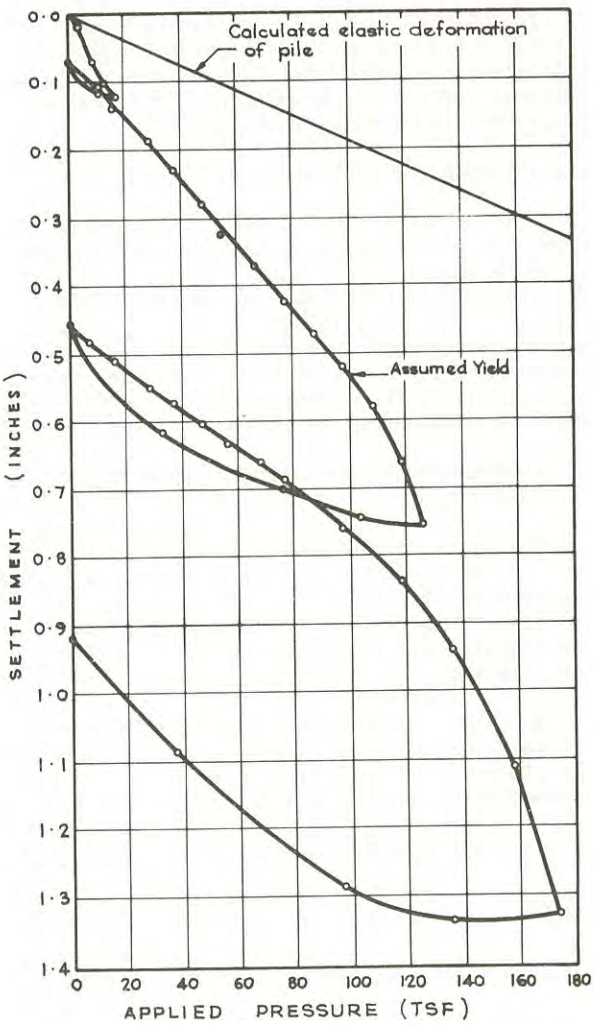


Fig. 6 : PRESSURE VS SETTLEMENT

16 TSF and then unloaded in two 24 hour cycles. During each increment of loading, deflection readings were taken at intervals identical to those of a normal consolidation test to determine the time-rate characteristics under load.

The second stage of loading, undertaken after a three-day break, consisted of a constant rate of loading test to assess the yield point bearing intensity. The applied pressure was increased in 10 TSF increments at 1 hour intervals until the plot of applied pressure against deflection and the rate of deflection in each loading cycle indicated that the yield point of the bearing material had been attained. The maximum applied pressure for this phase of testing was 130 TSF and the pile was unloaded in three, half-hour stages.

The third stage of testing was commenced after a further two day break. This test, to determine the ultimate bearing capacity of the foundation deposits, repeated the procedures of the constant rate of loading test. The applied pressure was increased in 10 TSF increments each hour to 80 TSF and thereafter in 20 TSF, hourly increments. The maximum applied pressure attained was 175 TSF at which point the pile yielded continuously under constant loading. The pile was then unloaded in four, half-hour intervals.

The results of the three loading stages are illustrated graphically in figures 5 and 6. The indicated settlements are the average of the four vertical deflection measurements recorded by dial gauges at each corner of the pile.

## VIII.-ANCHOR CABLE TESTS

Each of the three grouted cable anchors was subjected to loading tests subsequent to the completion of the pile test. An axial tensile load was applied individually to each cable by hydraulic jacks bearing against a surface grillage. Each cable was loaded to 170 tons or approximately 80 percent of the ultimate tensile strength of the cable. At these loads, no yielding of the anchor could be detected and the tests were abandoned for reasons of safety.

## IX.-CORRELATION OF THEORETICAL AND ACTUAL PILE CAPACITIES

The calculated ultimate capacity of the pile used in the load test was equal to an end-bearing pressure of 181 TSF. This value agrees remarkably (or fortuitously) closely with the measured ultimate bearing pressure of between 170 and 180 TSF under test loading.

The above capacity was based on shear test values available at the time of planning the load test. The ultimate strength parameters adopted for the predominantly sandstone basal deposits were:-

| | |
|---|---|
| apparent cohesion | $c_u$ = 2150 PSF |
| apparent angle of internal friction | $\phi_u$ = 40° Direct Shear. |

## X.- PILE DESIGN

In view of the confirming evidence provided by the load test, design capacities for bored piles at the site were evaluated by the Terzaghi "General Shear Failure" formula. It was assumed in analyses that piles may be underlain by weaker siltstones of the Waitemata series. The pile capacities were determined solely on the basis of end-bearing support and no allowance was made for frictional sidewall support on pile shafts by the soils above the base. Accordingly, and with the agreement of the local authority, drilled piles were proportioned to impose the following maximum end-bearing pressures:-

| | |
|---|---|
| Real loads: (dead plus permanently-applied live loads) | 15 TSF |
| Design gravity loads: (dead plus code live loads) | 20 TSF |
| Total design loads: (including seismic or wind loads) | 24 TSF |

These pressures were assessed to include an absolute minimum factor of safety of 2 with respect to failure under total design loading conditions. The equivalent theoretical factor of safety for real loads is in excess of 2.5. If the effects of sidewall friction were included, these factors would be considerably higher. The factor of safety for the sandstone deposits, as indicated by the pile load test results, is in excess of 5.

For contractural purposes, the founding depths of piles were selected directly from the correlated boring log data. Factors which governed the selection of pile depths included:-

(a) The random occurrence of weaker siltstones within the critical influence zone of two-base diameters of depth below piles; and

(b) Adequate depths below the surface of the Waitemata series deposits in which to found and bell the bases of bored piles.

In order to confirm selected founding depths, proof borings were drilled at approximately 50-foot centres in building areas ahead of piling construction. These borings were continuously cored to depths of at least two base diameters below the tentatively selected founding elevations. If siltstone deposits having equivalent triaxial deviator strengths of less than 50 pounds per square inch were encountered within this zone, the piles were deepened accordingly.

The total settlements of the multi-storey structures founded in this manner were conservatively estimated to be on the maximum order of 1 inch. Differential settlements between adjacent columns were not expected to exceed ½ inch. Approximately 80 percent of any settlement which did occur was expected to take place during construction on the initial application of permanent loads.

## XI.- CONCLUSIONS

(a) The decision to undertake this load test was vindicated by the satisfactory results and correlation achieved, notwithstanding the relatively high cost involved. The subsequent construction savings derived by the developers are estimated to be in excess of twenty times the cost of conducting the test.

(b) The success of any loading test, as confirmed by this project, depends more critically on preliminary planning than on any other single related factor.

## XII.-ACKNOWLEDGEMENTS

This paper has been presented with the permission and encouragement of the developers, Mainline-Dillingham-Fletcher.

The author is indebted to his colleagues, D.E.Hollands and K.H.Gillespie for their helpful criticism during its preparation.

## REFERENCES

1. Large Bored Piles, Institution of Civil Engineers, 1966, 159 pp.

2. A Performance Investigation of Pile Driving Hammers and Piles, Michigan State Highway Commission, 1965.

## APPENDIX

## LABORATORY STRENGTH TESTS

The shear strengths of the Waitemata series sandstones and siltstones were determined by three laboratory testing methods; unconfined compression, triaxial shear and direct shear.

Samples of the Waitemata series deposits were recovered as a continuous series of 3-foot long cores in an NX triple-tube core barrel. Although few cores were lost, the samples tended to break along horizontal bedding planes into 1 - to 12-inch lengths. All cores tested were of consistent diameter and required no preparation other than end trimming to the required test length. The samples were tested at their field moisture contents within 24 hours of recovery.

(a) Unconfined Compression Tests

All unconfined compression tests were performed at nominal confinement pressures of 10 PSI. A summary of the results of these tests is given in Table 1 below.

TABLE 1

UNCONFINED COMPRESSION TESTS

| | Siltstone | Sandstone |
|---|---|---|
| Number of Tests | 54 | 75 |
| Minimum Strength | 19 PSI | 12 PSI |
| Maximum Strength | 285 PSI | 383 PSI |
| Average Strength | 113 PSI | 106 PSI |
| Median Strength | 102 PSI | 95 PSI |

(b) Triaxial and Direct Shear Tests

Eleven quick, undrained triaxial shear tests were performed on selected cores of the Waitemata series deposits. In addition, 19 strain-controlled direct shear tests were carried out under quick, undrained conditions and surcharge pressures approximately equal to or greater than the natural overburden pressures.

(c) Strength Parameters

For the purpose of pile design, the strength parameters of the supporting foundation deposits were assessed from the combined results of the above strength tests. The apparent angles of internal friction were determined from a combination of the results of the triaxial and direct shear tests. These values are given in Section III of the main text.

# Analysis of the Movements of Battered Piles

By

H. G. Poulos, B.E., Ph.D., M.I.E.Aust.

(Senior Lecturer, School of Civil Engineering, University of Sydney)

AND

M. R. Madhav, M.E., Ph.D.

(Assistant Professor in Civil Engineering, Indian Institute of Technology, Kanpur, India—Presently Post-Doctoral Fellow, University of Sydney)

SUMMARY.- Analyses are made of the axial displacement of a battered pile in an elastic soil mass subject to axial loading, and of the normal displacement due to normal loading and moment. It is found that these displacements are almost independent of the angle of batter of the pile over a practical range of batter angles, so that available solutions for a vertical pile may be used to analyse relatively simply the movements of a battered pile under a general loading system. The simplified method of analyzing a single pile is extended to the consideration of groups containing battered piles.

## I.- INTRODUCTION

In recent years, several analyses have been made of the movements of pile foundations in which the soil is assumed to be an elastic mass (e.g. Refs. 1,2,3) and sufficient correlation has been found between predicted and observed behaviour to suggest that such approaches may be of practical value. To date, these analyses have dealt only with vertical piles subjected to axial or horizontal loads. However, piles are often battered in practice, especially when significant lateral loads and moments are to be resisted.

In this paper, extensions to previous analyses for single vertical piles are described for single battered piles. On the basis of these analyses, a relatively simple method of analyzing the movements of a battered pile is developed and an extension for pile groups is then described. The characteristics of a single battered pile and a group containing battered piles are examined in relation to two illustrative examples.

## II.- ANALYSIS

The analysis is considered in two stages:

(i) a battered pile subjected to an axial load

(ii) a battered pile subjected to a normal load and a moment.

In both cases, the soil is assumed to be an ideal elastic material with parameters $E_s$ and $\nu_s$ which are constant throughout the mass.

### (a) Battered Pile Subjected to Axial Load

The analysis follows directly from Poulos and Davis (Ref. 3). The pile of diameter d and length L, is assumed to be incompressible and the axial force is considered to mobilize only shear stresses on the periphery and a uniform normal stress on the base of the pile. The pile (Fig. 1a) is divided into n elements of equal length and each element is assumed to be acted upon by an average stress $p_i$, and the base by an average normal stress $p_b$. The axial displacement of the pile and the soil at the centre of each element are evaluated and equated, the resulting equations being solved to obtain the unknown stresses and displacements. In evaluating the soil displacements, the unknown force on each element is resolved into vertical and horizontal components, and vertical and horizontal displacements due to each of these components are calculated using Mindlin's equations (Ref. 4). These displacements are then combined to give the axial displacement.

A similar analysis may be carried out for a compressible pile, following the analysis of Mattes and Poulos (Ref. 5) for a vertical compressible pile. In this case, the compressibility of the pile relative to the soil is expressed conveniently in terms of the pile stiffness factor K,

$$K = \frac{E_p}{E_s} \cdot R_a \qquad (1)$$

where $E_p$ = pile modulus
$R_a$ = ratio of area of pile section to gross plan area of pile cross-section
($R_a$ = 1 for a solid pile.)

### (b) Battered Pile Subjected to Normal Load and Moment

The analysis in this case follows closely that of Poulos (Ref. 9). Here, it is assumed that only stresses normal to the pile are mobilized in the soil by the applied loads and

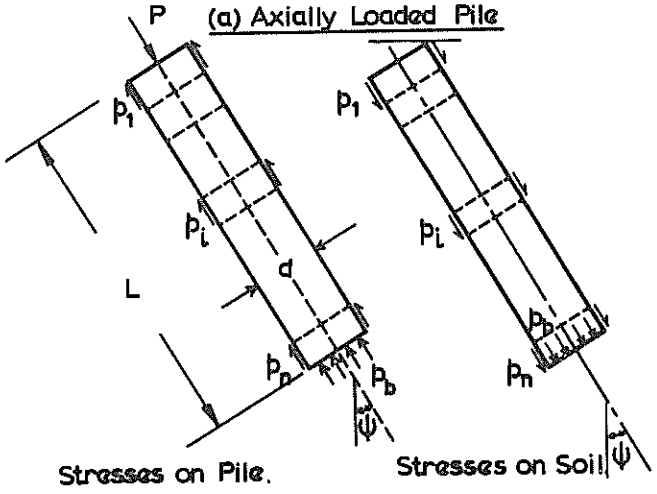


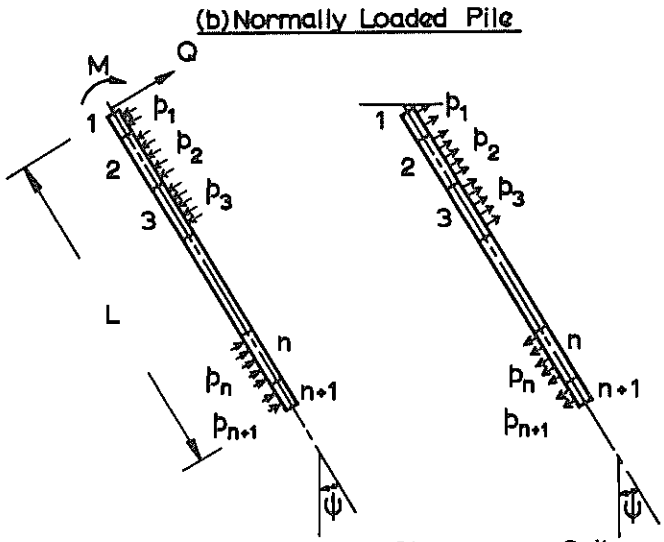


FIGURE 1

moments, and that the plane of the batter and of the loading are identical. The pile is divided into (n+1) elements as shown in Fig. 1(b), and the soil and pile displacements are evaluated at each element and equated, the resulting equations being solved for the unknown normal stresses and displacements. The soil displacements are evaluated in a similar manner to the axially-loaded pile, while the pile displacements are obtained from the beam equation.

The flexibility of the pile relative to the soil is conveniently expressed in terms of a pile flexibility factor $K_R$,

$$K_R = \frac{E_p I_p}{E_s L^4} \qquad (2)$$

where $E_p$ and $I_p$ are the pile modulus and moment of inertia.

For a rigid pile, $K_R = \infty$ while for an infinitely flexible or long pile, $K_R = 0$. In practice, a pile can be considered as rigid if $K_R \geq 1$.

The following cases have been studied:

1. Pile free at top and tip and subjected to
   (a) Normal load, and
   (b) Moment
2. Pile fixed at the top but free at the tip, and subjected to normal load.

## III.- RESULTS

Typical results for battered pile displacements are given in Table 1 for axial load and in Table 2 for normal load and moment. In each case, the appropriate displacement coefficient is given for piles with a batter angle, ψ, of 0 (a vertical pile) and 30°. It should be noted that the solutions for positive and negative batter angles are identical.

It is very significant that both the axial and normal displacements are almost unaffected by the batter of the pile; the maximum effect for a batter angle of 30° is only of the order of 4%. The virtual independence of the normal displacement on batter angle appears to be unaffected by the pile flexibility factor $K_R$ and the boundary condition at the pile head. It is therefore reasonable to assume that the compressibility of the pile in the axial direction will similarly not affect the independence of axial displacement on batter angle.

TABLE I

AXIAL DISPLACEMENT DUE TO AXIAL LOAD

Incompressible Pile
$\nu_s = 0.5$

| L/d | $I_{\rho a}$ | |
|---|---|---|
| | ψ = 0 | ψ = ±30 |
| 10 | 1.415 | 1.382 |
| 25 | 1.860 | 1.859 |
| 100 | 2.542 | 2.538 |

$$\rho_a = I_{\rho a} \cdot \frac{P}{L\, E_s}$$

The fact that the axial and normal displacements of a pile are almost independent of the pile batter means that solutions previously obtained for vertical and horizontal displacements of vertical piles may be applied to calculate the axial and normal displacements of battered piles. This in turn leads to a relatively simple method of calculating the horizontal and vertical displacements of a battered pile subjected to vertical and horizontal loads and moments. The vertical and horizontal loads V and H are first resolved into axial and normal components P and Q as follows:-

TABLE II

NORMAL DISPLACEMENT DUE TO NORMAL LOAD AND MOMENT

$\nu_s = 0.5$

| L/d | | $I_{\rho N}$ | | | | $I_{\rho M}$ | | | | $I_{\rho F}$ | | | |
|---|---|---|---|---|---|---|---|---|---|---|---|---|---|
| | $K_R$ | .0001 | | 10 | | .0001 | | 10 | | .0001 | | 10 | |
| | $\psi^\circ$ | 0 | ±30 | 0 | ±30 | 0 | ±30 | 0 | ±30 | 0 | ±30 | 0 | ±30 |
| 10 | | 7.29 | 7.35 | 3.22 | 3.37 | 39.89 | 39.78 | 3.90 | 4.05 | 5.81 | 5.92 | 1.04 | 1.09 |
| 25 | | 9.75 | 9.84 | 3.98 | 4.13 | 54.68 | 54.65 | 4.99 | 5.15 | 7.27 | 7.40 | 1.23 | 1.28 |
| 100 | | 12.21 | 12.33 | 4.79 | 4.95 | 68.28 | 68.32 | 6.16 | 6.33 | 8.67 | 8.82 | 1.44 | 1.49 |

Free-head pile: $\rho_N = \frac{1}{E_s L} \{I_{\rho N} \cdot Q + I_{\rho M} \cdot \frac{M}{L}\}$

Fixed-head pile: $\rho_F = \frac{1}{E_s L} \{I_{\rho F} \cdot Q\}$

- - - - -

$$P = V \cos \psi + H \sin \psi \quad (3a)$$

$$Q = H \cos \psi - V \sin \psi \quad (3b)$$

The axial and normal displacements $\rho_a$ and $\rho_n$ may then be calculated and resolved into vertical and horizontal components. The following expressions are then obtained for the battered pile (see Notation for definition of influence factors):

Vertical displacement:

$$\rho_v = \frac{1}{E_s L} \{V \cdot I_{vv} + H. I_{vh} + \frac{M}{L} \cdot I_{vM}\} \quad (4)$$

where

$$I_{vv} = I_{\rho a} \cos^2 \psi - I_{\rho N} \sin^2 \psi$$
$$I_{vh} = (I_{\rho a} - I_{\rho N}) \sin \psi \cos \psi$$
$$I_{vM} = - I_{\rho M} \sin \psi$$

Horizontal displacement of free-head pile:

$$\rho_h = \frac{1}{E_s L} \{V \cdot I_{hv} + H. I_{hH} + \frac{M}{L} \cdot I_{hM}\} \quad (5)$$

where

$$I_{hv} = (I_{\rho a} - I_{\rho N}) \sin \psi \cos \psi$$
$$I_{hH} = I_{\rho a} \sin^2 \psi + I_{\rho N} \cos^2 \psi$$
$$I_{hM} = I_{\rho M} \cos \psi$$

Rotation of free-head pile:

$$\theta = \frac{1}{E_s L^2} \{V. I_{\theta v} + H. I_{\theta H} + \frac{M}{L} \cdot I_{\theta M}\} \quad (6)$$

where

$$I_{\theta v} = - I_{\theta N} \sin \psi$$
$$I_{\theta H} = I_{\theta N} \cos \psi$$
$$I_{\theta M} = I_{\theta M}$$

Horizontal displacement of fixed-head pile:

$$\rho_{hF} = \frac{1}{E_s L} \{V. I_{FV} + H. I_{FH}\} \quad (7)$$

where

$$I_{FV} = (I_{\rho a} - I_{\rho F}) \sin \psi \cos \psi$$
$$I_{FH} = I_{\rho a} \sin^2 \psi + I_{\rho F} \cos^2 \psi$$

Since as found previously, the influence factors for axial and normal displacement and rotation of a battered pile are almost identical with those for the vertical and horizontal displacement and rotation of a vertical pile, $I_{\rho a}$ may be obtained from the values given by Poulos and Davis (Ref. 3) and Mattes and Poulos (Ref. 5) while $I_{\rho N}$, $I_{\rho M}$, $I_{FN}$, $I_{\theta N}$ and $I_{\theta M}$ may be obtained from the values given by Poulos (Ref. 6). For convenience, some values of the above influence factors are tabulated in Tables 3 and 4 for Poisson's ratio of the soil $\nu_s = 0.5$. $\nu_s$ has little influence on these factors.

Although the above analysis is strictly limited to a pile in which the plane of the batter coincides with the plane of the horizontal loading, the general case of horizontal loading out of the batter plane could be analyzed approximately by resolving the horizontal load into an in-plane component and a component normal to this. If the horizontal load H is inclined at an angle ω to the plane

TABLE III

AXIAL DISPLACEMENT FACTORS, $I_{\rho a}$, FOR PILE IN SEMI-INFINITE MASS

$\nu_s = 0.5$

| L/d \ K | 100 | 500 | 1000 | 5000 | ∞ |
|---|---|---|---|---|---|
| 10 | 1.80 | 1.49 | 1.45 | 1.41 | 1.40 |
| 25 | 3.58 | 2.33 | 2.10 | 1.90 | 1.86 |
| 50 | 6.36 | 3.73 | 3.07 | 2.39 | 2.24 |
| 100 | 10.63 | 6.58 | 5.16 | 3.26 | 2.54 |

TABLE IV

NORMAL DISPLACEMENT AND ROTATION FACTORS FOR PILE IN SEMI-INFINITE MASS

$\nu_s = 0.5$

| L/d | I \ $K_R$ | $10^{-6}$ | $10^{-5}$ | $10^{-4}$ | $10^{-3}$ | $10^{-2}$ | $10^{-1}$ | 1.0 | 10 |
|---|---|---|---|---|---|---|---|---|---|
| 10 | $I_{\rho N}$ | 10.84 | 10.10 | 8.249 | 5.951 | 4.076 | 3.397 | 3.304 | 3.294 |
| | $I_{\rho M} = I_{\Theta N}$ | 124.5 | 97.11 | 52.42 | 22.05 | 8.348 | 4.583 | 4.090 | 4.039 |
| | $I_{\Theta M}$ | 4957 | 2939 | 904.5 | 199.5 | 39.67 | 11.06 | 7.647 | 7.296 |
| | $I_{FN}$ | 10.36 | 8.256 | 5.630 | 3.667 | 2.401 | 1.532 | 1.123 | 1.061 |
| 25 | $I_{\rho N}$ | 17.44 | 15.03 | 11.12 | 7.468 | 4.973 | 4.234 | 4.141 | 4.132 |
| | $I_{\rho M} = I_{\Theta N}$ | 233.6 | 153.5 | 70.47 | 26.99 | 9.871 | 5.815 | 5.321 | 5.270 |
| | $I_{\Theta M}$ | 9418 | 4301 | 1101 | 224.7 | 43.49 | 13.47 | 10.05 | 9.700 |
| | $I_{FN}$ | 15.85 | 11.11 | 7.034 | 4.394 | 2.831 | 1.760 | 1.330 | 1.271 |
| 50 | $I_{\rho N}$ | 22.30 | 18.23 | 12.92 | 8.421 | 5.573 | 4.808 | 4.715 | 4.706 |
| | $I_{\rho M} = I_{\Theta N}$ | 314.3 | 188.2 | 80.70 | 29.82 | 10.84 | 6.660 | 6.165 | 6.115 |
| | $I_{\Theta M}$ | 12593 | 5034 | 1198 | 238.1 | 45.75 | 15.12 | 11.70 | 11.35 |
| | $I_{FN}$ | 19.56 | 12.88 | 7.917 | 4.862 | 3.113 | 1.913 | 1.473 | 1.415 |
| 100 | $I_{\rho N}$ | 26.40 | 20.91 | 14.34 | 9.191 | 6.076 | 5.296 | 5.203 | 5.194 |
| | $I_{\rho M} = I_{\Theta N}$ | 380.8 | 214.4 | 88.39 | 31.99 | 11.63 | 7.376 | 6.882 | 6.832 |
| | $I_{\Theta M}$ | 15092 | 6541 | 1266 | 247.2 | 47.53 | 16.52 | 13.10 | 12.76 |
| | $I_{FN}$ | 22.53 | 14.29 | 8.632 | 5.246 | 3.346 | 2.043 | 1.595 | 1.537 |

of batter, the horizontal displacement due to the in-plane component H cos ω may then be calculated as described above while the displacement in the direction normal to this may be calculated as the horizontal displacement of a vertical pile of length equal to the projected length of the pile, L cos ψ, and subjected to a load H sin ω. The resultant magnitude and direction of the horizontal displacement may thus be calculated from these two components.

EXAMPLE

To illustrate the effect of batter on pile displacements, the numerical example shown in Fig. 2 has been evaluated. The case considered corresponds to a concrete pile in a medium-stiff soil. The vertical and horizontal displacements, $\rho_v$ and $\rho_h$ and the rotation Θ of the pile head are plotted against batter angle ψ, for $-30° \leq \psi \leq +30°$. The effect of a positive batter in reducing $\rho_h$ and Θ is clearly shown. All displacements are significantly larger if a negative batter is employed. The vertical displacement $\rho_v$ is a minimum for a batter angle of about +15°, and this characteristic is also somewhat similar to that found from the experimental results on model piles in sand reported by Awad and Petrasovits (Ref. 7).

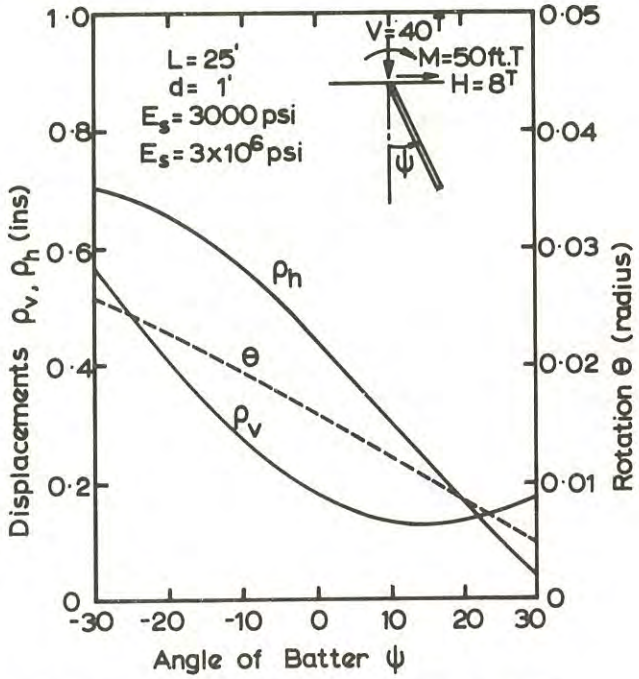


FIGURE 2 EXAMPLE OF SINGLE PILE ANALYSIS.

## IV.- ANALYSIS OF PILE GROUPS

A number of analyses have been developed for determining the movements and load distribution within a pile group. Analysis such as those described by Priddle (Ref. 8), Francis (Ref. 9) and Saul (Ref. 10) are of considerable generality in that battered piles can be considered, but they are based on subgrade reaction or "Winkler" theory and consequently cannot correctly consider the effects of interaction between the piles in the group. Analyses of group behaviour, assuming an elastic soil model rather than a Winkler model, have been proposed for axially-loaded groups (Refs. 11,12,13) and for laterally-loaded groups (Ref. 14), but these methods at present do not allow for consideration of battered piles. However, on the basis of the simplified approach described above for battered piles, it appears feasible now to extend the previous elastic analyses to groups containing battered piles.

Previous analyses for vertical piles (Refs.12,13,14) have been based on the use of "interaction factors", which express the increase in movement of a pile due to an adjacent loaded pile, and which are functions of the pile spacing, relative stiffness, and geometry, and for horizontal loads, on the direction of loading. By summation of the interaction factors for each pile in a group due to all the other piles in the group, the displacement of each pile may be written in terms of the loads on each pile in the group. For example, for a typical pile in a group of n vertical piles subjected to vertical load, the following expression is obtained:

$$\rho_{vi} = \rho_{vl}\{\sum_{\substack{j=1 \\ j\neq i}}^{n} \alpha_{ij} P_j + P_i\} \qquad (8)$$

where $\rho_{vl}$ = vertical displacement of a single pile due to unit vertical load
$\alpha_{ij}$ = interaction factor for vertical displacement corresponding to spacing between piles i and j
$P_j$ = vertical load on pile j.

Values of $\alpha_{ij}$ have been presented by Poulos (Ref. 12) and Poulos and Mattes (Ref. 13). Similar expression may be obtained for vertical piles subjected to horizontal load and moment. By solving the series of equations thus obtained for the appropriate boundary condition at the pile head (e.g. equal displacement of each pile or equal load in each pile), the load and displacement distribution within the group may be obtained.

A similar approach can be adopted for groups containing battered piles. The case will be considered first of a group in which all the piles are battered in the same plane and on which the horizontal load acts in the same plane. It will be assumed for simplicity that the interaction factors for battered piles are identical with those for vertical piles with a spacing corresponding to the centre-to-centre distance between the piles halfway along their length. Thus, on this assumption, which appears reasonable in view of the correspondence between displacements previously found, the interaction factor for normal displacement due to normal load is the same as that for vertical displacement due to vertical load on a vertical pile, and the rotation and normal displacement interaction factors due to normal load and moment are identical with those for rotation and horizontal displacement due to horizontal load and moment.

On the basis of the above assumption, the resulting equations for vertical and horizontal displacement and rotation may be written conveniently in matrix form. For a group of free-head piles, the following equation is obtained:

$$\begin{bmatrix} A_v & B_v & C_v \\ A_h & B_h & C_h \\ A_\theta & B_\theta & C_\theta \end{bmatrix} \begin{bmatrix} V \\ H \\ M \end{bmatrix} = \begin{bmatrix} \rho_v \\ \rho_h \\ \theta \end{bmatrix} \qquad (9)$$

where the coefficients of the sub-matrices are as follows:

$$A_{vij} = \rho_{al}\alpha_{ij}\cos\psi_i\cos\psi_j + \rho_{NQl}\alpha_{\rho Hij}\sin\psi_i\sin\psi_j$$

$$B_{vij} = \rho_{al}\alpha_{ij}\cos\psi_i\sin\psi_j - \rho_{NQl}\alpha_{\rho Hij}\sin\psi_i\cos\psi_j$$

$$C_{vij} = -\rho_{NMl}\alpha_{\rho Mij}\sin\psi_i$$

$$A_{hij} = \rho_{al}\alpha_{ij}\sin\psi_i\cos\psi_j - \rho_{NQl}\alpha_{\rho Hij}\cos\psi_i\sin\psi_j$$

$$B_{hij} = \rho_{al}\alpha_{ij}\sin\psi_i\sin\psi_j + \rho_{NQl}\alpha_{\rho Hij}\cos\psi_i\cos\psi_j$$

$$C_{hij} = \rho_{NMl}\alpha_{\rho Mij}\cos\psi_i$$

$$A_{\theta ij} = -\theta_{Nl}\alpha_{\theta Hij}\sin\psi_j$$

$$B_{\theta ij} = \theta_{Nl}\alpha_{\theta Hij}\cos\psi_j$$

$$C_{\theta ij} = \theta_{Ml}\alpha_{\theta Mij}$$

$\rho_{al}, \rho_{NQl}, \rho_{NMl}, \theta_{Nl}$ and $\theta_{Ml}$ are the displacements and rotations due to unit axial load and moment. They may be calculated from the theoretical relationships (see Notation) if values of the soil moduli can be estimated, or if pile load test data is available, from the pile deflections at the working loads. The interaction factors $\alpha$ may be found from Ref. 12 or 13, while values of the interaction factors $\alpha_{\rho H}, \alpha_{\rho M}, \alpha_{\theta H}$ and $\alpha_{\theta M}$ are given in Ref. 14.

The submatrices $A_v$, $B_v$ etc. are of order nxn while the vectors V, $\rho_v$ etc. are of order n. Equation (9), together with the three equations expressing vertical and horizontal load equilibrium and moment equilibrium, may be solved to obtain the 3n+3 unknown vertical and horizontal loads, moments, displacements and rotations, for the desired boundary conditions at the pile heads.

Equation (9) is formulated for free-head piles, but if the piles are fixed into a massive cap so that no head rotation will occur (i.e. the piles are now fixed-head piles), a similar equation to equation (9) may be derived except that now there are only 2n+2 equations and unknowns (the rotations and moments are not considered now) and the horizontal displacement and interaction factors are now those for a fixed head pile.

Groups in which piles are battered in different directions can be treated approximately by resolving the horizontal load into two components and calculating the in-line horizontal displacements due to each component, using, as the length of a pile, its projected length in the plane of loading. The resultant horizontal displacement can then be calculated from these displacement components.

The use of the above method of analysis obviously requires the use of a computer for all but the simplest groups. However, it should be emphasized that the fact that 3n+3 equations are required, rather than only 3 equations as in some other methods based on subgrade reaction theory (e.g. Ref. 8), is a consequence of considering the interaction between the piles rather than assuming that the displacements and rotation of a pile are a function only of the loads and moments on that particular pile. The consideration of inter-pile interaction in a logical manner in the present analysis thus obviates the necessity to make approximate allowances for group effects in estimating a modulus of subgrade reaction.

EXAMPLE

As an example of the application of the above method, a 6 pile group has been analysed. Two cases have been considered, the first in which all the piles are vertical and the second in which the outer piles are battered outwards. The group considered is shown in Fig. 3, the pile and soil moduli again being chosen to represent concrete piles in a medium stiff clay. The pile cap is assumed not to be in contact with the soil, and is taken to be rigid so that each pile has an equal horizontal displacement and head rotation. The results of the analyses are also shown in Fig. 3 and the beneficial effects of the battered piles may clearly be seen. The displacements and rotation, and the horizontal displacement in particular, are reduced when the outer piles are battered, while the loads and moments in the piles are generally reduced. The large vertical loads in the outer piles, compressive for piles C and tensile for piles A, are particularly noteworthy and in a problem involving a soil with finite strength, the outer piles would almost certainly fail under the loading system employed in this example.

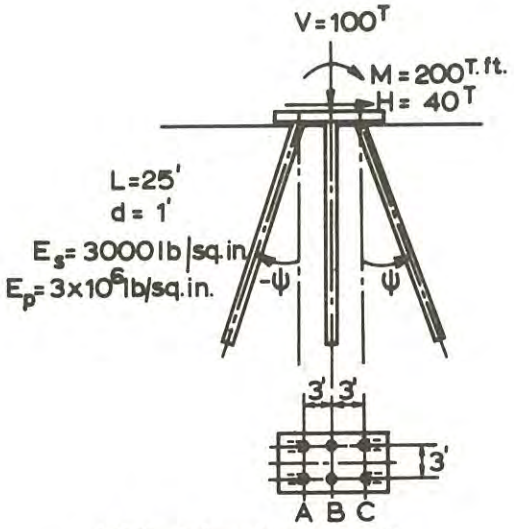


(a) $\psi = 0$ (vertical piles)

| Piles | V (T) | H (T) | M (T.ft) | $\rho_v$ (in.) | $\rho_h$ (in.) | $\theta$ (rad.) |
|---|---|---|---|---|---|---|
| A | -115·8 | 13·1 | 25·8 | -·27 | ·53 | ·0153 |
| B | 12·5 | -6·2 | 48·4 | ·29 | ·53 | ·0153 |
| C | 153·3 | 13·1 | 25·8 | ·85 | ·53 | ·0153 |

(b) $\psi = 15°$ (battered piles)

| Piles | V (T) | H (T) | M (T.ft.) | $\rho_v$ (in.) | $\rho_h$ (in.) | $\theta$ (rad.) |
|---|---|---|---|---|---|---|
| A | -37·8 | 10·6 | 26·4 | -·04 | ·19 | ·0080 |
| B | 12·7 | 7·7 | 16·6 | ·24 | ·19 | ·0080 |
| C | 75·1 | 1·7 | 57·0 | ·52 | ·19 | ·0080 |

FIGURE 3 EXAMPLE OF GROUP ANALYSIS.

V.- CONCLUSIONS

The analyses described in this paper have revealed that the axial displacement of a battered pile subjected to axial load, and the normal displacement and rotation of a pile subjected to normal load and moment, are virtually independent of the batter of the pile, at least for the range of batter angles employed in practice. This fact leads to a relatively simple method of analyzing the movements of a single battered pile subjected to a general loading system using available

solutions for the movements of vertical piles. It is shown that a reduction in displacements and rotation is obtained by employing a pile with a positive batter. Available solutions for a vertical pile may also be employed in analyzing a pile group containing battered piles.

## VII .- ACKNOWLEDGMENTS

The work described in this paper forms part of a general program of research into the settlement of all types of foundations being carried out at the University of Sydney under the general direction of Professor E.H. Davis, Professor of Civil Engineering (Soil Mechanics). The work is supported by a research grant from the Australian Research Grants Committee.

## REFERENCES

1. D'APPOLONIA, E. and ROMUALDI. J.P. - Load Transfer in End-Bearing Steel H-piles. J.Soil Mech.Fndns.Divn.A.S.C.E., 89, No. SM2, 1963, 1-25.

2. THURMAN, A.G. and D'APPOLONIA, E. - Computed Movement of Friction and End-Bearing Piles Embedded in Uniform and Stratified Soils. Proc. 6th Int.Conf.Soil Mech. 2, 1965, 323-327.

3. POULOS, H.G. and DAVIS, E.H. - The Settlement Behaviour of Single Axially-Loaded Incompressible Piles and Piers. Geotechnique, 18, 1968, 351-371.

4. MINDLIN, R.D. - Force at a Point in the Interior of a Semi-Infinite Solid. Physics, 7, 1936, 195.

5. MATTES, N.S. and POULOS, H.G. - Settlement of a Single Compressible Pile. J.Soil Mech.Fndn.Divn.A.S.C.E., 95, No.SM1, 1969, 189-207.

6. POULOS, H.G. - The Behaviour of Laterally-Loaded Piles. I. Single Piles. To be published in J.Soil Mech.Fndn.Divn,A.S.C.E. (May) 1971.

7. AWAD, A. and PETRASOVITS, G. - Considerations on the Bearing Capacity of Vertical and Batter Piles Subjected to Forces Acting in Different Directions. Proc. 3rd Budapest Conf.Soil Mechs. & Fndn.Eng., Budapest 1968, 484-497.

8. PRIDDLE, R.A. - Load Distribution in Piled Bents. Trans.Inst.Engrs.Aust., CE5, No.2, 1963, 43-51.

9. FRANCIS, A.J. - Analysis of Pile Groups with Flexural Resistance. J.Soil Mech. Fndns.Divn, A.S.C.E., 90, No.SM3, 1964, 1-32.

10. SAUL, W.E. - Static and Dynamic Analysis of Pile Foundations. J.Struct.Divn,A.S.C.E. 94, No.ST5, 1968, 1077-1100.

11. PICHUMANI, R. and D'APPOLONIA, E. - Theoretical Distribution of Loads Among the Piles in a Group. Proc.3rd Pan American Conf.Soil Mechs, 2, 1967, 547-564.

12. POULOS, H.G. - Analysis of the Settlement of Pile Groups. Geotechnique, 18, 1968 449-471.

13. POULOS, H.G. and MATTES, N.S. - Settlement and Load Distribution Analysis of Pile Groups. To be published in Australian Geomechanics Journal 1971.

14. POULOS, H.G. - The Behaviour of Laterally Loaded Piles. II. Pile Groups. To be published in J.Soil Mech.Fndns.Divn., A.S.C.E. (May) 1971.

## NOTATION

| | |
|---|---|
| $A_v, A_h, A_\theta$ | Submatrices for group analysis |
| $B_v$ etc. | |
| $C_v$ etc. | |
| $E_p$ | Young's modulus of pile |
| $E_s$ | Young's modulus of soil |
| $H$ | Horizontal load |
| $I_p$ | Moment of inertia of pile |
| $I_{\rho a}$ | Axial displacement factor for axial load |
| $I_{\rho N}$ | Normal displacement factor for normal load |
| $I_{\rho M}$ | Normal displacement factor for moment |
| $I_{\rho F}$ | Normal displacement factor for fixed-head pile |
| $I_{\theta N}$ | Rotation factor for normal load |
| $I_{\theta M}$ | Rotation factor for moment |
| $I_{vv}$ | Vertical displacement factor for vertical load on battered pile, and similarly for other values. |
| $K$ | Pile stiffness factor = $E_p/E_s \cdot R_A$ |
| $K_R$ | Pile flexibility factor = $E_p I_p / E_s L^4$ |
| $L$ | Pile length |
| $M$ | Moment |
| $P$ | Axial load |
| $Q$ | Normal load |
| $R_A$ | Area ratio of pile = area of pile section/gross area. |
| $V$ | Vertical load |
| $d$ | Pile diameter. |
| $n$ | Number of piles in group. |
| $\alpha$ | Interaction factors for vertical displacement due to vertical load. |
| $\alpha_{\rho H}$ | Interaction factor for horizontal displacement due to horizontal load, and similarly for $\alpha_{\rho M}, \alpha_{\rho F}, \alpha_{\theta H}$ and $\alpha_{\theta M}$. |
| $\theta$ | Rotation of pile head. |

$\theta_{N1}$ Rotation due to unit normal load = $I_{\theta N}/E_s L^2$

$\theta_{M1}$ Rotation due to unit moment = $I_{\theta M}/E_s L^3$

$\nu_s$ Poisson's ratio of soil

$\rho_a$ Axial displacement of pile head

$\rho_F$ Normal displacement of fixed-head pile.

$\rho_N$ Normal displacement of free-head pile

$\rho_V$ Vertical displacement of pile

$\rho_h$ Horizontal displacement of free-head pile

$\rho_{hF}$ Horizontal displacement of fixed-head pile

$\rho_{a1}$ Axial displacement due to unit axial load = $I_{\rho a}/E_s L$

$\rho_{NQ1}$ Normal displacement due to unit normal load = $I_{\rho N}/E_s L$

$\rho_{NM1}$ Normal displacement due to unit moment = $I_{\rho M}/E_s L^2$

$\psi$ Angle of pile batter

$\omega$ Angle between planes of horizontal load and pile batter.

# The Bearing Capacity of Strip Footings from the Standpoint of Plasticity Theory

By

E. H. Davis, B.Sc. (Eng.), F.I.E.Aust.

(Professor of Civil Engineering (Soil Mechanics), University of Sydney)

AND

J. R. Booker, B.Sc., Ph.D.

(Post-Doctoral Fellow, University of Sydney)

SUMMARY.- Solutions, by the theory for a perfectly plastic material with a non-associated flow rule, are presented over the full range from the limiting case of no body forces (the Prandtl solution) to the limiting case for no surcharge. It is shown that in between these limiting cases the principle of superposition implied in the ordinary concept of bearing capacity coefficients Nq and Nγ is approximately true, the error being no more than a maximum of 30%.

The results confirm previous solutions by Sokolovski and by Cox for smooth footings and also show that for such footings the nature of the flow rule of the material has no influence at all on the collapse load. On the other hand the results show that the ultimate bearing capacity of a rough footing may be as much as double that of a smooth footing when there is no surcharge although with increasing surcharge the effect of roughness decreases. Terzaghi's values of Nγ for a rough footing are shown to be significantly optimistic for high values of $\phi$. The nature of the flow rule also has a theoretical influence when the footing is rough but, over the full range from a constant volume material to one which dilates at the extreme rate required by an associated flow rule, the influence is so small as to have negligible practical importance.

## I.- INTRODUCTION

Most of the methods in common use in soil and rock mechanics for analysing the stability of slopes, earth pressures and ultimate bearing capacity of foundations suffer from lack of rigour when viewed from an applied mechanics point of view. In such methods, an arbitrary assumption with regard to the shape of a rupture plane or velocity discontinuity is frequently made and only the strength properties, often in incomplete form, are taken into account, whereas the complete specification of the failure properties of an ideal plastic involves not only a statement of the stress combinations for failure but also the interrelation between strains (as exhibited by dilatancy) during failure. This is not to say that approximate engineering methods of stability analysis are not satisfactory for most practical purposes; their continued successful use is evidence that they are, and they certainly have the advantage of greater flexibility in application to complicated practical situations as compared with the more restricted problem solving potential of rigorous methods. However it is clearly desirable that the accuracy of the approximate engineering methods should be checked against more rigorous solutions wherever possible. The purpose of this paper is therefore to examine the class of stability problems concerned with surface bearing capacity in the light of previously published and the authors' own solutions using the theory of plasticity, particular attention being paid to the effect of the plastic deformation properties or flow rule of the material and to the effect of footing roughness. This must be the authors' excuse for writing yet another paper on bearing capacity theory. A similar examination of retaining wall problems has been undertaken by Lee and Herington (Refs. 1 and 2).

## II.- BASIS OF PLASTICITY THEORY

A plasticity theory based on a class of simple ideal materials with a non-associated flow rule has been proposed by Davis (Refs. 3 and 4). Restricting attention to plane strain problems, the usual Mohr-Coulomb failure criterion is assumed,

$$\sigma_1 = N_\phi \sigma_3 + 2c\sqrt{N_\phi} \qquad (1)$$

where $N_\phi = \tan^2(\pi/4 + \phi/2)$

and the strain rates in plastically deforming regions are related by:

$$\dot{\varepsilon}_3/\dot{\varepsilon}_1 = -N_\psi \qquad (2)$$

where $N_\psi = \tan^2(\pi/4 + \psi/2)$

For the ideal material the parameters c, $\phi$ and $\psi$ are constants and, in relation to real soils or rocks, may be equated to experimentally determined values, in particular those at the peak or at ultimate strengths. At the ultimate, deformation is at constant

volume so that $\psi$ is then zero. Being for a non-work hardening (or softening) material, the theory cannot take into account the effect of transition from initial yielding up to peak strength and down to ultimate that accompanies increasing strain in real granular materials, but neither can the approximate engineering methods of solving stability problems properly take this effect into account.

The equations governing the distributions of stress and velocity throughout plastic fields can be shown to be hyperbolic. Thus these distributions are conveniently represented by their characteristics. The characteristic lines for stresses ($s_1$ and $s_2$ lines) are inclined at $(\pi/4-\phi/2)$ anti-clockwise and clockwise from the major principal stress direction whereas those for velocities ($k_1$ and $k_2$ lines) are at $(\pi/4-\psi/2)$. It can be shown that velocity discontinuities or rupture surfaces can only occur on velocity characteristics. This raises the interesting point (Ref. 4) that the shear stress on a rupture surface in a soil mass, on the horizontal failure plane in the conventional shear box, or at the surface of a rough wall where relative slip between wall and soil is occurring, is less than the value normally assumed of $(c+\sigma_n \tan\phi)$ when c and $\phi$ are determined by substituting experimental values of $\sigma_1$ and $\sigma_3$ into equation (1), unless $\psi = \phi$. Rowe (Ref. 5) has noted that this conclusion, and the resulting expression for the shear stress on rupture planes, is identical with his deduction from his stress dilatancy theory, although expressed in a somewhat different way.

Classical plasticity theory assumes normality or an associated flow rule and this requires that $\psi = \phi$, stress and velocity characteristics then coinciding. Only in this case do the limit theorems hold (Ref. 3) and a solution to any problem which is both statically and kinematically admissible is the unique solution. Unfortunately it seems certain that all real granular materials, even at their densest and at peak strength, exhibit values of $\psi$ which are very much less than $\phi$. Thus the theory which allows $\psi$ to take a value less than $\phi$ as dictated by experimental evidence, suffers the drawback that an exact solution to a problem is from a mathematical point of view not necessarily unique. However there is strong inferential evidence (Booker (Ref. 6)) that the range of collapse loads in the set of possible exact non-unique solutions is likely to be insignificant in problems of practical interest.

A solution to a plasticity problem must satisfy certain requirements. Briefly, the mass must be divided into two regions, a plastic region and an elastic-rigid region. A solution to the problem involves finding a stress field and velocity field such that

(i) The stress field satisfies the equations of equilibrium and the stress boundary conditions.

(ii) In a plastic region the stresses lie on the yield surface while in the elastic rigid regions the stresses lie within or on the yield surface.

(iii) In a plastic region the velocity field must satisfy the flow rule (this may be either associated or non-associated) of the material. In an elastic-rigid region the velocity must reduce to rigid body movements. The velocity field must satisfy the velocity boundary conditions and be such that the rate of internal plastic work is always positive.

(iv) The velocity field must be continuous except for possible velocity discontinuities, of a definite type, across velocity characteristics. The line separating a plastic and elastic-rigid regions must be a velocity characteristic.

## III.- THE SURFACE BEARING CAPACITY PROBLEM

Attention is restricted to plane strain conditions. In Fig.1, Ox is parallel to the direction of gravity. The half space $x \geq 0$ is occupied by a cohesive frictional soil of density $\gamma$. A'OA is a rough or smooth rigid die (or strip footing) of breadth B. The load on the die is P. The surface of the material other than A'OA is acted on by a uniform surcharge q.

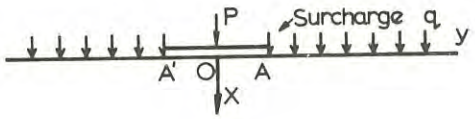


Fig. 1

Previously published solutions of an exact nature can be outlined as follows:

(i) The indentation of a smooth die into a purely cohesive material was first examined by Prandtl (Ref. 7). Prandtl only specified the stresses in the plastic region and thus his solution was incomplete. Prager and Hodge (Ref. 8) obtained the velocity solution. Hill (Ref. 9) proposed an alternative solution for a smooth die and found the stresses in the plastic region and the velocity field. Bishop (Ref.10) completed Prandtl's and Hill's solution by showing that the stresses in the rigid region were safe. It is readily shown that this solution is also valid if the die is perfectly rough.

(ii) The indentation of a smooth die into a weightless cohesive-frictional material was investigated by Prandtl (Ref. 7). His solution was incomplete and has been completed, for a material with an associated flow rule, by Shield (Ref. 11). Cox (Ref. 12) showed that a velocity field could be obtained for a mat-

erial with a non-associated flow rule ($\psi=0$). Cox's analysis is readily extended to materials with a general non-associated flow rule ($\psi\neq\phi$). It is again readily shown that this solution is also valid if the die is perfectly rough.

(iii) The indentation of a smooth die into a cohesive frictional material with weight has been investigated by Sokolovski. Sokolovski's solution is incomplete and has been completed by Cox (Ref. 13) for a material with an associated flow rule.

(iv) The indentation of a rough die into a cohesive frictional material with weight has been investigated by Lundgren and Mortensen (Ref. 14). Their solution is incomplete; it contains no discussion of the velocity field and does not show that the stress field can be extended into the rigid regions without violating the yield criterion. Also Lundgren and Mortensen s numerical results tend to be inaccurate and the results are in error by as much as 10%.

In the analysis described in this paper, it will be sufficient to consider only $\phi>0$, for if $\phi=0$, the failure load, as remarked in (i) above, is independent of density and footing roughness and is the well known Prandtl value

$$P = (2+\pi).B.c + qB \qquad (3)$$

It will also be sufficient to consider a purely frictional material. For suppose $P_1$ is the failure load for a material with an angle of internal friction $\phi$, a cohesion $c^*$ and acted on by a surcharge $q^*$. Let $P_2$ be the failure load for a purely frictional material with an angle of internal friction $\phi$ and acted on by a surcharge $q = q^* + c^*\cot\phi$ then it is easily shown

$$P_1 = P_2 - Bc^*\cot\phi \qquad (4)$$

In the remainder of this paper attention will therefore be restricted to a purely frictional material. Attention will also be restricted to rough footings since the adaptation of the analysis to the smooth case is relatively straightforward.

## IV.- PROPOSED SOLUTION

The assumed condition that the footing is rough allows of two possibilities in the material immediately beneath the footing.

Case (i) There is no relative movement between the footing and the soil. A wedge of material bounded by the footing and the velocity characteristics emanating from the edges must then move as a rigid body with the footing. This case will arise with narrower footings.

Case (ii) A wedge of material moving with the footing as in Case (i) may occur symmetrically about the centre for a limited width but there is slip between soil and footing for the remaining segments out to the edges. Since a velocity discontinuity occurs over these segments, the footing underside must here be a velocity characteristic or tangential to velocity characteristics. This case will clearly arise with wider footings.

(a) Proposed Stress Field

In Fig. 2, suppose that the material outside the footing is plastic, the data on the non-characteristic line AB then determines the region ABC bounded by the stress characteristics AC ($s_1$ line) and BC ($s_2$ line).

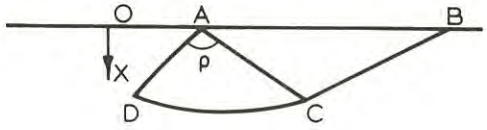


Fig. 2

The characteristics in ABC are all straight In general there is a discontinuity of stress at the point A known as a Prandtl singularity. This singularity and the characteristic line AC determine the region ACD. There are now two possibilities:

(i) If $\pi/2 \leq \rho \leq 3\pi/4+\psi/2$ then B may be chosen so that D lies on the x axis and $\theta(D) = 0$, ($\theta$ is the angle between the major principal stress direction and the vertical). The complete field is then obtained by reflection in Ox, see Fig. 3. This is the stress field for case (i).

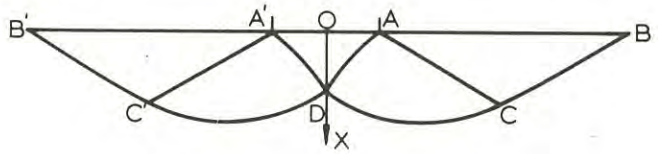


Fig. 3

Notice that if $\rho = \pi/2$ the Prandtl solution ($\Upsilon=0$) is obtained and if $\rho = 3\pi/4+\psi/2$ the velocity characteristic at A is tangent to the footing.

(ii) If $\rho = 3\pi/4+\psi/2$, that is if the velocity characteristic at A is tangent to the footing, the field may be continued in such a way that the velocity characteristics are tangent to the footing on the segment EA, see Fig. 4. The condition on EA with the known characteristic AD determines the region ADPE. For a particular footing width, the field may be completed by choosing B and E so that P lies on the x axis and $\theta(P) = 0$, and then by reflection in Ox. This is the stress field for case (ii).

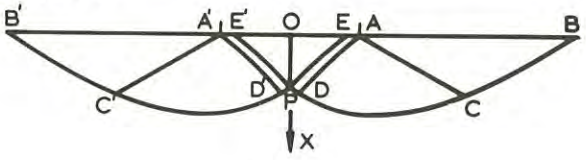


Fig. 4

These stress fields were suggested by Lundgren and Mortensen (Ref. 14) for the particular case $\psi = \phi$.

(b) Proposed Velocity Field

Considering case (i), the main features of the velocity field are shown by the dotted velocity characteristics in Fig.5. The material below tst' is at rest and the material in AsA' moves rigidly with the footing. These conditions are sufficient to define the velocity distribution throughout the deforming regions Ast and A'st'.


Fig. 5

The main features of the velocity field for case (ii) are shown in Fig.6. As before, the material below tst' remains at rest but now it is only the material within EsE' which moves rigidly with the footing. Note that SE and SE' are tangential to the footing at E and E'. These conditions, together with the special condition on the velocity discontinuity EA (for example, if $\psi = 0$ the soil must have a vertical component of velocity equal to that of the footing), are sufficient to define the velocity distribution throughout the deforming regions AEst and A'E'st'.

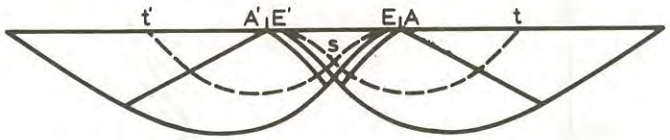


Fig. 6

V.- RESULTS OF NUMERICAL CALCULATIONS

The main calculation consists in evaluating the stress distribution in the plastic region. Apart from the modification to incorporate a rough footing, the mathematical development is similar to that given in Ref. 16. The validity of the failure load given by this calculation has then to be confirmed by checking that the corresponding velocity field involves no negative plastic work, and by checking that a statically admissible field of stresses can be devised which nowhere exceeds the strength of the material.

The stress distribution in the plastic region was evaluated on a computer using a numerical method (Ref. 15) which progressively constructs the net of stress characteristics from the initial data and which is more efficient and accurate than many methods previously published in that more than the nodes immediately adjacent to the new node to be evaluated are taken into account.

It can be shown from dimensional considerations that, for given values of $\phi$ and $\psi$, the solution depends only on the two non-dimensional parameters $P/qB$, $\gamma B/q$. The solution will be complete if the value of $P/qB$ for each value of $\gamma B/q$ can be found. This is most conveniently done by plotting $P/qB$ against $\gamma B/q$ when $0 \leq \gamma B/q \leq 1$ and $P/\gamma B^2$ against $q/\gamma B$ when $0 \leq q/\gamma B \leq 1$. This has been done for $\phi = 30°$, $\psi = \phi$, $\psi = 0$ in Figs. 7 & 8.

For a given value of $\phi$ the load should increase with $\psi$ when the solution is of the type case (ii). Thus the maximum load will be obtained for an associated flow rule ($\psi=\phi$) and the minimum load for the constant volume material ($\psi=0$). Whereas for case (i) solutions, the value of $\psi$ will not influence the collapse load. It can be seen from Fig.8 that the solutions coincide for all but small values of $q/\gamma B$. The maximum difference will occur when $q/\gamma B = 0$. The effect for the range $\psi=0$ to $\phi$, is tabulated in Fig.8. The maximum effect is of the order of 1% and thus it would seem that the deformation behaviour of the material makes a negligible difference to the failure load for this problem.

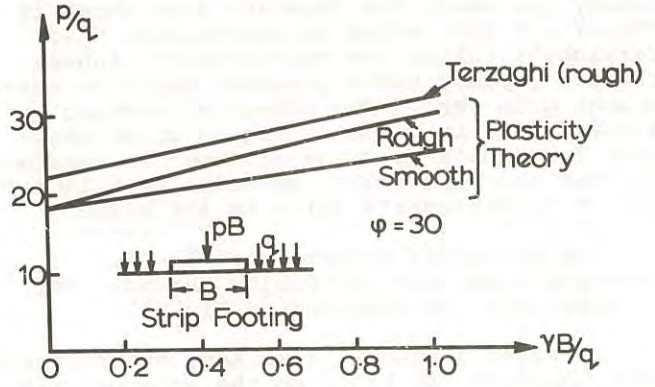


Fig. 7

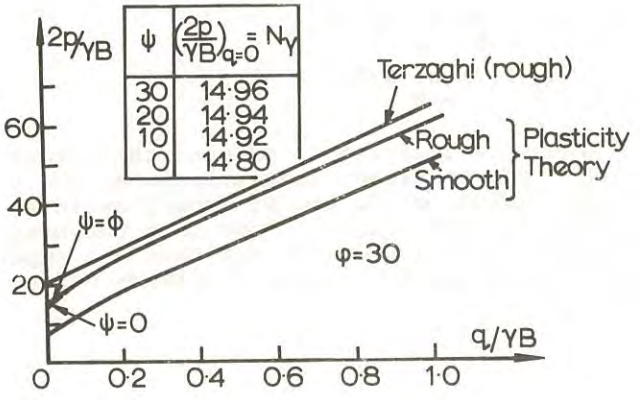


Fig. 8

A comparison between a perfectly rough footing and a perfectly smooth footing has been made for the particular case $\phi = 30°$. The smooth results agree precisely with those obtained by Cox (Ref. 13). The comparison is made in Figs.7 & 8, but the effect is demonstrated more dramatically by plotting the ratio of the rough load to the smooth load as in Fig.9. At its maximum, roughness nearly doubles the bearing capacity when $\phi = 30$ and for larger values of $\phi$ the effect would be even greater.

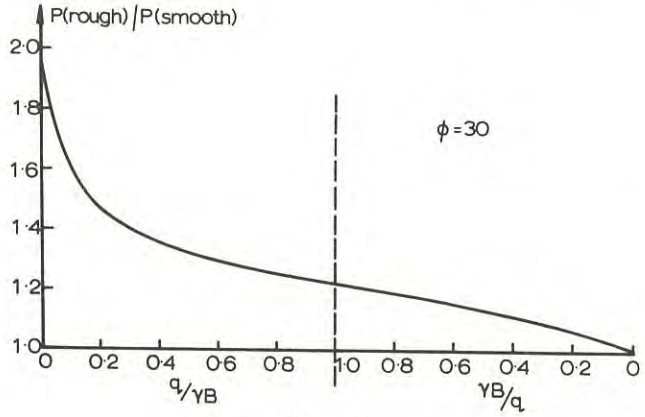


Fig. 9

The values from Terzaghi's approximate theory for rough footings are also shown in Figs.7 & 8 from which it can be seen that Terzaghi's values are consistently higher, the discrepancy being greatest when the surcharge q is zero. The effect of varying $\phi$ when $q = 0$ is given in Fig.10 which shows that Terzaghi's solution diverges increasingly from the plasticity solution as $\phi$ increases. At $\phi = 40$ Terzaghi's value is 40% higher.

For the other extreme when $\gamma = 0$, Terzaghi's and the plasticity (Prandtl Ref. 7) solutions are compared in Fig. 11.

Terzaghi's theory, like many other approximate theories, is based on the superposition assumption implicit in the equation:

$$P/B = qN_q + \gamma BN_\gamma/2 \qquad (5)$$

where $N_\gamma = \underset{q \to 0}{\text{Limit}}\ 2P/\gamma B^2$

$N_q = \underset{\gamma \to 0}{\text{Limit}}\ P/Bq$

It is interesting to examine the errors in this superposition assumption when the correct values of $N_q$ and $N_\gamma$ from plasticity theory are used. Fig.12 shows that the maximum error may be over 20% but that the superposition assumption itself is always on the safe side.

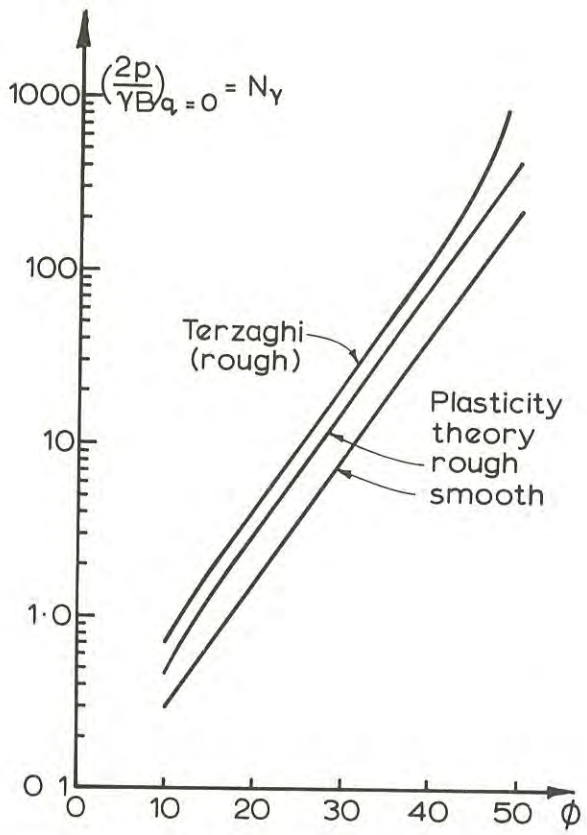


Fig. 10

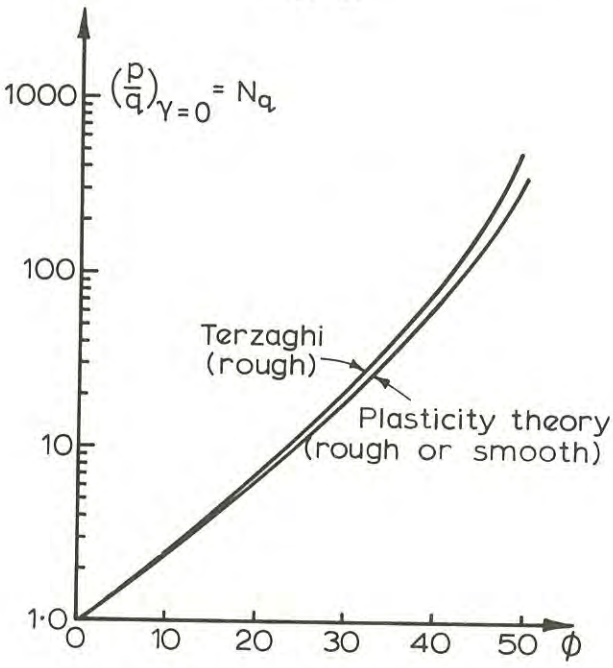


Fig. 11

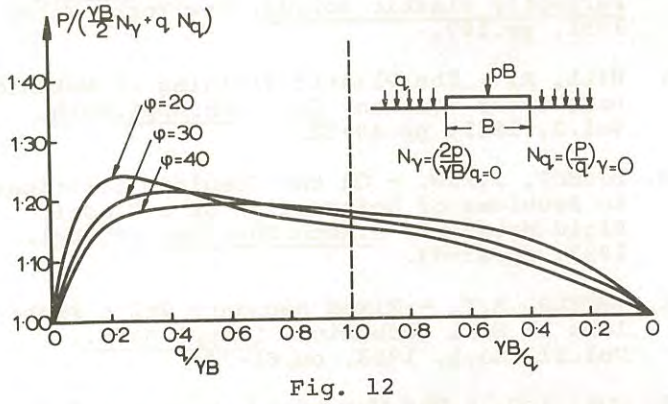


Fig. 12

## VI.- KINEMATIC AND STATIC VERIFICATION

As mentioned at the start of Section V, it is necessary to check that the solutions reported in that section are kinematically and statically admissible before finally accepting them as exact.

As part of the computer calculation, the velocity field was evaluated for each problem and the rate of plastic work calculated at the nodes of the characteristic net. In every case this rate was nowhere negative thus confirming the kinematic validity of the solutions. A typical pattern of stress and velocity characteristics (coincident in this example for which $\psi=\phi$) for a narrower footing (case i) is shown in Fig. 13. A typical pattern of stress characteristics for a wider footing (case ii) is shown in Fig.14 and the corresponding velocity characteristics, different since in this example $\psi<\phi$, are shown in Fig.15. It is clear that, although the nature of the flow rule, i.e. the value of $\psi$, has a negligible or no effect on the ultimate bearing capacity, it does have a considerable effect on the distance out from the edge of the footing affected by plastic deformation.

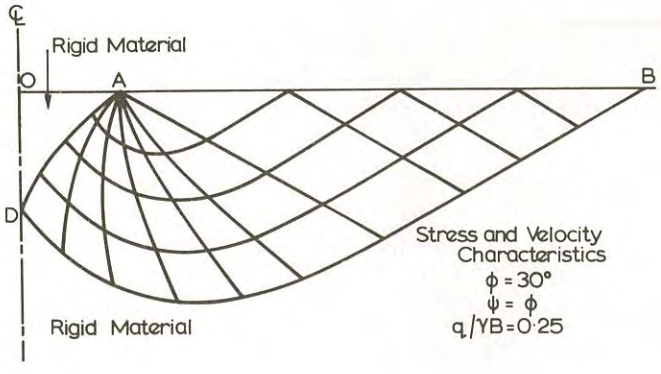


Fig. 13

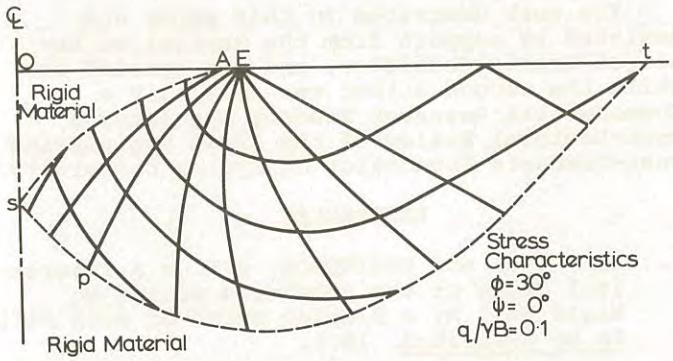


Fig. 14

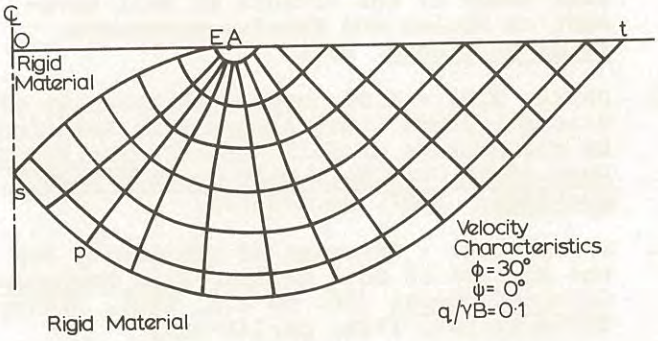


Fig. 15

The static admissibility of the solutions was proved by adapting the method for weightless material proposed by Cox, Eason and Hopkins (Ref. 16) to include body forces. The field of stress characteristics is extended sufficiently to meet the minor principal stress trajectory through the points B and B' as in Fig.16. It is then relatively easy to devise a simple extension field beyond this line by assuming it to have straight major principal stress trajectories. In all cases it was then found that the stresses satisfield equilibrium and did not exceed the strength of the material.

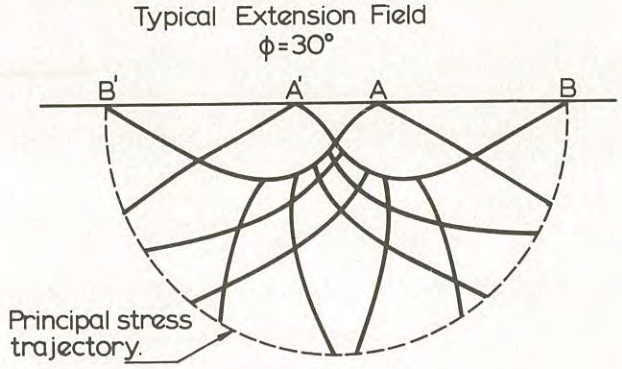


Fig. 16

## VII.- CONCLUSIONS

See summary.

VIII.- ACKNOWLEDGMENTS

The work described in this paper was assisted by support from the Australian Research Grants Committee, and was carried out while the second author was initially a Commonwealth Research Student and later a Post-Doctoral Fellow of the Civil Engineering Post-Graduate Foundation of Sydney University.

REFERENCES

1. LEE, I.K. and HERINGTON, J.R. - A Theoretical Study of the Pressures acting on Rigid Wall by a Sloping Earth or Rock Fill. To be published. 1971.

2. LEE, I.K. and HERINGTON, J.R. - A Theoretical Study of the Effects of Wall Movement on Active and Passive Pressures. To be published. 1971.

3. DAVIS, E.H. - A Discussion of Theories of Plasticity and Limit Analysis in Relation to the Failure of Soil Masses. Proc.Fifth Aust.-N.Z. Conf.Soil Mech. & Fndn.Engng., Auckland, 1967, pp.175-182.

4. DAVIS, E.H. - Theories of Plasticity and the Failure of Soil Masses. Soil Mechanics Selected Topics (Ed. by I.K. Lee), Sydney Butterworths, 1968, pp.341-380.

5. ROWE, P.W. - The Relation between the Shear Strength of Sands in Triaxial Compression, Plane Strain and Direct Shear. Geotechnique, Vol.19, No.1, March 1969, pp.75-86.

6. BOOKER, J.R. - Applications of Theories of Plasticity to Cohesive Frictional Soils. Thesis (Ph.D) Univ. of Sydney, 1970.

7. PRANDTL, L. - Ueber die Haerte plastischer Koerper; Goettinger Nachr; Math.-Phys. Kl. 1920, pp.74-85.

8. PRAGER, W. and HODGE, P.G. - Theory of Perfectly Plastic Solids. New York, Wiley 1951, pp.169.

9. HILL, R. - The Plastic Yielding of Notched Bars under Tension. Q.J.Mech.Appl.Math, Vol.2, 1949, pp.40-52.

10. BISHOP, J.F.W. - On the Complete Solutions to Problems of Deformation of a Plastic Rigid Material. J.Mech.Phys.Solids, Vol.2, 1953, pp.43-53.

11. SHIELD, R.T. - Mixed Boundary Value Problems in Soil Mechanics. Q.Appl.Math., Vol.11, No.1, 1953, pp.61-74.

12. COX, A.D. - The Use of Non-Associated Flow Rules in Soil Plasticity. R.A.R.D.E.Rep(B) 2/63, 1963.

13. COX, A.D. - Axially Symmetric Plastic Deformation in Soils - II Indentation of Ponderable Soils. Int.J.Mech.Sci., Vol.4, 1962, pp.371-380.

14. LUNDGREN, H. and MORTENSEN, K. - Determination by the Theory of Plasticity of the Bearing Capacity of Continuous Footings on Sand. Proc. 3rd Int.Conf.Soil Mech. & Fndn.Engng; Switzerland. Vol.1, 1953, pp.409-412.

15. BOOKER, J.R. - An Improved Method for the Numerical Inegration of Hyperbolic Equations. To be published. 1971.

16. COX, A.D., EASON, G. and HOPKINS, H.G. - Axially Symmetric Plastic Deformation in Soils; Phil.Trans.Roy.Soc.A. Vol.254, 1961, pp.1-45.

# Uplift Testing of Prototype Transmission Tower Footings

By
R. J. McKenzie, B.C.E., C.A.S.E. (Cantab.), M.I.E.Aust.
(Investigations Engineer (Civil), State Electricity Commission of Victoria)

SUMMARY.- This paper describes a series of uplift tests carried out by the State Electricity Commission of Victoria, Australia, on full size transmission tower footings. Tests were conducted on bored piles in basaltic clay and buried slab footings in basaltic clay and in a granitic soil. Comparison of the pile test results is made with a "tension limited shear" theory developed from the results of an earlier series of uplift tests on piles of smaller capacity. (Ref. 1 and 2.) The effect of compaction and compressibility of backfill above concrete slab footings subjected to uplift loading is discussed and the results are compared with a modified empirical cone theory.

## I.- INTRODUCTION

Footings for power transmission towers are required to restrain large vertical loadings at the tower legs within small margins of differential movement to prevent overstressing of the tower structure. This is one of the prime factors to be considered in the design. Other factors include the nature of foundation materials, the type of footing and the method of construction.

Transmission lines in Victoria traverse country with cohesive and non-cohesive type soils which can vary significantly along the route, even at one tower site. The type of footings used are the bored cast in situ pile and buried concrete slab and are designed to satisfy a range of loadings and soil conditions.

The design of tower foundations by the State Electricity Commission of Victoria takes into account both the ultimate uplift resistance and the load-displacement characteristic for a particular type of foundation. The actual methods based on soil mechanics principles have been developed to predict the ultimate uplift capacity of tower foundations but heavy reliance has also been placed on full scale testing of actual footing designs to check the theoretical approach and to obtain experience of their load-displacement behaviour. The results of such tests carried out for 220 kV tower foundations have been published (Ref. 1 and 2) and this paper deals with tests carried out in 1965/1966 on 500 kV tower footing designs which require uplift capacities of up to 500,000 lb.

It was necessary to rationalise the tests to determine the behaviour of pile footings in a clay, and buried slab footings in clay and in weathered granitic soil. These soils represent those types generally encountered within Victoria.

For overall economy the footing must be simple in form yet suit a wide variety of soil conditions and loadings. Flexibility of dimensional change to suit unexpected site conditions during construction is essential.

## II.- OBJECTIVE OF TEST SERIES

The objectives of the 1965/66 test series were as follows:

(a) To extend the testing of prototype footings up to a capacity of 500,000 lb uplift.

(b) To compare the test results for the bored type footing in clay soils with the theoretical values calculated by the "tension limited shear" theory postulated by Paterson and Urie in 1964 (Ref. 2).

(c) To check the validity of the empirical "cone of earth" method of design for buried slab type footings.

(d) To check the effect of the degree of compaction of the backfill and the value of fine crushed rock placed over the slab type foundation on the uplift capacity and load-displacement characteristic.

## III.- SELECTION OF TEST SITES

In order to exclude as many variables as possible, two sites were selected on the basis that one consisted of a cohesive soil and the other a non-cohesive soil and that the in situ materials were reasonably uniform to a depth of 18 feet.

The sites selected were at Keilor Terminal Station (approximately 8 miles N-W of Melbourne), and near Corryong (Tower 100 on 330 kV line, Snowy-Dederang).

(a) KEILOR SITE - IN SITU CLAY - The in situ soil at Keilor is a residual deeply fissured basaltic clay. Five bores were put down to 20' depth over the site and undisturbed samples (1.5" diameter) were taken at intervals of one foot. No water table was detected.

The soil properties for the in situ and remoulded states are given in Table I.

The indirect tensile strength of the clay was determined on undisturbed samples 1.5" x 1.5" diameter by the Brazilian method using a standard unconfined compression testing machine as the loading mechanism. The procedure is simple and tests were made in parallel with the unconfined compression strength test on samples cut from the same tube. Some scatter in the properties occurred throughout the soil profile with indication of a very slight increase in their mean value below 9' depth where the indirect tensile strength values increased from about 4 to 6 $lb/in^2$, apparent cohesion strengths increased from about 11 to 20 $lb/in^2$ and moisture contents reduced from 30% to 20%. Overall mean values of 5 and 15 $lb/in^2$ for tension and cohesion strengths respectively were used in the theoretical calculations of uplift capacity.

(b) CORRYONG SITE - IN SITU SILTY SAND - The soil at this site is a residual silty sand derived from weathered granite. It is poorly graded, and firm in the undisturbed state. Light usage of a pneumatic spade was required during excavation but the spoil collapsed to a cohensionless silty sand. Some slight fracturing of the soil mass occurred and light timbering was used to prevent minor collapses. Again no water table was detected within the 14' deep excavations. The soil properties are shown in Table I.

## IV.- METHOD OF APPLYING TEST LOAD

Test loads on the bored piles were applied by a hydraulic jack and yoke arrangement set at the centre of a 20' loading beam which was simply supported on timber packers at each end. The capacity of the loading jack and beam was 240,000 lb.

For the higher capacity buried slab footings the larger test beam and jacking system shown in Figure 1 was used. The beam, 36' long and 5' deep was supported clear of the ground on timber packing at each end. An uplift force of up to 500,000 lb was applied by hydraulic jack to a central yoke attached to the footing. A pair of 125,000 lb jacks at each end of the beam allowed a total uplift displacement of 10" at the test footing.

The load was read directly from a calibrated test pressure gauge fitted to the central jack. Displacements were measured by a scale fitted to the footing and a marker attached to an independent static beam. Displacements were also checked by survey level located some 30' from the footing.

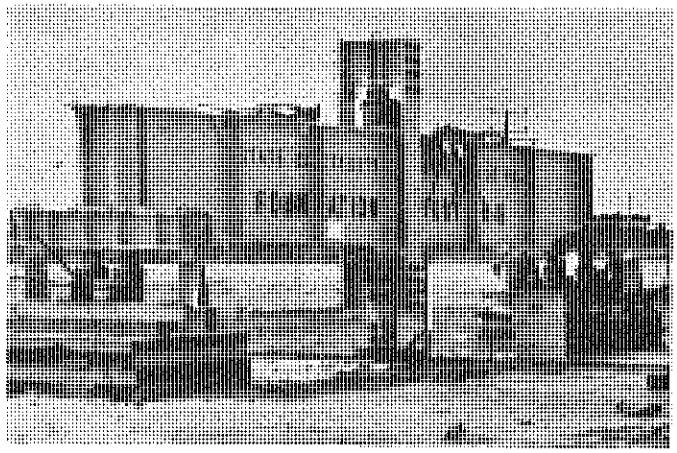

Fig. 1 Loading beam arrangement at site; 500,000 lb uplift capacity.

TABLE I

SOIL PROPERTIES AT KEILOR AND CORRYONG TEST SITES

| Site and Soil Type | Moisture Content (%) | Dry Density $\gamma_d$ ($lb/ft^3$) | Apparent Cohesion ($lb/in^2$) | Indirect Tensile Strength ($lb/in^2$) | Liquid Limit (%) | Plasticity Index (%) | Percentage Passing: Clay .002 mm (%) | Silt .06 mm (%) | Sand 2.0 mm (%) |
|---|---|---|---|---|---|---|---|---|---|
| (a) KEILOR Basaltic clay (CH) | | | | | | | | | |
| In Situ | 28 av.<br>17-32 | 93 av.<br>86-104 | 15 av.<br>8-29 | 5 av.<br>3-9 | 105<br>99-110 | 80<br>69-87 | 60 | 34 | 6 |
| Re-moulded | 25<br>Optimum | 95<br>$\gamma_d$ max.* | | | | | | | |
| (b) CORRYONG Granitic silty sand (SM) | | | | | | | | | |
| In Situ | 12 av.<br>9-15 | 96<br>90-102 | 3.0<br>$\phi = 34^o$ | 0 | Generally Indeterminate | | 9 | 25 | 64 |
| Re-moulded | 13-18<br>Optimum | 118-106<br>$\gamma_d$ max.* | | | | | | | |

* $\gamma_d$ max. = Maximum dry density (Aust. Standard A89 - 1966)

Two rates of load application were used in this series of tests. In the pile tests, excluding test Nos. 3, 7, 10 and 13, the load was applied at a constant rate of 20,000 lb per minute. For the slab footing tests and pile test Nos. 3, 7, 10 and 13 an incremental method of loading, as specified by the Conference Internationale des Grande Reseaux Electriques a Haute Tension, was used. (CIGRE Committee No. 7.) The load was applied at a uniform rate in approximately five increments each of 5 minute duration, and the load was held constant during intermediate rest periods of 10 minutes each. Each of the 5 incremental loads was predetermined on the basis of 20% of the estimated ultimate footing capacity and displacements were measured during the loading and rest periods.

The loading rate differs in each of these methods and the effect of this is discussed in Section VI.

## V.- FOOTING CAPACITY

The uplift capacity of a transmission tower footing is defined for these tests as the maximum uplift load applied to effect a 0.5 inch vertical displacement of the footing. This figure was originally chosen arbitrarily, but it has since been supported by an overall assessment of secondary stresses in the towers due to footing movements.

No load factor is specifically applied in determining the design capacity of the footing except those which are inherent either in the adopted design approach (for the footing) or in the structural analyses of the tower.

## VI.- BORED PILES AND TEST RESULTS

Tests were conducted in 1965 at Keilor on seventeen bored concrete piles in clay; of which seven were plain cylindrical shafts and ten with enlarged bases. The pile dimensions and test numbers are given in Table II.

TABLE II

TEST DATA FOR BORED PILES IN BASALTIC CLAY

| Bored Concrete Pile | | | | Uplift Load (lb x $10^3$) | | | |
|---|---|---|---|---|---|---|---|
| Test No. | Type | Diam. (in) | Depth (ft) | Test | | Theoretical | |
| | | | | At 1/2" displacement | Ultimate | Ultimate | 80% of Ultimate |
| 1 | Plain | 24 | 9.2 | 75 | 75 | 80 | 64 |
| 2 | " | " | 12.2 | 96 | 99 | 120 | 96 |
| 3 | " | " | 15.1 | 135 | 137 | 160 | 128 |
| 4 | " | " | 18.0 | 200 | 212 | 202 | 161 |
| 5 | " | 30 | 9.0 | 85 | 87 | 98 | 78 |
| 6 | " | " | 12.1 | 114 | 114 | 150 | 120 |
| 7 | " | " | 15.0 | 170 | 173 | 202 | 161 |
| 8 | Under-cut | 16/30 | 12.2 | 109 | 120 | 135 | 108 |
| 9 | " | 20/36 | 9.5 | 110 | 120 | 105 | 84 |
| 10 | " | " | 11.9 | 165 | 173 | 164 | 131 |
| 11 | " | " | 15.0 | 229 | 244 | 234 | 187 |
| 12 | " | 24/42 | 9.0 | 112 | 117 | 136 | 109 |
| 13 | " | " | 11.5 | 157 | 165 | 181 | 145 |
| 14 | " | " | 13.7 | 203 | 208 | 236 | 189 |
| 15 | Bulb | " | 8.9 | 108 | 113 | 130 | 104 |
| 16 | " | " | 11.3 | 175 | 181 | 188 | 150 |
| 17 | " | " | 13.8 | 220 | 222 | 242 | 193 |

NOTE: The diameters of pile shaft and under-ream are shown 16/30, 20/36 and 24/42 inches.

Augering was carried out by rotary Pengo type equipment for the plain cylindrical piles (test Nos. 1-7) and the shafts for those with enlarged bases (test Nos. 8-17). The spoil was removed frequently from the auger bit to prevent excessive plastering of the walls with remoulded clay.

Two methods of forming the enlarged bases were used. A cylindrical bucket with expandable side cutters was used for reaming the undercut holes (tests 8-14). The bulb-shape enlargements (tests 15-17) were reamed out by a special cutter with several vertically-mounted expandable cutting strips which could be adjusted at the drill head to form the required bulb dimensions. The bulb-shaped enlargements were cleanly cut with less disturbance to the in situ clay than those formed with the bucket. Typical shapes of the enlargements are shown diagrammatically in Fig. 3. The diameters of the reamed sections finished 1" oversize for test Nos. 10, 14, 16 and 17; 2" oversize for test Nos. 11 and 12 and 4" undersize for test No. 9. Concrete was placed into the holes and vibrated to ensure intimate contact with the in situ soil.

The test results are shown in Table II and the shape of the load-displacement curves related to the theoretical ultimate capacity is indicated in Figs. 2 and 3.

Differences in the curve characteristics for the cylindrical and under-reamed piles are clearly evident. In general the cylindrical pile reaches its ultimate capacity at 0.30 inches displacement, and 50% of its ultimate capacity at 0.05 inches, whereas the under-reamed piles displace 1.0 inch at ultimate capacity and 0.10 inches at 50% of ultimate capacity. The cylinder piles are more rigid in behaviour with little reserve capacity at the design displacement of 0.5"; approximately 2% reserve for cylinder piles and 6% for under-reamed piles.

In tests using the incremental loading method, creep effects were noted during the 10-minute periods when the load was held constant. In test Nos. 3, 7, 10, 13, the amount of movement resulting from creep at 0.5 inches total displacement was 0.05", 0.0", 0.10" and 0.10" respectively. Creep effects beyond this point could not be observed readily due to a rapid increase in displacement at the ultimate test load. It was not possible to determine creep effects in the constant loading rate method (20,000 lb/min) which was used for the other pile tests.

In comparing the test capacities given in Table II with respect to the depth of each pile type, the effect of loading rate is not apparent. In the incremental method the average loading rate over the whole test period was about 2,000 lb/min and during the loading period it varied from 5,000 to 10,000 lb/min. These rates are much less than that used in the constant rate method.

It is also noted that the capacities of piles with 42" diameter enlargements formed with the bucket (tests Nos. 12, 16 and 17) were only 3% greater than the smaller 36" diameter piles also formed by the bucket. There was also no apparent effect on the test capacity resulting from oversize or undersize enlargements noted above. However, piles with 42" diameter enlargements formed with the bulb cutter

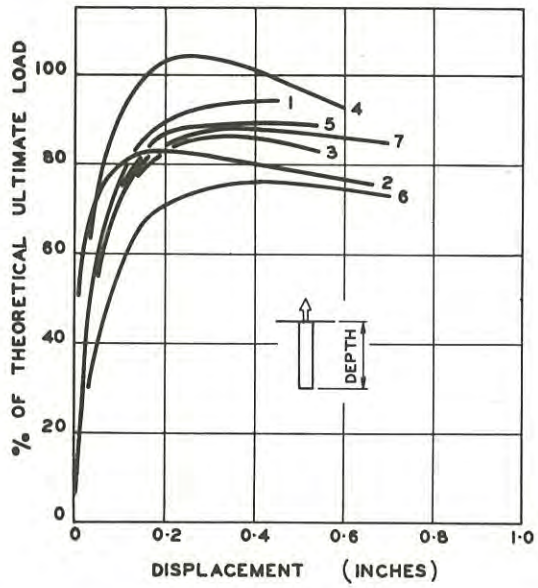


Fig. 2. Plain cylindrical Bored Piles in Basaltic Clay (Keilor, Oct., 1965). Test Nos. 1-7. Uplift load expressed as percent of theoretical ultimate load versus displacement.

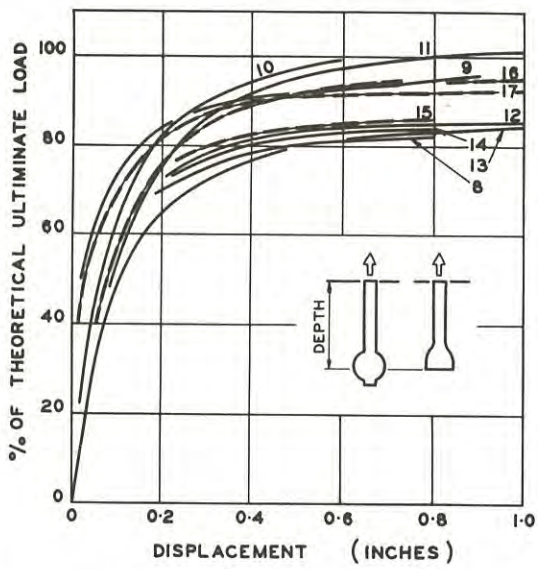


Fig. 3. Bored Piles with Enlarged Bases in Basaltic Clay (Keilor, Oct., 1965). Undercut pile test Nos. 8-14. Bulb Pile test Nos. 15-17. Uplift load expressed as percent of theoretical ultimate load versus displacement.

(test Nos. 16 and 17) generally contributed 10% more capacity than those formed with the bucket (tests 13 and 14).

## VII.- COMPARISON OF PILE TESTS WITH "TENSION LIMITED SHEAR" THEORY

The design capacity of the test piles was based on a "tension limited shear" theory proposed by Paterson and Urie in 1964 (Ref. 2) of which a brief summary is given in Appendix 1.

Figs. 2 and 3 show curves for the ultimate capacity of the cylindrical and under-reamed piles expressed as percent of the theoretical capacity versus the measured displacements and it is seen that the test capacities at 0.5 inches movement fall within the range of 76% to 104% of the theoretical capacity. The low value occurred in pile test No. 6 which was probably due to plastering of the augered hole with remoulded clay for the top 3 feet of its total 12 feet depth. Less variation (80% - 96%) resulted in the piles with under-reams.

The variations in the other tests could be attributed to an incorrect choice of mean values for the in situ tensile and cohesion strength parameters of the soil. In determining the theoretical ultimate capacities, the mean values adopted were 5 $lb/in^2$ for tensile strength and 15 $lb/in^2$ for cohesive strength. Precision in determining the ultimate capacity is dependent on the accuracy of the assessment of these values. For example, in test No. 14 the theoretical capacity is reduced by 10% if the assumed average value of the tensile strength is 4 $lb/in^2$ instead of 5 $lb/in^2$. For a cohesion strength value of 14 $lb/in^2$ instead of 15 $lb/in^2$ the loss in the theoretical capacity of the pile is only 2%.

In comparing the actual ultimate capacity with that calculated by the "tension limited shear" method (Figs. 2 and 3) it is seen that the ultimate test capacity of all the test piles, with the exception of No. 6, equalled or exceeded 80% of the theoretical capacity at 0.5 inches displacement.

As a result of the experience gained from these tests the procedure adopted for the design of bored pile footings by the State Electricity Commission is based on a modified version of the "tension limited shear" theory. Footing capacities are designed to exceed 80% of the theoretical ultimate capacity determined by the "tension limited shear" method. However, bored pile footings with enlargements are used only in the suspension or light strain type of towers. They are not acceptable at towers subjected to long-term uplift conditions because of their low reserve capacity at the design displacement limit.

## VIII.- SLAB FOOTINGS AND TEST RESULTS

The concrete slab footings tested in this series were constructed to uniform dimensions for the purpose of studying the effect of the density of backfill material on their uplift capacity.

Reinforced concrete slabs of 7' x 7' x 2' thickness were set at 14' depth and backfilled with 12' depth of compacted materials. The slabs were formed in the bottom of 7' x 7' x 14' deep excavations with vertical side walls. Open timber bracing was provided for the safety of personnel. The concrete was cast against the in situ soils at the walls of the excavation and no under-cutting of the walls of the excavation was permitted, particularly at the slab, so that the effect of the degree of compaction of the backfill materials could be observed during the test.

Backfilling was compacted in 4" layers into zones of predetermined densities representing various standards of compaction. Fine crushed rock material consisting of a well graded basaltic stone up to 3/4" size was compacted in 6" layers for 2' and 4' immediately above the slab (Zone A) in test Nos. 23, 27 and 28; the remainder of the hole was filled with compacted soil (Zone B).

The standard of compaction is referred to as the dry density of the compacted fill expressed as percent of the maximum dry density determined from a standard compactive effort of 12,375 ft lb/ft$^3$ (Australian Standard A89-1966).

A total of 11 footings were constructed, six in basaltic clay at the Keilor site (Nos. 18-23) and five in granitic soil at the Corryong site. (Nos. 24-28.) The soil properties are given in Table I. The 500,000 lb capacity test beam described in section IV was used for each test and loads were applied by the incremental CIGRE method. Actual loading rates varied from 8,000 to 21,000 lb/min and on the basis of overall time to reach ultimate capacity, the rate varied from 3,000 to 9,000 lb/min. No specific effects on the performance of the footings could be attributed to variation in loading rate.

The load capacities and displacements determined in the tests and the standards of compaction of the backfill within Zones A and B are shown in Table III.

TABLE III

TEST DATA FOR SLAB FOOTINGS IN BASALTIC CLAY AND GRANITIC SILTY SAND

| Concrete Footing (7' x 7' x 2' slab at 14' depth) | | | Uplift Load (lb x $10^3$) | | | |
|---|---|---|---|---|---|---|
| Test No. | Compacted Backfill ($\gamma_d/\gamma_{d\ max}$) x 100 | | Test | | Theoretical | |
| | Zone A (%) | Zone B (%) | At 1/2" displacement | Ultimate at stated displ. | "Cone of Earth" | 80% "Cone of Earth" |
| BASALTIC CLAY (12' depth of compacted backfill) | | | | | | |
| 18 | 75 | 75 | 163 | 225 @ 5" | 340 | 272 |
| 19 | 84 | 84 | 250 | 380 @ 6" | " | " |
| 20 | 87 | 87 | 220 | 357 @ 8" | " | " |
| 21 | 93 | 93 | 384 | 450 @ 1.6 | " | " |
| 22 | 2' zone - fine crushed rock | 86 | 306 | 352 @ 3.6 | " | " |
| 23 | 4' zone - fine crushed rock | 87 | 326 | 385 @ 2.2 | " | " |
| GRANITIC SOIL (12' depth of compacted backfill) | | | | | | |
| 24 (a) | no backfill - slab only | | 130 | 170 @ 1.1 | - | - |
| (b) | 85 | 85 | 220 | *495 @ 2.1 | 340 | 272 |
| 25 | 90 | 90 | 280 | *495 @ 1.7 | " | " |
| 26 | 92 | 92 | 315 | *460 @ 1.1 | " | " |
| 27 | 4' zone 92 | 90 | 320 | *496 @ 1 5 | " | " |
| 28 | 4' zone - fine crushed rock 95 | 90 | 430 | *500 @ 0.6 | " | " |

*less than ultimate load

NOTE: $\gamma_d$ max. = maximum dry density of soil (Aust. Standard A89-1966).

$\gamma_d$ = dry density of soil.

The load-displacement curves plotted in Figs. 4 and 5 clearly indicate the difference in behaviour of footings in a clay and a granular material. At 0.5 inches displacement, the capacity of the footings in clay ranged from 163,000 lb to 384,000 lb (236%), whereas in the silty-sand 220,000 lb to 430,000 lb (195%). The footings in clay provide less reserve capacity beyond the design displacement level to the ultimate capacity (12% to 62%) than that offered in the granular soil (estimated 60% to 100%).

In tests 18 to 21 it is evident that a high standard of compaction of the backfill significantly increases the footing capacity although tests 19 and 20 are inconsistent. The effect of a low compaction standard (75%) resulting in a low capacity is indicated in test No. 18.

The use of fine crushed rock in Zone A for footings in clay and silty sand, increased the capacity of the footing significantly at 0.5 inch movement from 220,000 lb to 326,000 lb (test Nos. 20 and 23) and from 320,000 lb to 430,000 lb (tests 27 and 28). The gain in capacity in each case was about 40%.

In Test 22(a) the load was applied to the slab before backfill was placed in order to ascertain the restraint offered by the slab. The average shear stress at the edges of the slab was 16 lb/in$^2$ and no suction effect was evident in the unsaturated clay. It was conducted in association with a theoretical study of displacement with respect to the compressibility of backfill related to its standard of compaction. Reference is made to this study in Section X. Backfill was then placed over the slab for test 22(b) in which the uplift load was released at 0.75 inch displacement then re-applied (Test 22, Fig. 4) incrementally after 80 minutes elapsed. On re-loading further displacement increased 0.5 inches from 0.4 inches to 0.9 inches at a capacity equivalent to 80% of that initially recorded at 0.5 inch displacement.

Observations of displacements due to creep effects could be made only during the 10 minute periods when the load was held constant. The total creep observed until the design displacement limit of 0.5" was reached indicated no clear trend with respect to the standard of backfill compaction or type of material. At footing displacements of 0.5 inches, the creep component recorded at Keilor was 0.10", 0.17", 0.06", 0.09", 0.18" and 0.11" (tests 18-23 respectively) and at Corryong 0.02", 0.07", 0.07", 0.02" and 0.05" (tests 24-28 respectively). The creep effect was greater in the clay which is significant for long-term loadings.

At ultimate test capacity when failure is occurring it is difficult to isolate creep effects with precision. However, values recorded in tests 18, 19, 21, 23 at Keilor and tests 24 to 28 at Corryong are 0.36", 0.54", 0.39", 0.24" and 0.26", 0.22", 0.17", 0.09", 0.06" respectively. Creep could not be isolated in tests 20 and 22 beyond the 0.5" displacement capacity. These results indicate the reduction of the creep displacements as the compaction standard of the backfill increases, particularly in the silty sand materials and also with the use of fine crushed rock in Zone A. The total time taken to reach the ultimate capacities varied from 80 to 110 minutes which is dependent on the loading method.

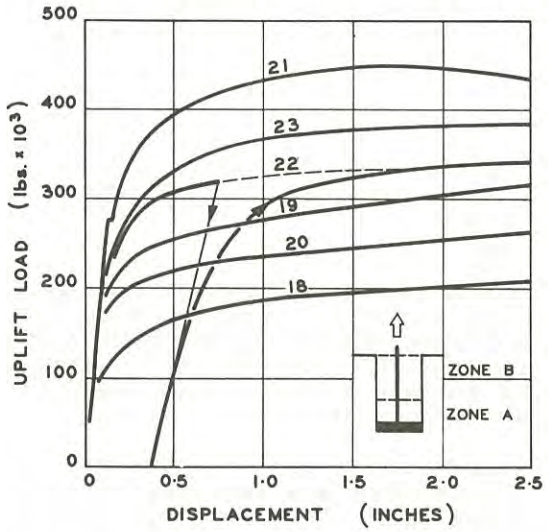


Fig. 4. Concrete Slab Footings in Basaltic Clay. (Keilor, Dec., 1966). Test Nos. 18-23.

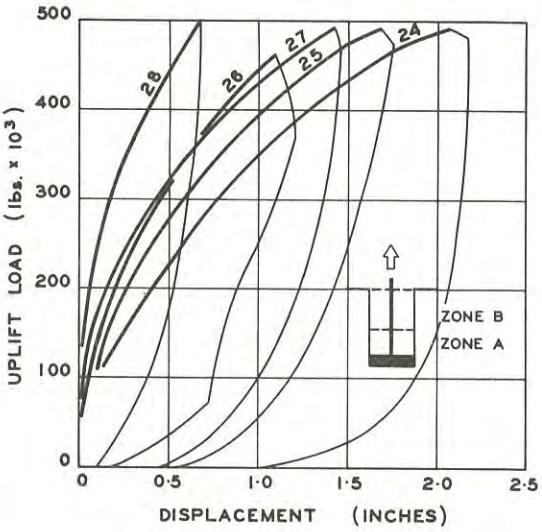


Fig. 5. Concrete Slab Footing in Granitic Silty Sand (Corryong, Nov., 1966). Test Nos. 24-28.

## IX.- DISPLACEMENTS WITHIN BACKFILL AND IN SITU MATERIALS

Observations of movements within the backfill and the in situ soils were made to study the compressibility of the backfill and to indicate the location of any potential failure planes. Levels at subsurface points were taken by means of steel rods set freely into 1" diameter holes. In backfill materials the rods stood on steel plates (12" x 12") which were set at various levels during compaction. For measurements in the in situ soils the lower end of the rods were cast into a handful of cement mortar.

Fig. 6 illustrates the distribution of displacements observed in the clays at Keilor during tests 19 and 23 for slab displacements of 0.8" and 3.0". The effect of increased restraint from the in situ soils can be noted when a 4' depth of fine crushed rock is included in Zone A above the slab.

In test 23 at 3.0" slab movement, a potential failure plane can be interpreted from Figure 6 to commence at the top of Zone A and rise on a 2 on 1 slope to the surface. In test 19 failure can only be interpreted to have occurred along the walls of the original excavation.

Maximum strains of approximately 50% at 3" slab movement were developed within the backfill immediately over the slab (test 19) and above the fine crushed rock (test 23) and reducing to zero at the surface. No strains within the fine crushed rock were observed. In comparing strain-depth plots not shown in the paper, it is apparent that the total strain energy applied to the footing, less shear forces developed at the slab edge, is absorbed in the clay backfill (test 19) and in both the backfill and the mobilised in situ material (test 23).

In comparing displacements in the clay footings without fine crushed rock (tests 18-21), some mobilisation of in situ material was only observed in test 21 in which the backfill was compacted to 93% of standard. In the granitic materials ultimate capacities of the footing were beyond that of the test loading beam but displacement patterns similar to that shown in Fig. 6 (test 23) were observed in all tests except 24(b) in which case the slab had been preloaded and then backfilled with compacted silty sand to 85% of standard.

## X.- COMPARISON OF SLAB FOOTING TESTS WITH "CONE OF EARTH" THEORY

The "cone of earth" method is an empirical method for determining the ultimate uplift capacity of a slab footing and relies on the weight of earth lying within a failure plane assumed to commence at the edge of the slab and reach the surface on a plane of slope 2 on 1.

In adopting a mean value for the density (115 lb/ft$^3$) of the backfill and in situ materials at Keilor and Corryong sites, the ultimate capacity of the test footings determined by this method is 340,000 lb. However, to meet the design requirements, displacements should not exceed 0.5 inches.

Only one footing at each site (tests 21 and 28) fulfilled these requirements. However, most of the tests achieved 80% of the cone of earth capacity within the 0.5" displacement limit provided the dry density of the backfill after compaction was greater than about 90% of the standard maximum dry density. Tests 18, 19, 20, 24, failed and were unacceptable for this reason.

The effect of a 4 ft layer of compacted fine crushed rock in Zone A (tests 23 and 28) considerably increased the uplift capacity at 0.5" displacement. The dilatent behaviour of a dense granular material is considered to be important in transferring increased shear forces to the in situ materials.

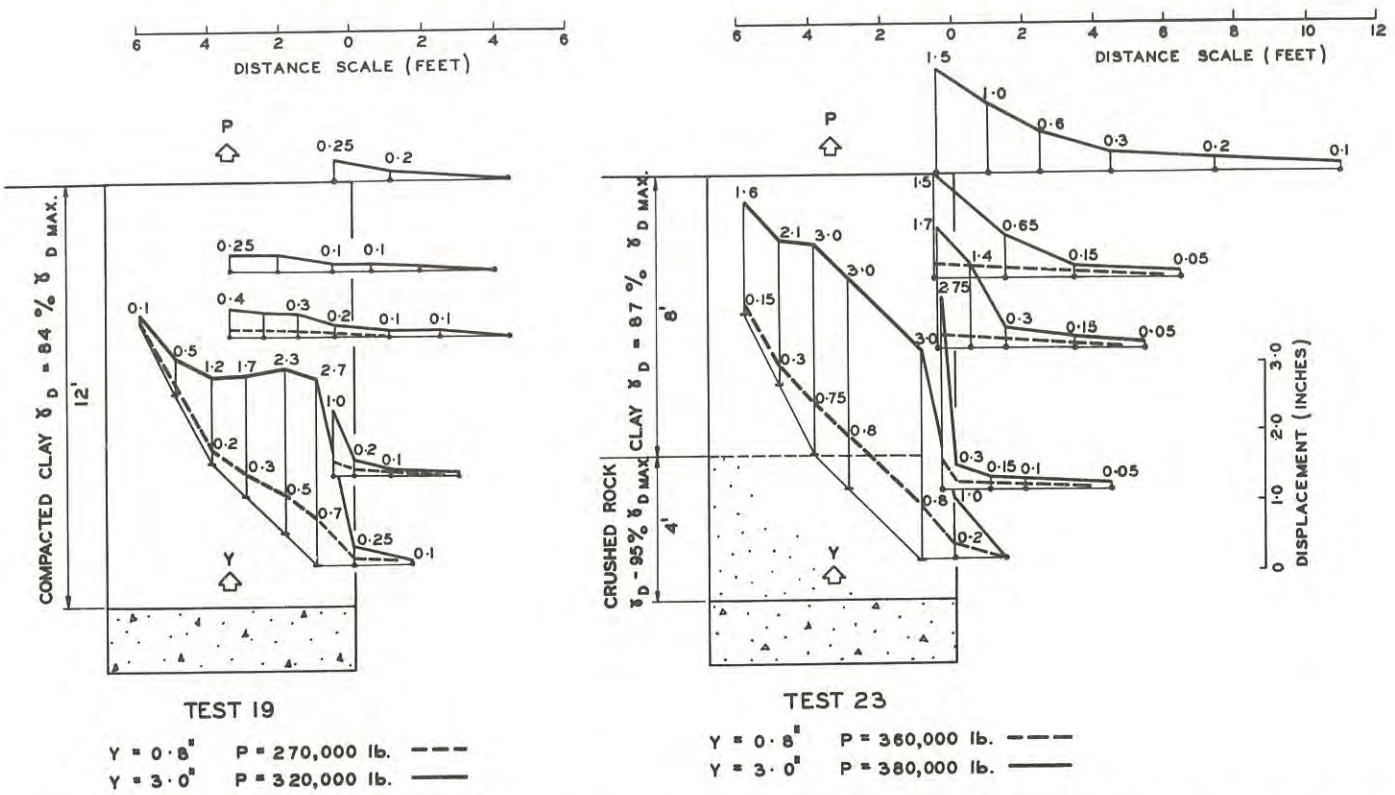


Fig. 6. Concrete Slab Footings in Basaltic Clay. (Keilor, Dec., 1966.) Observed displacements in compacted backfill and in situ soil for slab displacements of 0.8" and 3.0". Displacement values shown at top of ordinates which rise from the sub-surface point observed.

From observations during these tests, failure is interpreted to commence with a shear failure at the edge of the slab with some restraint being offered by the compacted backfill until the weight of the slab is taken up. At that stage the backfill is further compressed and shear forces are developed on the walls of the excavation, less restraint is now being provided by slab shear as lower residual strength values result. As the backfill now becomes fully mobilised it can either move as a plug or induce vertical movement of the in situ soils and at this stage the ultimate level of uplift restraint is reached.

An attempt was made to correlate the test results with a method of evaluation based on the compressibility of the backfill material. Limited agreement was achieved in the footings at Corryong but the method failed when applied to concrete slabs in basaltic clay at Keilor. In the latter case another method of calculation was tried, based on shear stress developed along the sides of the excavation, but this also proved unsatisfactory. Apart from their unreliability, these methods are not favoured on economic grounds because of time and expense required to gather precise data on the characteristics of the soil.

## XI.- CONCLUSIONS

In conducting the tests valuable experience and data on the field behaviour of bored piles and slab footings in uplift loading was gained resulting in a strengthened confidence in extending designs for tower footings to larger capacities up to 500,000 lb.

BORED PILES - The "Tension limited shear" theory consistently overestimates uplift capacity of the bored piles tested in stiff basaltic clay. However, footing capacities based on 80% of the "tension limited shear" resistance provides an adequate basis for determining the design capacity at displacements not exceeding 0.5 inches. The determination of cohesive and indirect tensile strength of the in situ clay can be readily obtained with sufficient accuracy from 1-1/2" diameter samples tested in a standard unconfined compression machine.

Bored piles have little reserve capacity at the design ultimate loading and are not recommended for use in conditions of long-term uplift loading. Some 20% of the design limit of 0.5 inches displacement resulted from the effect of creep. At least 10% loss in the design capacity can result from poorly excavated enlargements at the base of a bored pile.

BURIED SLAB FOOTINGS - The cone of earth method for the design of buried slab footings subjected to uplift loads overestimates the design capacity at the 0.5 inch limit of displacement. The uplift load-displacement characteristics are significantly improved with a higher standard of compaction (or stiffness) of the backfilled soils and a further improvement is gained from fine crushed rock, compacted in a zone immediately above the slab.

For the overall economy and simplicity of design, the capacity of slab footings at 0.5 inches displacement based on 80% of the "cone of earth" resistance is recommended, provided that the backfilling is compacted to a dry density not less than 90% of the standard maximum dry density and that a zone of compacted granular material is placed immediately above the slab. Slight under-cutting of the excavation at the edges of the slab is also recommended.

The "cone of earth" method is limited particularly in the case of loose or variable backfill material. Quantitative extrapolation of footing behaviour beyond the dimensional realms of the tests should be regarded with caution as the influence of scale was not investigated.

A slab footing provides adequate reserve capacity beyond the design capacity at 0.5 inches displacement and is recommended for use in conditions of long-term uplift loading.

## XII.- ACKNOWLEDGEMENTS

This paper is published with the permission of the Chief Civil Engineer of the State Electricity Commission of Victoria, Mr. R.L. Urie who initiated this study and contributed much from his previous experience in this field.

The work was carried out by members of the Civil and Architectural Department of the SECV and the author wishes to acknowledge their co-operation and assistance and in particular to Mr. W.T. Nicholas for the field organisation and to Mr. A.K. Szalla for the soil testing facilities.

## REFERENCES

1. CLEMENTS, B.J. - Full Scale Pull-out Tests on Transmission Line Tower Foundations. Proc. Third Aust. - N.Z. Conf. on Soil Mech. and Foundation Engineering, 1960.

2. PATERSON, G. and URIE, R.L. - Uplift Resistance Tests on Full Size Transmission Tower Foundations. Conference Internationale des Grandes Reseaux Electriques a Haute Tension, Paris, 1964.

## APPENDIX 1

## "TENSION LIMITED SHEAR"

SUMMARY:

A brief description of the theory by Paterson and Urie (Ref. 2) is given.

NOTATION:

- $d$, Diameter of Pile Shaft.
- $d_o$, Diameter of pile base.
- $h$, Depth of pile.
- $h_c$, Critical depth (tension limited shear in soil).
- $\gamma$, Soil density.
- $\gamma_c$, Concrete density.
- $\gamma_{av}$, Average density of soil and concrete within failure surface.
- $f_t$, Tensile strength of soil.
- $C$, Cohesion strength of soil.
- $V$, Uplift resistance of pile.
- $S$, Uplift resistance due to shear strength of soil.
- $W$, Uplift resistance due to weight of concrete and soil.

The theory is based on the observation of failure planes developed during uplift testing of bored piles and postulates that the shear strength of a fissured clay in a confined state is not controlled by the shear strength at the fissured surfaces. This is born out by noting that tensile cracks emanate from the cylindrical failure planes during the 1960 test series on cylindrical and under-reamed bored piles. It is suggested that uplift restraint is limited by the tensile strength of the soil rather than adhesion to the pile or shear strength on the failure plane of an under-reamed pile.

In developing the initial stress-strain relationships within the soil for the full depth of pile, the theory assumes the lateral stress level in the soil is raised by the fluid pressure exerted by vibrated concrete during placement and that the earth pressure coefficient K approximates to the ratio of the densities of the concrete and clay, i.e. K = 1.25. In the case of the under-reamed pile, K is adjusted by the ratio of the diameters of the shaft and pile enlargement, i.e. $K = 1.25 \times d_o/d = 0.75$.

During uplift of the pile, shear forces developed along the cylindrical failure plane (projected plane for under-reamed piles) and, if it is assumed that no increase in horizontal and vertical stress levels occur, then the limiting shear stress can be determined from the Mohr envelope for all depths of the pile.

It is shown that at greater depths the maximum shear stress is controlled by the cohesion strength of the clay. Above a critical depth a failure in tension occurs and below this depth failure in shear controlled by the cohesion strength of the clay occurs.

$$\text{i.e. } h = h_c \leq \frac{2}{1+K}\frac{1}{\gamma}(C - f_t)$$

The maximum uplift resistance of the pile can be expressed as the sum of the weight of the soil and concrete within the failure surface plus tension limiting shear stress on the failure plain.

$$\text{i.e. } V = S + W$$

where

$$S = \pi d h_c \left( f_t + \frac{1+K}{4}\gamma h_c \right) + C\pi d(h - h_c)$$

and

$$W = \frac{\pi}{4} d^2 h \gamma_{av}.$$

For plain piles,

$$K = \frac{\gamma_c}{\gamma}$$

For under reamed piles,

$$K = \frac{\gamma_c}{\gamma} \cdot \frac{d}{d_o}$$

# Stresses Beneath Granular Embankments

By

I. K. Lee, B.C.E., M.Eng.Sc., Ph.D., M.I.E.Aust.

(Associate Professor of Civil Engineering, University of Sydney)

AND

J. R. Herington, B.E., M.Eng.Sc.

(Engineer, Dames and Moore, Sydney)

293

SUMMARY.- A theoretical and experimental study of the stresses along the base of a granular embankment was completed. The experimental data consisted of normal and shear stress measurements on model embankments supported on a base which could be made rigid or deformed into any selected vertical profile. A comparison was made of the measured stresses with values predicted by the linear elastic, arching, and plasticity theories.

The model embankments were built up either as triangular wedges increased in height until the side slopes equalled the angle of repose, or in cumulative horizontal layers.

It is shown that the linear elastic theory manifests the progressive change in stress distribution as the embankment is formed on a rigid base, and that the peak stress values are approximately predicted. The arching theory appears to be inapplicable to the rigid base situation.

The imposition of a vertical settlement profile alone is not sufficient to develop a fully plastic state, and horizontal displacements would be necessary.

## I.- INTRODUCTION

Numerous theoretical analyses have been developed to predict the stresses within a soil embankment. Most of the investigators have treated the soil as a continuum of a linear elastic or rigid-plastic material (for example, Davis and Taylor (Ref 1), Goodman and Brown (Ref. 2), Clough and Woodward (Ref. 3) and other investigators have established solutions based on the statics of an idealized particulate mass of rigid elements (for example, Trollope (Ref. 4)). Trollope proposed two limiting solutions, the "no-arching" solution, assumed to apply to the stress distribution within a real soil wedge supported on a rigid foundation, and the "full-arching" solution which was considered to be the limiting case when a (theoretically unspecified) concave settlement of the foundation had occurred.

The present paper is concerned with the applicability of the solutions to a granular soil mass. Initially, attention is concentrated on the stress distribution beneath an embankment supported on a rigid foundation, and the concordance of experimental data with theoretical predictions is examined. The discussion is then extended to the change in stress distribution as the embankment is subject to settlement, and the applicability of the plasticity solutions is discussed.

The experimental data are the normal and shear stresses along the base of a symmetrical granular wedge supported on a foundation which could be held rigid or deformed vertically to a limited extent in a concave or convex profile. Previous laboratory studies (Hummel and Finnan (Ref. 5), Parry (Ref. 6), Lee (Ref. 7), Trollope (Ref. 4)) were limited to normal stress measurements, but as the shear stress distribution is a severe test of the effectiveness of a theoretical solution, it was essential to design the experimental equipment to record shear as well as normal stresses. As the first stage in these studies a monitored rigid base was constructed. To allow an examination of the trends in the stress distribution as foundation settlement occurred the base could be deformed to any selected vertical profile.

## II.- EXPERIMENTAL TECHNIQUES

After due consideration to the difficulties of interpreting shear stress measurements (Lee (Ref. 8)) the decision was made to initially construct an articulated base from independently supported narrow strips, each strip being monitored to measure the resultant vertical and horizontal forces. Each strip support was capable of adjustment in height but not in horizontal location. Any vertical settlement profile could then be imposed which was independent of the base stresses. As part of the second stage the development of the apparatus provision was made for the use of normal and shear stress cells but until the calibrations of the latter are finalized reliable results cannot be reported. However, the earlier normal stress measurmeents (Lee, (Ref. 7), are adequate to establish the pres-

sure distributions at large vertical base deflections for the purpose of comparison with the passive pressure plasticity solution.

The width of the monitored base was 52.1 inches, being composed of seven strips either 8.6 or 4.3 inches wide by 85.75 inches long. A clearance of 0.02 to 0.04 inches was maintained between adjacent strips. Each strip was supported at three points by calibrated thin metal straps operating in tension. Adjacent strips were horizontally connected by two similar calibrated straps. Actual strains in each strap were recorded by a pair of series connected electric resistance strain gauges attached to opposite sides of the strip. Details of the equipment are given by Herington (Herington (Ref. 9)).

All of the straps were calibrated by dead loading prior to assembly and an in-situ dead loading calibration after assembly produced identical calibration relationships. Although only a single dummy pair was used for all of the vertical straps, and a second single dummy pair for all of the horizontal straps, errors due to a drift caused by warming up of the active gauges was found to be negligible provided the gauge readings were taken immediately after switching to the active gauge.

In the present test series a quartz sand was used. The sand was intially washed to remove particles of silt - clay sizes. After washing the sand was dried and sieved to restrict the size range to 0.2 to 0.6 mm. This procedure rejected approximately 10 per cent of the sand. Finally, the sand was stored in sealed containers except during use. Exposure to the atmosphere over the testing periods caused an increase in moisture content of less than 0.04 per cent.

To provide suitable end restraint, vertical segments were attached to each strip. Thin overlapping metal items covered the gaps between the segments and a greased membrane was placed across the segments to form a "shear-free" continuous end support.

The results reported in this paper are confined to the sand placed in a relatively loose state, the average dry density being 95.6±0.5 p.c.f. Uniformity was achieved by fluvial pouring at a constant rate from 15 inches above the surface.

Three construction sequences were used in order to study the progressive development of the stress systems and to establish whether the loading history had a significant effect on the stresses when a final identical profile was formed. At this final stage the side slopes equalled the angle of repose (30 degrees). The construction sequences consisted of pouring the sand from a hopper moving back and forth along the centre line until the final profile was formed (final wedge sequence), secondly, forming the profile in three layers each layer being formed by continuous pouring over the plan area until the appropriate thickness had been built up (layered sequence), and finally, the wedge sequence in which the side slopes were increased in increments (slope sequence).

To translate the measured forces into stresses it was initially assumed that the stress distribution across the two outer strips was triangular and trapezoidal across the inner strips. Commencing at one stress free edge, an analysis was progressively completed across the full width which finally provides a statical check at the remaining stress-free edge. Such a procedure required extremely accurate load measurements since small errors had a dominant effects locally and despite the fact that the overall accuracy of total recorded weight was within 2 to 4 per cent, the normal stress at the "stress free" face was up to 10 per cent of the maximum stress. For this reason the alternative procedure of calculating the average stress over each strip from the forces applied to that strip alone was adopted. The position of the average stress was calculated for plotting purposes from moment equilibrium.

Taking into account the sensitivity of the straps, the zero drift over a test, the overall weight check, the consistency between replicate tests and the symmetry of the normal stress distributions, the accuracy of the local average pressure was found to be within ±2 -3 per cent of the calculated value. Although the shearing stress calculation required the difference of readings the force difference was, fortunately, quite large, and again taking all factors into account it was concluded that the accuracy of the shear stresses was similar to that for the normal stresses provided there was no deformation imposed on the base. When the base was deformed the bending strains in the horizontal strips affected the readings despite the use of a pair of strain gauges, and the procedure adopted was to place greatest significance on the measurements taken from the loaded to unloaded state since the base deformation was un-changed during unloading. By applying the corrections obtained by deforming the unloaded base to the unloaded-loaded sequence comparative results were obtained and taking into account the other checks available it was concluded that the recorded shear stresses were determined within a ±5 per cent accuracy for central deflections not exceeding 0.25 inches. The accuracy of the vertical stresses was unchanged at this deformation compared with no base deflection.

As shown in the following section, the stress distributions for a non-deforming base did not manifest severe local stress gradients so that the measurement of average stress over a finite width is a satisfactory technique. The technique is less satisfactory for the stress distributions associated with large deformations (Lee, (Ref. 7)) and use of pressure cells appears to be a better procedure.

The deformed profile used in the present series was confined to a circular arc.

As well as the in-situ dead load calibration previously mentioned, an in-situ sand calibration was also completed for the rigid base condition. Fig.1 shows the recorded pressures compared with the average pressure calculated from the total weight of sand on the base. The results were identical for sand depths of 3, 6 and 9 inches. One feature revealed by this calibration was a slight local arching between the central strips (points X and Y) with an over and corresponding under registration of 5 per cent of the recorded pressure. In the experimental results subsequently presented for the wedge this local error was evident but except in Fig.2 no correction in the plotted results was made. The correction in this figure was made to illustrate the order of this effect.

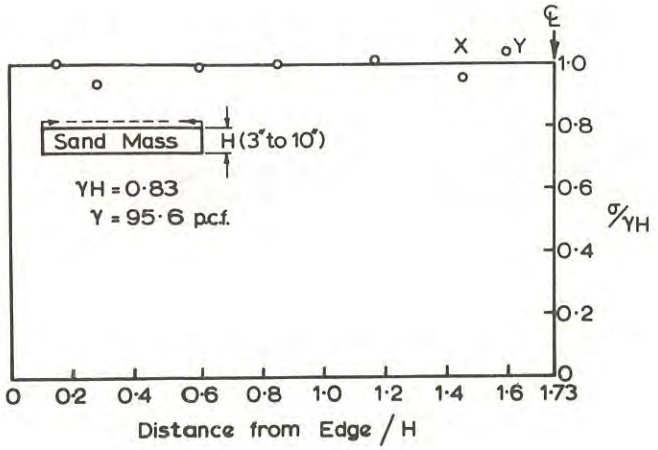


Fig.1 Normal Stress Distribution Layer of Uniform Depth

III.- RIGID BASE

Fig. 2 shows the experimental values of normal stress for the wedge in the final state, the side slopes being equal to the angle of repose (30°). The results for the three types of loading sequence were, within experimental accuracy, identical. In the earlier investigations (Lee, (Ref. 7)) a similar dried sand had been used but the angle of repose for these tests was 32½ degrees. Allowing for this difference by adjusting the location of the points at which the normal stresses were recorded by the pressure cells, the results can be superimposed on the present results. It is seen from the comparative values plotted in Fig. 2 that the correspondence was satifactory although the average pressure cell recording of central pressure was 0.79 γH compared with 0.84 γH obtained in the present tests. This difference may have been due to the fact that the supporting plate was slightly distorted in the earlier tests* and a small uniform or "zero" deflection could not be achieved over the whole width. (See also Fig. 7.)

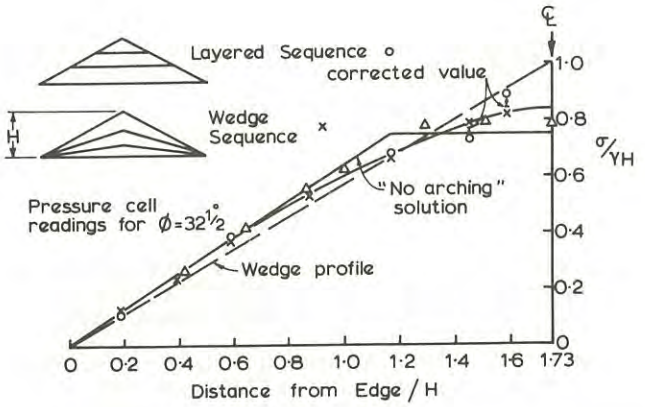


Fig.2 Normal Stress Distributions. Wedge and Layered Construction Sequences. Rigid Foundation

It is now possible to compare the data for the rigid base with the no-arching solution, that is, normal stresses should be trapezoidally distributed with a maximum ordinate of 0.75 γH. Although the differences between the theoretical and experimental normal stresses were relatively small the differences are real and significant.

The inapplicability of the no-arching solution to the experimental situation is more clearly demonstrated when a comparison of shearing stress distributions is made. According to the no-arching analysis the distribution is triangular over each half width with a maximum ordinate of 0.58 γH at a distance of 1.15 H from each stress-free edge. Fig. 3 shows that the shear stresses for side slopes equal to the angle of repose are symmetrically distributed over each half width with a peak value of approximately 0.11 γH. It is therefore clear that the no-arching solution is inapplicable to the rigid base condition when there is no horizontal displacement of the foundation.

*In these tests the base was a thin metal plate, the deflection being controlled by air pressure applied to the underside of the plate.

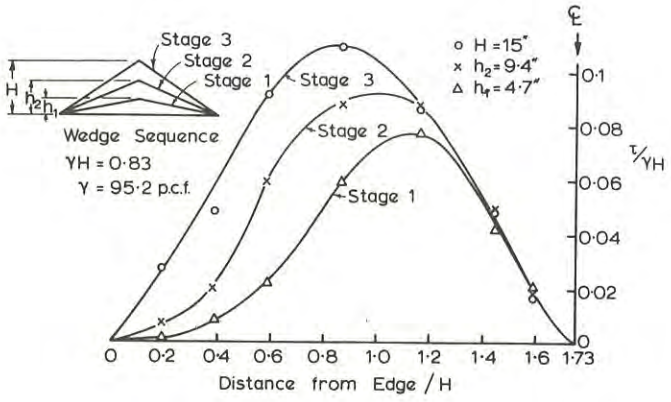


Fig.3 Experimental Shear Stress Distribution Intermediate Stages and Final Stage of Wedge Sequence. Rigid Foundation

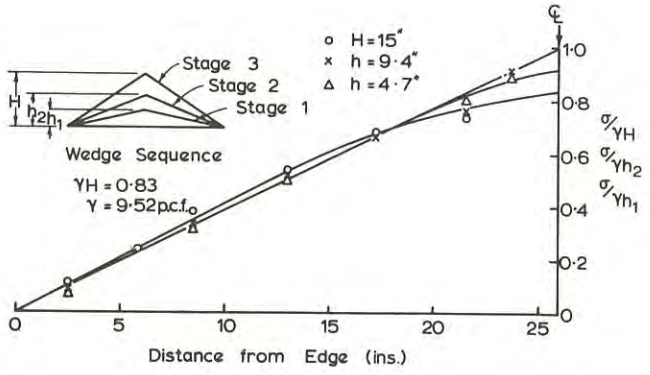


Fig.4 Normal Stress Distribution. Intermediate Stages and Final Stage of Wedge Sequence. Rigid Foundation. Experimental Values.

Existing theories which satisfy the fundamental requirements of equilibrium and strain compatibility involve the use of simplified constitutive equations. The latter equations express the stress-strain relationship for the real soil in some approximate fashion and as a first approximation one can make use of the linear elastic model. Provided the limitations are understood and the experimental parameters obtained by a suitable procedure, linear elastic solutions have been shown to be extremely valuable in many stress distribution problems.

Thus, a comparison of the data for the wedge was made with the corresponding linear elastic solutions. As shown in the following sections use of the simple linear elastic model leads to a relatively consistent prediction of measured values. Figs.4, 5 and 6 show the experimental results for the layered and wedge sequences. Table I summarizes the comparative values for the wedge sequence and the corresponding data for the layered sequence are given in Table II. Both the shear and normal stress values in these tables have been divided by the (density x mid height). The value of Poisson's ratio used in the elastic solutions was 0.40, an approximate value determined by independent shear tests at a representative stress state.

The observed trend, that the normal stress distribution is closer to the triangular distribution at side slopes less than the angle of repose, is in agreement with the linear elastic results. Similarly, the observed trend in normal stress distribution as the embankment is formed in layers is also predicted by the theory.

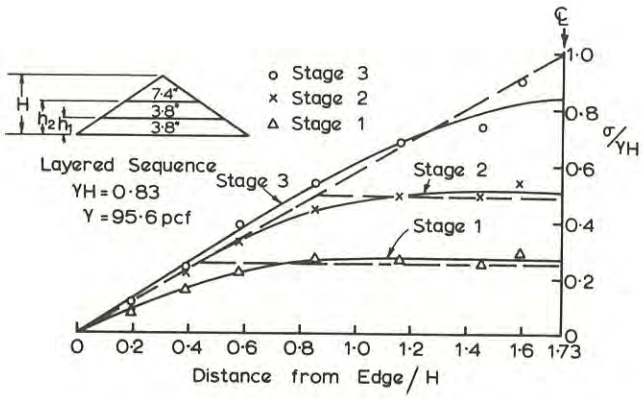


Fig.5 Normal Stress Distribution. Intermediate Stages and Final Stage of Layered Sequence. Rigid Foundation. Experimental Values.

TABLE I

THEORETICAL AND EXPERIMENTAL NORMAL AND SHEAR STRESSES. RIGID BASE. WEDGE SEQUENCE

| Mid Height | 0.4H | | 0.8H | | 1.2H | | CENTRE | |
|---|---|---|---|---|---|---|---|---|
| | $\sigma_{TH}$ | $\sigma_{EXP}$ | $\sigma_{TH}$ | $\sigma_{EXP}$ | $\sigma_{TH}$ | $\sigma_{EXP}$ | $\sigma_{TH}$ | $\sigma_{EXP}$ |
| 4.7" | 0.23 | 0.23 | 0.48 | 0.45 | 0.75 | 0.73 | 0.94 | 0.92 |
| 9.4" | 0.23 | 0.23 | 0.48 | 0.45 | 0.74 | 0.71 | 0.88 | 0.92 |
| 15.0" | 0.19 | 0.23 | 0.46 | 0.49 | 0.68 | 0.68 | 0.83 | 0.84 |
| | $\tau_{TH}$ | $\tau_{EXP}$ | $\tau_{TH}$ | $\tau_{EXP}$ | $\tau_{TH}$ | $\tau_{EXP}$ | $\tau_{TH}$ | $\tau_{EXP}$ |
| 4.7" | 0.016 | 0.025 | 0.035 | 0.160 | 0.049 | 0.240 | 0 | 0 |
| 9.4" | 0.033 | 0.035 | 0.062 | 0.135 | 0.056 | 0.135 | 0 | 0 |
| 15.0" | 0.040 | 0.060 | 0.075 | 0.105 | 0.068 | 0.085 | 0 | 0 |

TABLE II

THEORETICAL AND EXPERIMENTAL NORMAL AND SHEAR STRESSES. RIGID BASE. LAYERED SEQUENCE

| Mid Height | 0.4H | | 0.8H | | 1.2H | | CENTRE | |
|---|---|---|---|---|---|---|---|---|
| | $\sigma_{TH}$ | $\sigma_{EXP}$ | $\sigma_{TH}$ | $\sigma_{EXP}$ | $\sigma_{TH}$ | $\sigma_{EXP}$ | $\sigma_{TH}$ | $\sigma_{EXP}$ |
| 3.8" | 0.70 | 0.59 | 0.97 | 0.99 | 1.00 | 1.07 | 1.00 | 1.07 |
| 7.6" | 0.48 | 0.47 | 0.85 | 0.89 | 0.99 | 0.99 | 1.00 | 1.05 |
| | $\tau_{TH}$ | $\tau_{EXP}$ | $\tau_{TH}$ | $\tau_{EXP}$ | $\tau_{TH}$ | $\tau_{EXP}$ | $\tau_{TH}$ | $\tau_{EXP}$ |
| 3.8" | 0.080 | 0.095 | 0.010 | 0.030 | 0.000 | 0.000 | 0 | 0 |
| 7.6" | 0.100 | 0.080 | 0.085 | 0.055 | 0.027 | 0.036 | 0 | 0 |

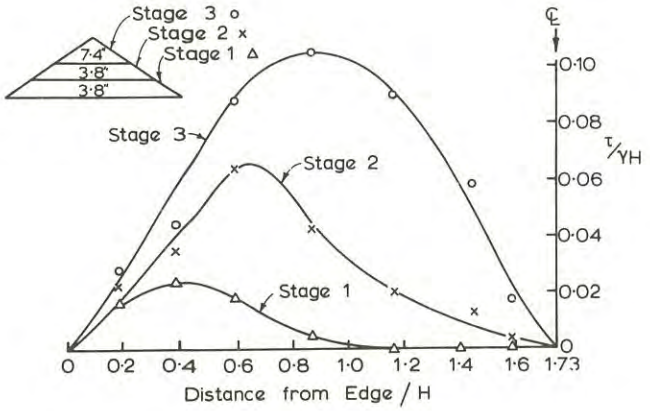


Fig.6 Shear Stress Distribution. Intermediate Stages and Final Stage of Layered Sequence. Rigid Foundation. Experimental Values.

Due to the significant changes in shear stress distribution as the embankment is formed the comparison of shear stress is a much more severe test on the effectiveness of a theory. The linear elastic theory predicts the observed trends and distributions (see Figs.3 and 6) as the embankment is constructed by either loading sequence. However, the measured values of base shear stress were in excess of the theoretical values as seen by a study of the values quoted in the tables. At side slopes equal to the angle of repose the predicted maximum shear stress is $0.077\gamma H$ compared with $(0.10\text{-}0.11)\gamma H$. Thus it follows, as anticipated, that the isotropic linear elastic model is not an adequate model for the granular mass and some of the more complex non linear stress-dependent parameter models should be used for more accurate stress predictions. Of greater importance at the present time is the recognition that the isotropic linear finite element solutions now in common use must be treated conservatively when applied to a granular soil.

IV.- DEFORMING BASE

To provide a practical technique for the measurement of stresses along the interface of a granular embankment supported on a compressible foundation, the monitored base of the model was deformed to selected convex and concave profiles. Horizontal displacements were not imposed, so that the data applies

only to a special deformation state, and the work will be later extended to impose both the vertical and horizontal displacement components which occur in a field embankment.

However, the normal stress distribution is not critically dependent on the horizontal displacements, and Fig.7 shows the normal stress distributions obtained for vertical displacements of ±0.1" at the centre of the embankment. There is a progressive transfer

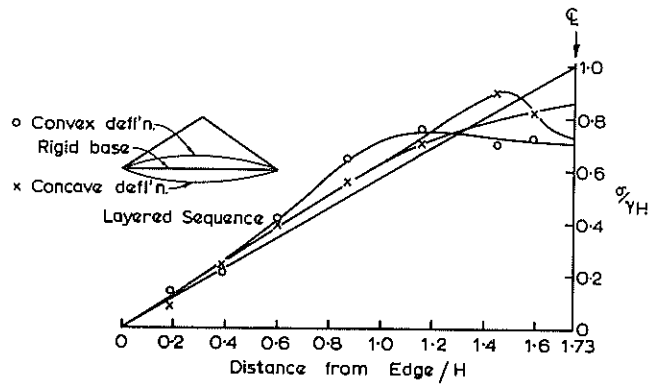


Fig.7 Experimental Normal Stress Distribution. Central Deflection of 0.1inch. Concave and Convex Foundation Deflection.

of normal stress from the central regions, and under large concave displacements the distribution is similar to that obtained for an infinite wedge in a passive state (Ref. 10). A further detailed quantitative comparison is not relevant as the passive state requires horizontal displacements along the base.

It is also of interest to note that convex base displacement also causes a reduction in normal stresses in the central region (Fig. 7), again in agreement with the plasticity solution - the relevant plasticity solution corresponds to the active state.

The shear stress distributions recorded when the base was deformed are shown in Fig.8. Here the direct influence of the finite slopes of the base appeared to have a dominant effect on the shear stresses, so that there was a progressive decrease in these stresses as the concave profile was developed. This trend is opposite to that expected by a consideration of the passive pressure plasticity solution. The shearing stresses increased rapidly as a convex base profile was developed and the distribution was similar to active

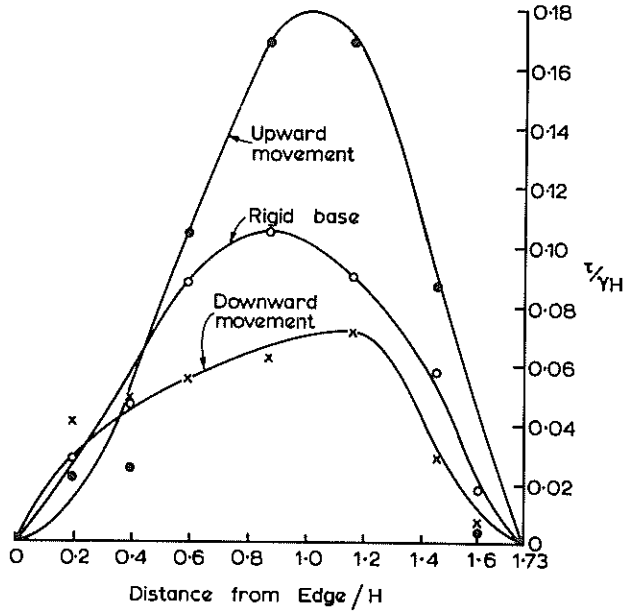


Fig.8 Experimental Shear Stress Distribution. Central Deflection of 0.1 inch. Concave and Convex Foundation Deflection.

pressure solution with theoretical and experimental peak values occurring at the section of the base 1.2H from the stress-free edge. The recorded maximum value of 0.18γH was 0.06γH in excess of the maximum theoretical value.

## V.- CONCLUSIONS

Use of the linear elastic model to predict the normal and shear stresses along the base of a loose granular embankment supported on a rigid foundation leads to a close prediction of the normal stresses, and an underestimate of the shearing stresses. The predicted trends in shear and normal stress distributions as the embankment is constructed agree with observed trends.

As the base of the embankment is deformed in a convex pattern there is a progressive decrease in normal stresses in the vicinity of the centre of the embankment. The passive and active plasticity solutions agree qualitatively with the observed limiting normal stress distributions but a proper comparison requires the development of the appropriate horizontal deformations in the model.

## VI. - ACKNOWLEDGMENTS

The work described in this paper was supported by a grant from the Australian Research Grants Committee. The equipment was manufactured in the Engineering General Workshop, University of Sydney and was assembled by Mr. K. Larrymore.

The authors are grateful to Professor E.H. Davis for discussions regarding the systematic arching theory, and to Dr. J. Booker for making available the plasticity solutions for an infinite wedge.

The linear elastic solutions were obtained by a finite element analysis carried out by Compunet Ltd.

## REFERENCES

1. DAVIS, E.H. and TAYLOR, H. - The Movement of Bridge Approaches and Abutments on Soft Foundation Soils. Proc.First Biennial Conf. Australian Road Research Board, Canberra. 1962, pp.740-755.

2. GOODMAN, L.E. and BROWN, C.B. - Dead Load Stresses and the Instability of Slopes. Jnl. of the Soil Mechancis & Foundation Engineering Division, A.S.C.E., Vol.89, No.SM3, May 1963, pp.103-134.

3. CLOUGH, R.W. and WOODWARD, R.J. - Analysis of Embankment Stresses and Deformations. Jnl of the Soil Mechanics & Foundation Engineering Division, ASCE., Vol.93, No.SM4, July 1967, pp.529-549.

4. TROLLOPE, D.H. - The Systematic Arching Theory Applied to the Stability Analysis of Embankments. Proc.Fourth Int.Conf.Soil Mechanics & Foundation Eng., London, 1957 pp.382-388.

5. HUMMEL, F.H. and FINNAN, E.J. - The Distribution of Pressure on Surfaces Supporting a Mass of Granular Material. Mins.Proc. Inst.Civil Engrs, Vol.212, Pt.2, 1920-21, pp.369-392.

6. PARRY, R.H. - Measurement of Pressure Distribution Across the Base of Triangular Section Granular Mass. Thesis (M.Eng.Sc.) Univ. of Melbourne. 1954.

7. LEE, I.K. - Design and Application of an Earth Pressure Cell. Thesis (M.Eng.Sc.) Univ. of Melbourne, 1956.

8. LEE, I.K. - Field Measurements at a Soil Structure Interface. Proc.Fourth Conf. Australian Road Research Board, Melbourne. 1968, pp.1785-1805.

9. HERINGTON, J.R. - Application of Earth and Rock Fill for Strengthening Existing Gravity Dams. Thesis (M.Eng.Sc.) Univ. of Sydney, 1969.

10. BOOKER, J.R. - Applications of Theories of Plasticity to Cohesive-Frictional Soils. Thesis (Ph.D), Univ. of Sydney. 1969.

# Abutment Stability Studies for the Gordon Arch Dam

By
D. T. Allen, B.E., M.I.E.Aust.
(Hydro-Electric Commission of Tasmania)

SUMMARY.- This paper deals with the foundation investigations that were carried out for a 460 ft. high arch dam on the Gordon River in Tasmania. A method was developed for computing the safety of an abutment block against sliding on two planes of weakness, each with wave angle shape, based on insitu observations and on an interpretation of the results of laboratory rock shear tests. This is followed by a brief description of the drainage measures adopted to improve the stability of the abutments.

## I.- INTRODUCTION

The Hydro-Electric Commission of Tasmania is constructing the first stage of power development on the Gordon River in the South West region of the state. This will have an installed capacity of 750,000 kilowatts and is estimated to cost $95,000,000. The maximum operating head is 638 ft. The storage formed by the Gordon dam will be 9.5 million acre feet.

The Gordon dam will be a 460 ft. high double curvature asymmetrical arch dam. When built it will be the highest concrete dam in Australia.

Before adopting the arch dam an extensive programme of foundation investigation was carried out. The work described in this paper formed a part of these investigations

## II.- NOTATION

$\theta_1$ angle between surface and horizontal
$\theta_2$ primary wave angle
$\theta_3$ secondary wave angle
$\phi$ basic friction angle
c cohesion
$\alpha$ angle between shear direction and horizontal in shear test
h hydrostatic head
$\mathbf{n}$ unit vector normal to plane
$\mathbf{n}'$ unit vector normal to wave angle face
$\mathbf{t}$ unit vector of intersection of base and side
$\mathbf{t}_T$ unit vector in direction of sliding
$\mathbf{W}$ rock weight vector
$\mathbf{R}$ resultant dam thrust vector
$\mathbf{V}$ combined load vector
u percolation pressure
$\mathbf{U}_C$ vector of percolation force on upstream crack
$\mathbf{U}_B$ vector of total percolation force on base
$\mathbf{T}$ vector resultant force in sliding direction
T scalar resultant force in sliding direction
$N'_B$ scalar total reaction on wave faces of base
$\mathbf{U}'_B$ vector percolation force on wave faces of base
$U'_B$ scalar percolation force on wave faces of base
$A_B$ area of active wave face of base surface
F factor of safety against sliding

Note: Suffixes "S" and "B" are used in the text to refer to side and base surfaces of the failure block.

## III.- GEOLOGICAL INVESTIGATION

### (a) TOPOGRAPHY

Site investigations commenced in 1962. Until the 55 mile long access road reached the damsite in the summer of 1966-67 all transport of men and equipment was by helicopter. Weather conditions restricted air operations to the summer months.

A prominent feature of the area in which the damsite is situated is a series of hard quartzite ridges running north south. The Gordon damsite is located in an extremely narrow gorge where the westward flowing river has cut through one of these ridges. The right abutment is overhanging for a vertical distance of 300 ft. immediately downstream of the dam and the average slope of the left abutment is 2:1 (vertical to horizontal).

### (b) METHODS OF GEOLOGICAL INVESTIGATION

The three methods used to obtain geological information were surface mapping, tunnelling or aditing, and diamond drilling.

The Commission's experiences with the foundations of Meadowbank and Cethana dams (Refs. 1 and 2) had shown that the stability was determined largely by the faulting and that faults could only be positively located and inspected by adits. Three adits were driven on the right abutment and

Fig. 1. - Gordon Damsite Gorge.

four were driven on the left abutment, the total length being approximately 5000 ft. A special feature of the investigation was the close control of aditing. Adits were driven in stages following discussion between the engineers and geologists concerning the extra information required. Parts of some adits were located where they could subsequently be used as drainage adits. The adits provided valuable information on the foundation weaknesses in the abutments. A complete exposure of each feature was obtained in the walls and roof of the adit. This revealed the roughness, planarity or irregularity of the contact surfaces and also the infilling material.

In the early stages of investigation the role of surface mapping was the identification of probable fault zones but in the gorge surface mapping was limited by the steepness of the topography and by vegetation. At a late stage valuable information was obtained when a portion of the left abutment was sluiced to expose the rock.

(c) GEOLOGY

The pre-Cambrian rocks at the damsite are intensively folded on north-south axes. The sequence up to crest level consists of fairly massively foliated quartzites containing thin inter-foliated lenses of schistose chloritic and micaceous materials. The quartzite layers are up to about two feet thick but are variable in thickness and lateral extent. Flecks of mica occur throughout the quartzite but are more numerous in the schistose bands where they are oriented parallel with the foliation. During the intense folding process shearing took place preferentially on the chlorite seams. However in most cases these seams are highly contorted and do not form extensive planar weaknesses in the rock.

The purpose of the diamond drilling was to check the general uniformity of the rock. Such information includes the spacing of joints, the location of faults and the watertightness of the rock. Most of the diamond drilling was concentrated in the riverbed. Three holes totalling 900 ft. were drilled in the left abutment to check the watertightness of the rock and to confirm fault locations. The total length of diamond drilling was 9000 ft. This is a relatively small amount of drilling for a dam of this size.

The principal joint directions and the surface trace of the faults are shown in Fig. 2. The joints are near vertical and in general are very tight.

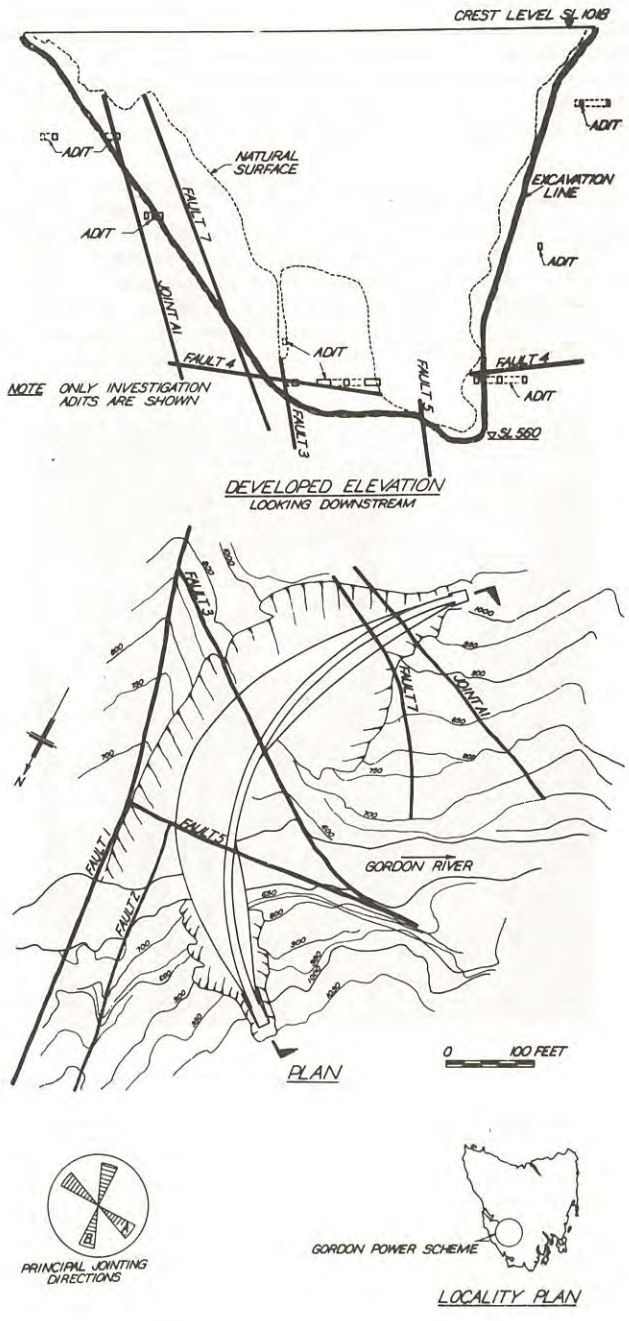


Fig. 2. - Gordon Damsite.

Joints have been designated "A" or "B" joints according to their direction.

Faulting and jointing tend to be in the same directions. The major faulting is along faults 1 and 2. When other faults approach these they become more open and show greater displacement. On the right abutment no near vertical faults could be found in the region downstream of fault 1. On the left abutment three faults occur dipping steeply towards the river. Of these, faults 3 and 5 do not constitute a stability problem as the rock wedges they form are supported at their downstream end.

Fault 4 is the only nearly horizontal fault at the site. It commences close to the riverbed near fault 1 and is continuous in a downstream direction. Fault 4 makes an angle of about 16° to the horizontal, rising in a downstream direction. It consists of a zone several feet thick containing sound quartzite separated by undulating shear planes of chlorite which are typically one half to three inches thick.

Fig. 3 is a photograph of a model which was constructed to aid interpretation of the geological data. It consists of a series of horizontal perspex plates. The plates are generally located at adit levels. All significant observations are recorded on the model. The value of the model as an aid in visualising the relationship between the dam and the underground features cannot be overemphasised.

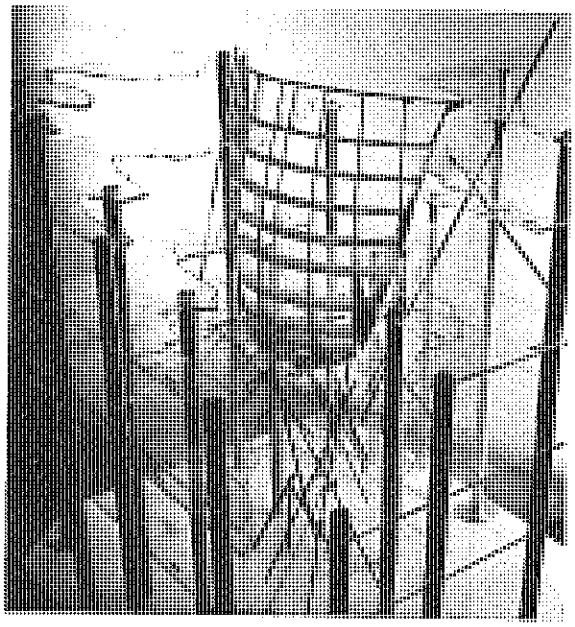

Fig. 3. - Perspex Model of Damsite.

IV.- INITIAL DESIGN

(a) During the course of the investigation the dam was moved progressively further downstream in order to lie completely clear of faults 1 and 2. (Refer to Fig. 2.) Fault 7 on the left abutment then lay immediately beneath the dam contact and emerged on the abutment a short distance downstream. Calculations showed that this block would be unstable under the dam thrust. It was decided to extend the dam profile and the excavation behind fault 7. This

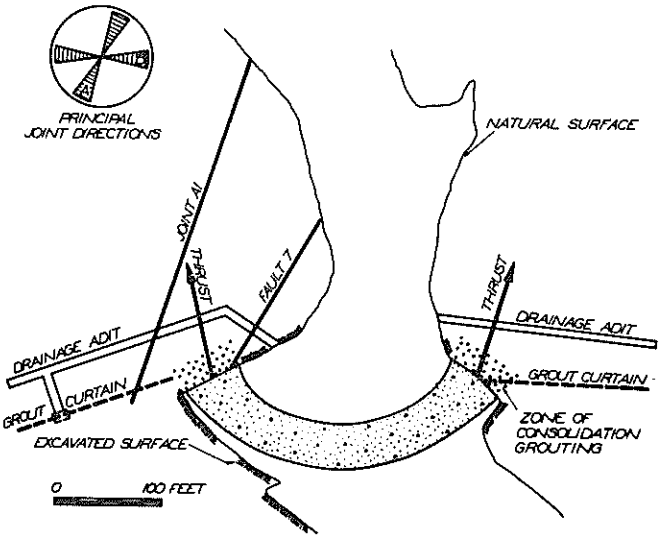


Fig. 4. - Horizontal Section.

accentuated the asymmetry of the dam and gave greater chord lengths across the arch. The volume of rock excavation on the left abutment was thereby increased. Total left abutment excavation volume was 170,000 cub.yds.

The dam is oriented in the gorge with its thrust directions approximately equally positioned with respect to surface contours. This is illustrated by Fig. 4 which is a horizontal section through the dam and the abutments.

(b) LEFT ABUTMENT STABILITY

Beyond the foundation contact lay a prominent tight joint designated joint A1. Sluicing of the abutment surface indicated that it emerged at the surface downstream of the dam (see Figs. 2, 4). Of the joints exposed by the aditing and sluicing this was the only joint that was continuous in the foundation immediately downstream of the dam. Joint A1 was oriented such that it made a small angle with the thrust and therefore its stability warranted scrutiny. As the vertical height between the adits was approximately 120 ft. there was some difficulty in identifying joint A1 in the different adits. In order to confirm the joint identification adits at three levels were driven along it thereby obtaining an exposure of the joint in the roof. The joint was limonite stained but very tight for most of its length.

The depth of joint A1 was such that it would have been very costly to extend the dam beyond it. Preliminary calculations were made using a polar plot to aid in the vector manipulations, and these confirmed that detailed study was received. The devastating failure of the Malpasset arch dam in France (Ref. 3) has also emphasized the necessity for detailed studies of rock defects below or behind arch dam foundations.

In order to avoid delays in the design programme

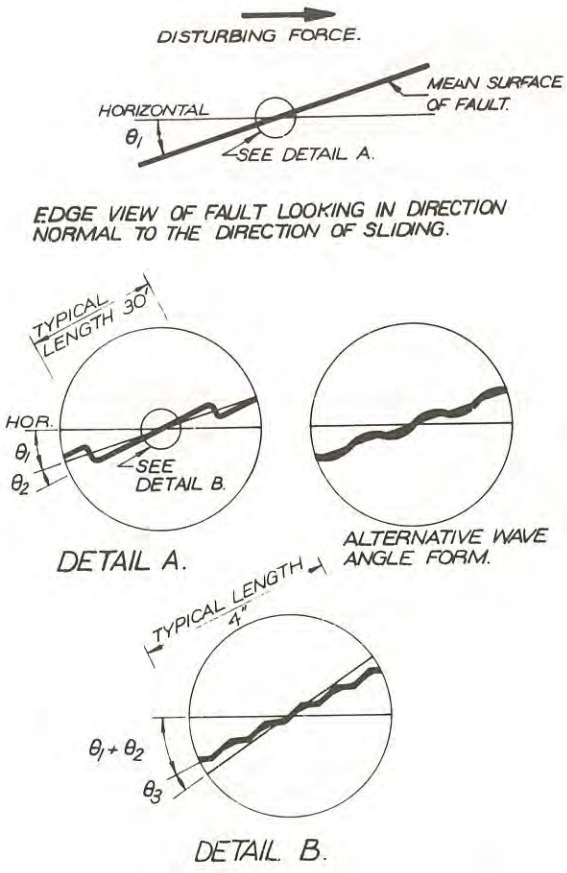


Fig. 5. - Wave Angle Concept.

for the dam itself it was decided to adhere to the dam profile and to ensure the stability of the abutment by other means if necessary. One such method would have been to drive a tunnel or shaft across the weakness transverse to the load and to provide the shear strength with concrete backfill (Ref. 4). Other methods considered were: flattening of the arches; rotating the dam at the expense of the stress state in the right abutment. Fortunately none of these measures were required.

## V.- WAVE ANGLE CONCEPT

A close inspection of joint A1 and fault 4 indicated that although their overall position was planar their surfaces exhibited substantial irregularities. A realistic stability analysis would need to take account of these. The concept used to describe these irregularities is referred to here as the wave angle concept. A similar approach has been used in Ref. 5.

The concept is illustrated in Fig. 5 by reference to fault 4. The profile of fault 4 in the direction of sliding consisted typically of straights about 30 ft. long making an angle of about 10 degrees to the mean plane surface. The rock forming these irregularities was sound and extremely hard. With a rock compressive strength of the order of 25,000 p.s.i. failure could not occur by crushing these irregularities. Thus for sliding to occur, the upper block must move at the angle $\theta_2$ to the mean surface. This is the primary wave angle effect.

The faces on the upstream portion of each wave shall subsequently be referred to in this paper as the active faces because the shear strength properties of these faces determine the resistance to sliding in the sliding direction described above.

Surface irregularities on a much smaller scale appeared again on each of the 30 ft. lengths. (See detail "B" in Fig. 5.) However, because of their small size, the likelihood of shearing through infilling material precluded the use of the secondary wave angle effect $(\theta_3)$.

Observations on the joint A1 in the roofs of adits indicated that its primary wave angle effect $(\theta_{2S})$ could be taken as 20 degrees.

## VI.- SHEAR TESTS

### (a) SAMPLING AND TESTING

In order to determine the strength parameters of the potential failure surfaces laboratory shear tests were carried out. Insitu shear tests were abandoned after several unsuccessful attempts to isolate a section of fault 4 in an adit.

The value of a laboratory shear test is dependent on the degree of disturbance obtained during sampling. Isolation of samples of rock straddling the joint (or fault) was carried out by line drilling in a Vee pattern, firing the holes with detonating fuse only, then removing the rock by hand chiselling. In every case some disturbance of the sample was caused. Taking care to retain any infilling material, the sample halves were then carefully matched together, marked with the shear directions corresponding with the sense of loads applied by the dam, and encased in wax for transport. In the laboratory, after embedding each half of the sample in plaster, the specimen was ready for testing.

The initial vertical stress was generally set at the computed insitu stress. The horizontal load was incremented to a maximum and then continued at reducing values until displacement took place at constant horizontal load thereby indicating the residual strength phase. Then the vertical stress was incremented and the shearing process repeated. Some specimens were tested at initial vertical stresses below the computed insitu stress to check whether this affected the shear resistance. Contact areas were typically 8 sq. in.

### (b) RESULTS

Vertical and horizontal loads in the test were resolved to obtain shearing and normal loads for the actual plane of shearing in the test. In Fig. 6 the slope of the line BC in the displacement plot is a direct measure of the slope of this plane. The range of values obtained for the angle between the plane of shearing and the horizontal (from +25 to -20 degrees) indicates the difficulties in predicting the probable plane of shearing.

Tests were carried out for shear displacements greater than could be tolerated in the abutment.

For stability calculations it was decided to use shear strength values for shear displacements up to 0.1 inches because greater displacements would have seriously increased the stresses in the dam and the uplift pressures. In some tests it was apparent that up to 0.05 inches shear displacement took place during the "bedding in" phase caused through sample disturbance. When the peak horizontal load (P1 in Fig. 6) occurred at less than 0.1 inches shear displacement a point was obtained on the initial shear strength envelope. However, for some samples, the first peak occurred beyond the displacement limit. In such cases the shear strength at the limiting displacement was plotted against the normal stress. By plotting the results for all the specimens it was possible to determine a mean strength envelope and a minimum strength envelope and hence the coefficient of friction and the cohesion. For tests on rock joints the term "cohesion" is a measure of the force required to shear through rock points or through infilling material when there is no normal load.

The small area constituting the plane of shearing in the test represents one of the small planes forming a secondary wave angle face. This face is superimposed on the active primary wave angle face of the joint. As it had previously been decided to ignore the secondary wave angle effect in order to be conservative, the shear strength parameters obtained for the plane of shearing in the test become the shear strength parameters of an active face of the primary wave angle surface.

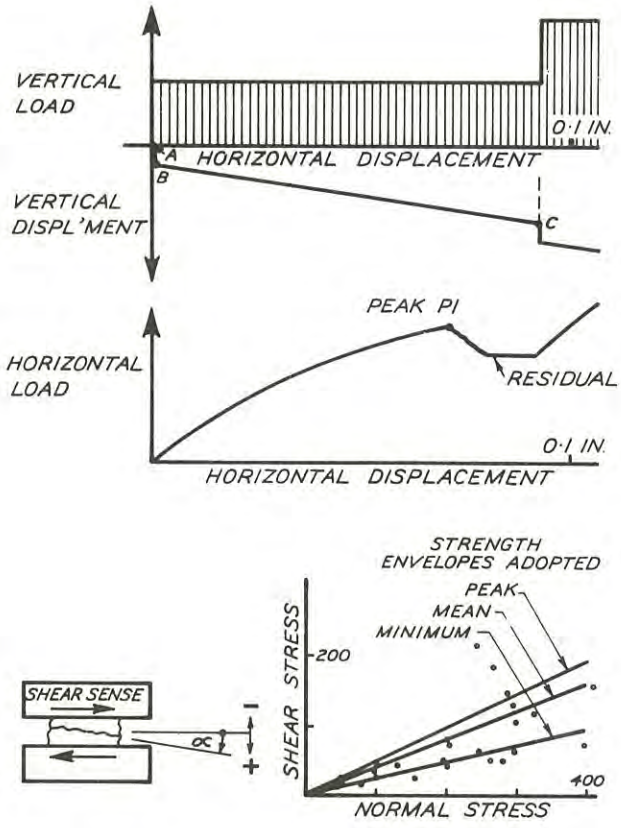


Fig. 6. - Typical Shear Test Graphs.

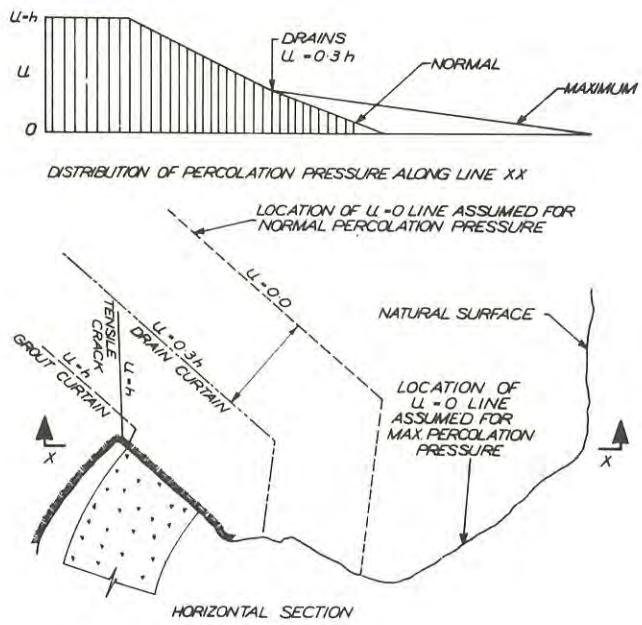


Fig. 7. - Percolation Pressure Distribution.

Nine shear tests were carried out on samples from fault 4 and twelve tests on samples from joint A1. As the results exhibited a considerable range a mean value and a minimum value were extracted:-

Fault 4 : tan $\phi_B$ : mean 0.4, min. 0.25
$C_B$ : mean 0 p.s.i., min. 0 p.s.i.
Joint A1: tan $\phi_S$ : mean 0.8, min. 0.6
$C_S$ : mean 50 p.s.i., min. 0 p.s.i.

## VII.- PERCOLATION PRESSURES

The watertightness of the rock was checked by means of water pressure tests on the diamond drill holes. Three holes totalling approximately 900 feet were drilled in the left abutment above fault 4. In general the rock was very watertight. One of the characteristics of the tectonicly jointed quartzite rock is that although most of the joints were limonite stained this was not necessarily indicative of leakage potential. Water loss from a 10 ft. stage rarely exceeded 2 g.p.m. when tested at stage pressures up to 350 p.s.i. This corresponds to a loss rate of .0006 g.p.m./ft./p.s.i. - a rate at which grouting is normally considered to be unnecessary. However in parts of the abutment where open joints were detected typical water losses were 10 g.p.m. at stage pressures of 45 p.s.i. All adits in the abutment were dry. No natural aquifers were detected in the left abutment.

The term "percolation pressure" is used to describe the pressure of water in joints and fissures. It is considered that for abutment studies this term is more meaningful than "uplift".

The prediction of percolation pressures within the abutment is overshadowed by the existence of the joints and faults which would invalidate an analytical solution based on the assumption of homogeneity. One of the conclusions from the water pressure testing at this site was that most of the flow would take place along a few relatively open joints. One consequence of the limited coverage of the abutment by diamond drilling was that, at the design stage, open joints may have been undetected for distances of 50 feet or more. It was considered that a more extensive drilling program was not economically justified. Unless all such potential aquifers were identified any mathematical model would very likely be a poor one. The mathematical problem for homogeneous conditions has been solved (Ref. 6).

The permeability of jointed rock also varies with applied stress (Ref. 7). The tensile zone in the abutment upstream of the dam will have greater permeability than the compressive zone downstream of the dam. It can be shown that this effect increases the percolation pressures in the abutment.

The view was taken that it would be reasonable to use empirical data as a guide to the percolation pressures and to review the drainage system if measured pressures exceed those assumed. Much data has been accumulated on the pressures that exist under gravity dams (e.g. Refs. 8 and 9) but very little exists on pressures within steep dam abutments. The differences between the two situations are significant. The drain holes beneath a gravity dam usually take the form of vertical drill holes within which a hydrostatic pressure distribution exists. Mean percolation pressure at the plane of the drains lies in the range 0.2 to 0.4 of the hydrostatic head of the reservoir.

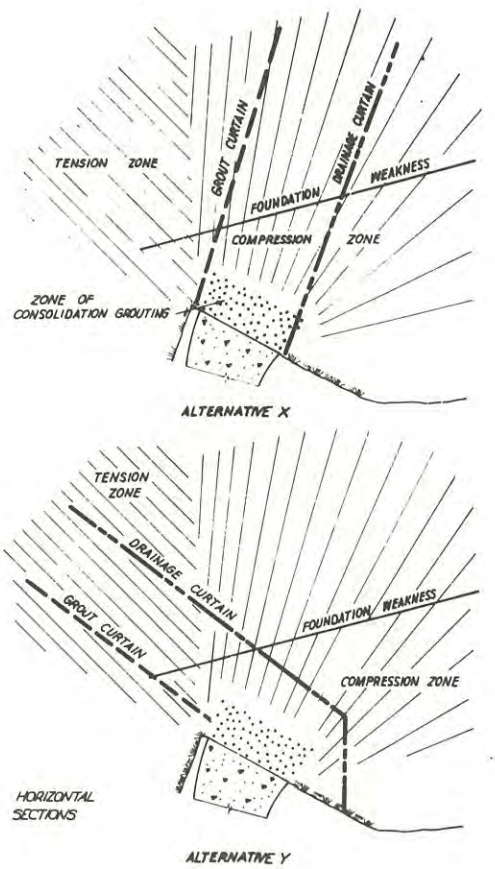


Fig. 8 - Alternative Locations for Drainage Curtains.

In steep abutments it is possible to provide drains that are free draining, thus lowering the mean pressure at the drain curtain. Drainage is further improved by orienting the drain holes to intersect the principal joints. The mean percolation pressure at the drainage curtain was assumed to be 0.3 of the hydrostatic head. The system was designed such that a blocked drain condition could not occur. (See Section XI.) Two alternative assumptions were made for the distribution of percolation pressure downstream of the drainage curtain. See Fig. 7.

The advantages of locating the drains well upstream have been pointed out in Ref. 7 by Minassian, Sabarly and Londe. This feature was adopted. In Fig. 8 the drain location "Y" intersects the foundation weakness further upstream than the conventional location shown in "X". This reduces the total percolation force on the weakness but is achieved at the expense of increased leakage because the drainage curtain extends into the tension (and hence more open) zone where the drains may function more effectively. The tight rock conditions at this damsite enable the upstream alternative to be used.

## VIII.- STRESS ANALYSES

Stress analyses of horizontal sections of the abutments were made using the finite element method and assuming that the rock has tensile strength. The studies showed tensile stresses upstream of the dam contact and oriented roughly normal to the "B" joints. As the tensile strength of the joints would be negligible it was evident that they would open and cause a redistribution of stress. Movement could tend to concentrate on one joint emanating from near the upstream corner of the dam. In order to determine whether it continued in the "B" joint direction a short crack was inserted and the section re-analysed. This process was repeated. These studies defined the probable crack direction at various levels in the abutment, but generally the crack made an angle of about 55° with the thrust direction. In the subsequent stability calculations it was assumed that full hydrostatic head existed in the crack.

## IX.- EARTHQUAKE LOADING

In recent years the possibility that earthquake activity may be associated with the filling of reservoirs of great depth or of great volume has been described in the literature, eg. Ref. 13. Studies were made of this effect but expert overseas opinion indicated that the problem was not sufficiently understood to make any firm statements about a particular locality.

The evidence of arch dams in Japan and elsewhere indicates that even high magnitude earthquakes close to a dam have not caused damage. The extraordinary acceleration - (0.62g) - sustained by Koyna dam in India without irreparable damage is but one example

of this. Tasmania is in an area of very low seismicity, the largest earthquake on record heing magnitude 5.3. Earthquakes of magnitude 5-6 require rupturing to occur simultaneously over a length of perhaps 10 miles of fault and they tend to occur on existing active faults (Ref. 14). The Lake Edgar fault scarp passes through the storage 15 miles from the damsite and has a length of approximately 20 miles. The decision was made not to include earthquake loading on the foundations after taking into account the complete absence of population downstream of the dam.

In order to obtain detailed information on the seismicity before and after filling, the State seismic net has been extended by five stations, microseismic recorders installed at Strathgordon, precise surveys carried out, and in the dam a strong motion instrument and four seismoscopes will be installed. A full time seismologist has been appointed.

## X.- STABILITY ANALYSES

### (a) POTENTIAL FAILURE BLOCK

The potential failure block analysed is illustrated in Fig. 9. The boundaries of the block are:

(i) A plane defining the base of the block (Fault 4)
(ii) A steeply dipping plane which intersects the base plane and forms the side of the block. Prominent joint A1 is the side plane.
(iii) The surface of the abutment after excavation.
(iv) An upstream boundary formed by the tension crack.

After considering the deformation characteristics of the foundation rock it was decided to assume that the potential failure block behaved as a rigid body. The weight of the block was computed assuming a rock density of 160 lb./cub.ft.

### (b) DAM THRUST

Stresses in the dam shell due to its own weight and due to water at maximum flood level were determined mainly by means of the Commission's computer programme for the analysis of arch dams. Stresses were confirmed by model studies. The results gave radial, tangential and vertical components of thrust at various levels on the foundation contact. As a check the thrust components acting downstream were integrated around the perimeter of the dam and compared with the water load. Finally the thrust components were used to determine the single resultant thrust vector applied by the dam to the potential failure block.

### (c) METHOD OF ANALYSIS

The literature on arch dam foundations contains many approaches to the problem (e.g. Refs. 10, 11, 12). For the Gordon damsite a lengthy computer programme was written to perform all stages of the analysis including the calculation of rock weight, dam thrust and percolation forces. The main value of the programme was that it enabled a large number of cases to be studied covering the many combinations of possible values of the parameters. It would also permit a rapid reassessment of the stability if other weaknesses were found during construction.

Unit vectors ($\mathbf{n_S}$ and $\mathbf{n_B}$) normal to the side and base planes are used to compute the unit vector ($\mathbf{t}$) of the plane intersection. This gives the direction of movement for zero wave angles. The true direction of incipient sliding ($\mathbf{t_T}$) makes an angle equal to the wave angle with each surface. (See Fig. 9). Using the vector cross product,

$$\mathbf{t} = \mathbf{n_S} \times \mathbf{n_B}$$

$$\mathbf{t_T} = \mathbf{t} - (\mathbf{n_B})(\sin \theta_B) - (\mathbf{n_S})(\sin \theta_S)$$

Unit vectors normal to the wave angle faces ($\mathbf{n'_S}$ and $\mathbf{n'_B}$) are then computed after making $\mathbf{t_T}$ a unit vector.

$$\mathbf{n'_S} = \mathbf{t_T} \times (\mathbf{n_S} \times \mathbf{t_T})$$

$$\mathbf{n'_B} = \mathbf{t_T} \times (\mathbf{n_B} \times \mathbf{t_T})$$

The external forces acting on the block are combined into a single load vector for convenience.

$$\mathbf{V} = \mathbf{W} + \mathbf{R} + \mathbf{U_C}$$

By neglecting the tensile strength of the upstream crack and using the vector dot product the total force in the direction $\mathbf{t_T}$ is given by the vector $\mathbf{T}$ from which its scalar magnitude ($T$) can be computed.

$$\mathbf{T} = \mathbf{t_T}(\mathbf{V} \cdot \mathbf{t_T} + \mathbf{U_S} \cdot \mathbf{t_T} + \mathbf{U_B} \cdot \mathbf{t_T})$$

It is to be noted that the wave angle concept required that there be a component of $\mathbf{U_S}$ and $\mathbf{U_B}$ in the direction of sliding. This effect is illustrated in Fig. 10. However the small increase thus obtained in $T$ is offset by the improved thrust directions relative to the wave angle faces. The reactions ($N'_S$ and $N'_B$) on the wave angle faces are obtained by apportioning $\mathbf{V}$ between them to satisfy the condition:

$$\mathbf{V} - (\mathbf{V} \cdot \mathbf{t_T})\mathbf{t_T} = -N'_S(\mathbf{n'_S}) - N'_B(\mathbf{n'_B})$$

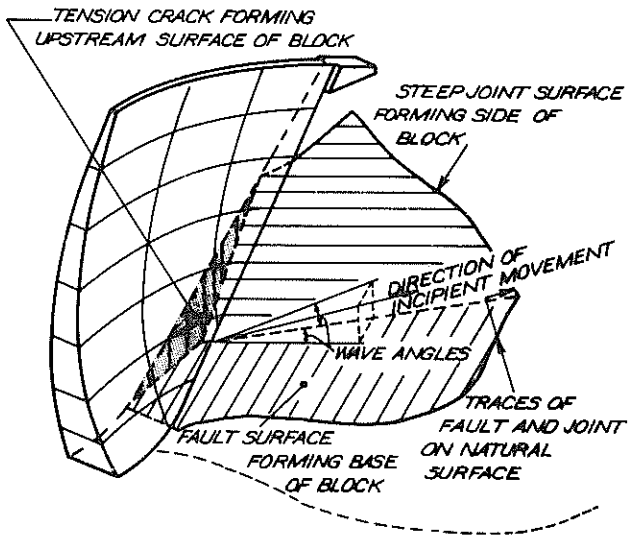


Fig. 9. - Potential Failure Block.

The solution, which is obtained by resection, is possible because there are two unknowns but three equations implied in this expression. The minus signs on the right correct for the convention adopted in Fig. 10.

The original percolation forces acting on the mean failure surfaces are then corrected to obtain the percolation forces applicable to the wave angle faces.

$$\bar{U}'_S = \bar{U}_S - (\bar{U}_S \cdot t_T)\, t_T$$

$$\bar{U}'_B = \bar{U}_B - (\bar{U}_B \cdot t_T)\, t_T$$

These are then converted to obtain the corresponding scalars $U'_S$ and $U'_B$.

The factor of safety is defined as the ratio of the forces resisting sliding to the forces tending to cause sliding. The only forces actively resisting the sliding are the shear forces mobilised on the active faces of the wave angle surfaces. The net force tending to produce sliding is T

$$F = \frac{(N'_S - U'_S)\tan \phi_S + (N'_B - U'_B)\tan \phi_B + A_S c_S + A_B c_B}{T}$$

Attention is drawn to the fact that, by this definition, the component of the rock weight acting upstream has been included in the denominator, thereby reducing the net sliding force. It is also worth noting that if $(N'_S - U'_S)$ is negative the problem must be re-analysed as a block sliding on a base plane, making suitable changes to the wave angle if necessary. In this condition, which did not occur, the side plane would not be providing any resistance to sliding.

(d) RESULTS

By means of the computer programme analyses were made not only for the most probable values of shear parameters but also for possible combinations of the range of parameters. It was considered unlikely that every parameter could have its most adverse value simultaneously. However the stability was checked when one parameter at a time had its most adverse value. For the most realistic case normal percolation pressure was assumed and mean values of shear parameters were used. The measured wave angles ($\theta_{2S} = 20°$ and $\theta_{2B} = 10°$) were used. This gave a value $F = 3.0$ for the factor of safety. For the assumption of maximum percolation pressure $F = 2.6$. For the most unfavourable case the assumptions were: maximum percolation pressure, minimum shear strength parameters, and measured wave angles. This case gave a factor of safety $F = 1.2$. Other studies showed that the stability was sensitive to changes in the predicted crack direction. Rotating the assumed crack direction 10° in a downstream direction gave a factor of safety $F = 1.6$ for all other conditions assumed normal.

It was required that the factor of safety be greater than 2.0 for normal conditions and that it should be greater than 1.0 for the worst case. On this basis it was concluded that the stability of the block was satisfactory.

XI.- DESIGN FOR STABILITY

(a) DRAINAGE DESIGN

It is essential that drainage be adequate to hold percolation pressures to the design limits. The drainage curtain as designed consists of 3" dia. holes drilled at 15 ft. centres. To prevent the possibility of the drains becoming blocked, all drain holes connect between the adits. The required drilling accuracy can be achieved with percussion equipment by the use of 2½" tuberod extensions and by restricting the adit spacing to 120 feet. This was verified by drilling trials. Within the inclined plane of the curtain all holes are inclined relative to the steepest line on the plane to give frequent intersections with the near vertical joints.

Supplementary drainage holes will be drilled from the adits to intersect any features that appear to be important aquifers. All significant weaknesses should be evident in the drainage adits. Other holes may be drilled to intersect fault 4 and joint A1 at wide spacings downstream of the curtain. As a check on the percolation pressures 33 Kyowa piezometers will be installed.

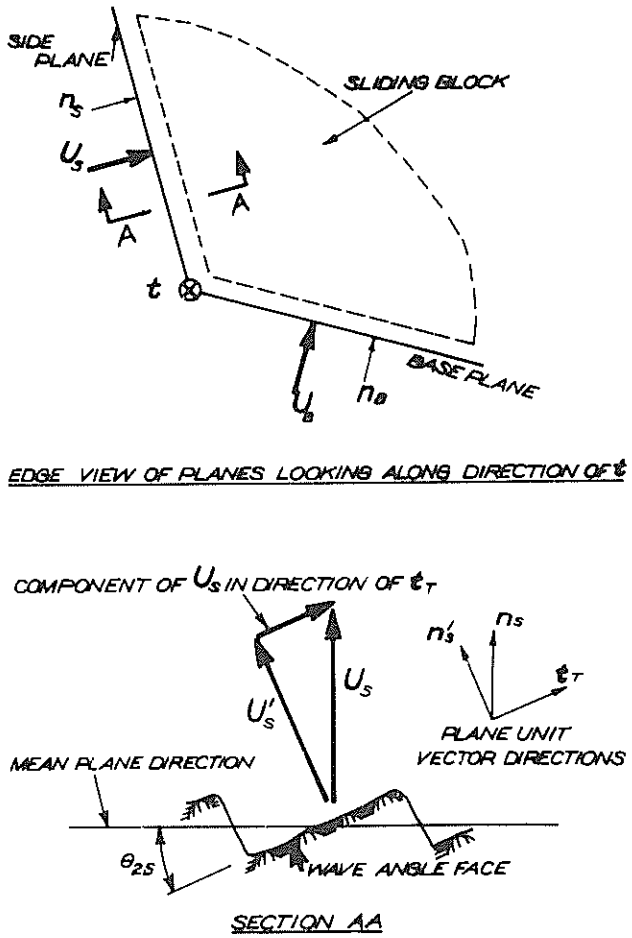


Fig. 10. - Percolation Force Directions.

(b) GROUTING

The grout curtain will be installed from chambers located as shown in Fig. 4. The quantity of grout injected will be limited to reduce the likelihood of grout travelling to the drainage curtain area and blocking the natural drainage paths.

(c) CONTROLLED FILLING

When filling the storage the rate of filling may be controlled after the water has risen to 210 feet below full supply level. Below this level the total load on the potential failure block is less than a quarter of its value with water at F.S.L. For the upper half of the storage the rate of increase in water level will be of the order of two feet per month if all water is stored. The control outlet at mid height will enable the lake level to be held if abutment measurements are unsatisfactory. For the extremely large volume of water stored in the upper levels of the lake it was considered not economically justified to install an outlet of sufficient size to produce a rapid fall in lake level if an emergency arose.

## XII. CONCLUSIONS

The possible failure mechanism revealed by the exploration required extensions to existing rock mechanics approaches to make a realistic assessment of the stability of the abutment. When storage filling is completed the piezometer readings will provide useful information on percolation pressures in abutments.

## XIII. ACKNOWLEDGEMENTS

The author is grateful to the Commissioner for the Hydro-Electric Commission, Sir Allan Knight, Kt., C.M.G., M.E., B.Sc., B.Comm., F.I.E.Aust., for permission to publish this paper. Mr. G. T. Colebatch, O.B.E., B.E., F.I.E.Aust. is the Chief Civil Engineer of the Commission. The author is also indebted to many other members of the Commission's staff. The work described was carried out under the direction of Mr. M. D. Fitzpatrick, M.I.E.Aust. Mr. N. O. Boughton, M.E., M.I.E.Aust. was the senior engineer responsible for the execution of the design work on the dam and the foundations and all work was carried out under his direct supervision. The computer programme for analysing the abutment stability was written in collaboration with Mr. P. J. Bullock, B.E., Grad.I.E.Aust.

## REFERENCES

1. Maddox, J.M., Kinstler, F.L. and Mather, R.P. - Meadowbank dam foundations. Civ. Engg. Trans. I.E. Aust., Vol. CE9, No. 2, Oct. 1967, pp. 321-333.

2. Boughton, N.O. and Hale, G.E. - Foundation studies for Cethana arch dam. Proc. Ninth I.C.O.L.D. Conf. Istanbul 1967, Q 32, R 10, pp. 143-164.

3. Jaeger, C. - Malpasset Report. Water Power Vol. 15, No. 2, Feb. 1963.

4. Artola, P.M. - Les travaux souterrains du barrage D'Aldeadavila. Proc. Seventh I.C.O.L.D. Conf., Rome 1961, pp 851-872.

5. Bray, J.W. - A study of jointed and fractured rock. Rock Mechanics and Engg. Geology, Vol. V, Nos. 2, 3, 4, 1967.

6. Zienkiewicz, O., Mayer, P. and Cheung, Y.K. - Solution of anisotropic seepage by the finite element method. Journal A.S.C.E., EMI, Vol. 92, Feb. 1966.

7. Minassian, W. Ter., Sabarly, F.L. and Londe, P. - How to protect arch dams from water pressure in the abutments. Proc. Ninth I.C.O.L.D. Conf., Istanbul 1967, Q. 32, R. 12, pp. 185-199.

8. Ginsbourg, M.B. - Study of the effect of grout curtains and drainage on uplift intensity in concrete dams. Proc. Sixth I.C.O.L.D. Conf., New York 1958, Q. 21, R. 130.

9. Casagrande, A. - Control of seepage through foundations and abutments of dams. Geotechnique, Vol. XI, No. 3, Sept. 1961.

10. Jaeger, C. - Rock mechanics and hydro power engineering. Water Power, Vol. 13, Nos. 9 and 10, Sept., Oct. 1961.

11. Muller, L. - Safety of rock abutments of concrete dams. Proc. Seventh I.C.O.L.D. Conf., Rome 1961, pp. 663-678.

12. Drnovsek, J. - Static and kinematic conditions of the stability of jointed and fissured rocky foundations of arch dams. Rock Mechanics and Engg. Geology, Vol. 6, No. 4, 1968.

13. Rothé, J.P. - Seismes artificiels. Tectonophys., 9, 1970, pp. 215-238.

14. Albee, A.L. and Smith, J.L. - Earthquake characteristics and fault activity in Southern California. Engg. Geology in Southern California. Assn. of Engg. Geologists, Oct. 1966.

# Rock Slope Stability—How far away are reliable design methods?

By
E. Hoek, M.Sc., Ph.D.
(Professor of Rock Mechanics, Imperial College of Science and Technology, London)

SUMMARY - Methods of slope stability analysis are briefly reviewed and it is concluded that the limit equilibrium technique is the only method currently available which offers the possibility of wide application in rock slope design. Discontinuum theories and model studies are seen as areas in which further development is likely to be productive. The problems of obtaining adequate input information on structural geology, rock properties and groundwater conditions are examined and methods of overcoming these problems are discussed. The influence of excavation techniques on the stability of rock slopes is briefly examined.

## I - INTRODUCTION

In both civil engineering and mining operations, the increasing size of excavated slopes is such that severe financial consequences as well as loss of life and damage to property can result from slope failure. The seriousness of this problem has been widely recognised and a considerable research effort has been devoted to the study of problems of rock slope stability. Significant advances have been made in these studies and , in this paper, an attempt will be made to take stock of the present position and to examine the question of whether reliable slope design methods are available or are likely to become available in the near future.

## II - METHODS OF STABILITY ANALYSIS

### (a) - Continuum Theories

Because of the successes which have been achieved in the application of continuum theories, particularly the theory of elasticity, to the design of underground excavations in high stress environments (Refs. 1,2), it is not surprising that attempts should have been made to apply the same theories to problems of rock slope stability (Refs. 3,4,5 ). Although the results which have been obtained have been interesting from the research point of view, it cannot be claimed that useful slope design criteria have emerged from these studies. This lack of success is due to the fact that, under the low stress conditions which exist in slopes, the behaviour of the rock mass is dominated by the structural discontinuities such as faults, joints and bedding planes. The normal stresses acting across these discontinuities are not high enough to permit the effective transmission of shear stress and hence stress and failure conditions determined on the basis of continuum theories are misleading.

In spite of the fact that some of the limitations of continuum theories have been overcome by the work of Goodman et al (Ref. 6 ), a detailed study of numerical methods of stress analysis , based on continuum theories, has lead the research team working under the author's direction to the conclusion that these methods are of limited practical value in rock slope design. These methods are useful, however, in the study of problems in which the scale is so large that individual discontinuities do not contribute significantly to the overall behaviour pattern. This applies to the study of the overall displacement or groundwater flow pattern in a large slope.

### (b) - Discontinuum Theories

The recognition that the behaviour of a rock mass under low stress conditions is dominated by the structural discontinuities present has resulted in an increased research activity involving attempts to treat the rock mass as a discontinuum. Experimental studies of the mechanical behaviour of interlocking granular systems (Refs. 7,8,9) have produced important results which have contributed to our understanding of this problem. Pioneering attempts to apply discontinuum theories to the design of rock slopes have been made by Trollope (Ref. 10) and, although these techniques have not been developed to the level at which they could be regarded as generally acceptable design tools, the philosophy underlying this approach deserves wider recognition and exploitation by rock mechanics research workers. The results of some recent work by Cundall (Ref. 11) in which the toppling failure of a system of regular blocks , separated by 'joints' having both cohesion and friction, was studies are reproduced in figure 1.

The development of more powerful numerical methods and of larger computers will almost certainly increase the usefulness of these methods which, at present, must be classed as research rather than design tools. The author believes that the most important application of these methods in the near future is the study of the behaviour and progressive failure of relatively simple discontinuous systems in an effort to build up a body of knowledge which can be used as a basis for the development of design techniques.

A discussion on the application of discontinuum theories to rock slope stability would not be complete without mention of the use of models for the study of

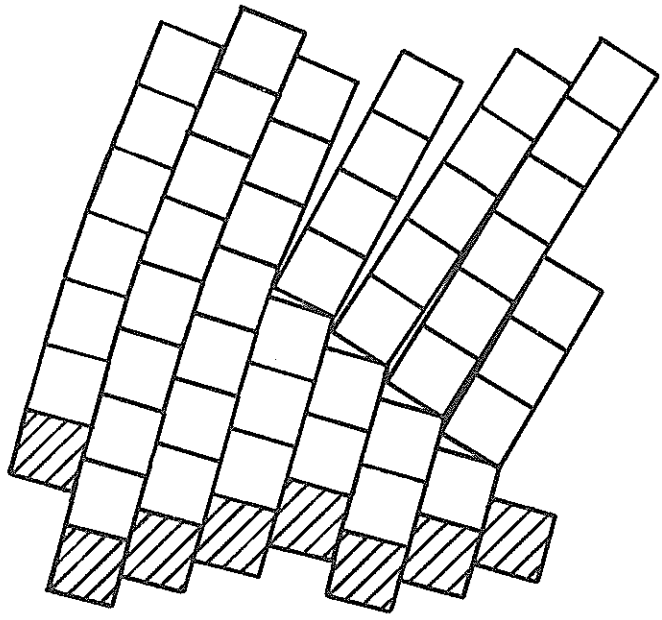

Fig. 1 : Toppling failure in a jointed system. ( After Cundall, Ref 11 ).

slope failure. Just as the computer produced diagram reproduced in figure 1 can give a useful insight into the mechanics of certain types of slope failure, so models can be used as tools for the communication of ideas and, if sufficient care is taken to satisfy the similitude requirements, for the quantitative study of slope failure. A recent model study by Barton (Ref. 12) provided useful information on both modelling techniques and on the mechanism of failure of a jointed slope.

(c) - Limit Equilibrium Methods

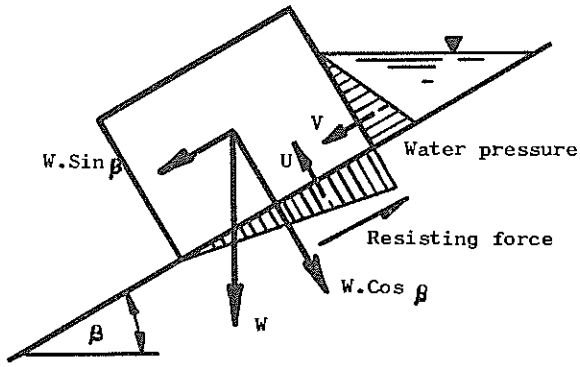


Fig. 2 : Forces acting on a block on an inclined plane.

The only form of slope stability analysis which has been developed to the extent that it can be classed as a widely accepted design tool is the method based upon the concept of limit equilibrium. The principle of this method is illustrated in figure 2 which shows a block of rock resting on an inclined plane and acted upon by the forces U and V generated by water pressure on the base and rear face of the block. The factor of safety against sliding of this block is given by

$$F = \frac{c.A + (W.\text{Cos}\,\beta - U)\,\text{Tan}\,\phi}{W.\text{Sin}\,\beta + V} \qquad (1)$$

where c is the cohesive strength of the base
$\phi$ is the angle of friction
and A is the base area of the block .

(i) - Soil slopes

The simple principles illustrated in figure 2 have been successfully applied to the stability analysis of soil slopes for many years and it is worth considering why the method works so well in soil. Skempton and Hutchinson (Ref. 13) have shown that, in most cases, the strength properties of soils, determined by triaxial or shear tests in the laboratory, bear a close relationship to the strength properties of those soils calculated by back-analysis of slope failures. This suggests that there is no serious scale effect in soil testing and that the process of progressive failure which takes place in a soil under laboratory test conditions is similar to the process of failure which occurs under field conditions. Since the laboratory test is an adequate model of field behaviour, one is justified in using the results of these tests as input information for a stability analysis and this convenient separation of the analysis into two relatively simple stages facilitates the production of practical engineering designs.

(ii) - Simple rock slopes

In the case of rock slopes containing planar discontinuities which strike parallel to the slope face and dip into the excavation at an angle greater than the angle of friction, the stability of the slopes can be calculated by means of simple two-dimensional limit equilibrium methods. The author has recently published a set of design charts which can be used to obtain estimates of the factor of safety for simple rock slopes (Ref. 14 ).

In the case of rock slopes , the intact material plays an almost insignificant part in the failure process since sliding occurs along structural discontinuity surfaces. The definition of the location of these structural surfaces and the determination of their mechanical properties are the most serious problems in rock slope stability and these problems will be discussed in greater detail in a later section of this paper.

(iii) - Three-dimensional slope problems.

The simple slopes discussed in the previous section are the exception rather than the rule and, generally, failure in a jointed rock slope occurs as a result of sliding, on two or more surfaces, of wedges or blocks of rock separated from the surrounding rock mass by a number of intersecting structural features. A relatively simple case of such a failure is illustrated diagrammatically in figure 3 which shows a wedge of rock sliding on two intersecting oblique planes.

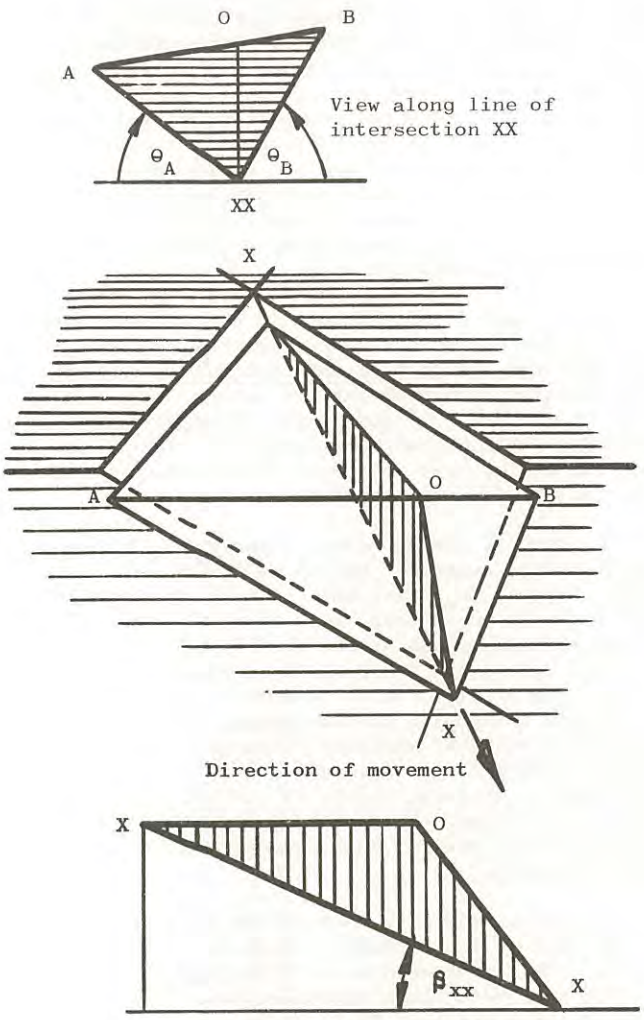


Fig. 3 : Sliding of a rock wedge on two intersecting oblique planes.

The factor of safety for the slope illustrated in figure 3 , assuming the material properties of the two planes to be the same and the slope to be drained, is given by

$$F = \left\{ \frac{c.A}{W.\mathrm{Sin}\beta_{xx}} + \frac{\mathrm{Tan}\,\phi}{\mathrm{Tan}\beta_{xx}} \right\} \frac{\mathrm{Sin}\,\Theta_A + \mathrm{Sin}\,\Theta_B}{\mathrm{Sin}(\Theta_A + \Theta_B)} \qquad (2)$$

It will be seen that this equation consists of three terms - a cohesion term, a friction term and a term which defines the wedging action of the two planes. For some simple slope geometries, the cohesion term can easily be evaluated (Ref. 15) but in many slope design situations it is preferable to ignore the cohesion term and base the design on frictional shear resistance only. Under these conditions , equation 2 reduces to a very simple form and Hoek and Boyd (Ref. 16) have recently published a set of charts which give the solution to this equation directly from the strike and dip of the two planes. These charts are intended for use where the quality of the input information does not justify a more detailed analysis but where a preliminary assessment of slope stability is required.

A more elaborate set of three-dimensional slope charts has been published by Londe et al (Ref.17) and these charts or the graphical methods based upon the use of stereographic projections (Ref. 18) are powerful tools for three-dimensional slopes stability analysis in cases where the structure of the rock mass has been reasonably well defined. Mathematical techniques for three-dimensional slope stability analysis are also available (Refs. 19,20,21,22 ) and have the advantage of being readily processed by computer.

(iv) Limitations of limit equilibrium methods

In spite of the fact that limit equilibrium techniques are currently the most satisfactory methods for slope stability analysis, it is important to recognise that these techniques have certain limitations which must be kept in mind when carrying out a stability analysis. The most important of these limitations are as follows:

A mode of failure must be assumed before a stability analysis can be carried out and this means that a judgement has to be made on the position and properties of the surface or surfaces upon which sliding will take place. Unless great care is taken in mapping the structural discontinuities in a rock mass and in checking the stability of a number of possible failure surfaces, it is relatively easy to miss the most dangerous failure mode and to arrive at an over-optimistic assessment of the factor of safety. In one case in which the author was involved, slope failure occurred on a one centimeter thick clay layer which had not been detected during the site investigation and was not, therefore, included in the considerations which resulted in this particular slope being pronounced safe.

Limit equilibrium calculations are restricted to the surface upon which sliding takes place and do not include any consideration of the behaviour of the mass of material resting on this surface. Observation of slope failures suggests that considerable movement can take place within the sliding mass and that this movement could have a significant influence upon the stability of the slope (Ref.23 ).Similarly, toppling failure of near surface blocks such as that illustrated in figure 1 cannot be incorporated into a normal limit equilibrium analysis.

The factor of safety calculated by means of the limit equilibrium method is only valid for the condition of limiting equilibrium , ie. the condition in which the material above the failure surface is just on the point of sliding. This restriction is due to the fact that the progressive failure of the surface and the changing stress distribution on the failure surface are not taken into account in the analysis. This means that factors of safety other than unity should only be used to give general guidance and their absolute value should not be relied upon too heavily.

Time dependent slope failure resulting from creep or weathering processes cannot be incorporated directly

into a limit equilibrium analysis and the only satisfactory method for dealing with this problem is to estimate the strength properties of the failure surface at various points in time and to use these values in the stability calculation.

## III - INPUT INFORMATION FOR STABILITY ANALYSIS

The reliability of any slope stability analysis depends not only upon the method of calculation used but also upon the quality of the input information used in this calculation. The most important items of input information are :

(a) The geometry of the slope and of the structural discontinuities in the rock mass.
(b) The mechanical properties of the surfaces upon which sliding can take place.
(c) The groundwater flow pattern and the resulting water pressure distribution in the slope.
(d) External factors such as accelerations imposed by nearby earthquakes or large blasts and superficial loads due to the placing of waste dumps or the passage of heavy equipment.

### (a) - Site Investigation for Stability Analysis

In the author's opinion, the most difficult problem associated with a rock slope stability analysis is the definition of the structural geology of the site. Surface exposures , where they exist, are frequently altered by weathering and care must be taken in extrapolating the information obtained from these exposures into the rock mass. Core drilling is expensive and, unless rigid specifications concerning core recovery are set out, the value of the information obtained is questionable since the critical weak zones are lost in drilling. The use of down-hole tools such as borehole television cameras and seismic or sonic probes is almost always associated with technical difficulties.

In view of these difficulties, what practical steps can be taken to ensure that an adequate site investigation is carried out before an attempt is made to assess the stability of a rock slope ?

In the first place, the author believes that a great deal of useful information can be obtained from airphotographs or from regional geology maps. All too often a slope problem is approached on the basis of the information available on site only and any information which could be obtained from a consideration of the regional geology of the area is ignored. Major structural features such as faults or folds, which have a significant influence upon the direction and frequency of jointing, are best studied on a regional scale and the maximum benefit is obtained when such a study is carried out by a competent geologist with some idea of the structural features which are important in slope stability.

The mapping of structural features on surface exposures is probably the most fruitful source of input information for a stability analysis and again, a geologist with some appreciation of the basic mechanics of slope failure should be responsible for such mapping if the maximum amount of information is to be obtained. There is considerable controversy upon the question of whether one should attempt to collect all avaliable structural information in order to build up a statistical picture of possible failure modes or whether one should first decide, from a superficial examination of the site, which structural features are likely to be the most dangerous and then to map only these features in detail. The author tends to favour the latter approach on the basis that the rock mass is not concerned with statistics - it finds the weakest structural plane and fails on that. On the other hand, it must be admitted that this plane may not be visible on the surface and it may only be possible to detect it by mapping a large number of small sympahthetic structures which will show up as a cluster on a stereographic projection .

Photogrammetric techniques in which stereoscopic pairs of photographs of rock exposures are used to determine the orientation and inclination of strucural features have been used by several research groups ( eg. Ref. 24) and it is anticipated that these techniques will become more useful in rock slope engineering as improved methods of analysing and presenting the results are evolved.

On opencast mining sites, diamond drill core is almost always available but on most civil engineering sites, special provision must be made for obtaining such core. During recent years there has been a considerable improvement in the quality of diamond drilling available and a few drilling companies will now accept a contract in which 98-100% core recovery is specified. In special circumstances, use can be made of Rocha's integral sampling technique (Ref. 25) in which a reinforcing rod is grouted into a small pilot hole before the final coring is carried out. The very good core recovery obtained in poor material justifies the additional cost of this technique in critical slope problems.

Even when 100% core recovery is obtained, the orientation of the structural features revealed in the core still represents a difficult problem and a variety of techniques have been used in order to overcome this problem. These techniques range from a reconstruction of the entire core from the collar of the hole ( Ref. 26 ) to the use of commercially available core marking devices. Examination of the walls of the borehole by means of a periscope or a borehole television camera, fitted with an orientation system, can provide useful information for the orientation of the structures in the rock mass. Devices such as the 'Televiewer', a sonic tool used in the oil industry (Ref. 27 ), have great potential for structural investigations in rock slope sites provided that these tools can be adapted to the conditions found on these sites.

All down-hole tools are expensive and, because of the severe conditions in which they operate, suffer from a high rate a breakdown and damage. Consequently, the use of these tools is probably best left in the hands of specialist consultants who have adequately trained crews available to service and operate the equipment and to interpret the results.

In general, there are no short-cuts in site investigation for rock slope stability analysis. Each site presents its own special set of problems and it is usually necessary to use a number of site investigation techniques and to be prepared to improvise to a considerable extent in order to obtain an adequate picture of the structural geology. Since it is an act

of gross irresponsibility to attempt to carry out a detailed stability analysis without an adequate structural picture of the rock mass, it is essential that provision be made, in terms of both finance and time, for this site investigation.

(b) - Mechanical Properties of Rock Masses

As already stated in this paper , the stability of a rock slope is controlled by the structural discontinuities in the rock mass and by the interlocking of rock elements separated by these dicontinuities. Since it is only possible to study the overall strength characteristics of an undisturbed jointed rock mass in a few special cases (Ref. 28 ), it is necessary to reduce the problem to the following relatively simple steps :

(i) Determination of the shear strength of the rock surfaces.
(ii) Correction of these shear strength values for surface roughness.
(iii) Consideration of the influence of interlocking of elements on rock mass behaviour.

(i)- Shear testing of rock surfaces

Goodman (Ref. 29 ) has recently published a review of methods of shear testing on rock and it would exceed the scope of this paper to enter into a full discussion on this subject here. In spite of the difficulty of interpreting the results of shear tests (Ref. 14 ), there does not appear to be any reasonable alternative to these methods available at present and the author believes that it is necessary to carry out some form of shear testing before attempting a slope stability calculation.

Figure 4 shows a large shear machine designed and constructed at Imperial College for the testing of rock surfaces . A small shear machine , designed for use in the field, is illustrated in figure 5. These two machines give very similar results and the author feels that shear strength values obtained from tests carried out in the small machine are adequate for most current forms of slope stability analysis (Ref. 14).

Fig. 4 : 100 ton shear machine at Imperial College.

Fig.5 : 10 ton capacity portable shear machine.

(ii) - Correction for surface roughness

Patton (Ref. 30) demonstrated the influence of surface roughness on the shear strength of structural discontinuities and suggested that a simple correction could be applied to account for this influence. A more refined correction has recently been suggested by Barton (Ref. 12) and the resulting curved relationship between shear strength and normal stress has been applied to the analysis of rock slope stability ( Refs. 14,15 ). Pentz (Ref. 22 ) has emphasised the importance of the curvature of this relationship at low normal stress and the author believes that research into methods for defining this curvature from simple field measurements is urgently required.

(iii) - Influence of interlocking of rock elements

Examination of any jointed rock mass in the field suggests that the interlocking of individual rock elements plays an important part in determining the strength of the rock mass. Since it is very difficult to study this effect at full scale, most of the information available has been derived from model studies (Refs. 7,8,9,12 ). These studies show that the influence of interlocking of blocks is similar to that of surface roughness and that a non-linear relationship between shear strength and normal stress is obtained. In terms of slope stability, this effect can be treated in exactly the same way as that due to surface roughness, provided that the shear strength versus normal stress relationship can be established (Ref.28).

(c) - Influence of Groundwater on Slope Stability

Equation (1) shows that the presence of groundwater in a slope can reduce the factor of safety since both forces U and V act in unfavourable directions. Estimates of the influence of water pressure on the stability of typical rock slopes ( Ref. 31) suggest that the safe slope angle can be reduced by approximately $10^{o}$ if a dry slope becomes saturated. If tension cracks in the slope crest become water-filled, the reduction in factor of safety is more serious ( Ref. 14 ).

Although it is widely recognised that water flow in rock masses is strongly dependent upon the frequency and direction of jointing, most forms of analysis are based upon the assumptions of porous media flow. More sophisticated forms of analysis are available (Ref. 32) but the difficulty of determining relevant hydraulic parameters is such that these techniques have not yet found general acceptance in rock mechanics (Ref. 33). Provided that sufficient allowance is made for changes in water level and for the filling of tension cracks and vertical fissure systems during heavy rains, the author feels that the results of stability calculations based upon the assumption of porous media flow are acceptable for most practical purposes ( Ref. 14). In order to carry out these calculations, it is important that some attempt should be made to locate the groundwater surface in the slope and this can be done by observation of the level of face seepage, measurement of the standing water level in adjacent wells and, where necessary, the installation of piezometric devices.

(d) - Influence of External Factors on Slope Stability

External factors such as accelerations imposed by nearby earthquakes or large blasts or the additional loading of the slope by the deposition of a waste dump or the passage of heavy equipment are sometimes blamed for slope failures. Whitman (Ref. 34 ) suggests that the most important of these factors, namely the accelerations due to a nearby earthquake, will only cause slope failure when the factor of safety is close to unity. Simple calculations of the loads imposed by these external factors confirm that these loads are normally small as compared with the gravitational loads in the rock mass. Exceptions can, however, occur if a fault passing through the site is activated by an earthquake or if liquefaction can occur in a soft saturated layer or tailings dam slope. For most practical rock slope problems, the author feels that it is acceptable to increase the factor of safety from say 1.3 to 1.5 to allow for additional loading in areas which are known to be prone to earthquakes or where it is intended to use very heavy blasting.

One form of damage which is seldom considered in rock slope design is that caused by the actual process of excavating the slope. It is becoming increasingly common to use large blasts in excavating slopes and the damage to the rock faces left by these blasts can have a significant influence on the stability of the slopes. Experienced slope engineers who have compared slopes which were excavated by hand tools and small charges with modern opencast mine slopes feel that a reduction of 5 to 10$^{o}$ in the safe slope angle is caused by blasting damage. The use of pre-split blasting techniques ( Ref. 35) can substantially reduce this damage and the author believes that research into this aspect of rock slope design is urgently required.

IV - CONCLUSIONS

How far away are reliable slope design methods ? There is no simple answer to this problem since the process of designing a rock slope cannot be compared with the design of a structure such as a bridge or an aircraft which is constructed entirely of man-made materials with known mechanical properties. A rock mass is a complex assembly of elements with widely differing properties in different directions and on different surfaces. The stability of this mass can be affected by the presence of groundwater and by factors such as the damage caused by blasting during excavation. The most serious problem in rock slope design is the definition of the location, orientation and inclination of structural discontinuities since these discontinuities control the mechanical properties and hence the stability of the rock slope.

In spite of these difficulties, the author feels that significant progress has been made in the development of a practical engineering approach to rock slope design. As the basic mechanisms which control slope behaviour are understood and applied in slope design, some of the malpractices which have grown out of ignorance will begin to dissappear. The implementation of simple and inexpensive surface drainage measures to prevent tension cracks from becoming water-filled, the use of pre-split blasting to avoid excessive damage to final slope faces and the re-routing of highways to avoid extremely difficult slope conditions - these are positive steps which can be taken to minimise the risk of major slope failure. Most important is the realisation that rock slopes can and do fail if they are made too high or too steep and several techniques are now available for estimating the limiting heights and angles of slopes under different conditions. Further research will certainly improve the accuracy and reliability of these techniques but such research will only be justified when available techniques have been applied and a need for greater accuracy in slope design has emerged.

V - ACKNOWLEDGMENTS

The thoughts presented in this paper derive from the author's participation in a research project concerned with the stability of rock slopes in opencast mines. This project is being carried out at the Royal School of Mines of the Imperial College of Science and Technology in London and is administered by the Rio Tinto-Zinc Corporation on behalf of the following mining companies : Anglo American International (UK) Ltd., on behalf of six member companies ; Bougainville Copper Pty., Ltd.; Consolidated Gold Fields Ltd.; English China Clays Ltd.; Iranian Selection Trust Ltd.; National Coal Board, Opencast Executive ; Palabora Mining Co., Ltd.;Rio Tinto Espanola, S.A.; Rio Tinto-Zinc Corporation Ltd.; Roan Selection Trust Ltd.,on behalf of two member companies operating in Zambia; and seven member companies of the Australian Mineral Industries Research Association Ltd .

The author is indebted to these companies and to Imperial College for their support and for permission to publish the information contained in this paper.

VI - REFERENCES

1. JAEGER,J.C and COOK, N.G.W. Fundamentals of Rock Mechanics. Methuen, London . 1969 . 513 p.

2. MOYE, D.G. Rock Mechanics in the investigation and construction of T.1. underground power station , Snowy Mountains, Australia . Engineering Geology Case Histories . Nos 1-5. Geol. Soc. pf America. New York. 1964. pp 123-154

3. BLAKE , W. Finite element model is excellent pit design tool . Mining Engg. AIME . Vol 29 , No.8 1969.

4. WANG, F.D. and SUN, M.C. Slope stability analysis by the finite element stress analysis and limiting equilibrium method. U.S.Bureau Mines. Rep. Inv.7341 Jan.1970. 16p.

5. STACEY,T.R. Application of the finite element method in the field of rock mechanics with particular reference to slope stability. S.Afr. Mech. Engnr. Dec. 1969. pp 131-134.

6. GOODMAN, R.E., TAYLOR,R.L. and BREKKE, T.L. A model for the mechanics of jointed rock. J. Soil Mech. and Found. Div. ASCE. Vol.94, No. SM 6, 1968.p 637

7. ROSENGREN,K.J and JAEGER, J.C. The mechanical properties of an interlocking low-porosity aggregate. Geotechnique. Vol.18, 1968. pp 317-326.

8. BROWN, E.T. Strength of models of rock with intermittent joints . J.Soil Mech. Found. Div. ASCE. Vol. 96. No. SM 6, 1970 pp 1935-1949.

9. JOHN, K.W. Engineering methods to determine strength and deformability of regularly jointed rock. Proc. 11 th Rock Mech. Symposium. Berkeley. Calif. 1969.

10. TROLLOPE, D.H. Mechanics of Rock Slopes. Trans. AIME.(Mining) Vol. 222, 1961 . pp 275-281.

11. CUNDALL , P.A. The measurement and analysis of accelerations in rock slopes . Ph.D Thesis. London University. 1971 . 182 p.

12. BARTON , N.R. A model study of the behaviour of steep excavated rock slopes. Ph.D Thesis. London University. 1971. 375 p.

13. SKEMPTON , A.W. and HUTCHINSON, J. Stability of natural slopes and embankment foundations , State of the art report . Proc. 7th Intnl. Conf. Soil Mech. Mexico . 1969. Vol 1. pp 291-340

14. HOEK, E. Estimating the stability of excavated slopes in opencast mines. Trans. Inst. Min. Metall London. Vol 79, 1970 pp A 109-A 132. Discussion and author's reply to be published in Trans. IMM, April 1971.

15. JAEGER, J.C. Rock friction and the stability of slopes. 1971 Rankine Lecture to be published in Geotechnique , June 1971.

16. HOEK, E and BOYD,J.M. Stability of slopes in jointed rock. Proc. Symposium on Highway slopes. Univ. Newcastle upon Tyne, 1971 . in press.

17. LONDE,P., VIGIER, G and VORMERINGER, R. Stability of rock slopes - graphical methods. J.Soil Mech. Found. Div. ASCE. Vol 94, No SM 4 , 1970 p 1411.

18. JOHN, K.W. Graphical stability analysis of slopes in jointed rock. J. Soil Mech. Found Div. ASCE. Vol. 94, No SM 2, 1968, pp 497-526.

19. WITTKE, W.W. A numerical method for calculating the stability of loaded and unloaded slopes. ( in German ). Felsmechanik und Ingenieurgeologie. Vol.30. Suppl. II, 1965. pp 52-79.

20. LONDE,P., VIGIER,G and VORMERINGER,R. Stability of rock slopes , a three-dimensional study . J.Soil Mech. Found. Div. ASCE.Vol 95, No SM 1,1969.

21. GOODMAN,R.E and TAYLOR,R.L. Methods of analysing rock slopes and abutments - a review of recent developments. Proc. 8th Rock Mech. Symp. Minnesota. 1967. pp 303-320.

22. PENTZ, D.L. Methods of evaluation and analysis of stability of rock slopes. Proc. Symp. Stability for open pit mining. Vancouver 1970. in press.

23. MENCL, V. The influence of the stiffness of a sliding mass on the stability of slopes. Rock Mech. and Engg. Geol. Vol. 4 ,1966, pp 127-131.

24. CALDER, P.N., BAUER,A. and MACDOUGALL,A.R. Stereo photography and open pit mine design. Canadian Inst. Min. Metall. Bull. in press.

25. ROCHA, M. An integral sampling technique for site investigation. Proc. 2nd Cong. Intnl. Soc. Rock Mech. Belgrade, 1970. Vol 4 . in press.

26. ROSENGREN,K.J. Rock Mechanics of the Black Star open cut, Mount Isa. Ph.D Thesis. Aust. Nat. Univ. 1968.

27. ZEMENEK, J. et al . The Borehole Televiewer - a new logging concept for fracture location and other types of borehole inspection. J. Petrol. Technol. 1969, p.762.

28. JAEGER,J.C. The behaviour of closely jointed rock. Proc. 11th Symp. Rock Mech. Berkeley, Calif.1969.

29. GOODMAN,R.E. The deformability of joints , in Determination of the in-situ modulus of deformation of rock. Amer. Soc. Testing and Matls. Special Tech. Publ. No 477 . 1970.

30. PATTON, F.D. Multiple modes of shear failure in rock. Proc. 1st Cong. Intnl. Soc. Rock Mech. Lisbon, 1966. Vol.1. pp 509-513.

31. HOEK,E and SHARP,J.C. Improving the stability of rock slopes by drainage. Proc. Symp. Planning Open Pit Mines. Johannesburg. 1970, in press.

32. LOUIS.C. A study of groundwater flow in jointed rock and its influence upon the stability of rock masses. Imperial College Rock Mech. Res. Rep. No. 10, Sept. 1969. 90 p.

33. LOUIS,C and MAINI,Y.N. Determination of in situ hydraulic parameters in jointed rock. Proc. 2nd Cong. Intnl. Soc. Rock Mech. Belgrage, 1970.

34. WHITMAN,R.V. Influence of earthquakes on stability. Proc. Symp. Stability for Open Pit Mining. Vancouver, Nov. 1970 . in press.

35. STEWART , R.M. and KENNEDY, B.A. The role of slope stability in the economics, design and operation of openpit mines. Proc. Symp. Stability for Open Pit Mining. Vancouver, Nov 1970. in press.